Cylinder Lubrication of Two-Stroke Diesel Engines

Investigation of Nozzle Flow and Spray Formation using Numerical Simulation and Experimental Visualisation

Ravendran, Rathesan

DOI (link to publication from Publisher):
10.5278/vbn.phd.eng.00069

Publication date:
2018

Document Version
Publisher's PDF, also known as Version of record

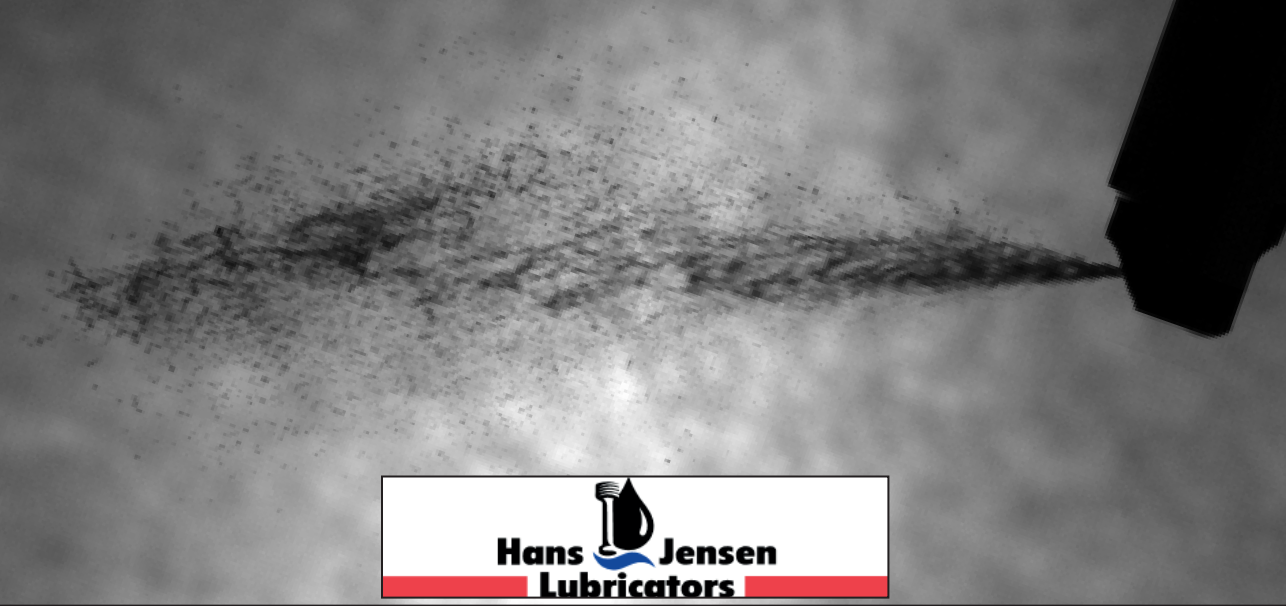

CYLINDER SPRAY LUBRICATION OF TWO-STROKE DIESEL ENGINES

INVESTIGATION OF NOZZLE FLOW AND SPRAY FORMATION
WITH NUMERICAL SIMULATION AND EXPERIMENTAL VISUALISATION

BY
RATHESAN RAVENDRAN

DISSERTATION SUBMITTED 2018

AALBORG UNIVERSITY
DENMARK

Cylinder Spray Lubrication of Two-Stroke Diesel Engines

Investigation of Nozzle Flow and Spray Formation

with Numerical Simulation and Experimental Visualisation

by

Rathesan Ravendran

PhD Dissertation
May, 2018

AALBORG UNIVERSITY
DENMARK

Dissertation submitted: May 2018

PhD supervisor: Prof. Jesper de Claville Christiansen
Aalborg University

Industrial PhD Supervisor: Peter Jensen
Hans Jensen Lubricators A/S

Assistant PhD Supervisor: Assoc. Prof. Benny Endelt
Aalborg University

PhD committee: Professor Lasse Rosendahl (chairman)
Aalborg Unviersity

Professor Jesper Hattel
Technical University of Denmark, DTU

Professor Cyril Crua
University of Brighton

PhD Series: Faculty of Engineering and Science, Aalborg University

Department: Department of Materials and Production

ISSN (online): 2446-1636
ISBN (online): 978-87-7210-055-5

Published by:
Aalborg University Press
Skjernvej 4A, 2nd floor
DK – 9220 Aalborg Ø
Phone: +45 99407140
aauf@forlag.aau.dk
forlag.aau.dk

Printed in Denmark by Rosendahls, 2018

Preface

This Industrial PhD thesis has been submitted to the Faculty of Engineering and Science at Aalborg University, Denmark, as partial fulfillment of the requirements for the Ph.D. degree. The underlying work of the thesis has been carried out during the period September 2014 to August 2017 at Department of Materials and Production.

The work has been supervised by Professor Jesper de Claville Christiansen, Associate Professor Benny Endelt, and Technical Manager Peter Jensen from Hans Jensen Lubricators A/S, to whom I express my sincere gratitude for their constant encouragement, their inspiring and supporting guidance and their success in providing good research conditions and facilities.

I would also like to thank Hans Peter Jensen and Rasmus Hans Jensen for many invaluable discussions, support and collaboration. Moreover, I would like to thank my colleagues and friends at Hans Jensen Lubricators for their advice and our discussions during my work, particular thanks to Nikolaj Kristensen, Arkadiusz Kucza, Lars Jespersen and Peer Bak. My colleagues and co-workers in the research group of Material Processing, and particularly thanks to Associate Professor Erik Appel Jensen, Anders Noel Thomsen and Professor Karl Brian Nielsen.

Furthermore, I would like to thank to thank Professor Bert Buchholz, Lehrstuhl für Kolbenmaschinen und Verbrennungsmotoren, Rostock University, for admitting me to his group at Rostock University, and for his engagement CFD simulations. Also thanks to the remainder of the group, especially M.S.c Martin Theile, Ph.D. Ibrahim Najar, Ph.D. Jören Ritzke, and M.S.c Sascha Andre.

Finally, thanks to my friends and family for their support throughout the project period.

August 2017, Aalborg, Denmark
Rathesan Ravendran

Abstract

Cylinder lubrication oil is an important component for the operation of large two-stoke marine diesel engines. It controls the mechanical friction loss and wear on cylinder liner and piston rings by providing a thin oil film between the sliding interfaces. The lubrication oil is injected as a spray into the scavenging air swirl inside the cylinder, thereby providing an even coverage of the oil at the top of the cylinder, where the need of lubrication is highest. Over the last decades, there has been an increasing focus on optimising the lubrication oil consumption in order to reduce the operational costs of marine diesel engines. As of today, the analysis has been documented by an experimental trial and error approach. Numerical investigations of the spray injection process have not been performed in order to establish an understanding of the complex process. This PhD thesis will serve as a starting point for the investigations by covering the topics influencing the flow of cylinder lubrication oil through the injection nozzle and the subsequent spray formation.

A computational fluid dynamics (CFD) model has been developed in open source CFD software package OpenFOAM. The modelling approach used is divided in two steps. Firstly, simulation of the liquid flow and cavitation inside the injection nozzle is performed using a multiphase approach. Secondly, simulation of the spray formation is performed using an Eulerian-Lagrangian framework using a Kelvin-Helmholtz and Rayleigh-Taylor (KHRT) secondary break-up model. The two simulation steps are connected using a coupling model, which translates the flow inside the nozzle to the first primary droplets at the nozzle exit. Thus, providing the boundary conditions for the spray formation. Experimental validation is performed using high-speed shadowgraphic imaging, which is able to visualise both the flow conditions inside the injection nozzle and the subsequent spray formation.

The numerical and experimental work has shown that cavitation inside the nozzle plays an important role in the spray formation, in terms of increased atomization. Cavitation is the formation of vapor cavities inside the

liquid due to evaporation, which takes place when, the local pressure of the liquid drops below the vapor pressure. The growth and collapse of these vapor cavities introduces disturbances to the liquid stream, which influences the spray formation.

Two types of cavitation are identified in the nozzle volume: edge-induced cavitation and string cavitation. Edge-induced cavitation is a result of a sudden change in geometry such as sharp edges, while string cavitation is due to the the non-symmetrical flow paths inside the nozzle that leads to a swirling liquid flow. The swirling flow results in the development of cavitation strings in the core of the liquid vortices. When these cavitation strings extend to the exit of the nozzle, the degree of atomization is significantly enhanced. In contrast, when the cavitation collapses in the nozzle volume, the viscous liquid is able to stabilize the stochastic behavior.

Knowledge gained from investigating the flow conditions inside the nozzle is used to develop a cavitation-induced primary break-up model for viscous liquids. The proposed model describes the boundary conditions for the discrete Lagrangian droplets on the basis of the conditions inside the nozzle. Thus providing the necessary information to calculate the spray formation and the secondary break-up in the surrounding gas. The coupling model divides the nozzle exit into a definite number of patches. Thereafter, liquid momentum and density from each patch are used to initialize the primary droplets. The model has been implemented in OpenFOAM and validation has been performed using high-speed shadowgraphic imaging. The simulated spray structure, spray tip penetration and spray cone angle show a good agreement with the experimental results.

In conclusion, the understanding of spray injection of cylinder lubrication oil is increased. The knowledge of cavitation-induced jet break-up in viscous pressure systems is also expanded. Factors affecting cavitation inside spray nozzles are mapped in order to enhance or oppress the degree of atomisation of viscous liquids. Finally, a number of tools, CFD models, and knowledge have been implemented at Hans Jensen Lubricators for further development of new products as well as for improvement of the existing ones.

Resumé

Cylindersmøring er en vigtig komponent i store totakts-marine-dieselmotorer. Smøreolien danner en tynd oliefilm mellem cylinderforingen og stempelringene, og således styrer den det mekaniske friktionstab og slid af kontaktfladerne. Smøreolien injiceres som en spray i motorens skylleluft, og derved opnås en jævn fordeling af olien øverst på cylinderen, hvor behovet for smøring er størst. I de seneste årtier har der været et stigende fokus på at optimere smøreolieforbruget for at reducere driftsomkostningerne på marine- dieselmotorer. Undersøgelserne er i dag baseret på en eksperimentel trial and error fremgangsmåde. Numeriske undersøgelser af injektionsprocessen er ikke tidligere blevet udført for at skabe en forståelse for den komplekse proces. Denne PhD- afhandling vil skabe et fundament og udgangspunkt for de numeriske undersøgelser, ved at behandle de emner, som påvirker strømmen af cylindersmøreolien igennem injektoren og dannelsen af den efterfølgende spray.

En computational fluid dynamics (CFD) model er udviklet i open-source CFD-programmet OpenFOAM. Modelleringsfremgangsmåden er opdelt i to trin. Først, simuleres strømningen og kavitationen inde i injektionsdysen ved hjælp af en flerfase- modelleringmetode. Derefter, simuleres spraydannelsen i et koblet Eulerian-Lagrangian domæne med en Kelvin-Helmholtz og Rayleigh-Taylor (KHRT) dråbeopbrydningsmodel. De to simuleringstrin er forbundet ved hjælp af en koblingsmodel, som omsætter strømmen inde i dysen til de første diskrete dråber ved dysens udgang. Derved etableres randbetingelserne for spraydannelsen. Eksperimentel validering er blevet udført ved hjælp af baggrundsbelyste højhastighedsoptagelser, hvorved det er muligt at visualisere både strømningsforholdene i injektoren og den efterfølgende spray.

Det numeriske og eksperimentelle studie viser, at kavitation inde i injektorens dysevolumen har en afgørende rolle for spraydannelsen, hvad angår øget forstøvning. Kavitation er dannelsen af damphulrum inde i væsken skabt af fordampning, som opstår, når det lokale tryk i væsken er lavere

end damptrykket. Udviklingen af disse dampkaviteter fører til forstyrrelser i strømningen, som påvirker sprayet.

To typer af kavitation er identificeret i dysevolumenet: kant-induceret kavitation og strengkavitation. Kant-induceret kavitation skabes af en pludselig geometrisk ændring f.eks. skarpe hjørner, mens strengkavitation skyldes ikke-symmetriske strømningsveje inde i dysen, der fører til en hvirvlende væskestrøm. Den hvirvlende væske skaber kavitationsstrenge i dens hvirvelcenter. Når disse kavitationsstrenge strækker sig til udgangen af dysen, forstærkes graden af forstøvning betydeligt. Hvorimod, når kavitationen kollapser i dysevolumenet, er den viskøse væske i stand til at stabilisere den stokastiske opførsel.

Viden opnået ved undersøgelse af strømningsforholdene inde i dysen anvendes til at udvikle en kavitations-induceret koblingsmodel for viskøse væsker. Modellen beskriver randbetingelserne for de diskrete Lagrangian-dråber på baggrund af tilstanden i dysen. Derved opnås de nødvendige informationer til at beregne spraydannelsen og dråbeopbruddet i den omgivne gas. Koblingsmodellen deler dysens udgang i et bestemt antal arealer. Derefter anvendes væskens momentum og densitet fra hvert areal til initialisering af de primære dråber. Modellen er implementeret i OpenFOAM, og validering er blevet udført ved hjælp af højhastighedsoptagelser. Der er en god overensstemmelse mellem de eksperimentelle resultater og den simulerede spraystruktur, spraypenetrering, spraykonusvinkel.

PhD afhandlingen har ført til, at forståelsen for injektion af cylindersmøreolie er øget. Viden omkring kavitation-induceret opbrud i viskøse tryksystemer er udvidet. For at forøge eller undertrykke graden af forstøvning af viskøse væsker, er faktorer, som påvirker kavitationen i injektoren, bestemt. Endelig er en række værktøjer, CFD-modeller og viden implementeret hos Hans Jensen Lubricators til videreudvikling af nye produkter samt til forbedring af de eksisterende.

Contents

Nomenclature

The important and non-trivial abbreviations and nomenclature used in this thesis are presented in the following. Conventional calculus and linear algebra notations, as well as the metric system are used throughout the thesis.

Abbreviations

BDC	Bottom Dead Center
BN	Base Number
CFD	Computational Fluid Dynamics
CLO	Cylinder Lubrication Oil
FPS	Frames Per Second
HFO	Heavy Fuel Oil
HEM	Homogeneous Equlibrium Mixture
HJL	Hans Jensen Lubricators
KHRT	Kelvin-Helmholtz and Rayleigh-Taylor
OpenFoam	Open Field Operation and Manipulation
PDF	Probability Distribution Function
PMMA	Poly(Methyl MethAcrylate)

RANS	Reynolds-Averaged Navier-Stokes
SIP	Swirl Injection Principle
TDC	Top Dead Centre
VOF	Volume Of Fluid

Greek Symbols

α	Phase fraction	[-]
ΔH_v	Molar enthalpy of vaporization	[kJ/mol]
ϵ	Dissipation of turbulent kinetic energy	[J/kg ·s]
μ	Viscosity	[Pa·s]
Λ	Wavelength	[m]
Ω	Growth rate	[-]
ρ	Density	[kg/m^3]
τ	Break-up time	[s]
σ	Surface Tension	[N/m]
ϕ	Spray cone angle	[$\circ$]
ϕ	Flow property	[-]
Φ	Dissipation function	[-]

Latin Symbols

a	Acceleration	$[m/s^2]$
A	Area	$[m^2]$
A_n	Nozzle area	$[m^2]$
B	Impact parameter	[-]
B_1	Constant in Kelvin-Helmholtz break-up model	[-]
C_3	Constant in Rayleigh-Taylor break-up model	[-]
C_d	Discharge coefficient	[-]
C_D	Droplet drag coefficient	[-]
C_v	Specific heat capacity	[J/K]
d_p	Particle diameter	[m]
D_n	Nozzle diameter	[m]
i	Internal Energy	[J]
k	Thermal conductivity	[W/(m·K)]
k	Turbulent kinetic energy	[-]
K	Cavitation number	[-]
L	Length	[m]
L_b	Break-up length	[m]
L_n	Nozzle length	[m]
m	Mass	[kg]
$\dot{m}$	Mass flow rate	[kg/s]
n	Refractive index	[-]

r	Radius	[m]
p_{col}	Probability of droplet collision	[-]
P	Pressure	[Pa]
P_{v}	Vapor pressure	[Pa]
R	Ideal gas constant	[J/(mol·K)]
R	Mass transfer rate	[-]
Re	Reynolds number	[-]
S	Spray tip penetration	[m]
S	Source term	[-]
t	Time	[s]
T	Temperature	[°C]
T_{b}	Boiling point	[°C]
T_{p}	Pour point	[°C]
Ta	Taylor number	[-]
u, v, w	Velocity components	[m/s]
We	Weber number	[-]
x, y, z	Coordinates	[-]
x_{p}	Droplet position	[-]
y_{p}	Droplet velocity	[m/s]
$\dot{y}_{\mathrm{p}}$	Droplet deformation	[m]
Z	Ohnesorge number	[-]

Part I

Introduction

1 Project Background

This chapter introduces the industrial challenges which have initiated the work carried out in this research. The primary terms used through the thesis are defined and the basic notation is presented. Finally, an overview of this thesis is given.

1.1 Motivation for cylinder lubrication research

Throughout the last century, maritime transport has evolved to become essential to the world economy. Increasing industrialization and the liberalization of national economies have driven free trade and a growing demand for consumer products. Today, more than 90% of the global trade is carried by sea, as this is the most cost-effective way to transport large quantities of raw materials and finished goods (Johansson et al., 2012; Wan, 2016). The majority of the merchant vessels utilize low-speed two-stroke diesel engines for the main propulsion power. There are three primary reasons for its dominance; superiority in efficiency, burning cheap heavy fuel oil (HFO), and direct coupling to the propeller without the need of a gearbox. The basic layout of two-stroke engines is illustrated in Figure 1.1.

Two-stroke marine engines have been exposed to a huge development since the first engine was introduced in M/S Selandia (1912). Since then, major improvements in engine performance have been achieved by increased thermal efficiency in order to reduce the size, and also increase power and reliability. For example, the introduction of the turbocharger in the 1950s had a significant impact (Woodyard, 2009). Today, thermal efficiency is approaching the optimal value, and therefore the focus has changed towards reducing operational costs in order to lower the costs of shipping goods (Toft and Thomsen, 2007; Vølund, 2003; Woodyard, 2009). From an economic point of view, cylinder lubrication oil is a significant part of a vessel's operational cost. Figure 1.2 shows an overview of the costs, excluding fuel consumption, for a typical engine.

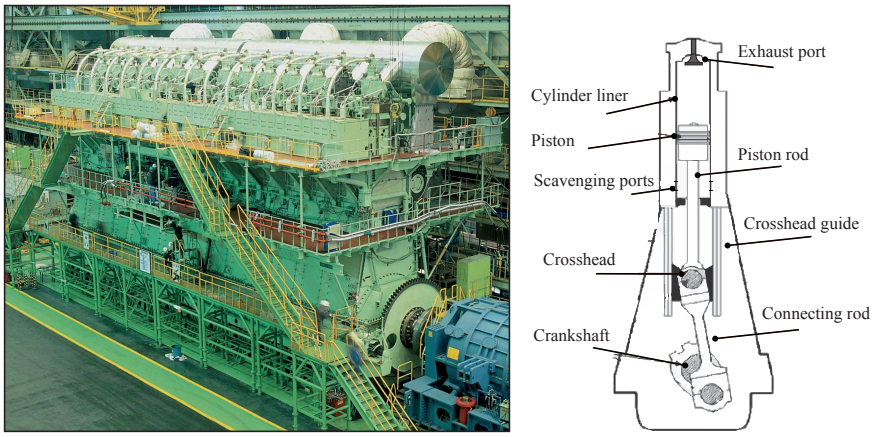

Figure 1.1: Photography of a two-stroke marine diesel engine and an illustration its cross-section.

Cylinder lubrication oil is essential for the performance of two-stroke diesel engines. It is the key component controlling the mechanical friction loss and wear on the cylinder liner and piston rings, by providing a thin oil film between the sliding interfaces, as shown in Figure 1.3. The tribology of cylinder liners and piston rings of marine diesel engines has been studied by researchers for many decades (Olander et al., 2013). The reasons are:

- Friction losses that occur at liner/ring interface lead to loss in propulsion power. Research has shown that this interface contributes about 20% of the engine's total mechanical frictional loss (Guo et al., 2013; Mohamad et al., 2015; Wolff, 2014).
- Wear near the top-dead-center (TDC) is often the limiting factor for the lifetime of engines (Jensen, 2002). High wear rates are caused by abrasive and adhesive wear, which is highly influenced by the operating conditions of the engine (Winkler, 2010; Wu et al., 2000).
- Heavy fuel oils (HFO) are of fairly low quality and generally have a high sulfur content (2-5%). The combustion of HFO leads to the formation of sulfuric acids (Olander et al., 2013; Ronnedal and Yamamoto, 2013). Sulfuric acids are damaging when they condensate on the cylinder liner, since this leads to corrosive wear (Schramm et al., 1994; Wu et al., 2000). These harmful compounds are neutralized by a large extent of reactive additives in the cylinder lubrication oil (described Appendix A).
- Provide a gas seal between the cylinder liner and the piston rings. Gas leakage leads to reduced compression pressure as well as power loss (Sherrington, 2011).

Increasing the dosage of lubrication oil does not mean less frictional losses and wear. It is as damaging as low oil dosage, as well as an environmental problem due to engine smoke formation and oil sludge production, which is naturally increased with the lubrication oil consumption (Jensen, 2002).

In the light of the abovementioned considerations, it is obvious that the right amount of lubrication oil is an economic and environmental advantage for the ship owner. However, achieving efficient cylinder lubrication of two-stroke marine diesel engines is very complicated. Harsh environments, reciprocating sliding, and fluctuations of loads cause consumption and deterioration of lubrication oil (Mohamad et al., 2015).

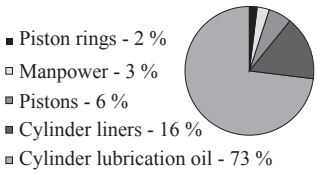

Figure 1.2: Typical cylinder cost distribution on MAN K90MC-engines (Jensen, 2002).

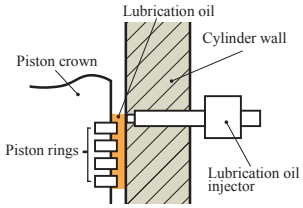

Figure 1.3: Illustration of the thin lubrication oil between the cylinder and piston rings.

1.2 Modern cylinder lubrication systems

Lubrication of cylinder liners has traditionally been provided by a number of low-pressure non-return valves, as shown in Figures 1.3 and 1.4. These valves are arranged circumferentially at either one or two levels. Each cylinder can be fitted with 4 to 16 valves, depending on the cylinder stroke and bore size. The lubrication oil is supplied by a lubricator, which controls the timing and dosage on the basis of the engine's operating conditions e.g. speed and load.

The disadvantage of non-return valves is that the vertical distribution of the oil is provided by the piston rings (Eriksen, 2003). This results in a tendency to over-lubricate lower regions in order to get the oil at the top of the cylinder liner, where the need of lubrication is highest.

An alternative and relatively new lubrication method, compared to traditional lubrication, is commercially called Swirl Injection Principle (SIP). It is a patented technology from Hans Jensen Lubricators, henceforth referred to as HJ SIP. It is based on the injection of a spray of lubrication oil into the scavenging air swirl inside the cylinder. This provides a more efficient coverage of the top of the cylinder.

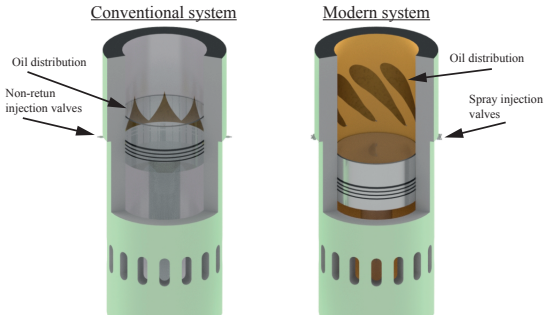

Figure 1.4: Illustration of a conventional and a Hans Jensen SIP lubrication system.

Figure 1.5 shows the process cycle of a typical two-stroke engine and the injection of lubrication oil using HJ SIP. The dosing takes place at the upward movement of the piston and before the piston top reaches the injectors. During the upward movement of the piston, the scavenging air in the two-stroke engine is subjected to a powerful rotation to exchange the combustion gases with fresh air. Thus, the gas follows a helical path or a swirl on its way from the scavenging air ports to the exhaust valve (Ingvorsen et al., 2013; Sigurdsson et al., 2014). An oil drop in this swirl will due to the centrifugal force be forced against the cylinder liner. As shown in Figure 1.6, the directions of the injection nozzles are arranged in such way that the interaction between the individual oil droplets and the gas flow ensures that the oil droplets hit the cylinder liner before it is caught by the piston top.

Practical studies on two-stroke engines have shown that the SIP lubrication principle is more efficient, meaning less oil is needed to lubricate, compared to traditional systems (Jensen, 2002).

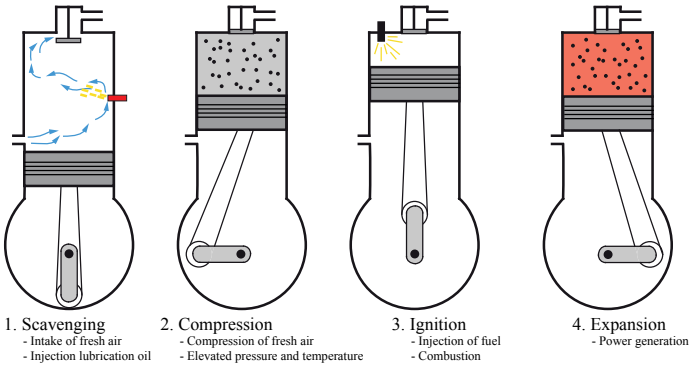

Figure 1.5: Engine cycle for a typical two-stroke marine engine with uniflow scavenging. Injection of cylinder lubrication oil with the SIP principle is performed under the engine scavenging.

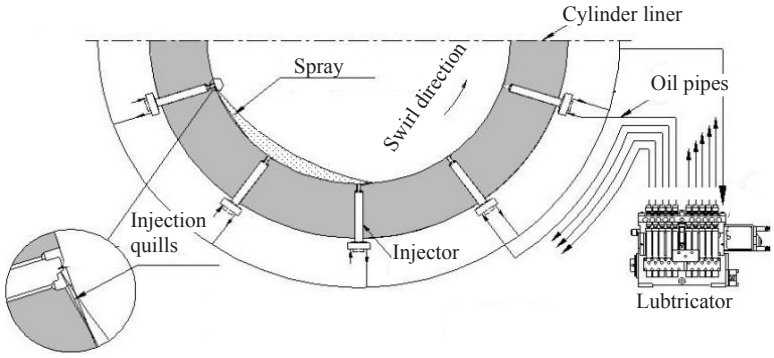

Figure 1.6: Overview of a lubrication system with spray injection valves and lubrication pump from Hans Jensen Lubricators.

1.3 Challenges of today

Cylinder lubrication systems have been undergoing a significant evolution over the last decade. A lot of work has been put into developing alternative lubrication strategies and lubrication oil formulations by the engine manufacturers and the oil companies, respectively. Figure 1.7 shows the development of engine manufacturers' recommended minimum dosage for any lubricating oil for hydrodynamic lubrication purposes. The dosage corresponds to the amount oil (g) needed per engine output (kWh).

Today, the recommended minimum is 0.60 g/kWh. However, practical studies by Jensen et al. (2016) have shown that the minimum oil dosage can be reduced to a new minimum using the HJ SIP lubrication system. Such low lubrication oil dosage has not previously been recommended and used

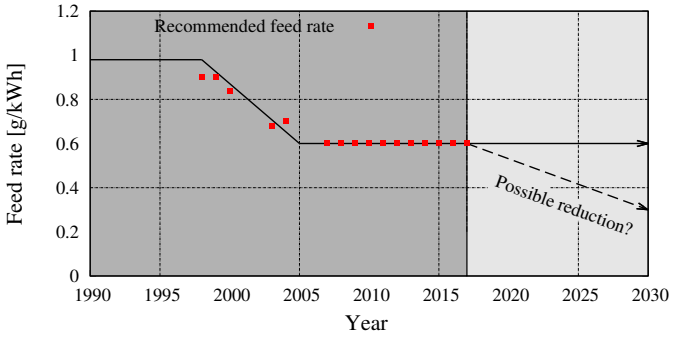

Figure 1.7: Development history of engine designers' recommended minimum feed rate.

in practice. The studies showed that the recommended minimum could be reduced to a feed rate of 0.30 g/kWh, and at the same time acceptable wear rates could be maintained.

Accepting a new minimum dosage is very difficult in the maritime industry. This is because the industry is conservative in terms of accepting new technologies. The practice of cylinder lubrication is based on a foundation of a large knowledge base, which dates back regarding methods process design. Much of this knowledge was, and is still today, passed on as experience (Weisser et al., 2004). This means that many decisions made during design phase are based on try-outs and non-optimal design methodologies, which have become acceptable and thus very hard to change. As most of the experiments were developed before the availability of computers and advanced measurement equipment, they can be considered to be somewhat crude compared to the numerical and experimental studies carried out today.

1.4 Scope of the PhD thesis

The scope of this PhD thesis is to create a scientific understanding of the spray lubrication system from Hans Jensen Lubricators A/S. This is due to the practice of cylinder lubrication is complex and still poorly understood. Knowledge has been based on real-scale tests and experience. Thus, establishing an understanding of the process will be beneficial for the further development of new products as well as the improvement of the existing ones at Hans Jensen Lubricators A/S. This leads to the following research question:

What is decisive in the spray lubrication process in order to achieve efficient lubrication of two-stroke diesel engines?

The term *efficient lubrication* relates to the task of operating the engine using low lubrication oil dosage, and at the same time having low frictional losses and wear. Between the first oil droplet leaving the spray injector to the oil film on the cylinder wall, there are several steps in the spray lubrication process that have to be covered in order to determine the lubrication efficiency.

Due to the time frame of this PhD project, the primary focus has been on the scientific problems related to spray atomization, droplet break-up and droplet flight in the scavenging air. Considerable attention has been given to computational fluid dynamics (CFD), in order to increase the understanding of the highly transient and physically coupled spray injection process. CFD

has already been utilized with great success in the industry and to simulate spray injection processes (Ghadimi et al., 2016; Schmidt and Corradini, 2001; Versteeg and Malalasekera, 2007).

1.5 Project methodology

The methodology used in this thesis is illustrated in Figure 1.8. A literature study provides an understanding of spray atomization and break-up liquid jets. From the knowledge obtained from the literature study, hypotheses investigating potential improvement with regard to the studied spray lubrication system are formulated. Numerical and experimental investigations into these hypotheses are performed and followed by analysis and interpretation of the observations made.

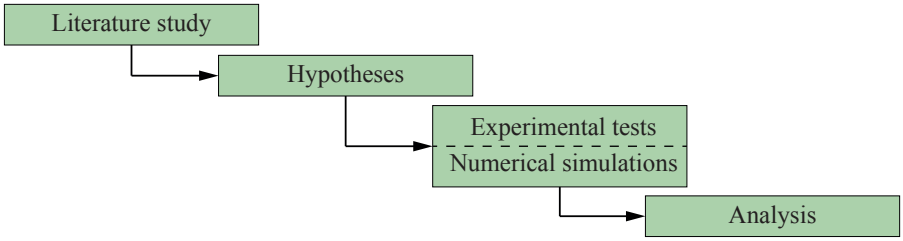

Figure 1.8: The methodology used in this thesis.

1.6 Thesis overview

This PhD thesis has been written in the format of collection of publications. Therefore, the main contributions and findings are included in the publications. The thesis is structured into ten chapters and seven parts, which provide the necessary background and a summary of the main findings to help the reader in understanding how the publications are related. The outline of the thesis is shown in the following pages.

Part I: Introduction

Chapter 1: Project background
This chapter introduces the industrial challenges which have initiated this research. The primary terms used through the thesis are defined and the basic notation is presented.

Part II: Literature Review

Chapter 2: Theory of sprays
In this chapter, the generally accepted theories of sprays are presented. This includes an introduction to the spray formation process and the used spray terminology, which might be new to the reader.

Chapter 3: State-of-the-art modelling
In this chapter, the state-of-the-art modelling of spray formation is presented.

Part III: Materials and Methods

Chapter 4: Presentation of hypothesis
Based on the knowledge and conclusions presented in Part II, four hypotheses are formed to constitute the basis of the publications presented in Part IV.

Chapter 5: Materials
This chapter introduces the cylinder lubrication oils and their properties, which are used for the experimental studies and numerical simulations, is given.

Chapter 6: Experimental setup
In this chapter, the experimental methods utilized to investigate the hypotheses are described. Initially, description of the experimental test setup is given and different aspects of the design are discussed in detail.

Chapter 7: Numerical setup
This chapter contains an overview of the numerical setup used to simulate the nozzle flow through the injector and the spray formation. Furthermore, an short introduction the CFD software package OpenFOAM version 3.0, which is utilized to perform the simulations.

Part IV: Results and Discussion

Paper A: **Rheological behavior of lubrication oils used in two-stroke marine engines**
This study presents useful information about the rheological behavior of lubrication oils, including how the oil properties are affected by shear rate, temperature and level of alkalinity.

Paper B: **CFD analysis of cavitation structures in viscous liquid spray systems**
This study shows that cavitation plays an important role in terms of droplet breakup and atomization. The developed simulation model is able to predict similar behavior as observed experimentally.

Paper C: **Coupling method for internal nozzle flow and the subsequent spray for viscous liquids**
In this study, a new model for cavitation-induced primary breakup is proposed. The model is able to map the influence of cavitating nozzle flow on spray formation.

Chapter 8: **Extended Summary**
This chapter sums up the findings and ties together the three papers. Furthermore, additional results that supports the observations presented in the papers are discussed.

Part V: Concluding Remarks

Chapter 9: **Conclusions**
The chapter concludes the work presented in this thesis based on the industrial and scientific objectives stated in the introduction.

Chapter 10: **Future work**
Future work involving both experimental work and numerical work are presented in this chapter.

Part VI: Appendices

Appendix A: **Determination of vapour pressure**
Vapour pressure of the cylinder lubrication oil is estimated in this Appendix using the Clausius-Clapeyron equation.

Appendix B: **Cold corrosion**
This Appendix describes the formation of cold corrosion inside two-stroke engines, and how it is prohibited by the additives in the cylinder lubrication oil.

Part VI: Additional publications

Paper D: **Numerical study of cavitation of high-viscous liquid spray systems**
In this study, a numerical simulation model of an injection nozzle is developed to predict cavitation of viscous liquids.

Paper E: **Model for cavitation-induced primary break-up of viscous liquid sprays**
In this paper, a model for cavitation-induced primary break-up is proposed, which is able to map the influence of cavitating nozzle flow on spray formation.

Paper F: **Consequences of oil film degradation**
In this review paper, the stresses leading to the degradation of cylinder oil film inside two-stroke engines as well as its consequences are described.

Patent A: **Method and system for dosing lubricating oil into cylinders, preferably in two-stroke diesel engines, and use of such method and system**
This patent describes a method for controlling the viscosity of cylinder lubrication oils in order to control the spray formation and break-up liquid jets.

Patent B: **Method for lubricating large two-stroke engines using controlled cavitation in the injector nozzle**
This patent describes a method for controlling the degree of cavitation inside injectors in order to regulate the degree of jet break-up.

Part II

Literature Review

2 Theory of Sprays

In this chapter, the generally accepted theories of sprays are presented, while the State-of-the-art is presented in Chapter 3. This includes an introduction to the spray formation and the used spray terminology, which might be new to the reader.

2.1 Introduction to sprays

A schematic layout of the spray injection process is shown in Figure 2.1. Immediately after the liquid jet leaves the nozzle hole, the jet starts to break up into a conical spray. The first break-up of the liquid is called primary break-up, and results in large ligaments and droplets that form the dense spray near the nozzle. The primary break-up is governed by the flow conditions of the liquid inside the spray nozzle, where, for example, turbulence and cavitation have an important role. The primary break-up is treated in Section 2.2.

After the primary break-up, the droplets are exposed to secondary break-up, which is caused by aerodynamic forces acting on the droplets. These forces are caused by the difference in velocity between droplets and surrounding gas. The aerodynamic forces decelerate the droplets. At the spray

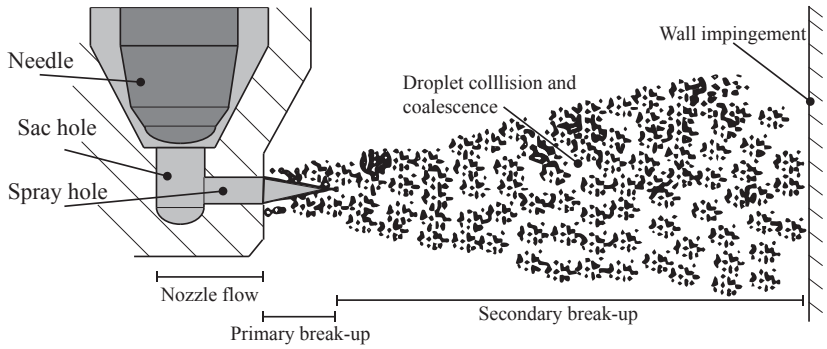

Figure 2.1: Schematic illustration of the four spray regimes.

tip, the drag force is highest, which means that the droplets at the spray tip are continuously replaced and droplets with low kinetic energy are pushed aside to the outer spray region. Thus, a conical spray is formed that is diluted downstream to the nozzle due to the entrainment of air. Droplet collisions may occur in a dense spray, which changes the droplet velocity and size. Collisions can lead to the break-up of droplets into smaller ones or coalescence to form larger drops. A detailed description of the secondary break-up is found in Section 2.3.

2.1.1 Spray characterization

Figure 2.2 shows the used parameters to characterize a spray under certain conditions. The most important are:

- Spray penetration (S) is defined as the distance between the nozzle and the leading spray boundary.
- Break-up length (L_b) is the distance from the nozzle to the end of the unbroken liquid phase.
- Spray cone angle (ϕ) is the angle between the two tangent lines of the side edge of the spray. In some cases, it is necessary to distinguish between the near and far spray cone angle.
- Droplet diameter (d_p) is the diameter of the droplet of interest.

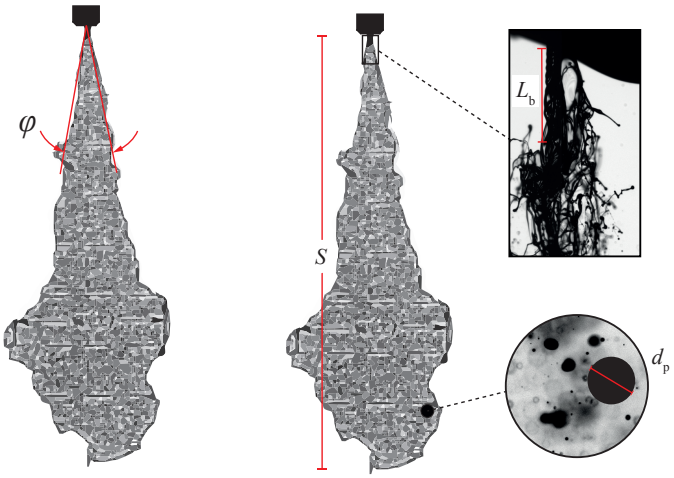

Figure 2.2: The spray definitions used in this thesis.

2.1.2 Spray regimes

When liquid is injected into the surrounding gas, the aerodynamic force, inertia force, viscosity and surface tension will act on the liquid and force it into separate liquid blocks, ligaments, or droplets (Baumgarten, 2006; Jing, 2005). The different break-up mechanisms are often characterized by the size of the droplet produced and the break-up length L_b. Figure 2.3 shows the four regimes into which sprays are generally classified (Dumouchel, 2008; Reitz and Bracco, 1982):

- **Rayleigh regime (Figure 2.3a):** Break-up occurs due to the growth of axisymmetric oscillations of the jet, which is initiated by liquid inertia and surface tension forces. The size of the droplets is greater than the nozzle hole diameter.
- **First wind-induced regime (Figure 2.3b):** In this regime, the relevant forces of the Rayleigh regime are amplified by aerodynamic forces. Break-up occurs many nozzle diameters downstream of the nozzle, and the droplet size is the size or slightly smaller than the diameter of the nozzle.
- **Second wind-induced regime (Figure 2.3c):** Break-up occurs due to the unstable growth of surface waves on the jet, which are initiated by jet turbulence and amplified by aerodynamic forces due to the relative velocity between gas and jet. The diameter of the resulting droplets is smaller than the nozzle diameter.
- **Atomization regime (Figure 2.3d):** Break-up in the atomization regime is more complex than the other regimes, as it strongly depends on the flow conditions inside the nozzle hole, which are usually unknown and chaotic. A spray develops immediately after the jet leaves the nozzle, and the resulting droplets are much smaller than the nozzle diameter.

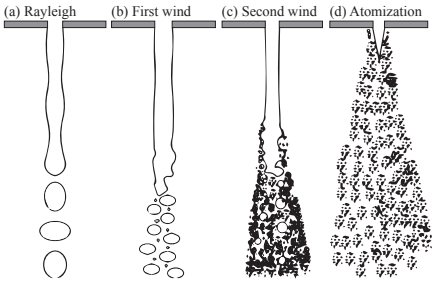

Figure 2.3: Schematic illustration of the four spray regimes classified by Ohnesorge.

Experimental studies by Ohnesorge have shown that the break-up regimes can be quantified using the two dimensionless numbers: Reynolds number Re and Weber number We, shown in equations 2.1 and 2.2 (Dumouchel, 2008; Lefebvre, 1989). The Reynolds number expresses the ratio of inertia to viscosity, whereas the Weber number expresses the ratio of inertia to surface tension. The inertia forces promote disintegration, due to the formation of unstable growth of surface waves on the liquid jet and the droplet surface. The surface tension force, on the other hand, tries to keep the droplet spherical and counteracts the deformation.

$$Re = \frac{u\rho_{\mathrm{l}} D_{\mathrm{n}}}{\mu_{\mathrm{l}}} \tag{2.1}$$

$$We_l = \frac{u^2\rho_{\mathrm{l}} D_{\mathrm{n}}}{\sigma} \tag{2.2}$$

where the u is the jet velocity, ρ_{l} is the density of the liquid, μ_{l} is the dynamic viscosity of the liquid, σ is the surface tension at the liquid-gas interface, and D_{n} is the nozzle hole diameter. The Ohnesorge number Z relates the viscous and surface tension forces:

$$Z = \frac{\sqrt{We_{\mathrm{l}}}}{Re} = \frac{\mu_{\mathrm{l}}}{\sqrt{\sigma\rho_{\mathrm{l}} D_{\mathrm{n}}}} \tag{2.3}$$

The different break-up regimes can thus be quantified using the Ohnesorge diagram shown in Figure 2.4. The diagram expresses the relationship between the viscous and surface tension forces Z and the inertia forces Re. However, only including the liquid properties in the description of the regimes is not sufficient, because atomization can be enhanced by increasing the gas density as well as turbulent and chaotic disturbances introduced to the flow inside the nozzle. This will be discussed in Section 2.2.

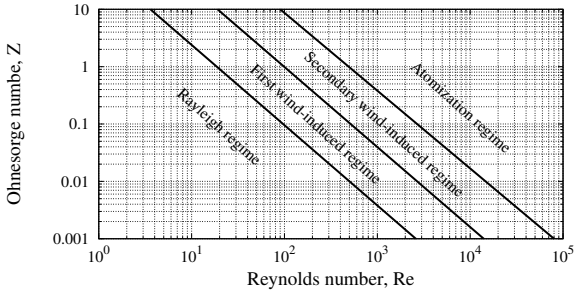

Figure 2.4: The Ohnesorge diagram with the different spray break-up regimes. This Figure is adapted from (Yarin et al., 2017).

2.2 Primary break-up

Primary break-up is the first disintegration of the liquid jet into large ligaments and droplets, resulting in a dense spray near the nozzle. The primary break-up is governed by different mechanisms due to the flow conditions of the liquid inside the spray nozzle (Dumouchel, 2008; Herrmann, 2011):

- **Aerodynamic break-up (Figure 2.5a)**: The surface of the exiting liquid jet is covered by small surface waves, which are amplified by the aerodynamic shear forces at the gas-liquid interface. When these surface waves become unstable, they separate from the liquid jet to form primary droplets.
- **Flow-induced break-up (Figure 2.5b)**: In the case of fully developed pipe flow inside the nozzle, the velocity profile changes when the flow exits the spray hole. The viscous forces inside the jet cause an acceleration of the outer jet region, due to the end of the wall boundary condition. This results in instabilities and in the break-up of the outer jet region.
- **Turbulence-induced break-up (Figure 2.5c)**: Turbulent velocity fluctuations generated inside the nozzle transfers to the exiting jet. Primary break-up occurs when the turbulent eddies in liquid are sufficient to overcome the surface tension.
- **Cavitation-induced break-up (Figure 2.5d)**: Vapor cavities created inside the nozzle introduces disturbances that enhance the break-up process. These disturbances are caused by the growth and collapse of vapor cavities. Cavitation occurs when the local pressure of the liquid drops below its vapor pressure, which may take place when liquid conformity to a rigid surface cannot be ensured.

Turbulence- and cavitation-induced primary break-up are considered to be the most influential primary break-up mechanisms. For this reason, these mechanisms are treated in detail in Sections 2.2.1 and 2.2.2, respectively.

Aerodynamic break-up is, on the other hand, considered to be the relevant mechanism for the secondary break-up. The growth of surface waves is a time-dependent process, which does not lead to the immediate break-up of the jet at the nozzle exit (Baumgarten, 2006). The secondary break-up due to aerodynamic forces is presented in Section 2.3

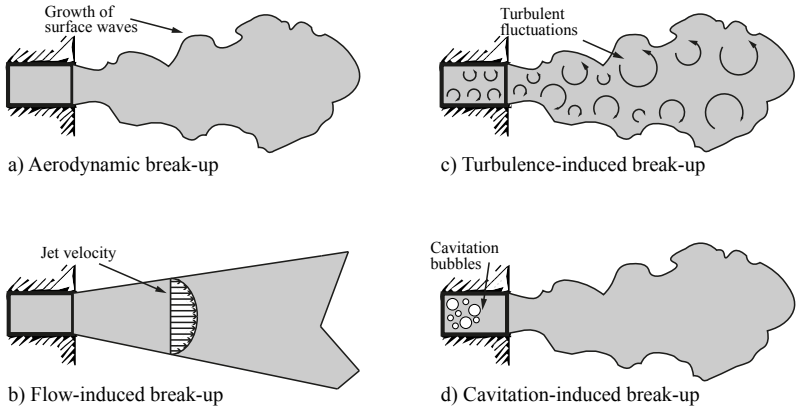

Figure 2.5: Overview of the possible primary break-up mechanisms.

2.2.1 Turbulence-induced break-up

Turbulence enhances the formation of surface waves on the liquid jet surface. The frequency and amplitude of the waves are dependent on the turbulent eddies generated in the flow inside the spray nozzle (Baumgarten, 2006; Lefebvre and Mcdonell, 2017). The surface waves are unstable and grow due to the aerodynamic interaction with the surrounding gas. When a critical amplitude is reached, the liquid wave breaks up into ligaments.

The liquid flow regimes can divided into the three flow regimes shown in Figure 2.6. These regimes can be identified by the the Reynolds number, which is shown in equation 2.1

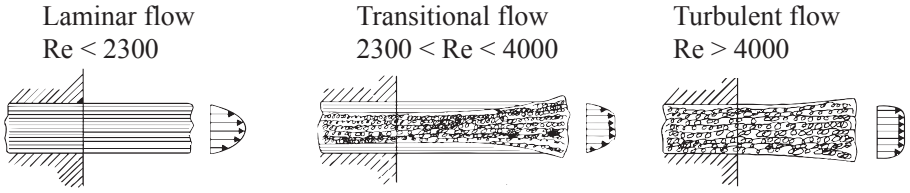

Figure 2.6: Illustration of laminar, transitional and turbulent flow regimes inside spray nozzles. Adapted from (Lefebvre and Mcdonell, 2017)

2.2.2 Cavitation-induced break-up

Cavitation is commonly known as the formation of vapor cavities inside a liquid due to evaporation, which takes place when the local pressure of the liquid drops below the vapor pressure P_v (Bergwerk, 1959; Franc and

Michel, 2006). The phenomena is known to occur in many hydrodynamical industrial applications such as valves, pumps, propellers and injection nozzles (Aleiferis et al., 2010; Hult et al., 2016; Tropea et al., 2007). In all these examples, cavitation is a result of a sudden change in the velocity due the change in flow direction, for example, changes in geometry. Figure 2.7 shows a schematic diagram of the phase change of water. The diagram shows that even though cavitation and boiling share the same phase change, the physical phenomenon is completely different. For boiling, the driving force is a barotropic change in temperature, while cavitation is caused by a isothermal change in pressure.

In spray injection systems, cavitation typically occurs at the nozzle entrance or in the region immediately adjacent to the vena contracta, as shown in Figure 2.8. The growth and collapse of the vapor cavities in this area, introduces large a number of disturbances, which in certain cases enhance the jet atomization (Dabiri et al., 2007). Figure 2.9 shows the four cavitation stages identified by researchers (Abderrezzak and Huang, 2016; He et al., 2016; Schmidt and Corradini, 2001; Sou et al., 2007):

- **No cavitation (Figure 2.9a)**: for short ($L_n/D_n = 0$) or smooth inlet nozzle orifice. The resulting spray is laminar in appearance.
- **Developing cavitation (Figure 2.9b)**: occurs due to the sharp-inlet nozzle orifice. It appears at the nozzle entrance and extends further downstream with increasing liquid velocity u_l. The degree of cavitation introduces instabilities from the growth and collapse of the cavitation bubbles, which affects the spray formation.
- **Supercavitation (Figure 2.9c)**: occurs when the cavitation extends almost until the nozzle hole aperture. The disintegration of the resulting spray is most violent in this case, which leads to the smallest ligaments and the maximum spray cone angle ϕ.

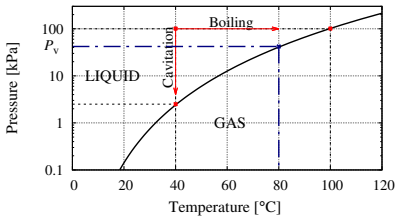

Figure 2.7: Phase diagram of water showing the difference between cavitation and boiling.

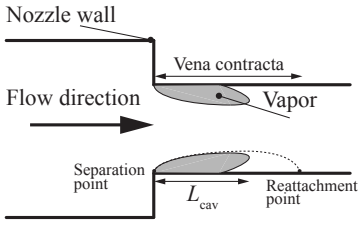

Figure 2.8: Cavitation at the nozzle entrance.

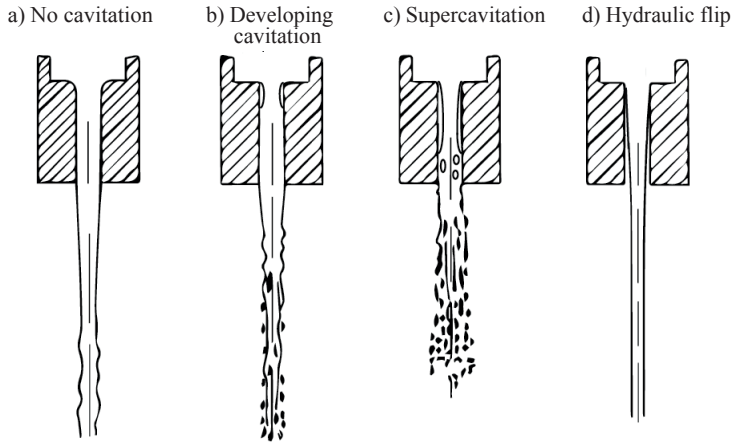

Figure 2.9: The four cavitation stages identified by researchers (Abderrezzak and Huang, 2016; He et al., 2016; Schmidt and Corradini, 2001; Sou et al., 2007).

- **Hydraulic flip (Figure 2.9d)**: occurs once the cavitation extends to the nozzle hole aperture, thus surrounding air outside the nozzle enters the recirculation region inside the nozzle hole. This results in the disappearance of cavitation, and the spray consists entirely of liquid and is laminar in appearance.

Investigating the mass flow rate at stationary conditions can give an indication of the appearance of cavitation. According to the Bernoulli's equation in equation 2.4, the mass flow increases as a function the pressure drop through the injection nozzle ΔP_{n}. However, a stagnation of the mass flow rate is reached when cavitational flow occurs, as shown by Payri et al. (2013) in Figure 2.10. This phenomenon is also known as choked flow (Wang and Su, 2009; Xue et al., 2017).

The choked flow is directly coupled to the discharge coefficient C_{d} in equation 2.4. This coefficient is defined as the relation between actual and theoretical mass flow rate. In non-cavitating conditions, C_{d} is a function of the Reynolds number. However, when the flow begins to cavitate, the discharge coefficient primarily depends on the degree of cavitation (Lefebvre and Mcdonell, 2017; Payri et al., 2004b).

$$\dot{m} = C_{\mathrm{d}} \cdot A_{\mathrm{n}} \cdot \sqrt{(2 \cdot \rho_{\mathrm{l}} \cdot \Delta P_{\mathrm{n}})} \tag{2.4}$$

where $\dot{m}$ is the actual mass flow rate, A_{n} is the area of the nozzle hole aperture, and ΔP_{n} is the pressure drop through the injector that is determined by the difference between injection pressure P_{i} and back pressure P_{b}.

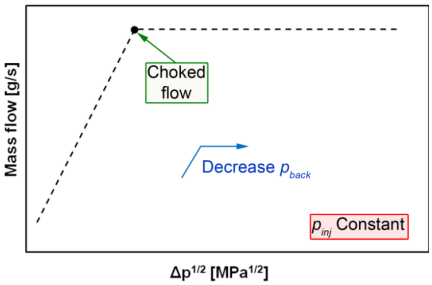

Figure 2.10: Mass flow rate through a cavitating nozzle with increasing back pressure p_b. Critical cavitation conditions are achieved at choked flow (Payri et al., 2013).

A dimensionless cavitation number K_c is used in order to characterize the potential of the flow to cavitate. There are several definitions of the cavitation number, but for this thesis the expression in equation 2.5 is found to be appropriate (Aleiferis et al., 2010; Brennen, 2005; Gavaises et al., 2015; Li, 2014; Payri et al., 2004a; Sou et al., 2007).

$$K_c = \frac{P_b - P_v}{\frac{1}{2}\rho_l \cdot u_l^2} \tag{2.5}$$

where P_b is the back pressure, P_v is the vapor pressure, and u_l is the mean velocity in the nozzle. The smaller the cavitation number, the higher tendency to cavitate (Payri et al., 2004a).

2.3 Secondary break-up

Secondary break-up is the disintegration of existing droplets into smaller ones due to the aerodynamic forces, which is a result of the relative velocity between the droplet and the surrounding gas (Baumgarten, 2006). The aerodynamic forces promote the growth of surface waves on the droplet surface or the whole droplet, which will lead to disintegration. The surface tension force counteracts the deformations from aerodynamic forces by keeping the droplet spherical. The ratio between aerodynamic and surface tension forces is expressed by the Weber number in equation 2.6.

$$We_g = \frac{\rho_g \cdot u_{rel}^2 \cdot d_p}{\sigma} \tag{2.6}$$

where ρ_g is the density of the gas, u_{rel} is the relative velocity between the droplet and surrounding gas, σ is the surface tension the liquid, and D_p is the droplet diameter. The smaller the droplet diameter, the greater the surface tension force and thus higher relative velocity is required for disintegration.

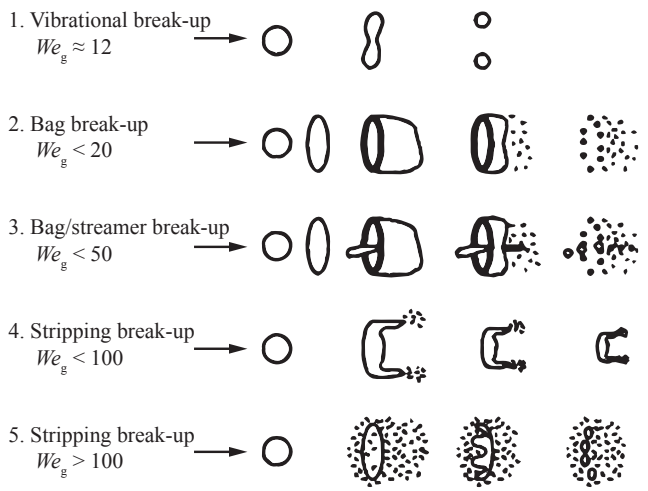

Figure 2.11: The different break-up modes and corresponding gas phase Weber number We_g. The modes are experimentally determined by (Wierzba, 1990)

Experimental investigations have shown that different break-up mechanisms exists, and that these depends on We_g. Figure 2.11 shows an illustration of the different break-up modes and the corresponding We_g that is experimentally determined. The different break-up modes are not further discussed in this thesis; however, a thorough description can be found in *Secondary droplet breakup in periodic aerodynamic flows* by Bruno (2000).

2.4 Droplet collision and coalescence

Collisions of liquid droplets can lead to several outcomes, as shown in Figure 2.12. The collisions are inelastic and result in an exchange of momentum, which influences the droplet break-up and spray formation (Pischke, 2014; Schmidt and Rutland, 2004). For example, coalescence of droplets opposes the droplet break-up, as larger droplets are created instead, whereas shattering collision enhances the droplet break-up. The outcome of the collision depends on the Weber number of the droplets and the impact parameter B, as shown Figure 2.12. The impact parameter B is defined by the angle of impact between the colliding droplets, where $B = 0$ is head-on collision and $B < 0$ is off-axis collision (Baumgarten, 2006).

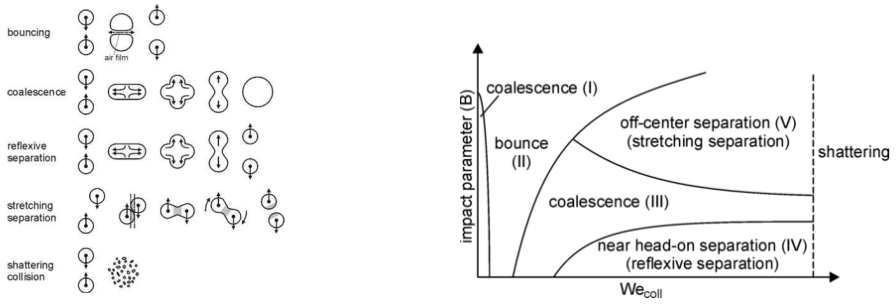

Figure 2.12: Droplet collision modes, which are influenced by the Weber number of the droplet We_{col} and impact parameter B (Baumgarten, 2006).

2.5 Discussion of spray lubrication systems

The theory presented in the previous sections is discussed in the following with respect to the studied spray lubrication system from Hans Jensen Lubricators A/S. The governing mechanisms influencing the spray formation are analyzed using the Ohnesorge diagram. As described in Section 2.1.2, the diagram is used to identify break-up regimes of liquid jets on the basis of inertial, viscous and surface tension forces.

Four different Ohnesorge diagrams are shown in Figure 2.13. In each of these diagrams, the effect of a single parameter in We and Re is studied by a parameter sweep. The sweep is shown in a range of relevance to the studied lubrication system. For example, the Ohnesorge diagram in Figure 2.13a shows that the liquid break-up changes from Rayleigh regime to Secondary wind-induced regime, when the jet velocity u_{l} increases from 10 to 100 m/s.

The jet velocity u_{l} of the commercial lubrication systems is approximately 40 m/s. According to the Ohnesorge diagram, this means that the Second wind-induced regime must be the governing break-up mechanism. It is also shown that fluid density ρ_{l} only has a minor impact, and that different fluid viscosities μ_{l} and surface tensions σ_{l} do not lead to the change in break-up regime. Concluding that the liquid break-up occurs within the Second wind-induced regime is, however, in contradiction to the reality, since atomization and instant break-up at the near-nozzle region are observed in experimental tests.

Cavitation inside the spray nozzle can explain why atomization is observed. As described in Section 2.2.2, the growth and collapse of cavitation vapor bubbles inside spray nozzles destabilizes and contributes to stochastic

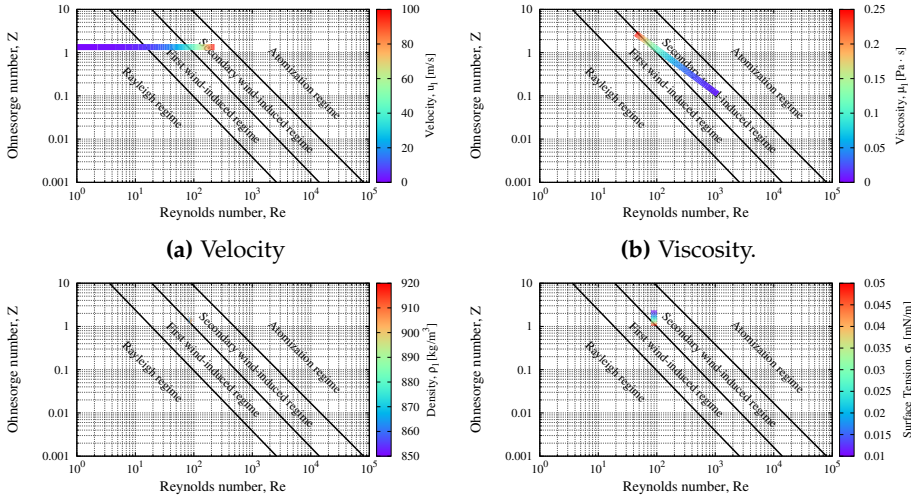

(a) Velocity

(b) Viscosity.

(c) Density.

(d) Surface tension.

Figure 2.13: Four Ohnesorge diagrams showing the effects of a single parameter by a parameter sweep. The selected parameter range is relevant for a commercial spray lubrication system from HJL. Reynolds and Weber number is calculated using equation 2.1 and 2.2 with the following properties, u_l = 40 m/s, $\mu_l = 0.12\,\mathrm{Pa \cdot s}$, $\sigma_l = 0.03\,\mathrm{N/m}$, $\rho_l = 900\mathrm{kg/m}^3$, and D_n = 0.3 mm

behavior of the liquid, which has shown to enhance the degree of atomization. In light of this analysis, it is believed that high injection pressure should be applied in order to obtain liquid atomization. However, cavitation inside the nozzle may influence the break-up, thus atomization can be achieved at lower injection pressures. This observation complies with the experimental studies performed by Tamaki and Shimizu (2002), which investigate the influence of cavitation on a pressure system with similar viscosity to the studied lubrication oil.

2.6 Summary

The spray terminology and generally accepted theories of sprays are presented in this chapter. There are several mechanisms that affect the break-up process. In particular, the flow conditions inside the spray injection nozzle have a great influence on the spray formation. Using the Ohnesorge diagram, it was shown that it is difficult to atomize viscous liquids using a pressure spray system unless high fluid pressure is applied.

The analysis conducted in Section 2.5 indicates that there is cavitation inside the spray nozzle. Cavitation is the formation of vapor cavities inside

the liquid due to evaporation, which takes place when the local pressure of the liquid drops below the vapor pressure. The subsequent collapse of these cavities introduces disturbances to the liquid stream that lead to a faster breakup of the exiting jet. Finally, turbulence does not influence the break-up, because the Reynolds number is $Re \ll 2300$.

3 State-of-the-art Modelling

The analysis performed in the end of Chapter 2 indicated that cavitation influences the liquid break-up and spray formation. There are two main methods for studying the cavitation inside spray nozzles: experimental visualisation methods based on high-speed imaging technology and numerical simulation methods based on Computational Fluid Dynamics (CFD). In this chapter, state-of-the-art modelling approaches are investigated with respect to modelling spray formation and cavitation-induced flow inside the injection nozzle.

3.1 Introduction to the modelling approach

In this thesis, spray formation is modelled using the combined Eulerian-Lagrangian method, which treats the surrounding gas as a continuum and the spray by a number of discrete points (Mostafa and Mongia, 1987; Subramaniam, 2013). The Navier stokes equations solve the gas phase transport over a fixed Eulerian computational grid, while the discrete points are tracked throughout the domain by solving Lagrangian equations of mass, momentum, and energy for each points.

The discrete points are assigned properties such as location, velocity, diameter and mass. These points only act as a marker and are of zero dimension, thus they do not occupy any space in the domain. The Eulerian-Lagrangian method therefore requires less computational time and power than an Eulerian-Eulerian treatment of the spray (Herrmann, 2011; Nordin, 2001). This is because an Eulerian description requires detailed resolution of the spray region in order to capture the break-up process. A detailed spray region is not desirable for this thesis, as a coarser resolution is preferred when modelling the spray injection process in large cylinder bores.

There are various studies where the Eulerian-Eulerian method is employed to simulate the spray formation. However, these will not be covered in this thesis. Examples of spray modelling studies using the Eulerian-Eulerian method can be found in (Demoulin et al., 2013; Ghiji et al., 2017; Salvador et al., 2016)

The spray formation is based on details from the internal nozzle flow, which is modelled using an Eulerian multiphase method, in order to capture cavitation phenomena. Thus, sub models are needed to describe the transition from the nozzle flow to the first discrete droplets. This coupling has been the focus of several authors, as the transition between the nozzle flow and spray formation is very complicated (Baumgarten, 2006; Mohan et al., 2014b; Soriano-Palao et al., 2014; Yu et al., 2016b). The majority of current coupling models employ simplified boundary conditions at the nozzle exit as an indirect coupling to the primary droplets. Such methods often dampen or lead to the loss of the nozzle flow characteristic, which is the drawback of the Eulerian-Lagrangian approach for simulating sprays.

Figure 3.1 shows an overview of the modelling approach used in this thesis, as well as the structure of the following sections in this chapter. Initially, the Eulerian-Lagrangian spray modelling approach is described throughout Sections 3.2 to 3.6, which includes state-of-the-art primary break-up models in Section 3.3. Finally, multiphase modelling of internal flow in Section 3.7.

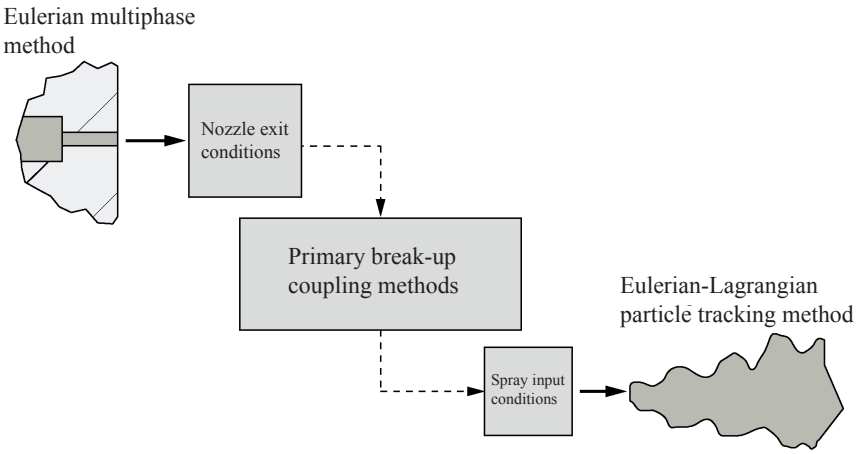

Figure 3.1: Overview of the numerical simulation approach used in the thesis.

3.2 Eulerian-Lagrangian spray modelling

An overview of the Eulerian-Lagrangian spray modelling method is shown in Figure 3.2. Both the Eulerian and Lagrangian phases consist of conservations equations and models that treat fundamental mechanisms. The coupling between the two phases is performed by source terms.

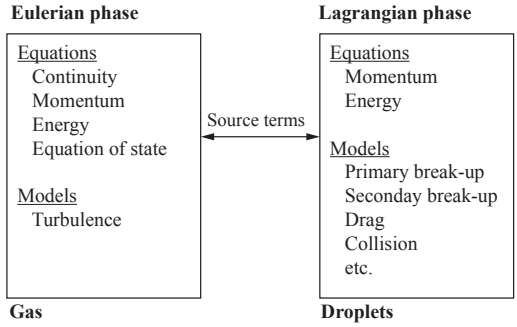

Figure 3.2: Overview of the Eulerian-Lagrangian method used for modelling the spray formation. This figure is adapted from (Gjesing et al., 2009).

The following description for modelling the Eulerian phase is based on the book *An Introduction to Computational Fluid Dynamics, The Finite Volume Method* by Versteeg and Malalasekera (2007).

3.2.1 Eulerian phase

According to Newton's second law, the fluid motion can be described when all forces are known. In fluid dynamics, it is difficult to determine the forces due to the viscous stress τ_{ij} that is applied on a element surface. The viscous stress force acts in three dimensions at each of the three different planes in a tree dimensional coordinate system. This leads to six viscous stress terms (due to symmetry) that need to be solved in order to describe the fluid motion.

The continuity equation (3.1) and the momentum equations (3.35 - 3.37) are used to describe the motion of a fluid element according to the viscous stress tensor and a sum of all other active forces. This leads to six unknown viscous stress variables in four equations and therefore it is not a mathematically closed system. Therefore, two equations of state (3.5) and an energy equation (3.6) are used to obtain a mathematically closed system with seven unknowns and seven equations.

Continuity equation:

$$\frac{\partial \rho}{\partial t} + \operatorname{div}(\rho \mathbf{u}) = 0 \tag{3.1}$$

Momentum equations:

$$\frac{\partial (\rho u)}{\partial t} + \operatorname{div}(\rho u \mathbf{u}) = -\frac{\partial p}{\partial x} + \operatorname{div}(\mu \operatorname{grad} u) + S_{Mx} \tag{3.2}$$

$$\frac{\partial (\rho v)}{\partial t} + \operatorname{div}(\rho v \mathbf{u}) = -\frac{\partial p}{\partial y} + \operatorname{div}(\mu \operatorname{grad} v) + S_{My} \tag{3.3}$$

$$\frac{\partial (\rho w)}{\partial t} + \operatorname{div}(\rho w \mathbf{u}) = -\frac{\partial p}{\delta z} + \operatorname{div}(\mu \operatorname{grad} w) + S_{Mz} \tag{3.4}$$

Equation of state:

$$p = p(\rho, T) \text{ and } i = i(\rho, T) \tag{3.5}$$

$$\text{e.g. perfect gas: } p = \rho \mathrm{R} T \text{ and } i = C_\mathrm{v} T$$

Internal energy equation:

$$\frac{\partial (\rho i)}{\partial t} + \operatorname{div}(\rho i \mathbf{u}) = -p \operatorname{div} \mathbf{u} + \operatorname{div}(k \operatorname{grad} T) + \mathbf{\Phi} + S_i \tag{3.6}$$

In equations 3.1 - 3.37, the variable ρ is the fluid density, p is pressure and μ is dynamic viscosity. The variables u, v and w define the flow velocity in the x, y and z-direction, and the velocity vector $\mathbf{u}$ contains all these velocity components. The variables S_M are the included source terms due to interaction with the liquid spray phase. In equation 3.5, i is the internal energy for the fluid element, R the specific gas constant, T the temperature and C_v the specific heat capacity at constant volume. In equation 3.6, k is the thermal conductivity of the fluid, $\mathbf{\Phi}$ is the dissipation function which describes the effects due to viscous stresses. The variable S_i is the source term due to heat transfer between the liquid phase and gas phase.

3.2.2 Reynolds-averaged Navier-Stokes equations

For Reynolds numbers above 2000, the gas phase becomes turbulent. Figure 3.3 shows the velocity fluctuations over time at a certain point. These random fluctuations are due to turbulent flow. In order to take turbulence into account, the Navier-Stokes equations are reformulated using the following averaging method.

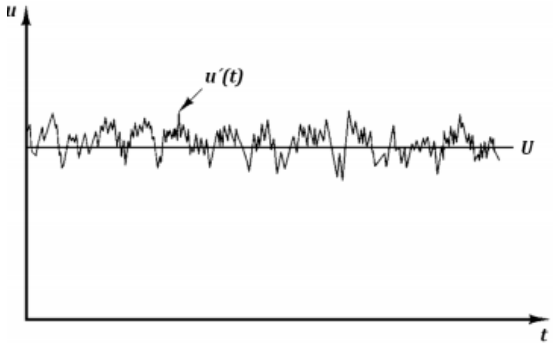

Figure 3.3: Measuring of velocity in an arbitrary point located in a turbulent flow (Versteeg and Malalasekera, 2007).

By introducing the flow property ϕ, which represents flow terms such as velocity, pressure, and temperature, the flow can be described in the overall definition shown in equation 3.7. This definition equals the decomposition of the velocity component (in Figure 3.3) into $\mathbf{u}(t) = \mathbf{U} + \mathbf{u}(t)$, where $\mathbf{U}$ is the mean velocity vector and $\mathbf{u}(t)$ is the fluctuating turbulent components. This is known as the Reynolds decomposition.

$$\phi = \Phi + \phi' \tag{3.7}$$

The Reynolds averaging is also known as time averaging of ϕ, which is described using equation 3.8.

$$\bar{\phi} = \bar{\Phi} + \bar{\phi}' \tag{3.8}$$

where

$$\bar{\Phi} = \Phi \tag{3.9}$$

$$\bar{\phi}' = \lim_{T\to\infty} \frac{1}{T} \int_0^T \phi'(t)dt = 0 \tag{3.10}$$

T equals averaging interval

The time averaged flow terms in equation 3.8 are substituted into equation 3.1 - 3.37. Thus, the Reynolds-averaged Navier-Stokes equations (RANS) and continuity equation for compressible flows are obtained.

Continuity equation:

$$\frac{\partial \bar{\rho}}{\partial t} + \text{div}\left(\bar{\rho}\tilde{\mathbf{U}}\right) = 0 \tag{3.11}$$

Momentum equation:

$$\frac{\partial\left(\bar{\rho}\tilde{U}\right)}{\partial t} + \text{div}\left(\bar{\rho}\tilde{U}\tilde{\mathbf{U}}\right) = -\frac{\partial \bar{P}}{\partial x} + \text{div}\left(\mu\,\text{grad}\,\tilde{U}\right) + \left[-\frac{\partial\overline{(\bar{\rho}u'^2)}}{\partial x} - \frac{\partial\overline{(\bar{\rho}u'v')}}{\partial y} - \frac{\partial\overline{(\bar{\rho}u'w')}}{\partial z}\right] + S_{Mx} \tag{3.12}$$

$$\frac{\partial\left(\bar{\rho}\tilde{V}\right)}{\partial t} + \text{div}\left(\bar{\rho}\tilde{V}\tilde{\mathbf{U}}\right) = -\frac{\partial \bar{P}}{\partial y} + \text{div}\left(\mu\,\text{grad}\,\tilde{V}\right) + \left[-\frac{\partial\overline{(\bar{\rho}u'v')}}{\partial x} - \frac{\partial\overline{(\bar{\rho}v'^2)}}{\partial y} - \frac{\partial\overline{(\bar{\rho}v'w')}}{\partial z}\right] + S_{My} \tag{3.13}$$

$$\frac{\partial\left(\bar{\rho}\tilde{W}\right)}{\partial t} + \text{div}\left(\bar{\rho}\tilde{W}\tilde{\mathbf{U}}\right) = -\frac{\partial \bar{P}}{\partial z} + \text{div}\left(\mu\,\text{grad}\,\tilde{W}\right) + \left[-\frac{\partial\overline{(\bar{\rho}u'w')}}{\partial x} - \frac{\partial\overline{(\bar{\rho}v'w')}}{\partial y} - \frac{\partial\overline{(\bar{\rho}w'^2)}}{\partial z}\right] + S_{Mz} \tag{3.14}$$

where $\bar{\rho}$ is the mean density for the fluid and $\bar{P}$ is the mean pressure. The variables $\tilde{U}$, $\tilde{V}$ and $\tilde{W}$ is the Favre-averaged velocity components in the x, y and z-direction and the velocity vector $\tilde{\mathbf{U}}$ contains all these velocity components. The terms located inside the brackets are the turbulent stresses, which are also known as the Reynolds stresses.

3.2.3 Turbulence modelling

In order to solve the RANS equations, the Reynolds stresses need to be modelled. Several turbulence models exists, such as Spalart-Allmaras, $k-\epsilon$, $k-\omega$, $SST\,k-\omega$, and the Reynolds stress model. These models contain different amount of equations in order to solve the turbulence in the flow. For example, the Spalart-Allmaras model uses one equation and the Reynolds stress model evaluates all Reynolds stresses independently with seven equations.

The $k-\epsilon$ model is a two-equation turbulence model, which is accurate in flows near smooth geometries. Due to its stability and fast convergence it is

used in many different industrial cases. As a fast convergence is desirable for testing and practical reasons, the $k-\epsilon$ turbulence model is used in this thesis.

The $k-\epsilon$ turbulence model consists of two transport equations, one for turbulent kinetic energy k, another for the dissipation of turbulent kinetic energy ϵ. These are shown in equation 3.15 and 3.16, respectively.

$$\frac{\partial(\rho k)}{\partial t} + \operatorname{div}(\rho k \mathbf{U}) = \operatorname{div}\left[\frac{\mu_\mathrm{t}}{\sigma_\mathrm{k}} \operatorname{grad} k\right] + 2\mu_\mathrm{t} E_{ij} \cdot E_{ij} - \rho\epsilon \tag{3.15}$$

$$\frac{\partial(\rho\epsilon)}{\partial t} + \operatorname{div}(\rho\epsilon \mathbf{U}) = \operatorname{div}\left[\frac{\mu_\mathrm{t}}{\sigma_\epsilon} \operatorname{grad} \epsilon\right] + C_{1\epsilon}\frac{\epsilon}{k} 2\mu_\mathrm{t} E_{ij} \cdot E_{ij} - C_2\rho\frac{\epsilon^2}{k} \tag{3.16}$$

where the E_{ij} tensor is the mean deformation rate of a fluid element and μ_t is the eddy viscosity expressed in equation 3.17.

$$\mu_\mathrm{t} = \rho C_\mu \frac{k^2}{\epsilon} \tag{3.17}$$

The five constants in equation 3.15 - 3.17 are set to default values (Versteeg and Malalasekera, 2007):

$$C_\mu = 0.09, \quad \sigma_k = 1.00, \quad \sigma_\epsilon = 1.30, \quad C_{1\epsilon} = 1.44, \quad C_{2\epsilon} = 1.92 \tag{3.18}$$

3.2.4 Lagrangian particle tracking

In the Lagrangian description, the spray is represented by a number of discrete droplets or particles. The motion of these droplets is solved by integrating the force balance (Subramaniam, 2013). The droplets are treated as points, but considered spherical with mass m_p and diameter D_p, in order to calculate droplet position $\boldsymbol{x}_\mathrm{p}$ and velocity $\boldsymbol{u}_\mathrm{p}$ using the following differential equations:

$$\frac{\partial \boldsymbol{x}_\mathrm{p}}{\partial t} = \boldsymbol{u}_\mathrm{p} \tag{3.19}$$

$$m_\mathrm{p}\frac{\partial \boldsymbol{u}_\mathrm{p}}{\partial t} = \sum F \tag{3.20}$$

In addition to droplet position $\boldsymbol{x}_\mathrm{p}$ and velocity $\boldsymbol{u}_\mathrm{p}$, there are a number of droplet parameters that have to be included i.e. radius r_p, temperature T_p, deformation y_p and deformation velocity $\dot{y}_\mathrm{p}$. A statistical description of the spray is therefore formulated using the droplet probability distribution function (PDF) in equation 3.21 (Baumgarten, 2006). This approach simplifies

the calculations of the spray, as only behavior and properties of some of droplets are calculated in detail. It is then assumed that the calculated subset of droplets represents the general features of all droplets.

$$f(\boldsymbol{x}_\mathrm{p}, \boldsymbol{u}_\mathrm{p}, t, r_\mathrm{p}, T_\mathrm{p}, y_\mathrm{p}, \dot{y}_\mathrm{p}) d\boldsymbol{x}_\mathrm{p} d\boldsymbol{u}_\mathrm{p} dt dr_\mathrm{p} dT_\mathrm{p} dy_\mathrm{p} d\dot{y}_\mathrm{p} \tag{3.21}$$

Equation 3.21 can be formulated in differential form by a transport equation 3.22, which is known as the spray equation (Nowruzi et al., 2014)

$$\frac{\partial f}{\partial t} + \mathrm{div}\,(f\boldsymbol{u}) + \mathrm{div}\left(f\frac{\partial \boldsymbol{u}}{\partial t}\right) + \frac{\partial}{\partial r}\left(f\frac{\partial r}{\partial t}\right) + \frac{\partial}{\partial T}\left(f\frac{\partial T}{\partial t}\right) + \frac{\partial}{\partial y}\left(f\frac{\partial y}{\partial t}\right) + \frac{\partial}{\partial \dot{y}}\left(f\frac{\partial \dot{y}}{\partial t}\right) = S_\mathrm{col} + S_\mathrm{break} \tag{3.22}$$

The two source parameters S_col and S_break are the contribution from the collision and breakup of the droplets, respectively. These source terms as well as the individual terms in the equation have to be modelled. The spray equation cannot be solved directly, since it is described by a number of complex functions and differential equations. Therefore, the Stochastic-Parcel Technique is used to obtain an approximation of the exact solution (Baumgarten, 2006). The method is based on the Monte-Carlo Method.

3.3 Primary break-up models

Primary break-up models are also known as coupling models, since they on the basis of the conditions inside the nozzle describe the boundary conditions for the discrete Lagrangian droplets. The Lagrangian droplets need initial size and velocity distribution to calculate the spray formation and the secondary break-up in the surrounding gas (Baumgarten, 2006).

There are only very few detailed models for the simulation of primary break-up of high-pressure sprays (Baumgarten, 2006; Soriano-Palao et al., 2014). Modelling the primary break-up is very complicated, as it is difficult to understand the relevant break-up processes involved (Soriano and Rotondi, 2008). Most researchers use therefore models that employ simplified boundary conditions at the nozzle exit as an indirect coupling to the primary spray droplets (Andriotis et al., 2008; Baumgarten, 2006; Herrmann, 2011; Mohan et al., 2014b; Moyne, 2010; von Berg et al., 2005). Such methods often dampen or lead to loss of the nozzle flow characteristic, thus leading to insufficient prediction of the structure and starting conditions of the first spray near the nozzle.

The simplest method for introducing the Lagrangian droplets is by the blob-method. The blob method is based on the assumption that detailed description of the atomization and drop break-up processes within the dense spray near the nozzle is not required. The Lagrangian droplets are therefore initiated by spherical droplets with a diameter equal to the nozzle hole diameter D_{n}. The break-up occurs due to secondary aerodynamic-induced break-up. The velocity of the inital droplets and the number of drops injected per unit time is determined from the mass flow rate $\dot{m}$ using equation 3.23.

$$u_{\mathrm{inj}}(t) = \frac{\dot{m}(t)}{A_{\mathrm{n}} \cdot \rho_{\mathrm{l}}} \tag{3.23}$$

Cavitation-induced break-up models have been developed by some researches in the recent years. The proposed break-up models are either based on one dimensional or phenomenological models of the cavitation inside the nozzle volume (Mohan et al., 2014a; Santos and Moyne, 2011). Arcoumanis et al. (1997) included cavitation in the primary break-up by calculating an effective hole diameter (the total area of the nozzle aperture occupied by cavitation) in order to determine the initial droplet diameter of droplets (Martinez et al., 2010). Nishimura and Assanis (2000) proposed a cavitation and turbulence-induced primary break-up model for diesel sprays. This model determines the bubble dynamics inside the injector and transfers collapse energy to turbulent kinetic energy, which is then transformed to an additional break-up force included in the secondary break-up (Moyne, 2010).

Baumgarten et al. (2002) proposed a cavitation-induced break-up model based on experimental investigations of a quasi-stationary spray. The model defines two different zones in the nozzle volume as shown in Figure 3.5. The first zone contain the liquid core of the jet, while the second zone consists of a mixture of cavitation bubbles and liquid ligaments. Break-up of the different zones is treated separately. The energy from the collapse of cavitation bubbles is transferred both to the outer surface and break-up of the mixture zone, as well as to the interface between the two zones to increase turbulent energy of liquid core.

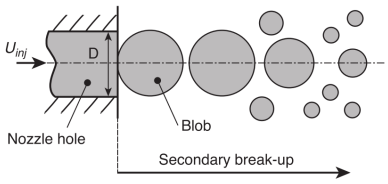

Figure 3.4: The blob-method used for primary break-up (Santos and Moyne, 2011).

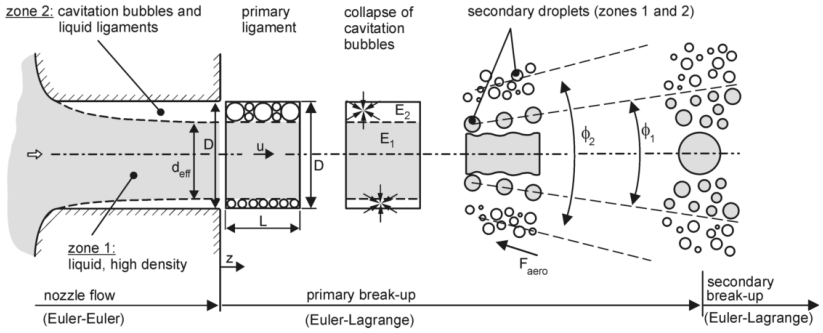

Figure 3.5: Overview of the primary break-up model proposed by Baumgarten et al. (2002).

The short review presented in this section shows, that the presented models are related to low-viscous liquids such as diesel fuels. This means that the models are based on assumptions, which may not valid for cavitation-induced break-up of viscous liquids. Therefore further investigations have to be performed to determine whether the proposed models can be applied for the studied injection system.

3.4 Secondary droplet break-up

The secondary breakup process is often modelled using the hybrid Kelvin-Helmholtz wave model and Rayleigh-Taylor model, known as the KHRT model (Kayhani et al., 2012; Pischke, 2014; Shi et al., 2011). The Kelvin-Helmholtz (KH) model is based on liquid jet stability analysis (Reitz and Beale, 1999), and describes the effect of KH waves on the jet surface due to aerodynamic forces. The Rayleigh-Taylor (RT) model is based on the theoretical work of Taylor (1950). RT instabilities appear from deceleration and drag of the liquid in the ambient gas (Reitz and Beale, 1999; Santos and Moyne, 2011).

Figure 3.6 shows an overview of the break-up mechanicsms. The aerodynamic force on the drop flattens it into the shape of a liquid sheet, and the decelerating sheet breaks into large-scale fragments by means of RT instability. The KH waves with a much shorter wavelength originate at the edges of the fragments, and these waves break into micrometer-size drops. It is assumed both instabilities occur simultaneously, and therefore they are used in combination the models describe the break-up the droplets (Baumgarten, 2006).

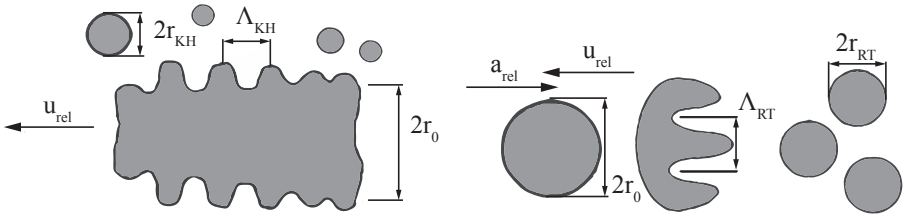

(a) Kelvin-Helmholtz (KH) model. **(b)** Rayleigh-Taylor (RT) model.

Figure 3.6: Illustration of the hybrid Kelvin-Helmholtz wave model and Rayleigh-Taylor (KHRT) model, which is used to describe the secondary break-up process. This figure is adapted from (Baumgarten, 2006).

3.4.1 Kelvin-Helmholtz instabilities

A stability analysis for round liquid jets leads to the fastest growing surface wave with a wavelength Λ_{KH} and growth rate Ω_{KH} in equation 3.24 and equation 3.25, respectively (Reitz and Beale, 1999).

$$\Lambda_{KH} = \frac{9.02 r_0 \left(1 + 0.45\sqrt{Z}\right)\left(1 + 0.4 Ta^{0.7}\right)}{(1+Z)\left(1 + 0.865 {We_g}^{1.67}\right)^{0.6}} \tag{3.24}$$

$$\Omega_{KH} = \frac{\left(0.34 + 0.38 {We_g}^{\frac{3}{2}}\right)}{(1+Z)\left(1 + 1.4 Ta^{0.6}\right)} \sqrt{\frac{\sigma}{\rho_l {r_0}^3}} \tag{3.25}$$

where r_0 is the droplet radius before the breakup, σ is the surface tension, ρ_l is the liquid density, u_{rel} is the relative velocity between droplet and the surrounding gas, Z is the Ohnesorge number for the liquid, We_g is the Weber number for the gas, and Ta is the Taylor number defined as $Ta = Z\sqrt{We_g}$.

The initial droplet of radius r_0 breakdowns to new droplets of radius r_{KH}. The new droplets are assumed to be sheared off from the surfaces waves of the parent droplet, and the size of these droplets is assumed to proportional to the wavelength Λ_{KH}:

$$r_{KH} = B_0 \Lambda_{KH} \tag{3.26}$$

The constant $B_0 = 0.61$ by Reitz and Beale (1999). According to this model, the parent droplet radius, r decreases constantly until it reaches stable droplet radius, which is defined by the rate equation in 3.27

$$\frac{\partial r}{\partial t} = \frac{r - r_{KH}}{\tau_{KH}} \tag{3.27}$$

where τ_{KH} is the break-up time is given by equation 3.28.

$$\tau_{KH} = 3.276 \frac{B_1 r}{\Omega_{KH} \Lambda_{KH}} \tag{3.28}$$

where the B_1 is an adjustable model constant that includes the influence of the nozzle flow e.g. nozzle design, liquid evaporation and turbulence level. Values between $B_1 = 1.73$ and $B_1 = 60$ are proposed in the literature (Baumgarten, 2006; Mohan et al., 2014a).

3.4.2 Rayleigh-Taylor instabilities

Similar to KH instabilities, the Rayleigh Taylor model also determines the break-up by determining the wavelength of the fastest growing disturbances. However, the disturbances in this model are due to acceleration instabilities on the surface of the liquid droplet. Liquid viscosity and gravity are neglected in these calculations, and only surface tension is considered. The fastest growing surface wave with a wavelength (Λ_{RT}) and growth rate (Ω_{RT}) is determined using equation 3.29 and 3.30 (Baumgarten, 2006; Mohan et al., 2014a).

$$\Lambda_{RT} = C_3 2\pi \sqrt{\frac{3\sigma}{a\left(\rho_l - \rho_g\right)}} \tag{3.29}$$

$$\Omega_{RT} = \sqrt{\frac{2}{3\sqrt{3\sigma}} \frac{\left[a\left(\rho_l - \rho_g\right)\right]^{3/2}}{\rho_l + \rho_g}} \tag{3.30}$$

where a is the acceleration observed by the droplet, and the constant C_3 is similar to the adjustable constant B_1 in the KH-model. However, in this thesis a value of $C_3 = 0.1$ is used.

In the RT-model, a droplet can only breakdown if the wavelength Λ_{RT} is smaller than the diameter of the droplet. The break-up leads to new droplets with a diameter that equals the wavelength and a mass determined through mass conservation.

3.5 Droplet drag

In this thesis, gravity and drag forces ($\boldsymbol{F}_G$ and $\boldsymbol{F}_D$) are the only external forces considered to act on the Lagrangian droplets. Other forces, such as Magnus force, Virtual mass force, and Basset force are neglected. This is primarily due to the small size of the droplets and the high ratio of droplets to the gas

density. The drag force on a sphere particle is described using equation 3.31 (Tropea et al., 2007).

$$\boldsymbol{F}_{\mathrm{D}} = \frac{1}{2}\rho_{\mathrm{g}} {u_{\mathrm{rel}}}^2 C_{\mathrm{D}} A_{\mathrm{f}} \tag{3.31}$$

where the u_{rel} is the relative velocity between gas phase and the droplet. The value A_{f} is the projected area of the spherical drop: $A_{\mathrm{d}} = \pi r_{\mathrm{d}}^2$. The value C_{D} is the drag coefficient shown in equation 3.32 (Ghadimi et al., 2016; Nordin, 2001). This empirical formulation shows the relation between particles' Reynolds number Re_{d} and the its drag coefficient. At higher Reynolds numbers, the level of turbulence behind the droplet increases, which leads to more drag.

$$C_D \begin{cases} \frac{24}{Re_{\mathrm{d}}}\left(1 + \frac{Re_{\mathrm{d}}^{(2/3)}}{6}\right) & Re_{\mathrm{d}} < 1000 \\ 0.424 & Re_{\mathrm{d}} > 1000 \end{cases} \tag{3.32}$$

where the Reynolds number for a droplet is calculated by equation 2.1. The droplet drag can be modelled using other formulations (Crowe et al., 2012), but this simple method is found sufficient in this thesis.

3.6 Droplet collision and coalescence

One approach for simulating the collision of droplets is the trajectory method proposed by Nordin (2001), which is a modified version of the statistical O'Rourke model. This trajectory model calculates the paths of all parcels and collides those that will intersect within the same timestep, as shown in Figure 3.7. There are only two outcomes of droplet collisions: permanent coalescence (region III in Figure 2.12) and stretching separation (region V).

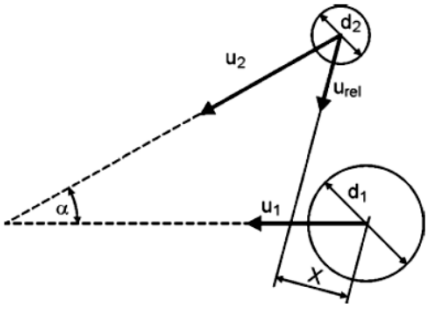

Figure 3.7: The designations used for calculating droplet collision and coalescence (Ghadimi et al., 2016).

The model calculates whether a pair of parcels are heading towards each other and whether the parcels can reach each other within the given timestep Δt. On basis of these criteria, the probability p_{col} for collision is given by equation 3.33 (Ghadimi et al., 2016; Nordin, 2001).

$$p_{\text{col}} = \left(\frac{\frac{1}{2}\left(d_1 + d_2\right)}{\max\left(\frac{1}{2}d_1 + d_2, \Delta x_{12}\right)} \right)^{C_{\text{space}}} e^{\frac{-c_{\text{time}}|t_\alpha - t_\beta|}{\Delta t}} \tag{3.33}$$

In equation 3.33, $\Delta x_{12} = |x_{1,\text{new}}(t_\alpha) - x_{2,\text{new}}(t_\alpha)|$ is the smallest distance between the two parcels during the timestep Δt. As this value decreases, the probability of collision increases. The two model constants C_{space} and C_{time} control the collision rate in space and time, respectively (Nordin, 2001).

3.7 Multiphase flow modelling

This section treats the modelling of the liquid flow through the spray nozzle. As discussed in Section 2.5, cavitation may occur inside the liquid, and therefore the system has to be considered as a multiphase system in order to simulate transfer of liquid to vapor. Furthermore, the model has to simultaneously treat both the liquid and cavitation (vapor) phases with different physical properties and their interactions.

In general, the difficulties of modelling cavitating flows include: sharp changes in the fluid density, existence of a moving boundary, and the requirement of modelling phase change (Giannadakis et al., 2008; Roohi et al., 2013; Zhu et al., 2015). Thus, a number of methods for modelling has been proposed in the literature (Lee and Reitz, 2010; Zhu et al., 2015). Figure 3.8 shows a classification of the existing cavitation modelling approaches in the literature (Xue et al., 2017). Common for these approaches is that there is a two-phase treatment of the liquid and gas, and as well as a separate treatment of the phase transition between vaporization and condensation.

A short overview of the models is given in the following:

- **Volume of fluid (VOF)** assumes that there is a clear and discontinuous interphase between the liquid and vapor (Ghiji et al., 2017; Koch et al., 2016). The interphase tracking scheme used in this method, requires the resolution of all involved length and time scales to accurately predict the interface between liquid and vapor (Marcer and LeGouez, 2001; Roohi et al., 2013; Yu et al., 2016a).

- **Two-Fluid model** assumes the liquid and vapor co-exist in each cell, thus treating two sets of conservation equations: one for the liquid phase and one for the vapor (von Berg et al., 2005; Wang and Su, 2009).

The interaction between the phases are included by additional source terms in the conservation equations (Bicer, 2015; Giannadakis et al., 2008).

- **Homogeneous equilibrium mixture (HEM)** assumes the vapor and liquid are perfectly mixed in each cell (Hoyas et al., 2012; Salvador et al., 2010). There is therefore only one set of equations. Phase transfer is treated by either a barotropic equations of state or mass transfer models (Baldwin et al., 2016; Morgut et al., 2011; Sou et al., 2014; Wang and Su, 2009).

In this PhD thesis, the HEM model is chosen for modelling the internal nozzle flow, because it is less computational demanding than VOF and Two-Fluid model (Bicer, 2015). The VOF model requires high resolution in order to track the interface, while the Two-Fluid model uses a more detailed description of the flow (Bicer, 2015; Wang and Su, 2009). The HEM method is a popular method for simulating the cavitation phenomenon inside injection nozzles (Karrholm, 2008; Salvador et al., 2010; Schmidt and Corradini, 2001; Sou et al., 2014; Vallier, 2013).

The HEM model calculates the phase transfer using a variable density field, which is defined by either a barotropic model or mass transfer model (Hejranfar et al., 2015; Roohi et al., 2013; Schmidt and Corradini, 2001). Barotropic models use an equation of state to relate the pressure with the thermodynamic properties (Huang and Wang, 2011; Zhu et al., 2015). Whereas, mass transfer models use a mass fraction transport equation, in which, the source terms define the condensation and evaporation rates (Morgut and Nobile, 2012).

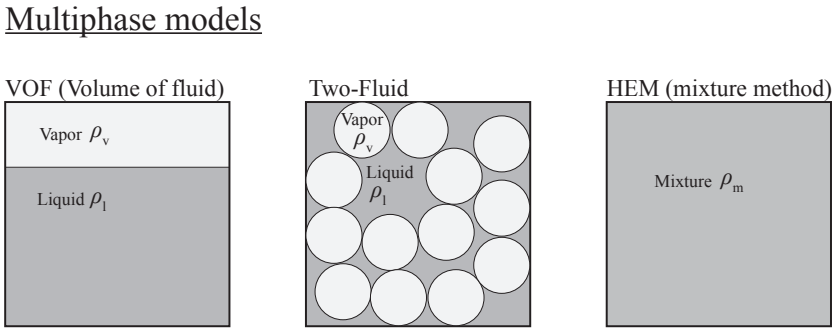

Figure 3.8: The multiphase models used are mainly divided into three groups.

Barotropic models are based on the assumption of complete thermodynamic equilibrium between the phases. Therefore, these models cannot take into account the physical details occurring in the cavitation phenomenon such as mass exchange and thermal transfer (Giannadakis et al., 2008). This is the advantage of mass transfer models, which are able to predict the impact of inertial forces on cavities, such as elongation and the detachment of cavity bubbles (Hejranfar et al., 2015; Wang et al., 2001).

On basis of the abovementioned considerations, it is assumed a HEM model together with a mass transfer model is suitable for simulating cavitating flows inside the studied injection nozzle.

3.7.1 Homogeneous mixture model

The homogeneous mixture model is based on a number of assumptions (Bicer, 2015; Morgut et al., 2011):

- The fluid consists of a single mixture of liquid and vapor.
- The relative velocity between the two phases is negligible compared to the high velocity of the average flow inside the nozzle.
- The phases are assumed to be in thermodynamic equilibrium i.e. isothermal, which means that interphase heat and mass transfer occurs instantaneously.
- The flow is considered isentropic (frictional less) and therefore energy equation can be neglected.

These assumptions allows the formulations of the continuity equation and the momentum equations for the mixture are described as follow:

Continuity equation

$$\frac{\delta \rho_m}{\delta t} + \mathrm{div}(\rho_m \mathbf{u}) = 0 \tag{3.34}$$

Momentum equations

$$\frac{\partial (\rho_\mathrm{m} u)}{\partial t} + \mathrm{div}\,(\rho_\mathrm{m} u \mathbf{u}) = -\frac{\partial p}{\partial x} + \mathrm{div}\,(\mu_\mathrm{m}\,\mathrm{grad}\,u) + S_{Mx} \tag{3.35}$$

$$\frac{\partial (\rho_\mathrm{m} v)}{\partial t} + \mathrm{div}\,(\rho_\mathrm{m} v \mathbf{u}) = -\frac{\partial p}{\partial y} + \mathrm{div}\,(\mu_\mathrm{m}\,\mathrm{grad}\,v) + S_{My} \tag{3.36}$$

$$\frac{\partial (\rho_\mathrm{m} w)}{\partial t} + \mathrm{div}\,(\rho_\mathrm{m} w \mathbf{u}) = -\frac{\partial p}{\delta z} + \mathrm{div}\,(\mu_\mathrm{m}\,\mathrm{grad}\,w) + S_{Mz} \tag{3.37}$$

where ρ_m and μ_m is the mixture density and mixture viscosity, which is determined by the volume fraction of the liquid phase α_l using the following equations:

$$\rho_m = (1 - \alpha_l)\rho_v + \alpha_l\rho_l \tag{3.38}$$

$$\mu_m = (1 - \alpha_l)\mu_v + \alpha_l\mu_l \tag{3.39}$$

The subscripts l and v indicates the liquid and vapor phase, respectively. The mass transfer rate between liquid and vapor phase is described using equation 3.40 (Sauer and Schnerr, 2000; Yu et al., 2016a).

$$\frac{\delta\alpha_l\rho_l}{\delta t} + \nabla \cdot (\alpha_l\rho_l\mathbf{u}) = S_c + S_e \tag{3.40}$$

where R_c and R_e are the mass transfer source terms for condensation and evaporation, respectively. There are different methods for determining these source terms e.g. full cavitation model, Zwart model, Kunz model, Singhal Full model, Schnerr-Sauer model (Morgut et al., 2011; Wang et al., 2001; Yuan et al., 2001). The main difference between the methods is the assumption of how to treat the growth and collapse of the cavitation bubbles inside the liquid volume (Zhu et al., 2015). The cavitation model proposed by Sauer and Schnerr (2000) is used in this PhD thesis.

The Schnerr–Sauer model is a simplified form of the Rayleigh-Plesset equation, where viscous terms, surface tension, incondensable gas, and high-order terms are ignored (Bicer and Sou, 2015). The mass transfer rate for the evaporation R_e and the condensation R_c is given in equation 3.41 and 3.42 (Bicer and Sou, 2015; Vallier, 2013). The equations takes vapor saturation pressure P_v, as a threshold for evaporation and condensation.

$$R_e = -C_v\frac{3\rho_l\rho_v}{\rho_m}\frac{\alpha_l(1-\alpha_l)}{R_b}\mathrm{sgn}(P_v - P_l)\cdot\sqrt{\frac{2|P_v - P_l|}{3\rho_l}},\quad P_l < P_v \tag{3.41}$$

$$R_c = -C_c\frac{3\rho_l\rho_v}{\rho_m}\frac{\alpha_l(1-\alpha_l)}{R_b}\mathrm{sgn}(P_l - P_v)\cdot\sqrt{\frac{2|P_v - P_l|}{3\rho_l}},\quad P_v < P_l \tag{3.42}$$

where R_b is the initial bubble radius, C_c and C_v are the rate constants for condensation and evaporation. The main challenge in using the Schnerr-Saur model, as well as the other mass transfer model, is to determine tunable parameters involved for vaporization and condensation processes.

3.8 Summary

In this chapter, state-of-the-art modelling approaches were investigated in order to determine an appropriate modelling strategy in this PhD thesis.

The simulation approach is divided into two steps. Firstly, the simulation of the liquid flow and cavitation inside the nozzle is performed using multiphase approach with a Schnerr-Saur cavitation model. Secondly, the simulation of the spray formation is performed using an Eulerian-Lagrangian approach using a KHRT secondary break-up model. The two simulations are connected using a primary break-up model, which translates the flow inside the nozzle to the first primary droplets at the nozzle exit.

Most primary break-up models use simplified models that employ simplified boundary conditions at the nozzle exit as an indirect coupling to the primary spray droplets. Such methods often dampen or lead to loss of the nozzle flow characteristic. This means that the models are based on assumptions, which may not valid for cavitation-induced break-up of viscous liquids. Therefore further investigations have to be performed to determine whether the state-of-the-art primary break-up models can be applied for the studied injection system.

Part III

Materials and Methods

4 Presentation of Hypotheses

At the end of Chapter 2, it was shown that it is difficult to atomize viscous liquids such as cylinder lubrication oil. In Chapter 3.2, the mechanisms of cavitation-induced break-up and different modelling strategies were discussed and conclusions were drawn. Based on the knowledge and conclusions presented in Part II, three hypotheses are formed to constitute the basis of the publications presented in Part IV.

4.1 Hypothesis I: The influence of lubrication oil properties

Viscosity is the most influential property of the cylinder lubrication oil that affects the jet break-up. This is according to the Ohnesorge diagram for the studied injection system in Figure 2.13 on page 26. The viscosity of lubrication oils might be Newtonian or non-Newtonian. In most studies, cylinder lubrication oils are considered as Newtonian fluids in order to simplify the calculations (Livanos and Kyrtatos, 2007; Mohamad et al., 2015; Valenti et al., 2013). However, this may be a crude assumption. At sufficiently high shear rates, all liquids become non-Newtonian (Barnes, 2001; Reiner, 1964). In case of a non-Newton lubrication oil, the break-up of the liquid becomes complicated (Aliseda et al., 2008).

Cylinder lubrication oils are not very well defined. The oil itself varies in temperature and chemical composition, providing different rheological behavior. Additives like calcium carbonate is dispersed into the base oil, in order to reduce the corrosive wear by neutralizing sulphuric acid formed during combustion (Fu et al., 2006; Sautermeister and Priest, 2012). This leads to the following hypothesis:

The rheological behavior of cylinder lubrication oils is affected by the additives incorporated into the oil formulation.

This hypothesis is treated by investigating the viscosity of different commercial cylinder lubrication oils. In order to detect non-Newtonian behavior,

viscosity measurements are performed at shear rates equivalent to the shear rates observed during the injection process.

4.2 Hypothesis II: Cavitation-induced break-up

Cavitation inside spray nozzles is of great importance in the break-up of liquid jets (Dong et al., 2016; Fansler and Parrish, 2015; Kastengren et al., 2012; Moyne, 2010; Sou et al., 2007). In simple pressure spray systems, liquid jets do not atomize greatly when disturbances caused by cavitation are not present (Dabiri et al., 2007; Dumouchel, 2008). This is especially true for viscous liquids, which are difficult to atomize unless high fluid pressure is applied (Khmelev et al., 2006; Tamaki and Shimizu, 2002). Cavitation occurs when the local pressure of the liquid drops below its vapor pressure (Franc and Michel, 2006), thereby forming vapor cavities inside the liquid. The collapse of these cavities introduce disturbances to the liquid, which leads to faster break-up and greater atomization of the exiting jet (Baumgarten et al., 2002; Bergwerk, 1959; Crua and Heikal, 2014; Dumouchel et al., 2013).

The internal nozzle cavitation has been studied intensively, and research has shown that cavitation is promoted by a variety of factors such as sharp inlet orifices, needle lift, curvature of the inlet edge, liquid properties, and system pressure (Andriotis et al., 2008; Dumouchel et al., 2013; Jollet et al., 2014; Pratama et al., 2015; Schmidt and Corradini, 2001). Identifying the factors influencing cavitation inside viscous liquids can lead to a more robust design of injection systems.

A study by Gardhouse et al. (2014) has shown that cavitation may influence the spray from an injection valve from Hans Jensen Lubricators. Nevertheless, the behaviour of the cavitation and its effects are still poorly understood. This leads to the following hypothesis:

Cavitation enhances the break-up viscous liquid jets.

Experimental tests and numerical simulations are used to investigate this hypothesis. The investigation is conducted on a commercial setup from Hans Jensen Lubricators, where cylinder lubrication oil is injected into ambient conditions.

4.3 Hypothesis III: Modelling spray formation

The spray process is complex, as it involves highly transient and coupled phenomena. To increase the understanding of such a complex process, numerical modelling and simulation can be used. Several methods exist and are implemented in commercial CFD codes for simulating the spray formation using the Eulerian-Lagrangian method, such as, the Taylor Analogy, Kelvin-Helmholtz and Rayleigh-Taylor break-up (Moyne, 2010). However, these models need sub models to describe the transition from the nozzle flow to the primary droplet. This coupling has been the focus of several authors, as accurate simulation of droplet flight is important (Andriotis et al., 2008; Baumgarten, 2006; Herrmann, 2011; Mohan et al., 2014b; von Berg et al., 2005).

First of all, the majority of current coupling models employ simplified boundary conditions at the nozzle exit as an indirect coupling to the primary spray droplets. Such methods often dampen or lead to loss of the nozzle flow characteristic. Secondly, these models are related to spray modelling of low-viscous liquids such as diesel fuels. This means that the current models are based on assumptions, which are not valid for cavitation-induced break-up of viscous liquids. This leads to the following hypothesis:

Cavitation-induced break-up of viscous liquids can be simulated using coupled state-of-the-art numerical models.

This hypothesis is investigated by developing a coupling model, which translates the viscous and cavitating flow conditions inside a nozzle to the first primary droplets. In order to imitate physical behavior, the model is based on observations made in Hypothesis II.

5 Materials

Based on the hypotheses presented in Chapter 4, seven different cylinder lubrication oils are selected for the experimental studies and numerical simulations. These lubrication oils are, together with their material properties, presented in this chapter.

5.1 Introduction to the lubrication oils

In this thesis, seven commercial cylinder lubrication oils are investigated, see Table 5.1. The chosen materials are considered to be representative of the commercial lubrication oils on the current market. As shown, the different lubrication oils consist of different levels of BN.

Table 5.1: Studied cylinder lubrication oils.

Product Name	Supplier	Base number
Castrol Cyltech 40SX	BP Castrol	40 BN
Castrol Cyltech 70	BP Castrol	70 BN
Castrol Cyltech CL 100 ACC	BP Castrol	100 BN
Mobilgard 525	ExxonMobil	25 BN
Mobilgard 560 VS	ExxonMobil	60 BN
Mobilgard 570	ExxonMobil	70 BN
Mobilgard 5100	ExxonMobil	100 BN

5.2 Material properties of lubrication oils

The primary lubrication oil used for the spray investigations is Mobilgard 570. The material properties for this oil are presented in Table 5.2, which are similar to the commercial cylinder lubrication oils presented in Table 5.1. The properties that are highly affected by temperature change are expressed as a function.

Table 5.2: Material properties of Mobilgaard 570 from ExxonMobil. In the following equations R is the ideal gas constant, and T_{L} is the temperature of the lubrication oil expressed in Celsius.

Property	**Value**
Boiling point [°C] *Material safety data sheet from ExxonMobil.	$T_{\mathrm{b}} = 316.0$
Pour point [°C] *Material safety data sheet from ExxonMobil.	$T_{\mathrm{p}} = -3.0$
Flash point [°C] *Material safety data sheet from ExxonMobil.	$T_{\mathrm{f}} = 225.0$
Surface tension [N/m] *Estimated from (Sautermeister and Priest, 2012).	$\sigma = 0.03$
Density [kg/m^3] *Measured by the supplier using ASTM D4052.	$\rho_{\mathrm{l}}(T_{\mathrm{L}}) = -6.087 \cdot 10^{-4} \cdot T_{\mathrm{L}} + 0.944$
Viscosity [Pa · s] *Determined using rotational rheometry in Paper A.	$\mu_l(T_{\mathrm{L}}) = 0.00610 \cdot e^{1246/(R \cdot T_{\mathrm{L}})}$
Vapour pressure [kPa] *Derived using the Clausius-Clapeyron equation in Appendix B. The dimensionless constants are $A = 1094$, $B = 3.458 \cdot 10^5$, and $C = 5463.0$.	$P_{\mathrm{v}}(T_{\mathrm{L}}) = 10 \cdot \mathrm{e}^{(A \cdot T_{\mathrm{L}} - B)/((20.0 \cdot T_{\mathrm{L}} + C)) \cdot R}$
Refractive index [-] *Estimated from (Stachowiak and Batchelor, 2013).	$n_{\mathrm{clo}} = 1.51$

6 Experimental Setup

In this Chapter the experimental methods utilized to investigate the hypotheses in chapter 4 are described. Initially, a description of the experimental test setup is given and different aspects of the design are discussed in detail. This is followed by a presentation of the high-speed shadowgraphic imaging setup, and finally the image processing approach. This chapter will present some of the details not treated in the publications.

6.1 Introduction to the experimental setup

Experiments have been carried out at Aalborg University on a test rig developed during this PhD project. The parts for the test rig have been provided by Hans Jensen Lubricators A/S, and the components for the imaging system is provided by the Department of Materials and Production at Aalborg University. A photograph of the test rig is shown in Figure 6.1.

A schematic overview of the test setup is shown in Figure 6.2. The setup consists of a lubricator (1), which delivers lubrication oil to a heated injection valve (2). The lubrication oil is injected in to a chamber (3) with ambient atmospheric conditions. To actuate the lubricator, hydraulic pressure is supplied from a standard pump station (4). Fresh lubrication oil to the lubricator is delivered from a heated reservoir (5).

The high-speed camera (6) and illumination source (7) are set up at either side of the spray in order to capture the images using the shadowgraphic method, where the spray is visualized as dark in front of an illuminated background. A control system (8) is developed in order to regulate the temperature on the lubrication oil, and to initialize both the high-speed camera and the lubricator.

The components in the experimental setup will be discussed throughout this chapter.

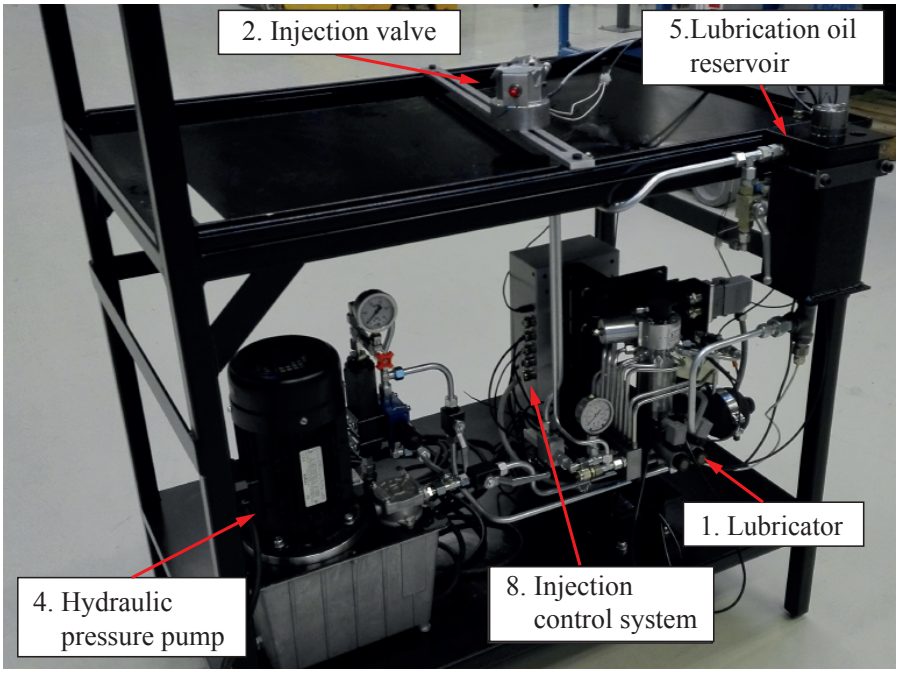

Figure 6.1: Photograph of the experimental setup used in this thesis. A schematic overview of the test setup is shown in Figure 6.2.

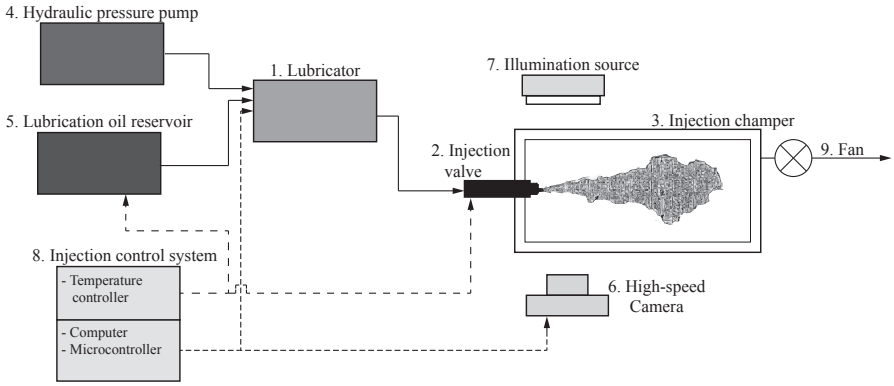

Figure 6.2: A schematic overview of the test setup used in the thesis. A picture of the test rig is shown in Figure 6.1.

6.2 HJ SIP spray injection valves

The spray injection valve used is a third generation HJ SIP valve from Hans Jensen Lubricators. A cross-sectional view of the valve is shown in Figure 6.3 and a detailed overview of the nozzle geometry is shown in Figure 6.4.

Lubrication oil to the SIP valve is supplied from the lubricator, which is a commercial HJ Lubtronic system. A comprehensive description of the lubricator can be found in Appendix C.

6.2.1 Working principle of the injection valve

The following description is based on Figure 6.3. The oil pipe from the lubricator is connected to the inlet (1) and the oil is lead through the space between the valve housing (2) and the inner part (3). From there it travels to the nozzle (4) which also contains the seat for the valve needle (5). The valve is kept closed by the spring (6). When the axial forces on the needle from the oil pressure exceeds the spring force, the valve opens for oil to enter the sac hole (7) and thereafter the oil leaves the injector through the spray hole (8). The spring force (opening pressure) of the valve can be adjusted using the adjustment screw (9). The leak oil is carried off through a return pipe (10).

The opening pressure on commercial HJ SIP valves is set to 3.7 MPa. In general, the injection pressure is higher under the injection phase. Figure 6.5 shows the characteristics of the pressure for an injector for different stroke

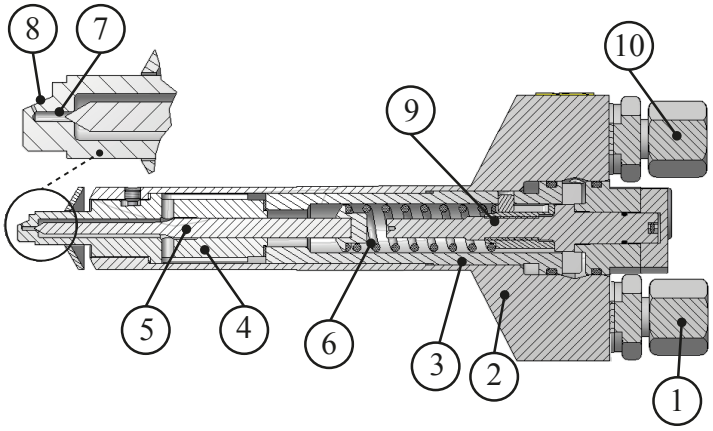

Figure 6.3: A third generation HJ SIP injection valve from Hans Jensen Lubricators. Consisting of (1) inlet, (2) valve housing, (3) inner part, (4) nozzle, (5) needle, (6) spring, (7) sac hole, (8) spray hole, (9) adjustment screw, and (10) return pipe.

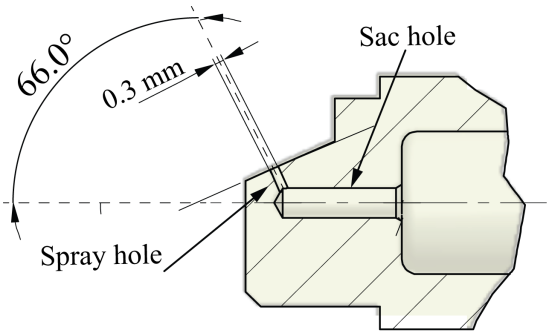

Figure 6.4: A detailed overview of the internal nozzle geometry and its dimensions.

length. Increased lubricator stroke length means higher injection pressure.

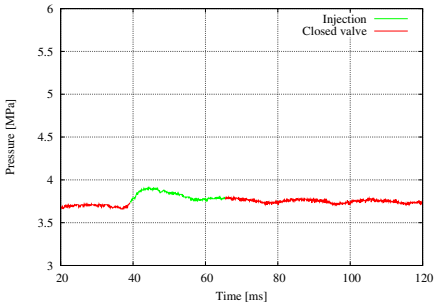

(a) Stroke length S_L = 2 mm

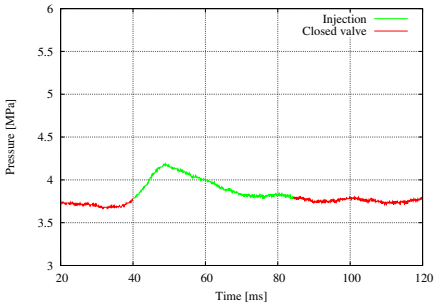

(b) Stroke length S_L = 4 mm

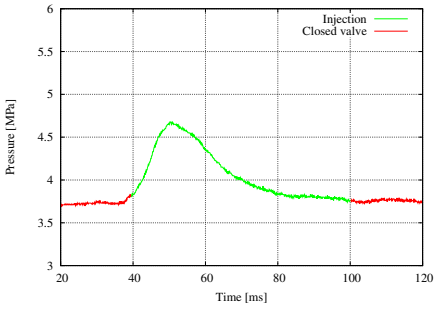

(c) Stroke length S_L = 6 mm

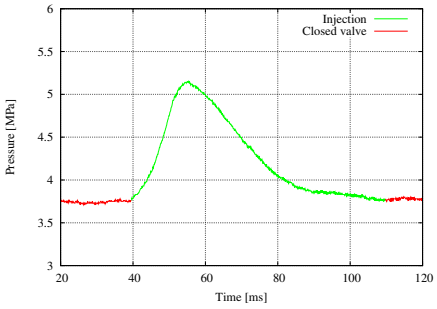

(d) Stroke length S_L = 8 mm

Figure 6.5: The opening pressure on commercial HJ SIP valves is set to 3.7 MPa. In general, the injection pressure is higher during the injection phase.

6.2.2 Manufacturing transparent spray nozzles

A transparent spray nozzle is manufactured in poly(methyl methacrylate) (PMMA) material, in order to investigate the flow inside the nozzle using the shadowgraphic imaging method. This imaging method can be applied because the lubrication oil and PMMA material have a matching refractive index. The refractive index for PMMA is n_{acr} = 1.491 (Jollet et al., 2014), the lubrication oil is estimated to have an index around n_{clo}= 1.51 (Stachowiak and Batchelor, 2013), and the vapor phase have an index of n_{vapor} = 1.0. This means that refraction will appear at the phase interface between the liquid and vapor, which leads to dark regions on the image, as shown in Figure 6.6.

The transparent nozzle has the same interior geometry as the HJ SIP nozzle shown in Figure 6.4. However, the outer geometry is changed to minimize the distortion of light due to the curved outer surfaces. The outer surfaces are therefore machined as plane surfaces that are parallel to the focal plane of the high-speed camera.

The complete nozzle (no. 4 in Figure 6.3) was initially manufactured in PMMA material. Unfortunately, this led to some challenges. PMMA is more brittle and have a lower yield strength than steel, which meant that the high fluid pressure and the repeated impact from the needle on the seat led to local deformations and thus failure of the nozzle.

To overcome the problem, the nozzle design shown in Figure 6.7 was proposed. By this design, the damaging stresses are distributed on the nozzle body made from steel, and at the same time, the flow inside the sac hole and spray hole can be observed using the nozzle tip made in PMMA material. The cap at the end is screwed onto the nozzle body and has two purposes: aligning the flow between the transparent tip and nozzle body, and providing the clamping force that prevents leakage between the parts.

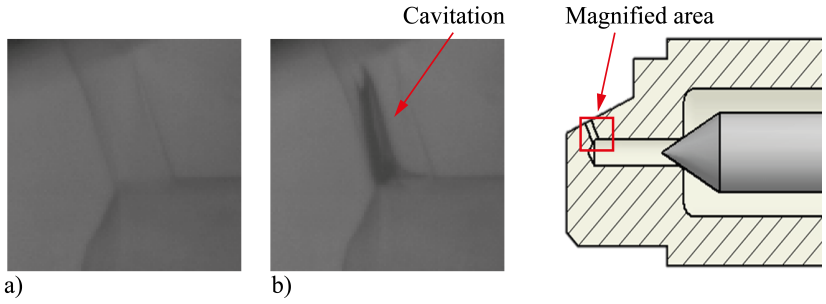

Figure 6.6: Image of the internal nozzle volume. The nozzle is manufactured in PMMA material, in order to investigate the flow inside the nozzle using the shadowgraphic imaging method.

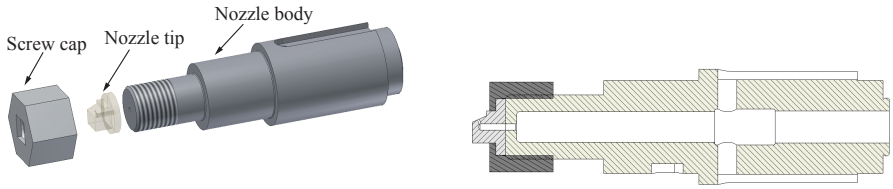

(a) Exploded-view drawing **(b)** Cross-sectional view

Figure 6.7: The transparent spray nozzle consists of three parts: a transparent nozzle tip machined in PMMA material, a screw cap, and nozzle body machined in steel. Figure 6.4 shows the internal dimensions of the transparent nozzle tip.

6.3 Injection control system

The injection control system consists of two sub-systems, as shown in Figure 6.8. One system, consisting of a computer and a micro-controller, initializes the process parameters and activates data acquisition. A separate system controls the temperature on the studied lubrication oil. The control system integrates a number of functions:

- **Initialization of process parameters**, such as stroke length and activation of the solenoid, is done by a custom written MATLAB Simulink program. There is a Simulink support package for Arduino hardware, which enables Simulink models to be created and run on the Arduino Mega 2650 board.
- **A process triggering signal** activates the high-speed camera, pressure measuring instrument, and the lubricator at the same time. Thereby a common time can be ensured on the measurements, which is relevant when comparing different test results. The triggering signal sent by the Arduino board is a 5V square wave pulse, and activates the camera using the TRIG TTL IN port and equivalently the I/J port on the pressure instrument.
  In the experiments, there is an electrical and hydraulic delay of approximately 40 ms between activation of the solenoid and opening of the injection valve. Obviously, this delay is dependent on the system setup and especially the length of the pipe.
- **Temperature** is controlled by a CAREL IR33 controller, which uses two separate circuits, able to regulate the temperature of the liquid inside the oil reservoir and the injection valve. This is done using a heating element built in to the oil reservoir and in the valve block. Feedback is achieved using two PT100 thermocouples. The temperature is regulated using an on/off control system with a hysteresis of 1 °C in the range of 50-150 °C.

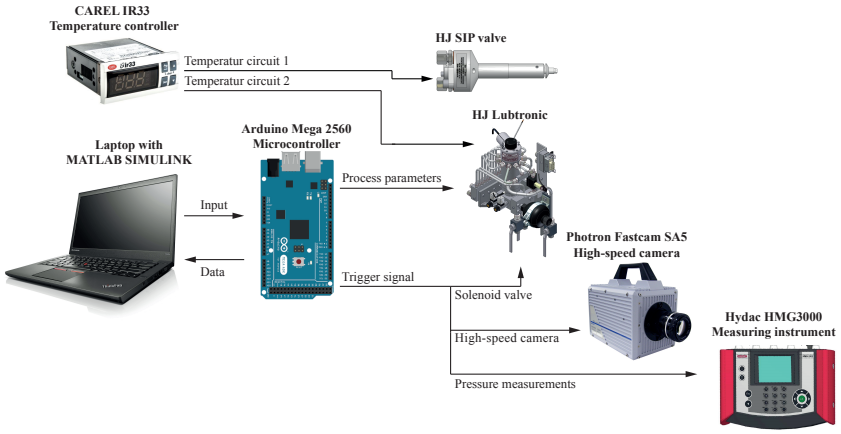

Figure 6.8: Overview of the control setup. The system consists of a computer and a microcontroller, which initializes the process parameters and activates data acquisition. A separate system controls the temperature on the studied lubrication oil.

6.4 Shadowgraphic imaging method

Shadowgraphic imaging is used to visualize the spray formation and the flow conditions inside the injection nozzle. Figure 6.9 shows a schematic overview of the shadowgraph system used in this thesis. The system consists of two main components: a high-speed camera and illumination source. They are set up on either side of the injector in order to capture the images using the shadowgraphic method.

In general, the shadowgraph highlights the difference in refractive index at the interface between an object and its surroundings, or between liquid media. The light that is illuminated from the behind of the object and that does not interact with the object produces a bright background. Whereas, the light refracted at the interface is dispersed and thus the interface appears dark. The refractive index of cylinder lubrication oil is assumed to be around $n_{\text{clo}} = 1.51$ and the surrounding atmospheric air has an index of $n_{\text{air}} = 1$, which means that the use of shadowgraphy is appropriate for spray visualization. Furthermore, it is also suited for observing cavitation inside the injection nozzle, as discussed in Section 6.2.

The shadowgraphic imaging method has been preferred by a number of researchers in studying the motion of particles, liquids or gases (Castrejón-Garcia et al., 2011; Fansler and Parrish, 2015). One of the advantages of using this method for spray measurements is that a high contrast between the spray and the background leads to a high level of detail.

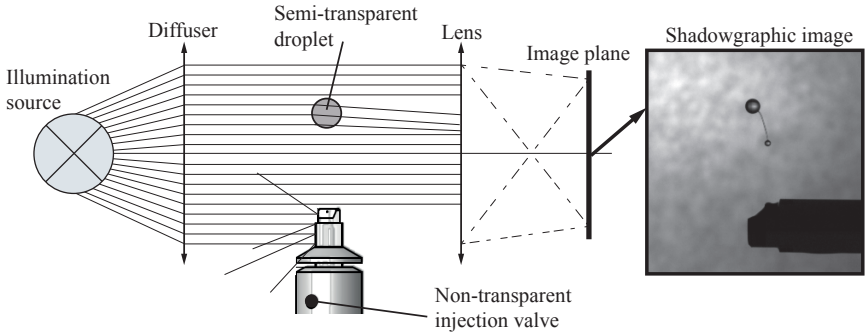

Figure 6.9: Illustration of the shadowgraphic imaging method. Light interacting with transparent objects becomes refracted, whereas light interacting with non-transparent objects is blocked. The shown setup lead to the shadowgraphic image to the right.

6.4.1 High-speed camera and illumination

The high-speed camera used is a Photron SA5 from Fastcam. The camera is a CCD-based imaging technology. It is capable of capturing 25,000 frames per second at a resolution of 512 X 512 pixels per image. A 1000W halogen lamp is used as illumination source, and a thin paper is used to diffuse the light.

Two types of lenses are used: a zoom lens to visualize centimeter-scale objects such as the spray formation, and a macro lens to visualise milimeter-scale objects such as the near-nozzle spray formation and nozzle flow. The zoom lens is a 35 mm Nikon, and the macro lens is a *Navitar Zoom 6000* solution from Navitar.

The imaging specifications chosen on the camera software are adjusted for different setups. This is because contrast, sharpness and brightness of the shadowgraphic images depend on parameters such as the magnification, light sensitivity, field of view, depth of field and focal length of the optical system. To detect the spray formation with the zoom lens a frame rate of 15000 fps and a shutter-speed of 1/171000 s was found to appropriate. For images captured with the macro lens, a frame rate of 1000 fps and a shutter speed of 1/ 161000 s is required.

Examples of shadowgraphic images with different lenses are shown in Figure 6.10.

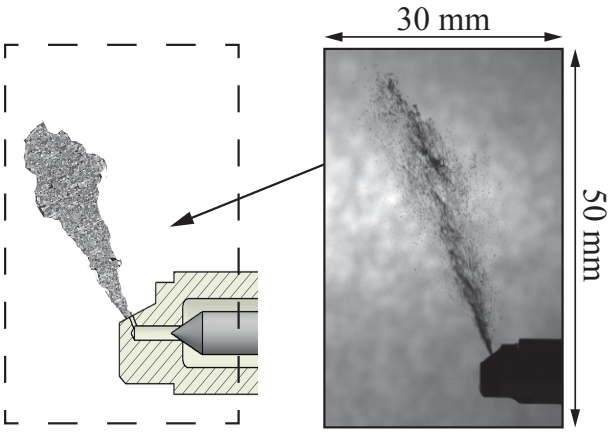

(a) Spray formation is captured using the zoom lens. This image shows the spray angle and penetration.

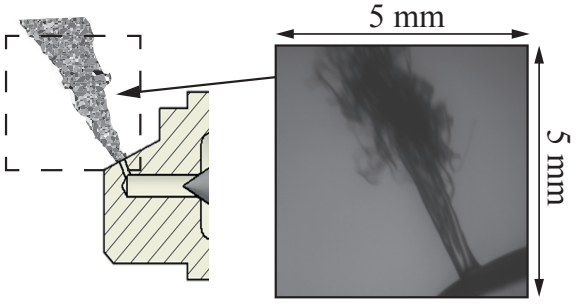

(b) Near-nozzle spray formation is captured using the macro lens. This image shows the primary-breakup.

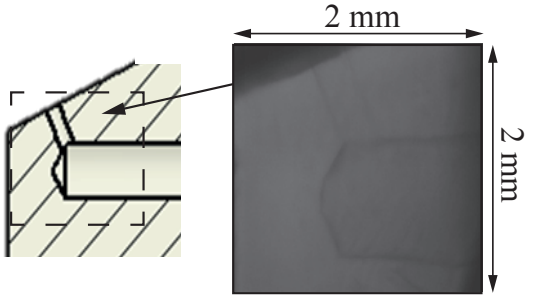

(c) Internal nozzle flow is captured using the macro lens. This image shows the internal nozzle conditions such as cavitation.

Figure 6.10: Examples of different types of shadowgraphic images captured by different lenses.

6.5 Post-processing shadowgraphic images

Each image is digitally processed using a custom algorithm in MATLAB, which detects the spray boundary and computes the spray tip penetration and cone angle. The algorithm consists of several image processing steps in order to distinguish the spray from the background sufficiently. The steps are described in the following and shown in Figure 6.11.

1. **Unprocessed shadowgraphic image (6.11a)** is a grayscale image consisting of a 2D array of pixels. The value of each pixel is a single sample carrying intensity information. The intensity is represented by values in the range of 0-255, where black is 0 and white is 255. The image is represented as $f(x,y)$, where x is the horizontal position of the pixel and y the vertical position (Moeslund, 2012).

2. **Background subtraction(6.11b)** is performed to separate the spray boundary from the background. The subtraction results in a grayscale image $g(x,y)$, where the spray is shown as white contour on a black background:
$$g(x,y) = f(x,y) - Background(x,y) \tag{6.1}$$

3. **Contrast stretching** is performed to normalize the grayscale image linearly in the range of 0 to 255. This leads to enhanced brightness of the spray contour in the contrast stretched image $c(x,y)$:
$$c(x,y) = \frac{255}{f_2 - f_1} \cdot (g(x,y) - f_1) \tag{6.2}$$
where f_1 is the lowest pixel intensity value in the input image $g(x,y)$, and f_2 is the highest value (Moeslund, 2012).

4. **Thresholding (6.11c)** is performed to convert the grayscale image into a binary black/white image $h(x,y)$. This is performed using the following segmentation algorithm:
$$\text{if } \; c(x,y) \leq T \; \text{ then } \; h(x,y) = 0 \tag{6.3}$$
$$\text{if } \; c(x,y) > T \; \text{ then } \; h(x,y) = 255 \tag{6.4}$$
The threshold value T is one of the most important features that can introduce measurement uncertainties. The value of 25 was selected to be applied in this thesis. However, it must be adjusted if contrast, sharpness and brightness of the original unprocessed image $f(x,y)$ changes.

5. **Blob detection** is performed in order to distinguish the spray from noise and smaller single droplets outside the spray region. If more

than 4 white pixels are connected in the image, they are considered to be as a blob. The largest of these blobs is considered to be the spray region, whereas the smaller blobs are removed.

6. **Edge detection (6.11d)** is used to define the contour of the spray region. The Sobel filter is used, in order to detect when the colour of a pixel and its neighbouring pixel changes from 0 to 255 or vice versa. These edges or spray boundaries are used to calculate spray angle and spray penetration.

7. **Curve fitting(6.11e)** is performed to calculate the spray cone angle. Two linear lines, having a starting point at the nozzle tip, are fitted to each spray edge. The angle between these lines is the spray cone angle. The length of these fitted lines can be adjusted to determine the accuracy of the spray cone angle.

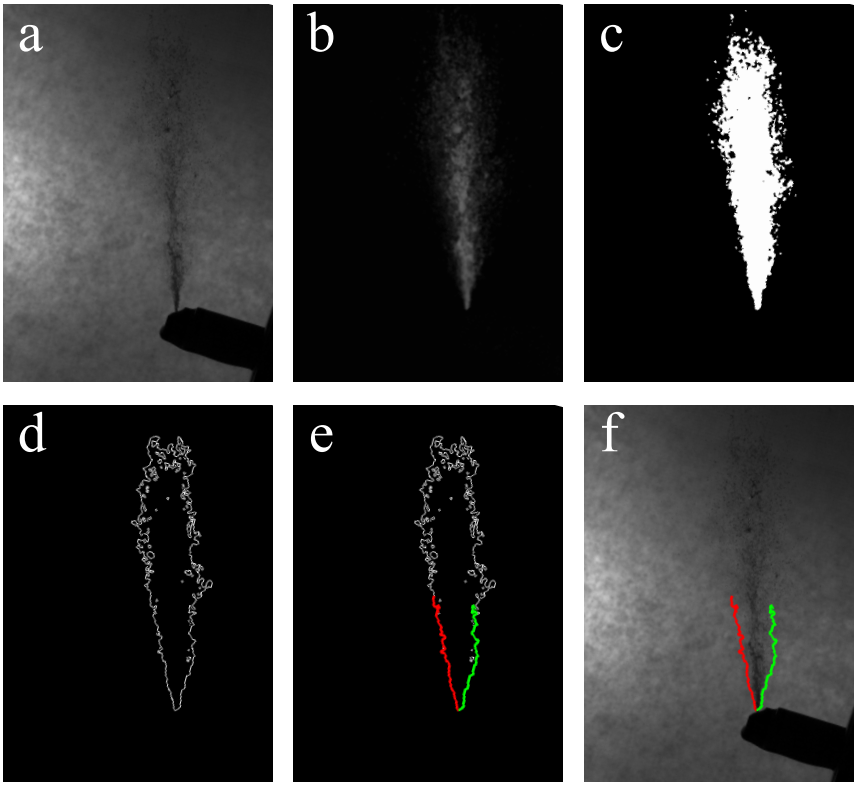

Figure 6.11: The image processing algorithm: (a) Unprocessed original image (b) Background subtraction and Contrast stretching (c) Thresholding and Blob detection (d) Edge detection (e) Curve fitting (f) Processed final image.

6.6 Recommendations for the experimental setup

Recommendations for improving the experimental studies are discussed in the following.

- Instead of the halogen lamp used for background illumination, it is recommended to use high-power, short duration light pulses e.g. from Nd:YAG double-cavity laser sources. Such illumination lasers produce short-exposure images (Hult et al., 2016). Thereby reducing motion blur on the images.
- The transparent nozzle can lead to some uncertainties compared to production nozzles made in steel. Differences in material and manufacturing cause difference in surface roughness and inlet geometries, both features are known to affect turbulence and cavitation inside the nozzle (Crua and Heikal, 2014). High-speed phase-contrast x-ray imaging (Kastengren et al., 2012; Powell et al., 2011; Zhang et al., 2016) can capture the cavitation and also needle motion for metal injectors, but the procedure is still complex and expensive for industrial applications (Fansler and Parrish, 2015).
- For each setup, much time were spent on calibration. Aligning the camera, injector and illumination is cumbersome process. It is recommended to use translation stages (Gardhouse et al., 2014) in order to adjust the camera and illumination precisely and eliminate alignment errors.
- Droplet size measurements cannot be performed using the setup presented in this chapter. There are a difference imaging techniques to perform droplet size measurements. A thorough description of droplet measurements techniques is found in *Spray measurement technology: a review* by Fansler and Parrish (2015).

6.7 Summary

The experimental methods utilized to investigate the hypotheses are described in this chapter. A HJ SIP injection valve and HJ Lubtronic lubricator are used for the investigations. A transparent nozzle is manufactured to capture cavitation inside the nozzle. High-speed shadowgraphic imaging is used to visualize cavitation and the spray formation, and the captured images are processed by a custom algorithm.

7 | Numerical Setup

This chapter contains an overview of the numerical setup used in this PhD thesis. The numerical setup includes geometry, mesh, imposed boundary conditions, and convergence criteria, as well as the solution and discretization schemes. The numerical modelling is performed in the CFD software package OpenFOAM.

7.1 Introduction to the numerical approach

Based on the conclusions from Chapter 3, the simulation approach is divided into two steps, as shown in Figure 7.1. Firstly, the simulation of the liquid flow and cavitation inside the nozzle is performed using multiphase approach with a Schnerr-Saur cavitation model. Secondly, the simulation of the spray formation is performed using an Eulerian-Lagrangian approach using a KHRT secondary break-up model. The two simulations are connected using a coupling model, which translates the flow inside the nozzle to the first primary droplets at the nozzle exit.

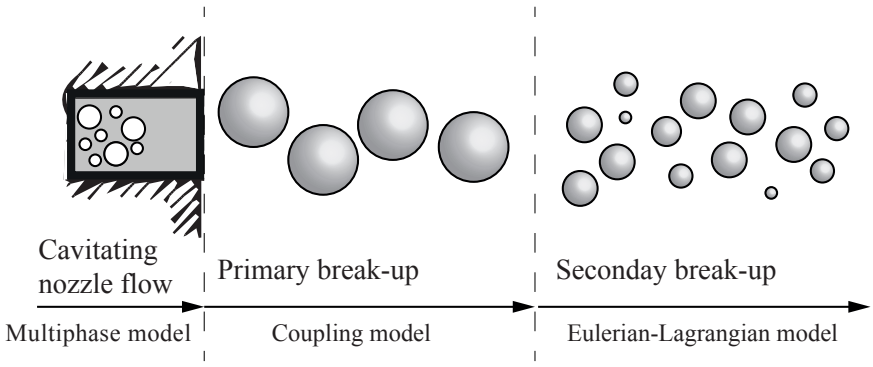

Figure 7.1: Overview of the numerical approach used in this thesis. The cavitating nozzle flow is modelled using a multiphase model, and the Eulerian-Lagrangian approach is used to simulate the spray formation. The two models are connected using a coupling model.

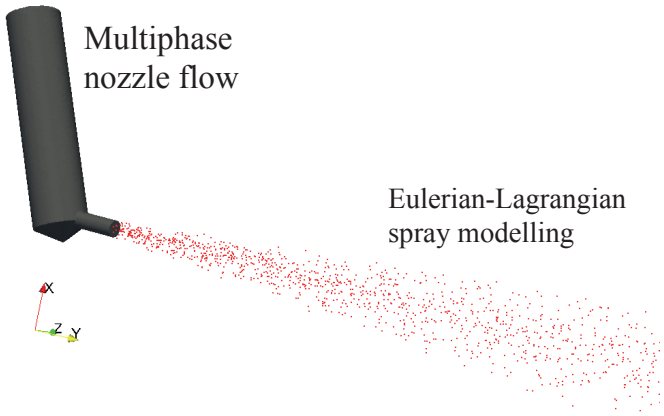

Figure 7.2: The coupled CFD simulations. The cavitating viscous nozzle flow is modelled using a multiphase model, and the subsequent spray is modelled using Eulerian-Lagrangian particle tracking approach.

Figure 7.2 shows the coupled CFD simulation model. The Lagrangian droplets are initiated at the center of the nozzle aperture, and from there they travel in y-direction. The center of the nozzle aperture is placed at the origin in the three-dimensional Cartesian coordinate system.

7.2 Finite volume method and OpenFOAM CFD

The finite volume method is used to solve the system of differential equations that governs the fluid. The method consists of discretizing the domain into a finite number of control volumes (cells). Thereafter, the differential equations are integrated over each control volume, and by the Gauss's theorem, converted to surface integrals (Versteeg and Malalasekera, 2007). The derivative terms are evaluated with discrete values at the center of the control volume. This results in a set of linear algebraic equations, which can be solved iteratively using solution algorithms (Galindo-Rosales, 2017).

The numerical simulations were performed using OpenFOAM 3.0 (Open Field Operation and Manipulation). The program is an open source CFD software based on an object-oriented C++ framework, which means that it is free and that it is to possible incorporate new code or modify existing code (Desantes et al., 2016; Nowruzi et al., 2014).

As a variety of solvers, libraries and utilities have been implemented in recent years by its users, the program has gained popularity in both academia

and industry (Chen et al., 2014). The structure of the OpenFOAM is shown in Figure 7.3 For an introduction to OpenFOAM and the options available in the code, see the *OpenFOAM User Guide* (OpenFOAM Foundation, 2014).

There are several solvers available in OpenFOAM ranging from basic CFD solvers to compressible, incompressible, multiphase, LES, DNS, combustion, heat transfer, stresses and electromagnetics (Chen et al., 2014; OpenFOAM Foundation, 2014). Since OpenFOAM is an open source CFD program, the solvers can be customized to compute the user's requirements. This is a convenient option that, in comparison to developing the entire code from scratch, saves time and resources. In this thesis, the following solvers have been modified:

- ***InterphaseChangeFoam*** is a solver for two incompressible, isothermal immiscible fluids. The fluid is treated as a homogeneous mixture, and phase change is based on a VOF interface capturing approach. The Kunz, Merkle, and Schnerr-Sauer models are included to simulate phase change.
- ***SprayFoam*** is a solver for compressible, laminar or turbulent flow of spray parcels in the Eulerian-Lagrangian framework. A variety of droplet models are implemented, including combustion, droplet break-up, collision, wall impingement, etc.

There is no graphical user interface in OpenFOAM, which means that every parameter that needs to be set for an application, is set in a text file called dictionary in a certain directory. Figure 7.4 shows the directory structure of OpenFOAM solvers.

In Figure 7.4, the directory *system* includes the used computational and solution schemes for the numerical simulations. The dictionary *fvSchemes*

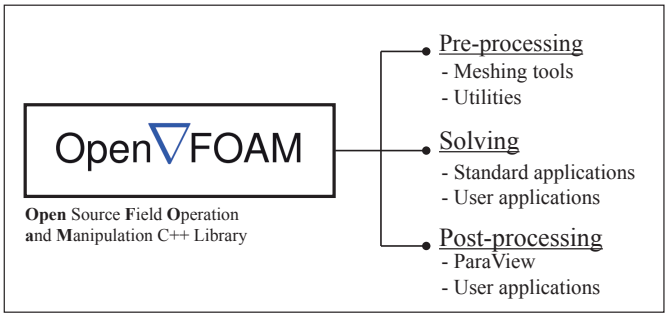

Figure 7.3: Structure of the open source OpenFOAM CFD program. There are several options available for pre-processing, solving CFD problems, and post-processing.

describes numerical schemes for terms, such as derivatives in equations. The *fvSolution* controls solution schemes, i.e. solvers, tolerance and algorithms. The dictionary *controlDict* determines the time steps, maximum Courant number, simulation start time, simulation end time, and writing time of the output files, etc. The directory *constant* contains information about mesh, transport properties, and employed turbulence model. Finally, the *time directories* contain the defined boundary conditions.

The several possibilities and advantages of OpenFOAM have been described in this section, but there is also a number of disadvantages using the open source program. For example, there is limited documentation compared to commercial software, and support can be bought directly from the founders of OpenFOAM (Chen et al., 2014; Gjesing, 2008).

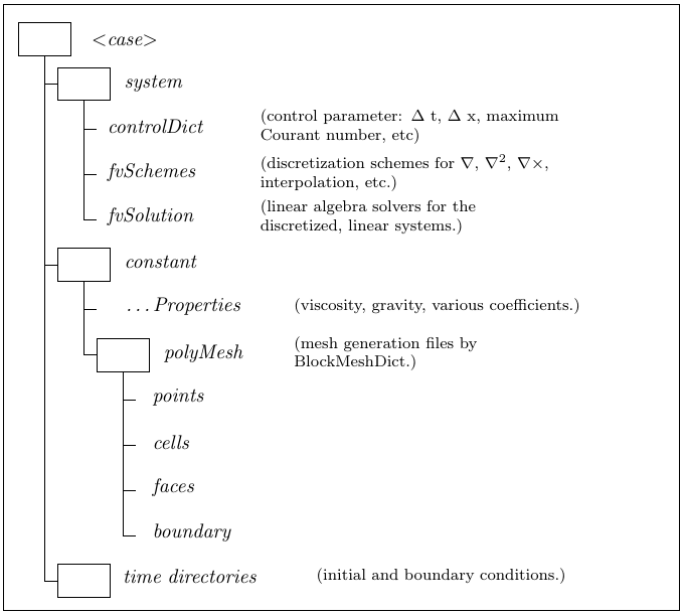

Figure 7.4: The directory structure of solvers in OpenFOAM. There is no graphical user interface, which means that model parameters are set in a dictionary text file (Chen et al., 2014).

7.3 Mesh generation

Mesh generation is an important step in CFD, as the accuracy of the simulation results are affected by the quality of the mesh (Versteeg and Malalasekera, 2007). In general, meshes can be divided into two categories: structured and unstructured meshes. The structured mesh is generated in a regular arrangement and consists of hexahedral cells in the three-dimensional domain. The unstructured mesh is not regularly built and the control volumes are distributed arbitrarily through the computational domain (Roohi et al., 2013).

In this thesis, the meshes are generated using the tools *blockMesh* and *SnappyHexMesh* that are both supplied with OpenFOAM. The *blockMesh* tool is used to create structured meshes for the spray simulations, while *SnappyHexMesh* is used to create unstructured meshes for complex geometries such as the internal nozzle volume. The quality of a mesh is evaluated using the *checkMesh* utility in OpenFOAM, which provides information about the employed cell volumes, domain size, aspect ratio, skewness and mesh non-orthogonality, etc.

7.4 Computational hardware

The CFD simulations are carried out on a Linux computer cluster (called Hill) from the Materials Processing Group at Aalborg University. The computer cluster is a Dell solution with 5 nodes, each containing two Intel Xeon E5-2697v3 (2.6 GHz) processors with 14 cores and 256 GB RAM. Every simulation in this thesis is computed in parallel with 16 processors. Once the simulations are have been completed, the results are viewed and processed using the post-processing software ParaView and MATLAB.

7.5 Numerical setup of the internal nozzle flow

This section treats the setup used for simulating the internal nozzle flow using the homogeneous equilibrium two-phase mixture method. The cavitation modelling is comprehensively described in Paper B.

An overview of the internal nozzle domain is shown in Figure 7.5. The dimensions of the geometry are the same as the studied nozzle, see Figure 6.4 on page 58.

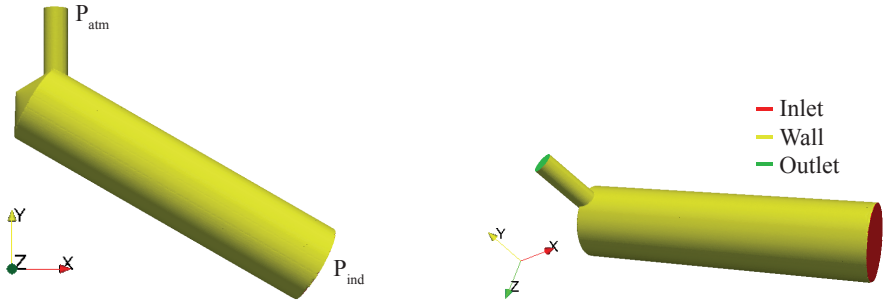

Figure 7.5: Overview of the nozzle volume domain and boundary conditions. The flow through the nozzle is driven by the pressure difference between the inlet and outlet. The center of the nozzle aperture is placed at the origin (x,y,z) = (0,0,0).

The flow through the nozzle is driven by the pressure difference between the inlet and outlet. Therefore, only three boundary conditions are necessary for the simulations:

- **Pressure inlet boundary** is based on the supply pressure from the lubricator. Effects from the needle opening and closing are included by exponential ramp-up and -down functions based on experimental tests. The pressure losses due to flow restrictions through the injector are not considered and this assumption adds uncertainty to the validity of the results.
- **Pressure outlet boundary** is based on the atmospheric pressure conditions.
- **Wall boundary** is no-slip conditions, which means that the tangential velocity is explicitly set to zero.

Symmetry boundary conditions in the xy-plane could be applied in order to reduce the computational time. However, this has not been performed, as this will complicate the coupling between the nozzle flow and Lagrangian particles.

7.5.1 Determination of mesh resolution

Figure 7.6 shows the generated mesh through the cross-section of the nozzle volume. There is a finer mesh resolution at the wall boundary layer and at the nozzle aperture region. It is important to have an high-quality mesh at the nozzle region, as the development of cavitation is highly dependent on sharp edges. Even minor changes in roundness between the sac and spray hole may lead to different results (Dabiri et al., 2007).

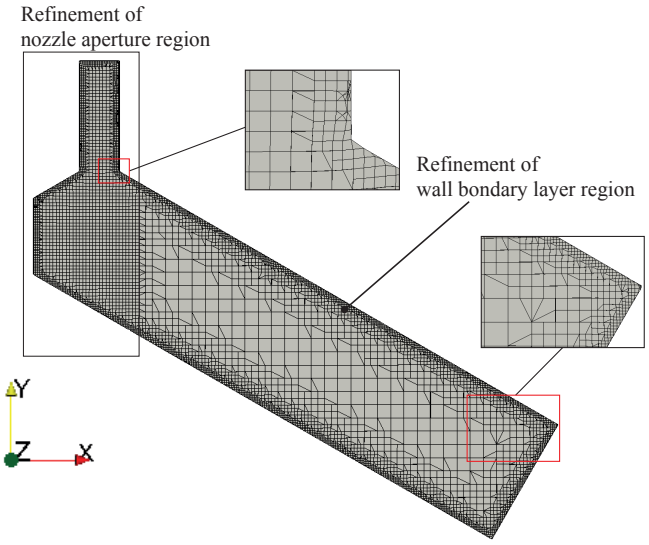

Figure 7.6: The cross-sectional view of the nozzle volume shows the generated mesh. A finer mesh resolution at the wall boundary layer and the nozzle aperture region is applied. This mesh equals the properties for the medium case in Table 7.1.

Four different mesh resolutions have been investigated in order to determine an appropriate mesh resolution. The properties of the meshes are shown in Table 7.1. The table shows that the number of cells across the diameter of the nozzle hole increases at higher mesh resolutions, which has an influence on the accuracy of the results.

Table 7.1: The properties of the four mesh resolutions analyzed.

Mesh quality	**Coarse**	**Medium**	**Fine**	**Ultra-fine**
Number of cells	33,477	404,098	620,643	1,990,126
Cells across hole	8	16	24	48
Maximum aspect ratio	19.53	22.31	22.31	22.31
Maximum skewness	1.46	1.85	1.85	2.27
Maximum non-orthogonality	64.99	65.19	65.00	65.00
Computational time in hours*	0.36	11.48	17.48	82.47
*time of simulation = 0.001 s				
**number of cores = 8 cores				

Figure 7.7 shows the velocity of the liquid at the nozzle exit hole for different mesh resolutions. It should be noticed that the velocity is represented by the three velocity components (u_x, u_y, u_z), and that the colour scales are different for the three components.

The results show that the coarse mesh does not predict the velocity components accurately. Accurate results are obtained by increasing the mesh resolution. In particular, mesh resolution has an significant influence on the prediction of velocities near the wall boundary layer. The disadvantage with a high mesh resolution is the high computational costs.

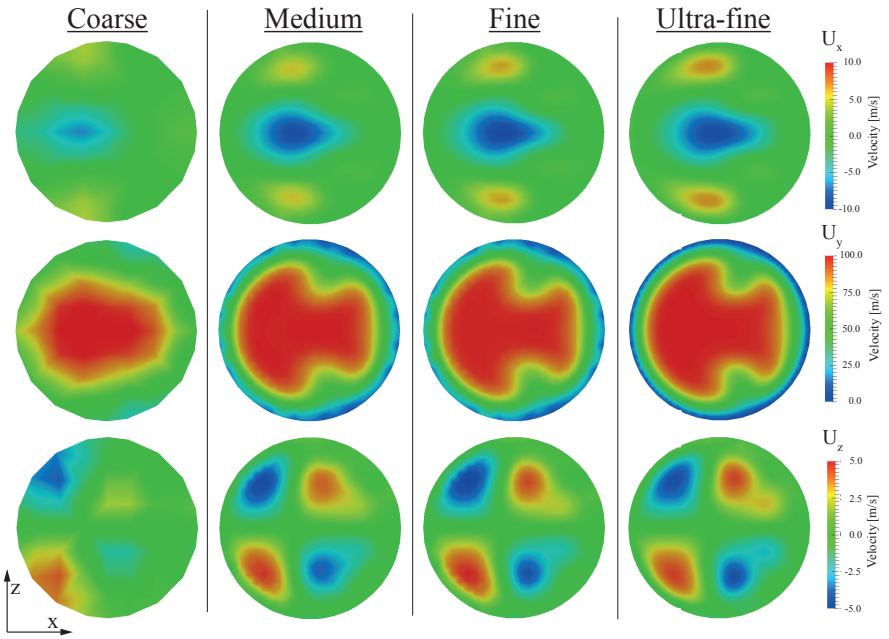

Figure 7.7: The velocity of the liquid at the nozzle exit hole for different mesh resolutions. It should be noticed that the velocity is represented by the three velocity components (u_x, u_y, u_z), and that the colour scales are different for the three components. On basis of the observations, the medium mesh is chosen.

Figure 7.8 shows the calculated mass flow rate for the different mesh resolutions. It is shown that the coarse mesh predicts an higher mass flow rate compared to the medium, fine and ultra-fine mesh. On basis of the observations made in this section, the medium mesh is preferred in order to ensure an adequate prediction of the flow conditions.

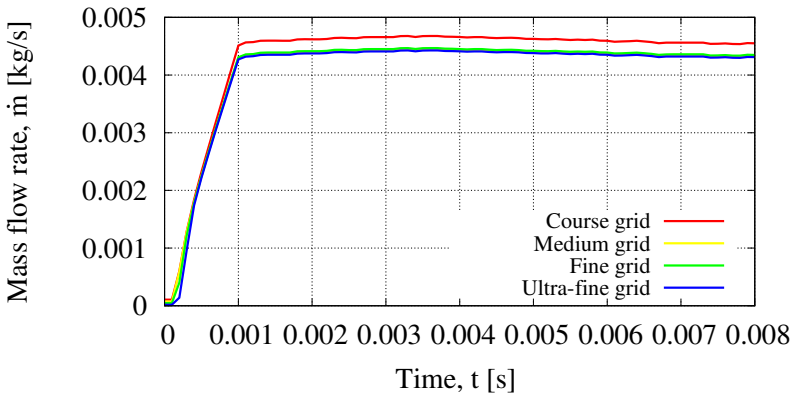

Figure 7.8: Calculated mass flow measurement from numerical simulations of different mesh resolutions.

7.6 Numerical setup of the spray formation

This section deals with the numerical simulations of the spray formation in the Eulerian-Lagrangian framework. The spray domain and its dimensions are shown in Figure 7.9. The spray, which consists of discrete Lagrangian droplets, is injected into the ambient conditions with an injection velocity u_{inj}. The injection occurs in y-direction from the nozzle aperture placed at the origin of the three-dimensional cartesian coordinate system. The droplets are allowed to escape the spray domain in any direction, as no wall model is implemented.

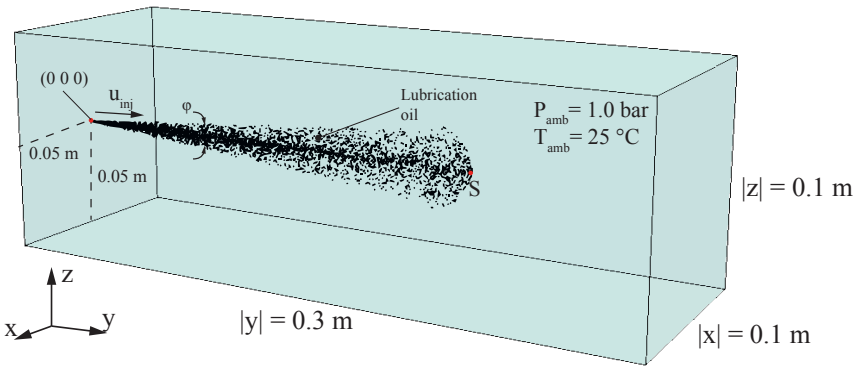

Figure 7.9: Overview of the spray domain and boundary conditions. The injection of discrete Lagrangian droplets occurs from the nozzle aperture placed in (x,y,z) = (0,0,0).

An overview of the implemented models is provided in Table 7.2. The numerical simulations presented in this section is performed using a standard blob-injection method that introduces the Lagrangian droplets. The blob-method is described in Section 3.3. In the publications, this injection method is replaced by a model that couples the internal flow simulations to the discrete Lagrangian droplets.

Table 7.2: Overview of the implemented models.

Models	**Value**
Injection model	Blob-method
Injection velocity, u_1	150.0 m/s
Injection direction, $\boldsymbol{r}$	(0, 0, 1)
Spray angle, ϕ	10°
Nozzle diameter, D_n	0.30 mm
Initial droplet diameter, $d_{\mathrm{p}0}$	0.30 mm
Parcels per second	$1.0{\cdot}10^6$
Number of particles	$1.0{\cdot}10^2$
Break-up model	KHRT
Tuning constant, B_1	20.0
Tuning constant, C_3	0.1
Turbulence model	Standard $k-\epsilon$
Drag model	Sphere drag
Collision model	None
Wall treatment	None

7.6.1 Determination of mesh resolution

Contrary to the Eulerian approach, where more accurate results can be obtained at finer mesh resolutions, there is a theoretical best mesh size in the Eulerian-Lagrangian approach. This means that refining the mesh could make the result worse, primarily due to the coupling between the Eulerian and Lagrangian phases (Nordin, 2001). A conventional mesh independency study can therefore not be conducted, but instead mesh resolution has to be assessed through less stringent evaluation (Dam, 2007).

When determining an appropriate mesh resolution, the following considerations have to be taken into account (Dam, 2007; Shi et al., 2011):

- A number of errors identified due to too coarse mesh resolution:
  - **Unresolved gradients:** The gradients of velocity and temperature are not accurately calculated.
  - **Inaccurate local values:** Local cell properties are not accurately calculated, which leads to inaccurate coupling between the Eulerian and Lagrangian phase. For example, when the relative velocity between droplet and surrounding gas is inaccurate, the drag and break-up calculations will also be inaccurate.
  - **Turbulence parameters:** The applied RANS turbulent model is not able to calculate the turbulent parameters when the gradients are not accurate.
- Errors identified due to too fine mesh resolution:
  - **Negligible liquid volume fraction:** Decreasing the cell size will correspondingly increase the liquid volume fraction. A high liquid volume fraction violates the assumption used for the current Eulerian-Lagrangian approach. This causes numerical instabilities.
  - **Droplet collisions:** The applied collision model only considers collision between droplets located in the same cell. Decreasing the cell size will therefore reduce the number of parcels interactions.

In order to determine an adequate mesh resolutions, numerical simulations are performed using four different mesh resolutions. The investigated mesh is structured and consists only of hexahedral cells. In the x and z direction, which is plane to spray axis, a cell size of 2, 5, 10, and 25 times the nozzle diameter d is used. In y direction, which is the direction of the spray, a cell size of 3 times the size of x and z direction is used i.e. 6, 15, 30, and 75.

To provoke droplet break-up of the lubrication oil in atmospheric conditions, the simulations are performed at constant injection velocity $u_{\text{inj}} = 150.0$ m/s and liquid temperature $T_{\text{L}} = 100°\text{C}$.

Figure 7.10 shows the numerical results for cases with and without a KHRT break-up model. The results show no significant influence of cell size on spray structure, but that cell size has an effect on the droplet break-up. Finer mesh leads to more details close to the nozzle region, more accurate prediction of large droplets and dense spray core at the center, as well as smaller droplets and diluted spray at outer regions. The influence of mesh size on spray penetration and droplet break-up is also shown in Figures 7.11 and 7.12, where the penetration S and Sauter mean diameter D_{32} is given as a function of time. The results show that refining the mesh resolution does not lead to an convergence in droplet size, as the finest mesh size $\Delta xy = 2d$

leads to a significantly higher D_{32} compared to the other mesh resolutions. This indicates that the mesh resolution is too fine, therefore leading to the aforementioned computational errors.

In the light of the observations made in this analysis, a mesh resolution of $\Delta xz = 10d$ and $\Delta y = 30d$ is found acceptable.

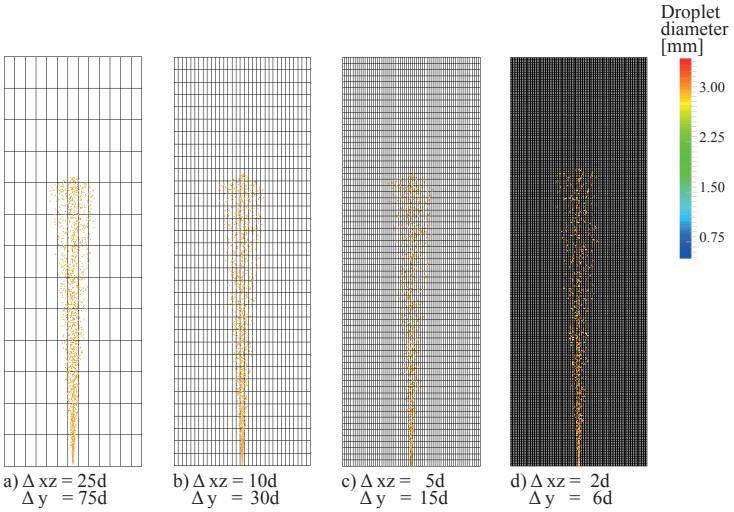

(a) Simulations are performed without a break-up model.

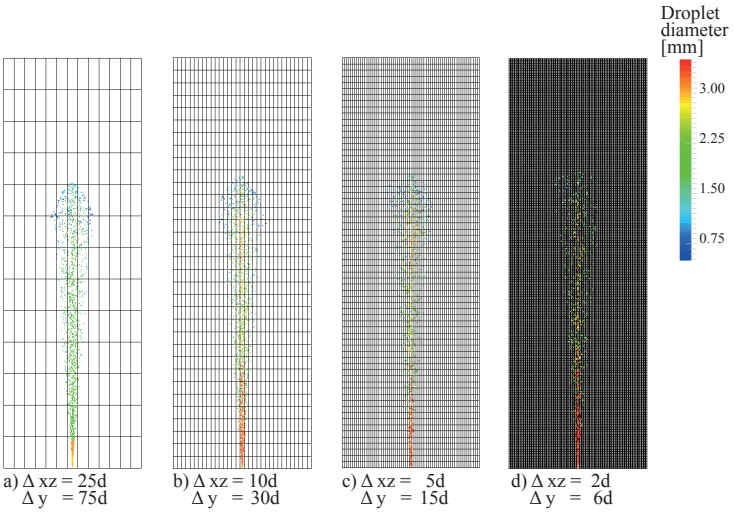

(b) Simulations are performed with KHRT break-up model.

Figure 7.10: The simulated spray formation at different mesh size in x-, y- and z-direction.

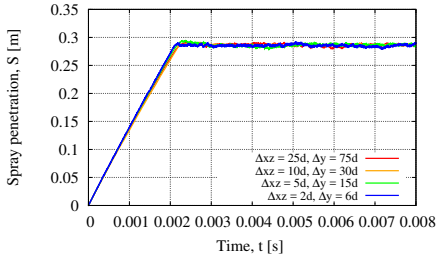

Figure 7.11: Spray penetration S at different mesh resolutions.

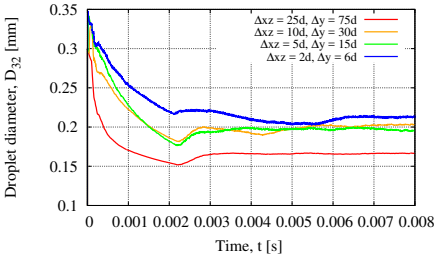

Figure 7.12: Mean diameter D_{32} at different mesh resolutions.

7.6.2 Tuning parameters in KHRT model

There are two adjustable model constants in the KHRT break-up model which are applied to include nozzle flow conditions in the break-up process. These are conditions such as turbulence flow and cavitation. The first value is B_1 in equation 7.1 and second value is C_3 in equation 7.2. In order to simplify the tuning process, the constant C_3 is set to 0.1 and only B_1 is used as a tuning parameter. Values of B_1 between 1.73 and 60 are proposed in the literature (Baumgarten, 2006; Mohan et al., 2014a).

$$\tau_{KH} = 3.276 \frac{B_1 r}{\Omega_{KH} \Lambda_{KH}} \tag{7.1}$$

$$\Lambda_{RT} = C_3 2\pi \sqrt{\frac{3\sigma}{a\left(\rho_l - \rho_g\right)}} \tag{7.2}$$

The influence of the value B_1 in the interval from 0.1 to 60 is shown in Figures 7.13 - 7.15. The simulations are performed using the same injection conditions described in Section 7.6.1, and a mesh solution of $\Delta xz = 10$.

Figures 7.13 and 7.15 show that the value of B_1 have an significant influence on the break-up process. A lower B_1 leads to enhanced break-up and smaller droplets. At $B_1 = 0.1$ an immediate droplet break up is observed, whereas increased B_1 leads to higher break-up length L_B. As shown in Figure 7.14, spray penetration is not influenced by B_1 and the existence of smaller droplets in the spray. This is considered to be due to injection in ambient conditions.

It is not possible to select an appropriate B_1 without experimental data. Validation against droplet size measurements is therefore necessary, as measurements of spray cone angle and spray penetration do not directly couple

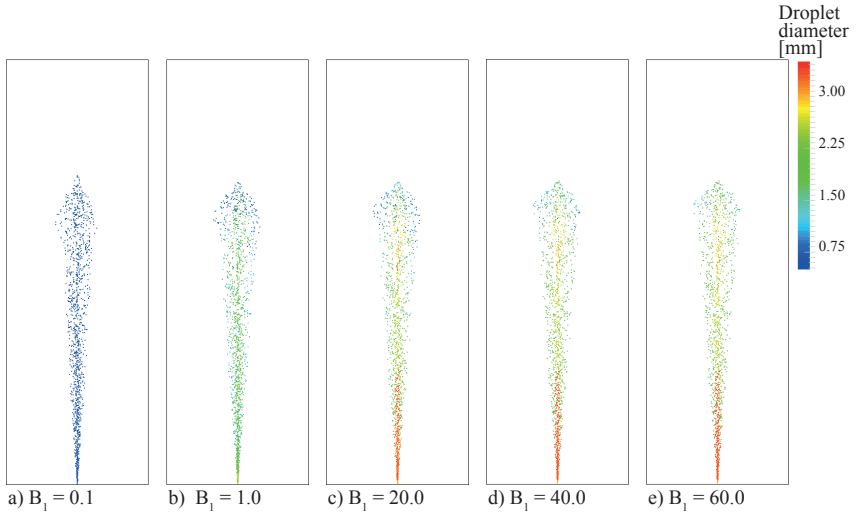

Figure 7.13: Simulation results of droplet size and spray structure for different values of B_1. The injection conditions are shown in Table 7.2.

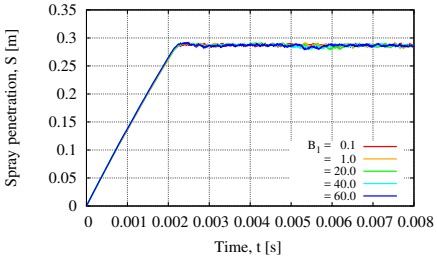

Figure 7.14: Spray penetration S for different values of B_1.

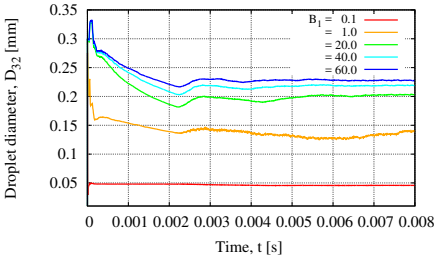

Figure 7.15: Mean diameter D_{32} for different values of B_1.

to droplet size. Therefore, $B_1 = 20$ is initially used for the simulations in this thesis, since this value is proposed for simulate fuel sprays in the literature (Baumgarten, 2006; Mohan et al., 2014b).

7.6.3 Effect of injection velocity

The injection velocity u_{inj} of the studied spray lubrication velocity is estimated to be approximately 40-50 m/s, which, according to the Ohnesorge diagram in Figure 2.13, does not lead to atomization. For this reason, the influence of injection velocity u_{inj} on the spray formation is investigated in this section. The investigation is performed using four injection velocities; $u_{\text{inj}} = 50, 100, 150, 200$ m/s, and the conditions presented in Table 7.2.

Figure 7.18 shows that droplet break-up process is highly affected by the injection velocity. There is almost no droplet break-up, when the $u_{\text{inj}} = 50$ m/s, and increasing velocity leads to a decrease in mean droplet diameter. Additionally, Figure 7.17 shows that spray penetration is naturally affected by the u_{inj}, as a lower injection velocity leads to slower penetration in the spray domain.

The spray structure for the different u_{inj} is shown in Figure 7.16. The results are shown for same penetration length, meaning simulation time t is different for the presented simulation results. It is shown that the break-up length decreases as the velocity increases. The simulation results are in agreement with the conclusions made from analyzing the Ohnesorge diagram at the end of Chapter 2, i.e. break-up of the viscous liquids are not due to the aerodynamic and turbulence forces.

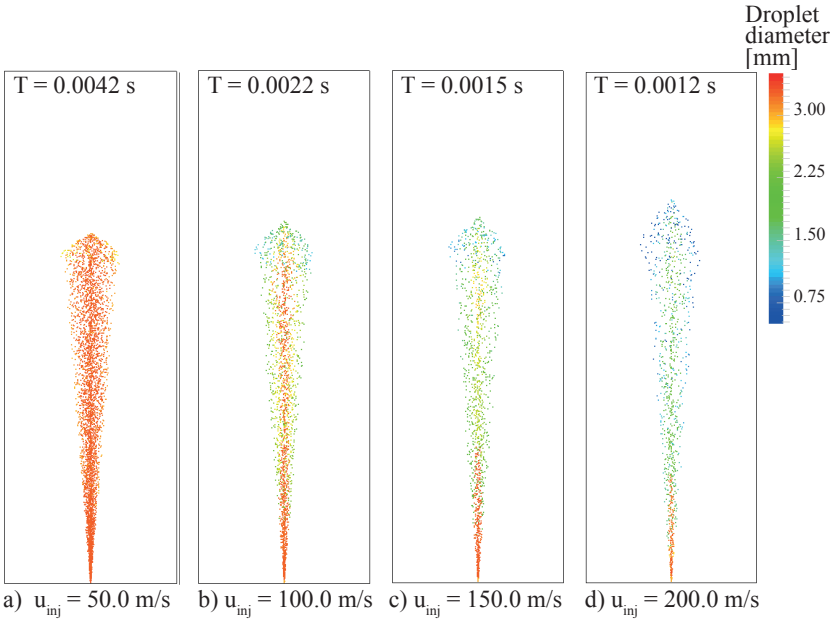

Figure 7.16: Numerical simulations of the spray structure for different injection velocities u_{inj}

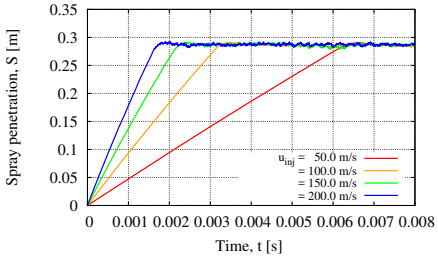

Figure 7.17: Spray penetration S for different injection velocities u_{inj}.

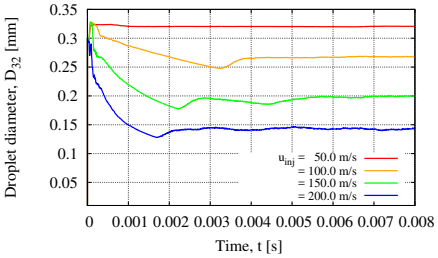

Figure 7.18: Mean diameter D_{32} for different injection velocities u_{inj}.

7.7 Summary

The numerical setup utilized to investigate the hypotheses was described in this chapter. The simulations are performed using the open source CFD program OpenFOAM using a computer cluster on Aalborg University. The following settings have been chosen for the numerical simulations:

1. Nozzle flow simulations:

   Geometry and boundary conditions are shown in Figure 7.5.

   An unstructured mesh is created using the snappyHexMesh tool. The appropriate mesh resolution is the medium mesh shown in Table 7.1.

   A homogeneous mixture method is used to simulate the nozzle flow, and cavitation is captured with the Schnerr-Saur model.

2. Spray simulations

   Geometry and boundary conditions are shown in Table 7.9.

   Spray formation is modelled in the Eulerian-Lagrangian framework, and the implemented models are shown in Table 7.2.

   A structured mesh is created using blockMesh tool. The appropriate mesh resolution is the $\Delta xz = 10d$ mesh shown in Figure 7.10.

Part IV

Results and Discussion

Paper A

Title: Rheological behavior of lubrication oils used in two-stroke marine engines

Authors: R. Ravendran*, J. d. Christiansen, P. Jensen, B. Endelt and E. A. Jensen.

Publisher: Emerald Group Publishing Limited [ISSN 0036-8792]

Journal: Industrial Lubrication and Tribology, 69(5) - 2017

DOI: https://doi.org/10.1108/ILT-03-2016-0075

Background: This paper originates from hypotheses I in chapter 4.

Abstract: The purpose of this study is to investigate the rheological behavior of commercial lubrication oils used for cylinder lubrication in two-stroke marine diesel engines. Furthermore, it is of interest to investigate if the viscosity of lubrication oils is affected by different levels of alkalinity.
Viscosity measurements are performed using both rotational and capillary rheometry. It was possible to measure oil viscosity in the shear rate from 0.1 to 3000 s^{-1} using rotational rheometry, whereas capillary rheometry allowed measurements in higher shear rates from $5 \cdot 10^5$ to $1.3 \cdot 10^6$ s^{-1} at 50 °C
The viscosity measurements show that the studied lubrication oils behave as a Newtonian fluid and that the viscosities are insensitive to the level of alkalinity. Furthermore, the viscosity/temperature dependency for the lubrication oils was found to fit the Arrhenius model.
This study presents useful information about the rheological behavior of lubrication oils, more precisely how the oil properties are affected by shear rate, temperature and level of alkalinity. The value of this research is considered to be important for designing two-stroke diesel engines and cylinder lubrication systems.

Rheological behaviour of lubrication oils used in two-stroke marine engines

Rathesan Ravendran and Peter Jensen
Research and Development, Hans Jensen Lubricators A/S, Hadsund, Denmark, and
Jesper de Claville Christiansen, Benny Endelt and Erik Appel Jensen
Department of Mechanical and Manufacturing Engineering, Aalborg University, Aalborg, Denmark

Abstract

Purpose – The purpose of this study is to investigate the rheological behaviour of commercial lubrication oils used for cylinder lubrication in two-stroke marine diesel engines. Furthermore, it is of interest to investigate whether the viscosity of lubrication oils is affected by different levels of alkalinity.

Design/methodology/approach – Viscosity measurements are performed using both rotational and capillary rheometry. It was possible to measure oil viscosity in the shear rate from 0.1 to 3,000 s^{-1} using rotational rheometry, whereas capillary rheometry allowed measurements in higher shear rates from 5×10^5 to 1.3×10^6 s^{-1} at 50°C.

Findings – The viscosity measurements show that the studied lubrication oils behave as a Newtonian fluid and that the viscosities are insensitive to the level of alkalinity. Furthermore, the viscosity/temperature dependency for the lubrication oils was found to fit the Arrhenius model.

Originality/value – This study presents useful information about the rheological behaviour of lubrication oils, more precisely how the oil properties are affected by shear rate, temperature and level of alkalinity. The value of this research is considered to be important for designing two-stroke diesel engines and cylinder lubrication systems.

Keywords Rheology, Base number, Calcium carbonate, Cylinder lubrication, Internal combustion engines, Marine diesel engines

Paper type Research paper

1. Introduction

Cylinder lubrication for large two-stroke marine diesel engines has been studied intensively in the recent years (Sautermeister *et al.*, 2013, 2014; Sautermeister and Priest, 2012; Cordtz *et al.*, 2013; Stolarski and Zhou, 2002; Mohamad *et al.*, 2015; Voelund and Felter, 2010; Eriksen, 2003). Environmental legislations force the maritime industry to reduce harmful exhaust gas emissions such as sulphur and nitrogen oxides (Cordtz *et al.*, 2013; Sigurdsson *et al.*, 2014). Today, marine diesel engines burn refined but mostly residual fuels with sulphur content between 0.005 and 4.5 wt.% (Sautermeister *et al.*, 2013; Sherrington *et al.*, 2002). In some environmentally controlled areas only 0.1 wt.% fuel sulphur is allowed unless equipment to treat the exhaust gas such as scrubbers are installed on-board (Cordtz *et al.*, 2013). This legislation regarding fuel sulphur content is even stricter from 2020 where a global legalisation of maximum 0.5 wt.% fuel sulphur is enforced (Cordtz *et al.*, 2013).

The choice of oil for cylinder lubrication is highly dependent on the sulphur content in the fuel oil. As the purpose of lubrication is, besides minimising wear between piston and cylinder, to neutralise liquid sulphuric acid (H_2SO_4) formed during combustion (Olander *et al.*, 2013). Sulphuric acids are damaging when it condensate on the liner, as it leads to corrosive wear (Wu *et al.*, 2000; Schramm *et al.*, 1994; Huijbregts and Leferink, 2004; Yahagi, 1987). To neutralise the acid and inhibit corrosion, commercial lubrication oils are formulated with a high level of alkalinity expressed by the base number (BN). The BN corresponds to the amount of potassium hydroxide (KOH) in mg necessary to neutralise the alkalinity in 1 g oil (Cordtz *et al.*, 2013). Commercial lubricants contain 25 to 100 BN, and higher sulphur in the fuel means that higher BN is required to neutralise the sulphuric acids.

The alkalinity reserve is usually added into the lubrication oil by dispersing calcium carbonate particles as reversed micelles (Sautermeister and Priest, 2012; Fu *et al.*, 2006). In general, the calcium carbonate exists as sulphonates, salicylates or phenates. When these complex molecules contain a large excess of base, they are referred to over-based detergents. The over-based sulphonates and salicylates form reverse micelles with mixed alkyl-aryl shell which makes the detergent soluble. The over-based phenates forms likewise a reverse micelle, though with a shell having a polymeric structure (Wu *et al.*, 2000). The calcium carbonate core and surfactant layer has a diameter between 8 and 18 nm (Wu *et al.*, 2000; Fu *et al.*, 2006). Agglomeration of the particles may happen; however, this is not considered as an issue for this study.

Commercial cylinder oils are chemically complex, as they, besides over-based calcium carbonate detergents, consist of a

The current issue and full text archive of this journal is available on Emerald Insight at: **www.emeraldinsight.com/0036-8792.htm**

Industrial Lubrication and Tribology
69/5 (2017) 750–753

[DOI 10.1108/ILT-03-2016-0075]

Received 31 March 2016
Revised 17 August 2016
Accepted 23 October 2016

wide variety of additives which serves different purposes, e.g. dispersants, anti-wear additives and anti-oxidants. The viscosity of dispersions is first of all controlled by the continuous liquid phase which might be Newtonian or non-Newtonian, and then the added dispersed phase. Particle size, shape, amount, deformability and even the interaction between the particles affect the viscosity (Barnes, 2000). In most studies, cylinder oils are considered as Newtonian fluids to simplify the calculations (Livanos and Kyrtatos, 2007; Valenti *et al.*, 2013; Mohamad *et al.*, 2015). However, this may be a crude assumption. At sufficiently high shear rates causing a high Deborah number, all liquids become non-Newtonian (Reiner, 1964; Barnes, 2000). For instance, the values of the critical shear rates for glycerol and mineral oils are above $10^5\ s^{-1}$ (Barnes, 2000).

The viscosity of most liquids decrease with an increase in temperature because of the increasing Brownian motion, and generally, the higher the viscosity, the greater is the rate of decrease (Barnes, 2000). In this paper, the Arrhenius model was found to describe the viscosity/temperature dependence, well:

$$\eta(T) = A_0 \cdot e^{E/(R \cdot T)}$$

where

A_0 = constant;
E = activation energy for viscous flow;
R = universal gas constant; and
T = temperature.

The objective of this work is to investigate the rheological behaviour of commercial cylinder oils, as knowing these properties are important to consider for designing two-stroke diesel engines and cylinder lubrication systems.

2. Materials

For this study, the commercial lubrication oils shown in Table I were investigated. The chosen materials are considered representative of the commercial cylinder lubrication oils on the current market. As shown, the different lubrication oils consist of different levels of BN.

3. Experimental methods

3.1 Rotational rheometry

Rotational rheometry (Figure 1(a)) is used to determine the viscosity in shear rates $\dot{\gamma}$ from 0.1 to 3,000 s^{-1} at 50°C, 60°C, 70°C and 80°C. The measurements are performed using a in a double gab configuration with gap sizes of G_1 = 0.465 and G_2 = 0.417 mm. Each specimen was heated and equilibrated for 5 min before measurement.

Table I Table of studied lubrication oils

Product name	Supplier	Base no.
Castrol Cyltech 40SX	BP Castrol	40 BN
Castrol Cyltech 70	BP Castrol	70 BN
Castrol Cyltech CL 100 ACC	BP Castrol	100 BN
Mobilgard 525	ExxonMobil	25 BN
Mobilgard 560 VS	ExxonMobil	60 BN
Mobilgard 570	ExxonMobil	70 BN
Mobilgard 5100	ExxonMobil	100 BN

Figure 1 Schematic illustration of the experimental methods – (a) rotational rheometry and (b) capillary rheometry. A detailed description of the methods can be found in Barnes (2000)

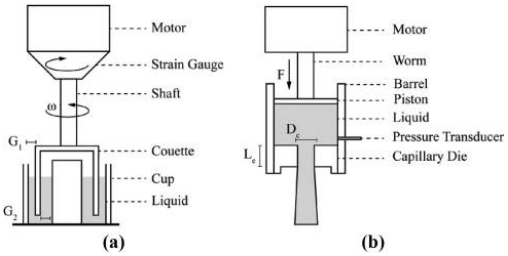

3.2 Capillary rheometry

Capillary rheometry (Figure 1(b)) is performed on Instron Ceast SR50 rheometer using a capillary die with a diameter of 0.3 mm and capillary length of 5 mm. This setup allows measuring the viscosity in shear rates $\dot{\gamma}$ from 5×10^5 to $1.3 \times 10^6\ s^{-1}$ at 50°C, because of the limits of instrument. Each specimen was heated and equilibrated for 5 min before measurements. No Bagley correction was performed on the test. This might lead to a slightly higher viscosity, as the measured pressure drop includes the entrance pressure drop.

For both methods, five repetitions of each experiments have been made, which is considered to be sufficient because of the reliability of the measuring devices.

4. Results and discussion

Figure 2 shows the viscosity as a function of shear rate for different lubrication oils. The results from both rotational and capillary rheometer are shown in the same figure, even though the two methods cannot be directly compared with each other. However, presenting the results in this way gives an indication of whether the oils behave as a Newtonian or non-Newtonian fluid.

The viscosities measured by the capillary rheometer is in general lower than the viscosities measured by the rotational rheometer, which might be due to the viscous heating induced in high shear rates or wall slip. The maximum viscosity

Figure 2 Viscosity of different cylinder oils as a function of shear rate at 50°C

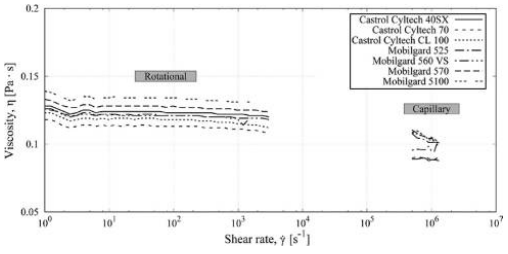

difference between rotational and capillary rheometer is 37.8 per cent with Castrol Cyltech 40SX and the lowest difference is 11.9 per cent with Castrol Cyltech CL100. Viscosity measurements performed by capillary and rotational rheometry have in other studies shown good correlation (Dao *et al.*, 2009). Even though there is a variation in viscosity between the two methods, the lubrication oils can be considered as Newtonian fluids because of no significant change in viscosity at different shear rates. The average viscosity values of the measured lubrication oils are shown in Table II. This shows that the viscosities of the studied lubrication oils are similar no matter the level of BN. It cannot be concluded whether the level of BN affects the viscosity of lubrication oils, as additives such as viscosity modifiers can be incorporated in the oils to ensure unchanged viscosity between the commercial lubrication oils.

4.1 Viscosity/temperature dependency

Figure 3 shows the viscosity/temperature dependency for the lubrication oils. The figure shows an exponential correlation between the viscosity and temperature. As shown in Table III, the tested lubrication oils are found to obey the Arrhenius model which is expressed in equation (1). The results show that the viscosity–temperature dependency is similar for the commercial lubrication oils on the market.

Table II Average viscosity values of the lubrication oil at 50°C

Product name	Base no.	Rotational (Pa·s)	Capillary (Pa·s)	Difference (%)
Castrol Cyltech 40SX	40 BN	0.122	0.089	37.8
Castrol Cyltech 70	70 BN	0.116	0.090	24.5
Castrol Cyltech CL 100 ACC	100 BN	0.116	0.104	11.9
Mobilgard 525	25 BN	0.120	0.103	16.7
Mobilgard 560 VS	60 BN	0.120	0.097	23.9
Mobilgard 570	70 BN	0.126	0.105	20.4
Mobilgard 5100	100 BN	0.132	0.106	25.0
Mean		0.122	0.099	

Figure 3 The viscosity of lubrication oils as a function of temperature

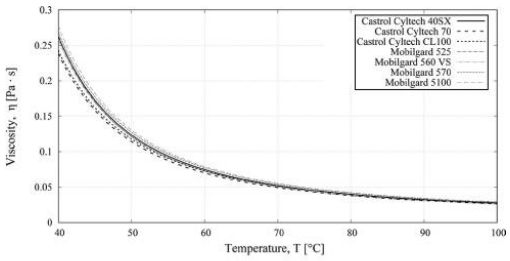

Notes: The measured values are fitted to the Arrhenius model. The Arrhenius parameters are shown in Table III

Table III This table shows the Arrhenius parameters of the lubrication oils

Product name	Base no.	A	E	R^2
Castrol Cyltech 40SX	40 BN	0.00601	1256	0.9915
Castrol Cyltech 70	70 BN	0.00593	1224	0.9931
Castrol Cyltech CL 100 ACC	100 BN	0.00650	1204	0.9934
Mobilgard 525	25 BN	0.00548	1286	0.9948
Mobilgard 560 VS	60 BN	0.00590	1256	0.9929
Mobilgard 570	70 BN	0.00641	1242	0.9941
Mobilgard 5100	100 BN	0.00641	1253	0.9939
Mean		0.00610	1246	

Note: The R^2 values indicate how well the Arrhenius model fit the measured data

5. Conclusion

In this study, the rheological behaviour of seven commercial lubrication oils for two-stroke marine diesel engines has been investigated. The lubrication oils consist of different levels of BN, which is an expression of alkalinity. The following main conclusions can be drawn from the present work:

- Viscosity measurements using rotational and capillary rheometry show that the studied lubrication oils behave as a Newtonian fluid in shear rates from 0.1 to $1.3 \times 10^6\ s^{-1}$. A minor drop in viscosity is observed in the capillary measurements compared to the rotational, but this is thought to be due to effects from, for example, viscous heating or wall slip.
- The viscosities of the studied lubrication oils are similar no matter the level of BN.
- The viscosity/temperature dependency was found to fit the Arrhenius model. Furthermore, the viscosity/temperature dependency of the studied lubrication oils is similar no matter the level of BN.
- It cannot be concluded whether the level of BN affects the viscosity of the commercial lubrication oils, as additives can be incorporated to ensure the same viscosity range for the commercial lubrication oils. To investigate whether BN affects the viscosity, the analysis has to be performed on compounds of BN and base oil without any additives.

References

Barnes, H.A. (2000), *A Handbook of Elementary Rheology*, University of Wales, Institute of Non-Newtonian Fluid Mechanics, Wales.

Cordtz, R., Schramm, J., Andreasen, A., Eskildsen, S.S. and Mayer, S. (2013), "Modeling the distribution of sulfur compounds in a large two stroke diesel engine", *Energy & Fuels*, Vol. 27 No. 3, pp. 1652-1660.

Dao, T.T., Ye, A.X., Shaito, A.A., Roye, N. and Hedman, K. (2009), *Capillary Rheometry: Analysis of Low-Viscosity Fluids, and Viscous Liquids and Melts at High Shear Rates*.

Eriksen, L. (2003), *Developments in Cylinder Liner Lubrication. In Recent Developments in Marine Engineering Operations*, Hans Jensen Lubricators A/S, Flensburg, pp. 1-8.

Fu, J., Lu, Y., Campbell, C.B., Papadopoulos, K.D., Che, V., Company, O. and Way, C.V. (2006), "Acid neutralization by marine cylinder lubricants inside a heating capillary:

strong/weak-stick collision mechanisms", *Industrial & Engineering Chemistry Research*, Vol. 45, pp. 5619-5627.

Huijbregts, W. and Leferink, R. (2004), "Latest advances in the understanding of acid dewpoint corrosion: corrosion and stress corrosion cracking in combustion gas condensates", *Anti-Corrosion Methods and Materials*, Vol. 51 No. 3, pp. 173-188.

Livanos, G.A. and Kyrtatos, N.P. (2007), "Friction model of a marine diesel engine piston assembly", *Tribology International*, Vol. 40 Nos 10/11/12, pp. 1441-1453.

Mohamad, S.A., Lu, X. and Zheng, Q. (2015), "Numerical modeling of lubrication of piston ring of two-stroke marine diesel engine considering the effect of multi-scale grooves on the cylinder liner", *Proceedings of the Institution of Mechanical Engineers, Part J: Journal of Engineering Tribology*, Vol. 229 No. 8, pp. 989-1002.

Olander, P., Hollman, P. and Jacobson, S. (2013), "Piston ring and cylinder liner wear aggravation caused by transition to greener ship transports–comparison of samples from test rig and field", *Wear*, Vol. 2, pp. 1345-1350.

Reiner, M. (1964). "The Deborah number", *Physics Today*, Vol. 17 No. 1, p. 62.

Sautermeister, F.A. and Priest, M. (2012), "Physical and chemical impact of sulphuric acid on cylinder lubrication for large 2-stroke marine diesel engines", *Tribology Letters*, Vol. 47 No. 2, pp. 261-271.

Sautermeister, F.A., Priest, M. and Fox, M.F. (2014), "FTIR lubricant analysis: concentration of dispersed sulphuric acid", *Industrial Lubrication and Tribology*, Vol. 66 No. 4, pp. 555-559.

Sautermeister, F., Priest, M., Lee, P. and Fox, M. (2013), "Impact of sulphuric acid on cylinder lubrication for large 2-stroke marine diesel engines: contact angle, interfacial tension and chemical interaction", *Tribology International*, Vol. 59, p. 47-56.

Schramm, J., Henningsen, S. and Sorenson, S.C. (1994), "Modelling of corrosion of cylinder liner in diesel engines caused by sulphur in the diesel fuel", SAE Technical Paper, 940818, SAE International, pp. 1-10, available at: http://papers.sae.org/940818/

Sherrington, I., Rowe, W.B. and Wood, R.J.K. (2002). *Total Tribology: Towards an Integrated Approach, Volume Tribology*, Professional Engineering, Wiley, available at: www.amazon.com/Total-Tribology-Integrated-Approach-Practice/dp/1860583938

Sigurdsson, E., Ingvorsen, K., Jensen, M., Mayer, S., Matlok, S. and Walther, J. (2014), "Numerical analysis of the scavenge flow and convective heat transfer in large two-stroke marine diesel engines", *Applied Energy*, Vol. 123, pp. 37-46.

Stolarski, T. and Zhou, Q. (2002), "Temperature–friction characteristics of used lubricant from two-stroke cross-head marine diesel engines", *Wear*, Vol. 252 Nos 3/4, pp. 300-305.

Valenti, G., Colombo, L., Murgia, S., Lucchini, A., Sampietro, A., Capoferri, A. and Araneo, L. (2013), "Thermal effect of lubricating oil in positive-displacement air compressors", *Applied Thermal Engineering*, Vol. 51 Nos 1/2, pp. 1055-1066.

Voelund, A. and Felter, C. (2010), "Experimental investigation of lubrication regimes on piston ring - cylinder liner contacts for large two-stroke engines", in 26 CIMAC World Congress; CIMAC, Bergen, 2010.

Wu, R.C., Campbell, C.B. and Papadopoulos, K.D. (2000), "Acid-neutralizing of marine cylinder lubricants – effects of nonionic surfactants", *Industrial & Engineering Chemistry Research*, Vol. 39 No. 10, pp. 3926-3931.

Yahagi, Y. (1987), "Corrosive wear of diesel engine cylinder bore", *Tribology International*, Vol. 20 No. 6, pp. 365-373.

Corresponding author

Rathesan Ravendran can be contacted at: rra@hjlubri.dk

Paper B

Title: CFD analysis of cavitation structures in viscous liquid spray systems

Authors: R. Ravendran*, J. d. Christiansen, B. Endelt, P. Jensen, and J. A. Kepler

Submitted to Journal: Engineering Applications of Computational Fluid Mechanics

Publisher: Taylor & Francis [ISSN 1994-2060]

Background: This paper investigates hypothesis II in chapter 4.

Abstract: In order to understand spray process of lubricating the cylinder liner of large two-stroke marine diesel engines, the internal nozzle flow of spray injection valves has been studied using high-speed shadowgraphic images and CFD simulations. The modelling is carried out in the open-source CFD software package OpenFOAM using a standard incompressible multiphase flow solver.
The experimental work showed that cavitation plays an important role in terms of droplet breakup and atomization. The simulation model is able to predict similar behavior as observed experimentally. Two types of cavitation where identified in the nozzle volume; edge cavitation and vortex/string cavitation. For this specific nozzle geometry, cavitation extends to the nozzle exit when the liquid temperature is above 100 °. This increases the degree of atomization significantly.

CFD analysis of cavitation structures in viscous liquid spray systems

Engineering Applications of Computational Fluid Mechanics

Rathesan Ravendran[*a], Jesper de Claville Christiansen[b], Benny Endelt[b], Peter Jensen[a] , Jørgen Asbøll Kepler[b],

a) Hans Jensen Lubricators, Smedevænget 1-3, 9560 Hadsund, Denmark.
b) Department of Materials and Production, Aalborg University, Aalborg, Denmark

Abstract: In order to understand spray process of lubricating the cylinder liner of large two-stroke marine diesel engines, the internal nozzle flow of spray injection valves has been studied using high-speed shadowgraphic images and CFD simulations. The modelling is carried out in the open-source CFD software package OpenFOAM using a standard incompressible multiphase flow solver.

The experimental work showed that cavitation plays an important role in terms of droplet breakup and atomization. The simulation model is able to predict similar behavior as observed experimentally. Two types of cavitation where identified in the nozzle volume; edge cavitation and vortex/string cavitation. For this specific nozzle geometry, cavitation extends to the nozzle exit when the liquid temperature is above 100 ℃. This increases the degree of atomization significantly.

Keywords: Atomization, Cavitation, Viscous liquids, Nozzle internal flow, CFD, OpenFOAM.

NOMENCLATURE:

A, B, C = Dimensionless constants	**Greek letters**
D = Diameter	α = Vapor volume fraction
n_c= nuclei number density per unit volume	μ = Viscosity
p = Pressure	ρ = Density
T = Temperature	σ = Cavitation number
R = Ideal gas constant	
U_n = Mean velocity	**Subscripts**
u = velocity	a = atmospheric
R = Source terms	c = condensation
Re = Reynolds number	e = evaporation
t = time	l = liquid
	m = mixture
	v = vapor

INTRODUCTION

Atomization of viscous liquids using pressure spray systems require high pressure, compared to similar atomization of low-viscosity liquids. To enhance the degree of liquid atomization, the internal nozzle geometry can be designed to promote cavitation. Cavitation is the formation of cavities where the pressure difference is insufficient to enforce fluid conformity to a rigid surface. The low pressure in the cavities promotes evaporation, when the local pressure of the liquid drops below its vapor pressure (Franc & Michel, 2006; Li, 2014). The most well-known type of cavitation in spray nozzles is geometrically induced cavitation (Dumouchel, Leboucher, & Lisiecki, 2013). This is when a change in geometry, through which the liquid flows, leads to a pressure drop sufficient to evaporate the liquid.

Cavitation in the nozzle enhances the jet atomization, because it introduces large a number of disturbances which results in a stochastic behavior of the liquid stream that destabilizes the jet (Bergwerk, 1959; Gavaises, Villa, Koukouvinis, Marengo, & Franc, 2015). Not only sharp inlet orifices promote cavitation, but also parameters as e.g. needle lift, length to diameter ratio of the discharge orifice, curvature of the inlet edge, liquid properties, and system pressure (Dong, Inaba, Nishida, & Shimo, 2016; Jollet, Hansen, Bitner, Niemeyer, &

Dinkelacker, 2014; R H Pratama, Sou, Wada, & Yokohata, 2015; Schmidt & Corradini, 2001; Taghavifar, Shervani-Tabar, & Abbasalizadeh, 2013). Andriotis et al. (2008)(Andriotis et al., 2008) investigated non-axial injection conditions, and showed that the swirling liquid flow inside the nozzle leads to complex phenomena, as string cavitation or vortex cavitation.

Due to the complex nature of cavitation and difficulties in observing cavitation in real-scale nozzles, development of accurate Computational Fluid Dynamics (CFD) simulation models for capturing the in-nozzle cavitating flow has been studied intensively (Dabiri, Sirignano, & Joseph, 2007; Mariasiu, 2013; Schmidt & Corradini, 2001; Soriano-Palao, Sommerfeld, & Burkhardt, 2014). One of the popular approaches to model cavitation inside the nozzle is the homogenous equilibrium mixture two-phase method (HEM) (Roohi, Zahiri, & Passandideh-Fard, 2013; Schmidt & Corradini, 2001), which assume that the liquid and gas phases are perfectly mixed in a cell. This means that there is only one set of equations, hence reducing computational time. The most difficult part of this method is to determine the boundary conditions. A bartropic law is often used to calculate the growth and collapse of cavitation (Biçer & Sou, 2016; Roohi et al., 2013).

State-of-the-art modeling approaches focus on low viscous liquids such as water and diesel fuel, and not much work has been performed on modelling high-viscous cavitating flow inside spray nozzles (Andriotis & Gavaises, 2009; Anvari, Taghavifar, Khalilarya, Jafarmadar, & Shervani-Tabar, 2016; Biçer & Sou, 2016; Brusiani, Falfari, & Pelloni, 2014; Soriano-Palao et al., 2014; Yuan, Sauer, & Schnerr, 2001). This leads to the objective of this paper; to investigate if the HEM-method can be applied to simulate the in-nozzle cavitation for high-viscous liquids. The analysis is performed on a spray lubrication system used to lubricate the cylinder liner of large two-stroke marine diesel engines. The viscosity grade of commercial lubrication oils is typically SAE50, and is therefore considered as being viscous compared to e.g. diesel fuel oil and water. The CFD simulations verified with experiments using high-speed shadowgrapic visualization to determine the cavitation structures inside the nozzle volume.

EXPERIMENTAL SETUP

In this study, cavitation inside the spray nozzle is captured using a shadowgrapic imaging technique. In general, the shadowgraph highlights the difference in refractive index at the interface between an object and its surroundings, or between liquid media. The light that is illuminated from the behind of the object and that does not interact with the object produces a

bright background. Whereas, the light refracted at the interface is dispersed and thus the interface appears dark.

The tip of the nozzle is manufactured in a transparent Poly(methyl methacrylate) (PMMA) material. It was found that the refractive index of lubrication oil and PMMA material matched, and therefore refraction appears only at the phase interface between the liquid and vapor. This means that phase interfaces, such as cavitation, will appear as a dark shadow on the image. The nozzle configuration and its internal geometry is shown in Figure 1.

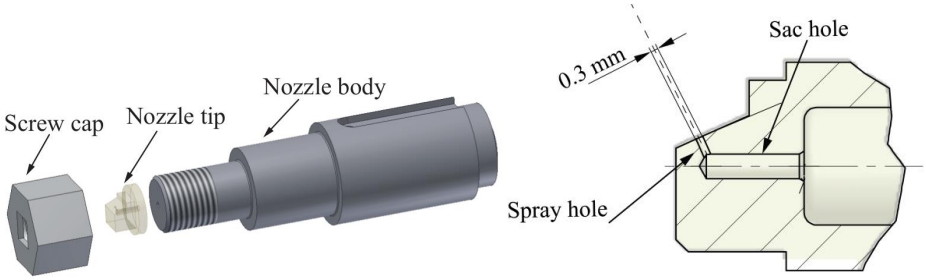

Figure 1: The nozzle configuration and its internal geometry of the HJ-SIP spray injection valve.

The experimental setup is illustrated in Figure 2. The setup consists of a HJ Lubtronic system (Figure 2a) from Hans Jensen Lubricators A/S, which delivers 50 mg lubrication oil per injection to a heated HJ-SIP injection valve (Figure 2b). The opening pressure of the injection valve is 4.0 MPa. The lubrication oil is injected in to ambient atmospheric conditions. The lubricator is supplied with 6 MPa in hydraulic pressure from a pump station (Figure 2c) and fresh lubrication oil from a heated reservoir (Figure 2d). The high-speed camera (Figure 2e) used in this study is a Photron Fastcam SA5. Images are taken with a frame rate of 1000 fps with a shutter speed of 1/161000. A 1000W halogen lamp is used as illumination source (Figure 2f). Both the high-speed camera and the lubricator are controlled by a computer (Figure 2g). The lubrication oil used is Mobilgard 570, which is a commercial lubrication oil from ExxonMobil. The properties of the lubrication oil are shown in Table 1.

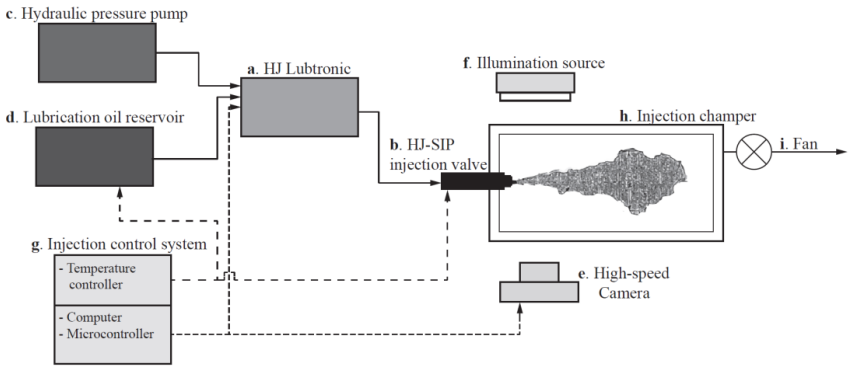

Figure 2: The experimental setup used to detect the internal nozzle cavitation.

The experiments are conducted at various Reynolds numbers Re and cavitation numbers σ, which are described in equation 1 and 2 respectively. The cavitation number is a dimensionless quantity like the Reynolds number, but describes the degree of cavitation. The smaller cavitation number, the probability of cavitation is higher.

$$\mathrm{Re} = \frac{\rho_l \cdot U_n \cdot D}{\mu_l} \tag{1}$$

$$\sigma = \frac{P_a - P_v}{0.5 \cdot \rho_l \cdot U_n^2} \tag{2}$$

where P_a is the atmospheric pressure, P_v is the liquid vapor pressure, ρ_l the liquid density, U_n the mean liquid velocity in the nozzle, μ_l is the viscosity, and D is the diameter of the spray hole. The Reynolds number and cavitation number are in this study controlled by the liquid temperature. The change in temperature has the highest impact on the Reynolds number, as an increase liquid temperature reduces the liquid viscosity and vice versa. The Reynolds number for the experiments is between 200 and 800, and therefore the flow inside the spray nozzle is considered to be laminar.

Table 1. Lubrication oil properties used in this study. In the following equations R is the ideal gas constant, and T is the temperature of the lubrication oil expressed in Celsius.

Oil property	**Value**	**Reference**
Vapor Pressure	$P_v(T) = 10 \cdot e^{(A \cdot T - B)/((20.0 \cdot T + C)) \cdot \mathrm{R}}$ The dimensionless constants are A = 1094, B = $3.458 \cdot 10^5$, and C = 5463.0.	Derived using the Clausius-Clapeyron equation
Liquid Density	$\rho_l(T) = 0.6087 \cdot T + 943.97$	Measured
Liquid Viscosity	$\mu_l(T) = 0.00610 \cdot e^{1246/(\mathrm{R} \cdot T)}$	(Ravendran, Christiansen, Endelt, Jensen, & Jensen, 2017)
Vapor Density	$\rho_v = 16.05\ \mathrm{kg \cdot m^{-3}}$	(Assael, Dalaouti, & Vesovic, 2001)
Vapor Viscosity	$\mu_v = 11.58\ \mu\mathrm{Pa \cdot s}$	(Assael et al., 2001)

NUMERICAL SETUP

In general, the difficulties of modelling cavitating flows include: sharp changes in the fluid density, existence of a moving boundary, and the requirement of modelling phase change (Giannadakis, Gavaises, & Arcoumanis, 2008; Roohi et al., 2013; Zhu, Chen, Zhao, & Zhang, 2015). Thus, a number of methods for modelling has been proposed in the literature. The existing cavitation modelling approaches can be classified into three categories; Volume of fluid (VOF), Two-Fluid model, and Homogeneous equilibrium mixture (HEM). Common for these approaches is that there is a two-phase treatment of the liquid and gas, and as well as a separate treatment of the phase transition between vaporization and condensation.

A short overview of the models is given in the following:

- *Volume of fluid (VOF)* assumes that there is a clear and discontinuous interphase between the liquid and vapor (Ghiji, Goldsworthy, Brandner, Garaniya, & Hield, 2017; Koch et al., 2016). The interphase tracking scheme used in this method, requires the resolution of all involved length and time scales to accurately predict the

interface between liquid and vapor (Marcer & LeGouez, 2001; Roohi et al., 2013; H. Yu, Goldsworthy, Brandner, & Garaniya, 2016).

- *Two-Fluid model* assumes the liquid and vapor co-exist in each cell, thus treating two sets of conservation equations: one for the liquid phase and one for the vapor (von Berg et al., 2005; X. Wang & Su, 2009). The interaction between the phases are included by additional source terms in the conservation equations.
- *Homogeneous equilibrium mixture (HEM)* assumes the vapor and liquid are perfectly mixed in each cell (Hoyas, Gil, Fajardo, Khuong-Anh, & Ravet, 2012; Salvador, Romero, Roselló, & Martínez-López, 2010). There is therefore only one set of equations. Phase transfer is treated by either a barotropic equations of state or mass transfer models (Baldwin et al., 2016; Mohan, Yang, & Chou, 2014; Morgut, Nobile, & Biluš, 2011; Sou, Bicer, & Tomiyama, 2014; X. Wang & Su, 2009).

In this publication, the internal flow is modelled using the homogeneous equilibrium two-phase mixture method (HEM), because it is less computational demanding than VOF and Two-Fluid model (Bicer & Sou, 2015). The VOF model requires high resolution in order to track the interface, while the Two-Fluid model uses a more detailed description of the flow. The HEM method is a popular method for simulating the cavitation phenomenon inside injection nozzles (Bicer & Sou, 2015; Karrholm, 2008; Salvador et al., 2010; Schmidt & Corradini, 2001; Vallier, 2013)

Governing equations

The continuity equation and the momentum equations for the mixture are described as follows:

$$\frac{\delta \rho_m}{\delta t} + \mathrm{div}(\rho_m \mathbf{u}) = 0 \tag{3}$$

$$\frac{\delta \rho_m}{\delta t} + \mathrm{div}(\rho_m \mathbf{u}\mathbf{u}) = -\mathrm{div}\,\mathbf{p} + \mathrm{div}(\mu_m\, \mathrm{grad}\,\mathbf{u}) \tag{4}$$

where t is time, **u** and **p** is the velocity and the pressure of the mixture. ρ_m and μ_m is the mixture density and mixture viscosity, which is determined by the volume fraction of the liquid phase α_l using the following equations:

$$\rho_m = (1-\alpha_l)\rho_v + \alpha_l \rho_l \tag{5}$$

$$\mu_m = (1-\alpha_l)\mu_v + \alpha_l \mu_l \tag{6}$$

The subscripts l and v indicate the liquid and vapor phase, respectively.

Cavitation model

The mass transfer rate between liquid and vapor phase is described using equation 7.

$$\frac{\delta \alpha_l \rho_l}{\delta t} + \nabla \cdot (\alpha_l \rho_l \mathbf{U}) = R_c + R_e \tag{7}$$

where R_c and R_e are the mass transfer source terms for condensation and evaporation, respectively. There are different methods for determining these source terms e.g. full cavitation model, Zwart model, Kunz model, Singhal Full model, Schnerr-Sauer model (Morgut et al., 2011; G. Wang, Senocak, Shyy, Ikohagi, & Cao, 2001; Yuan et al., 2001). The main difference between the methods is the assumption of how to treat the growth and collapse of the cavitation bubbles inside the liquid volume. The cavitation model proposed by Sauer and Schnerr (2000) is used in this study.

The Schnerr-Saur cavitation model is a simplified form of the Rayleigh-Plesset equation, where viscous terms, surface tension, incondensable gas, and high-order terms are ignored (Bițer and Sou, 2015; Yuan et al., 2001). The mass transfer rate for the evaporation R_e and the condensation R_c is given in equation 8 and 9. The equations take vapor pressure P_v, as a threshold for evaporation and condensation.

$$R_e = -C_v \frac{3\rho_l \rho_v}{\rho_m} \frac{\alpha_l (1 - \alpha_l)}{R_b} \operatorname{sgn}(P_v - P_l) \cdot \sqrt{\frac{2|P_v - P_l|}{3\rho_l}} \tag{8}$$

$$R_c = -C_c \frac{3\rho_l \rho_v}{\rho_m} \frac{\alpha_l (1 - \alpha_l)}{R_b} \operatorname{sgn}(P_l - P_v) \cdot \sqrt{\frac{2|P_v - P_l|}{3\rho_l}} \tag{9}$$

where R_b is the initial bubble radius, C_c and C_v are the rate constants for condensation and evaporation. The initial bubble radius b is set to $10 \cdot 10^{-4}$ m in all the present simulations. The rate constant for evaporation is set to 100, and the constant for condensation is set to 0.01. Furthermore, the nuclei number density per unit volume n_c is set to be 10^{16} m^{-3}. These constants are fitting parameters and are hold constant for the calculations.

The Schneer-Saur model allows turbulence viscosity to be included (Yuan et al., 2001). However, turbulence is not taken into account in the present simulations, because a Reynolds number below 2000 indicates a laminar flow. If turbulence viscosity is taken into account, it

will lead to a higher total viscosity which results in decreased dynamic pressure and therefore less cavitation.

Computational grid and boundary conditions

The operating conditions were set according to the experimental conditions with an inlet pressure P_{inlet} = 4.0 MPa and outlet pressure P_{atm} equal to the environment pressure at 0.1 MPa (see Figure 3). The transient needle movement is not included in this model, as the length of the sac hole is assumed to cancel out the turbulence effect from the needle motion.

The interPhaseChangeFoam solver in OpenFOAM 3.0 is used to perform the numerical simulations. Gauss Upwind scheme is used for numerical discretization. The simulations are performed with adjustable time step limited by the Courant number. The Courant number is set to 0.5 and the initial time step Δt is set to 10^{-7} s. The results in this study show the steady state solution at 0.002 s.

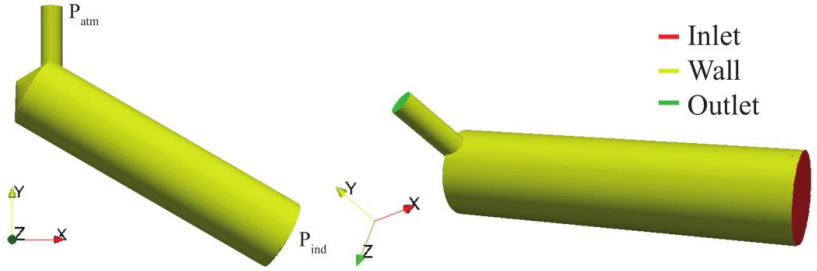

Figure 3: Overview of the nozzle volume domain and boundary conditions. The flow through the nozzle is driven by the pressure difference between the inlet and outlet.

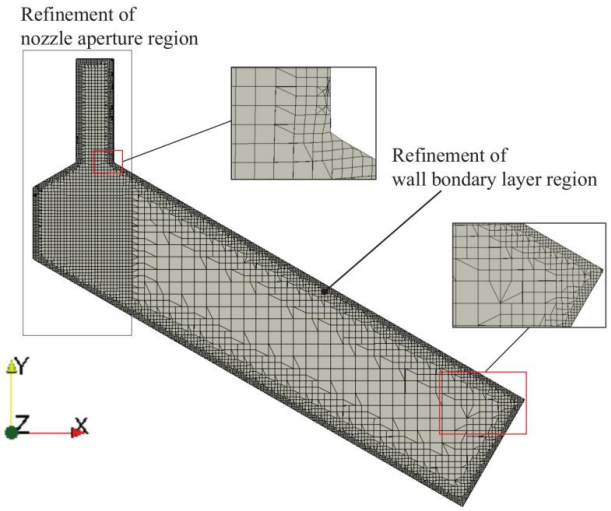

Figure 4: The cross-sectional view of the nozzle volume shows the generated mesh. A finer mesh resolution at the wall boundary layer and the nozzle aperture region is applied.

The computational grid is shown in Figure 4, which is made of a structured grid with 404,098 hexahedral cells and 16 cells across the diameter of the nozzle aperture. The quality of the mesh plays a significant role in the accuracy of the numerical model, as the flow behavior and cavitation is highly dependent on the sharpness of edges. Even minor changes in roundness between the sac and spray hole may lead to differences (Dabiri et al., 2007).

RESULTS AND DISCUSSION

A description of the formed cavitation and its behavior inside the nozzle is given first. Hereafter, the CFD simulations are compared to the experimental images to conclude whether similar behaviors can be observed. From the experimental images and simulations, a number of questions may be raised regarding the dynamics of cavitation, the origin of cavitation and how cavitation influences the nozzle flow and the subsequent spray. These questions will be addressed in the following sections.

Dynamics of cavitation and its origin

Figure 5 shows shadowgraphic images of the internal nozzle flow at different liquid temperatures. It is shown that cavitation is not present, when the liquid temperature is 60 ℃. As temperature increases, cavitation emerges at the center of the spray hole. The size of cavitation is highly dependent on the liquid temperature, as both length and width of the

cavitation increases with increasing temperature and thus reduced viscosity. When the liquid temperature is above 100 ℃, the cavitation extends to the nozzle exit. This is an indication of hydraulic flip (Sou, Hosokawa, & Tomiyama, 2007), which will suppress liquid atomization. However, CFD simulations indicate the presence of vortex/string cavitation formed by the swirling flow inside the spray hole. Figure 6 show, the simulation results where the level of vapor fraction indicate the zones with cavitation.

The simulations show similar behavior as the experimental images, and correlate with the observations shown in Figure 5. Cavitation is not present at 60 ℃, but emerges as the temperature increases. At the beginning of the spray hole, a high degree of cavitation is attached at one side of the wall. This mechanism is known as edge cavitation, and is created by the pressure drop in the liquid at the wall. Towards the exit of the spray hole, two converging cavitation strings perpendicular to spray hole are developed at the center. In general, cavitation strings are created in strong recirculation zones in the liquid, where the liquid pressure drops below its vapor pressure (Andriotis et al., 2008; Miranda, Chaves, & Obermeier, 2002; Mitroglou & Gavaises, 2013; Raditya Hendra Pratama, Sou, Tokihiro, & Shigeru, 2017; Watanabe et al., 2015). In this case, these recirculation zones are provoked by the the asymmetrical geometry of the nozzle volume which create a swirling motion of the liquid. Figure 7 shows a illustration of the two separate mechanisms forming the cavitation structures inside nozzle volume.

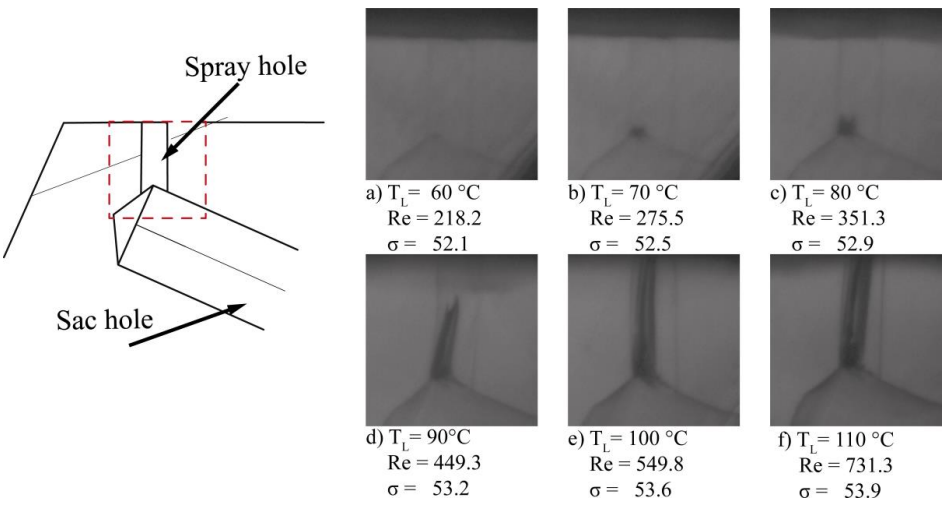

Figure 5: High-speed shadowgraphic images of the internal nozzle flow. The images are taken after 0.002 s after injection.

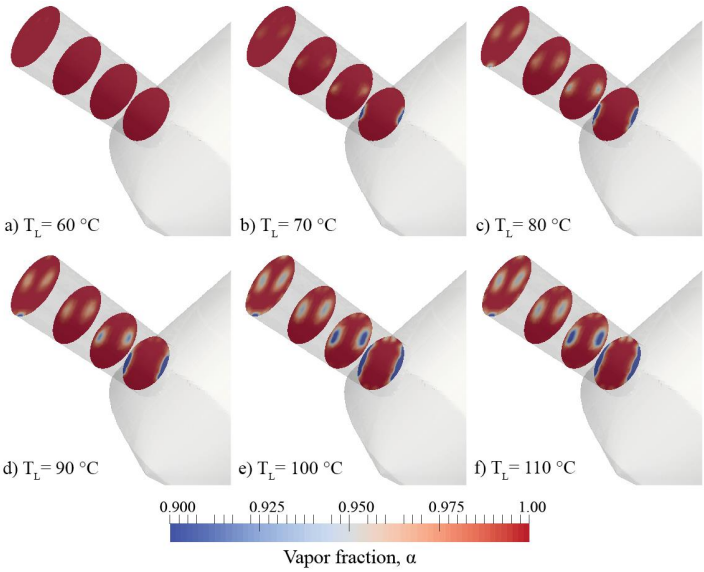

Figure 6: Results from the numerical simulations showing the cavitation structures.

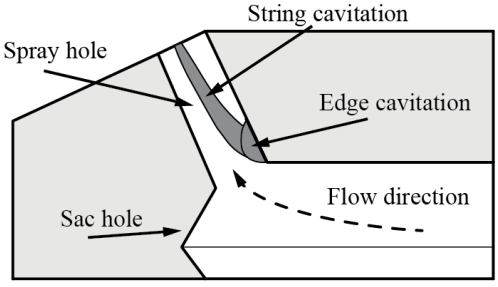

Figure 7: Illustration of the cavitation structures in the nozzle volume.

Figure 8 shows velocity of the liquid throughout the spray hole for different injection conditions. It should be noticed that the velocity is represented by the three velocity components (U_x, U_y, U_z), and that the colour scales are different for the three components. It is seen that the swirling flow is prominent at higher temperatures, and at low temperatures the flow is non-swirling and axisymmetric.

When the liquid temperature is 60 ℃, the velocity component U_y is uniform at the nozzle exit and can be described using an elliptic paraboloid with maximum at center. Furthermore, the velocity components U_x and U_z are small compared U_y. As temperature increases two recirculation zones develop at the center of the spray hole and symmetry is only kept across

the x-axis. These recirculation zones are the reason to the observed cavitation strings. Furthermore, the velocity component U_y becomes non-uniform and the magnitude of U_x and U_z increases at increasing temperature. A smaller ratio between U_y and the velocity components in x- and z-direction means that more disturbances are introduced to the liquid flow, which leads to an increased degree of droplet breakup (Moon et al., 2015; Y. Yu, Li, Wang, & Ding, 2016).

Though the nozzle flow is considered laminar due to the high viscosity of the liquid, it should be investigated how dissipation and heat from cavitation changes the local liquid properties. These effects are not considered in the simulations, and may influence the accuracy of the results.

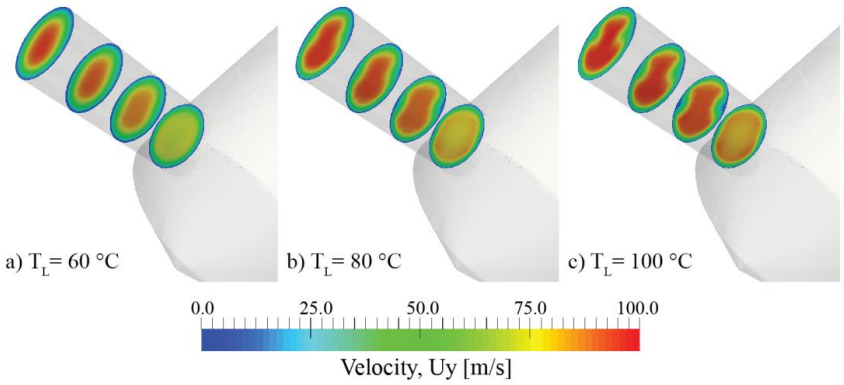

a) Velocity Uy for three different injection cases.

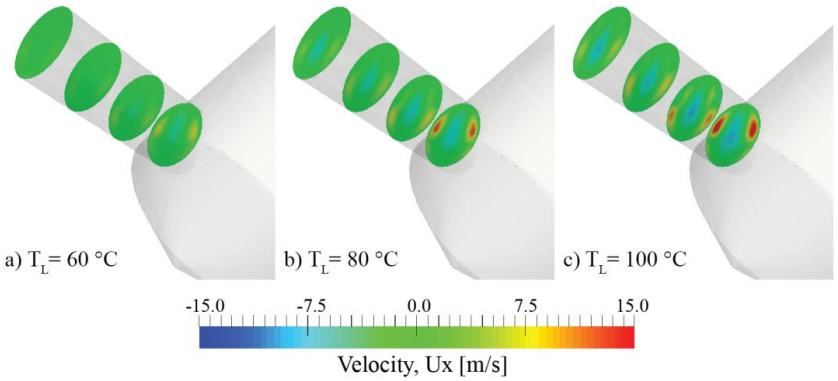

b) Velocity Ux for three different injection cases.

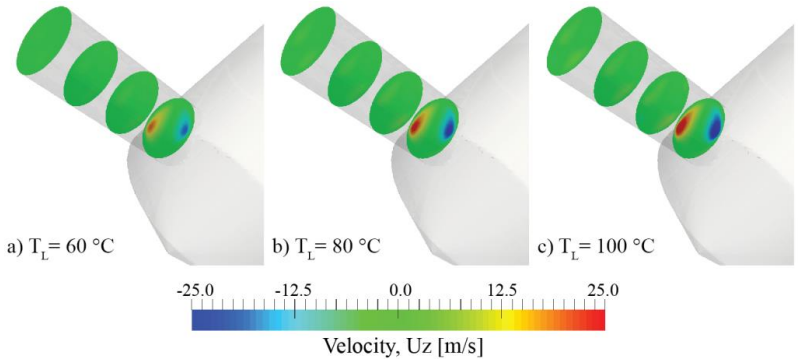

c) Velocity Uz for three different injection cases.

Figure 8: Results from the numerical simulations showing the velocity of the liquid through the nozzle exit.

The effect of vortex cavitation on spray formation

Having identified the mechanisms leading to the cavitation structures and their dependence on liquid temperature, it is considered important to investigate the effects on the subsequent spray. Figure 9 shows shadowgraphic images of the liquid stream injected into the atmosphere. The images show that the liquid is undisturbed and jet shaped at temperatures up to 100 ℃. Whereas at 100 ℃ and 110 ℃, the liquid stream is more disrupted and the spray angle is increased. Furthermore, this also leads to shorter breakup-length and enhanced degree of liquid atomization.

Comparing the observations made from the internal flow (Figure 5) and subsequent spray (Figure 9), it is obvious that the degree of atomization increases significantly if the cavitation extends to end of the spray hole. This is in contrast to cases where the cavitation collapses in the nozzle volume, which results in a jet-shaped liquid stream. It is assumed, that the different behavior is due to viscoelastic damping of the liquid. If the cavitation collapses inside the nozzle volume, the liquid will stabilize the stochastic disturbances introduced and when the cavitation extends to the exit the disturbances are directly transferred to the spray.

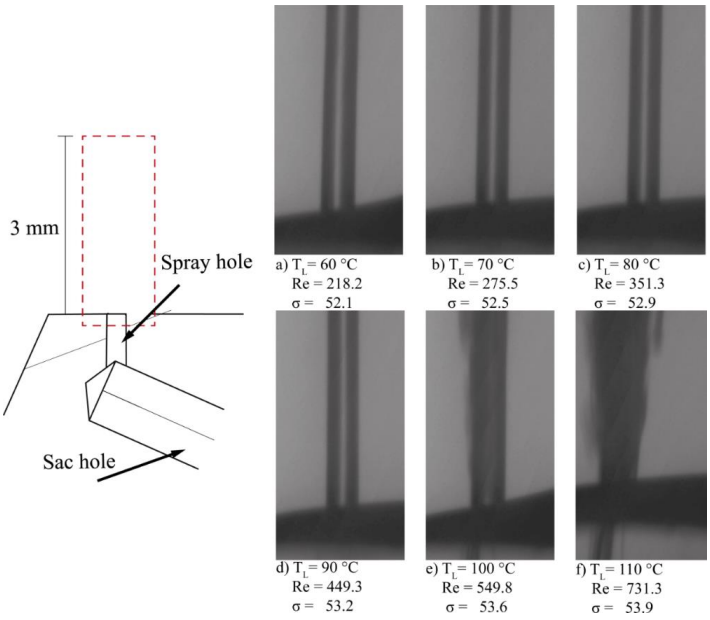

Figure 9: High-speed shadowgrapic images of the subsequent spray. Images are taken 0.002s after injection.

CONCLUSION

In this study, the internal nozzle flow of HJ-SIP spray injection valves has studied using high-speed shadowgraphic images and CFD simulations. The liquid medium is cylinder oil, which is high-viscous compared to e.g. diesel fuel and water, and therefore it was found out that cavitation plays an important role in terms of droplet breakup and atomisation. Following conclusions can be drawn from the present work:

- Two types of cavitation are identified in the nozzle volume; edge cavitation and string cavitation.
- The size of cavitation is highly dependent on the liquid temperature, as both length and width of the cavitation increases with increasing temperature.
- For this specific nozzle geometry, cavitation extends to the nozzle exit when the liquid temperature is above 100 ℃. This increases the degree of atomization significantly. However, when the cavitation collapses in the nozzle volume, the viscous liquid is able to stabilize the stochastic disturbances introduced by the cavitation.

- The homogenous mixture model together with Schneer-Saur cavitation model can be applied to simulate the cavitation in high-viscous liquids. The simulation model is able to predict similar behavior as observed experimentally.

ACKNOWLEDGEMENTS

We thank Hans Jensen Lubrication A/S for financial and equipment support for the work. Furthermore, equipment used for the work was also supported by the Poul Due Jensen Foundation.

REFERENCES

Andriotis, A., & Gavaises, M. (2009). INFLUENCE OF VORTEX FLOW AND CAVITATION ON NEAR-NOZZLE DIESEL SPRAY DISPERSION ANGLE. *Atomization and Sprays*, *19*(3).

Andriotis, A., Gavaises, M., & Arcoumanis, C. (2008). Vortex flow and cavitation in diesel injector nozzles. *Journal of Fluid Mechanics*, *610*, 195–215. https://doi.org/10.1017/S0022112008002668

Anvari, S., Taghavifar, H., Khalilarya, S., Jafarmadar, S., & Shervani-Tabar, M. T. (2016). Numerical simulation of diesel injector nozzle flow and in-cylinder spray evolution. *Applied Mathematical Modelling*, *40*(19–20), 8617–8629. https://doi.org/10.1016/j.apm.2016.05.017

Assael, M. J., Dalaouti, N. K., & Vesovic, V. (2001). Viscosity of Natural-Gas Mixtures: Measurements and Prediction. *International Journal of Thermophysics*, *22*(1), 61–71. https://doi.org/10.1023/A:1006784814390

Baldwin, E. T., Grover, R. O., Parrish, S. E., Duke, D. J., Matusik, K. E., Powell, C. F., … Schmidt, D. P. (2016). String flash-boiling in gasoline direct injection simulations with transient needle motion. *International Journal of Multiphase Flow*, *87*, 90–101. https://doi.org/10.1016/j.ijmultiphaseflow.2016.09.004

Bergwerk, W. (1959). Flow pattern in Diesel Nozzle Spray Hole. *Proceedings of the Institution of Mechanical Engineers*, *173*. https://doi.org/10.1243/PIME_PROC_1959_173_054_02

Bicer, B., & Sou, A. (2015). NUMERICAL MODELS FOR SIMULATION OF

CAVITATION IN DIESEL INJECTOR NOZZLES. *Atomization and Sprays*, *25*(12).

Biçer, B., & Sou, A. (2016). Application of the improved cavitation model to turbulent cavitating flow in fuel injector nozzle. *Applied Mathematical Modelling*, *40*(7–8), 4712–4726. https://doi.org/10.1016/j.apm.2015.11.049

Brusiani, F., Falfari, S., & Pelloni, P. (2014). Influence of the diesel injector hole geometry on the flow conditions emerging from the nozzle. *Energy Procedia*, *45*, 749–758. https://doi.org/10.1016/j.egypro.2014.01.080

Dabiri, S., Sirignano, W. a., & Joseph, D. D. (2007). Cavitation in an orifice flow. *Physics of Fluids*, *19*. https://doi.org/10.1063/1.2750655

Dong, P., Inaba, T., Nishida, K., & Shimo, D. (2016). Characteristics of the internal flow and the near-field spray of a single-hole injector and a multi-hole injector for diesel engines. *Proceedings of the Institution of Mechanical Engineers*, *230*(5), 632–649. https://doi.org/10.1177/0954407015591299

Dumouchel, C., Leboucher, N., & Lisiecki, D. (2013). Cavitation and primary atomization in real injectors at low injection pressure condition. *Experiments in Fluids*, *54*(6), 1–17. https://doi.org/10.1007/s00348-013-1554-y

Franc, J.-P., & Michel, J.-M. (2006). *Fundamentals of Cavitation*. Springer Science + Business Media, Inc. Retrieved from https://books.google.dk/books/about/Fundamentals_of_Cavitation.html?id=QJOQYa_oo24C&pgis=1

Gavaises, M., Villa, F., Koukouvinis, P., Marengo, M., & Franc, J.-P. (2015). Visualisation and les simulation of cavitation cloud formation and collapse in an axisymmetric geometry. *International Journal of Multiphase Flow*, *68*, 14–26. https://doi.org/10.1016/j.ijmultiphaseflow.2014.09.008

Ghiji, M., Goldsworthy, L., Brandner, P. A., Garaniya, V., & Hield, P. (2017). Analysis of diesel spray dynamics using a compressible Eulerian/VOF/LES model and microscopic shadowgraphy. *Fuel*, *188*, 352–366. https://doi.org/10.1016/j.fuel.2016.10.041

Giannadakis, E., Gavaises, M., & Arcoumanis, C. (2008). Modelling of cavitation in diesel injector nozzles. *Journal of Fluid Mechanics*, *616*, 153–193.

https://doi.org/10.1017/S0022112008003777

Hoyas, S., Gil, A., Fajardo, P., Khuong-Anh, D., & Ravet, F. (2012). Evaluation and Validation of ELSA Model in Diesel Sprays - 3D Cavitating Nozzles Case. *ICLASS-2012*.

Jollet, S., Hansen, H., Bitner, K., Niemeyer, D., & Dinkelacker, F. (2014). Experimental and numerical investigations of 90 micrometer real-size transparent nozzles with high pressure conditions. *ILASS-Europe 2014*.

Karrholm, F. P. (2008). *Numerical modelling of diesel spray injection, turbulence interaction and combustion*. *Thesis*. Chalmers University of Technology.

Koch, M., Lechner, C., Reuter, F., Köhler, K., Mettin, R., & Lauterborn, W. (2016). Numerical modeling of laser generated cavitation bubbles with the finite volume and volume of fluid method, using OpenFOAM. *Computers and Fluids*, *126*, 71–90. https://doi.org/10.1016/j.compfluid.2015.11.008

Li, Z. (2014). Criteria for jet cavitation and cavitation jet drilling. *International Journal of Rock Mechanics and Mining Sciences*, *71*, 204–207. https://doi.org/10.1016/j.ijrmms.2014.03.021

Marcer, R., & LeGouez, J. M. (2001). Simulation of unsteady cavitating flows in diesel injector with an improved VOF method. *ILASS-Europe 2001*. https://doi.org/10.13140/RG.2.1.4853.5129

Mariasiu, F. (2013). Numerical Investigation of the Effects of Biofuel Characteristics on the Injector Nozzle Erosion Process. *Tribology Transactions*, *56*(2), 161–168. https://doi.org/10.1080/10402004.2012.709918

Miranda, R., Chaves, H., & Obermeier, F. (2002). Imaging of Cavitation, Hollow Jets and Jet Branching at Low Lift in a Real Size VCO Nozzle. *ILASS-Europe 2002*, *i*(September), 2–6. Retrieved from http://www.ilasseurope.org/ICLASS/ilass2002/sessions.html

Mitroglou, N., & Gavaises, M. (2013). Mapping of cavitating flow regimes in injectors for medium-/heavy-duty diesel engines. *International Journal of Engine Research*, *14*(6), 590–605. https://doi.org/10.1177/1468087413500491

Mohan, B., Yang, W., & Chou, S. (2014). Cavitation in Injector Nozzle Holes – A Parametric

Study. *Engineering Applications of Computational Fluid Mechanics*, *8*(1), 70–81. https://doi.org/10.1080/19942060.2014.11015498

Moon, S., Gao, Y., Park, S., Wang, J., Kurimoto, N., & Nishijima, Y. (2015). Effect of the number and position of nozzle holes on in- and near-nozzle dynamic characteristics of diesel injection. *Fuel*, *150*, 112–122. https://doi.org/10.1016/j.fuel.2015.01.097

Morgut, M., Nobile, E., & Biluš, I. (2011). Comparison of mass transfer models for the numerical prediction of sheet cavitation around a hydrofoil. *International Journal of Multiphase Flow*, *37*(6), 620–626. https://doi.org/10.1016/j.ijmultiphaseflow.2011.03.005

Pratama, R. H., Sou, A., Tokihiro, K., & Shigeru, N. (2017). String cavitation in fuel injector. *Atomization and Sprays*, (3).

Pratama, R. H., Sou, A., Wada, Y., & Yokohata, H. (2015). Cavitation in Mini-Sac Nozzle and Injected Liquid Jet. *ICLASS-2015*.

Ravendran, R., Christiansen, J. deClaville, Endelt, B., Jensen, E. A., & Jensen, P. (2017). Rheological behavior of lubrication oils used in two-stroke marine engines. *Industrial Lubrication and Tribology*, *69*(5).

Roohi, E., Zahiri, A. P., & Passandideh-Fard, M. (2013). Numerical simulation of cavitation around a two-dimensional hydrofoil using VOF method and LES turbulence model. *Applied Mathematical Modelling*, *37*(9), 6469–6488. https://doi.org/10.1016/j.apm.2012.09.002

Salvador, F. J., Romero, J.-V., Roselló, M.-D., & Martínez-López, J. (2010). Validation of code model cavitation phenomena in diesel injector nozzles. *Mathematical and Computer Modelling*, *52*(7), 1123–1132. https://doi.org/10.1016/j.mcm.2010.02.027

Schmidt, D. P., & Corradini, M. L. (2001). The internal flow of diesel fuel injector nozzles: a review. *International Journal of Engine Research.*, *2*(1), 1–22. https://doi.org/10.1243/1468087011545316

Soriano-Palao, O. J., Sommerfeld, M., & Burkhardt, A. (2014). Modelling the influence of the nozzle geometry on the primary breakup of diesel jets. *International Journal of Spray and Combustion Dynamics*, *6*(2), 113–146. https://doi.org/10.1260/1756-

8277.6.2.113

Sou, A., Bicer, B., & Tomiyama, A. (2014). Numerical simulation of incipient cavitation flow in a nozzle of fuel injector. *Computers and Fluids*, *103*, 42–48. https://doi.org/10.1016/j.compfluid.2014.07.011

Sou, A., Hosokawa, S., & Tomiyama, A. (2007). Effects of cavitation in a nozzle on liquid jet atomization. *International Journal of Heat and Mass Transfer*, *50*(17–18), 3575–3582. https://doi.org/10.1016/j.ijheatmasstransfer.2006.12.033

Taghavifar, H., Shervani-Tabar, M. T., & Abbasalizadeh, M. (2013). Numerical study of the effects of injector needle movement and the nozzle inclination angle on the internal fluid flow and spray structure of a group-hole nozzle layout. *Applied Mathematical Modelling*, *39*(23–24), 7718–7733. https://doi.org/10.1016/j.apm.2015.04.032

Vallier, A. A. (2013). *Simulations of cavitation – from the large vapour structures to the small bubble dynamics*. Lund University.

von Berg, E., Edelbauer, W., Alajbegovic, A., Tatschl, R., Volmajer, M., Kegl, B., & Ganippa, L. C. (2005). Coupled Simulations of Nozzle Flow, Primary Fuel Jet Breakup, and Spray Formation. *Journal of Engineering for Gas Turbines and Power*, *127*(4), 897. https://doi.org/10.1115/1.1914803

Wang, G., Senocak, I., Shyy, W., Ikohagi, T., & Cao, S. (2001). Dynamics of attached turbulent cavitating flows. *Progress in Aerospace Sciences*, *37*(6), 551–581. https://doi.org/10.1016/S0376-0421(01)00014-8

Wang, X., & Su, W. (2009). A numerical study of cavitating flows in high-pressure diesel injection nozzle holes using a two-fluid model. *Chinese Science Bulletin*, *54*(10), 1655–1662. https://doi.org/10.1007/s11434-009-0301-5

Watanabe, H., Nishikori, M., Hayashi, T., Suzuki, M., Kakehashi, N., & Ikemoto, M. (2015). Visualization analysis of relationship between vortex flow and cavitation behavior in diesel nozzle. *International Journal of Engine Research*, *16*(1), 5–12. https://doi.org/10.1177/1468087414562459

Yu, H., Goldsworthy, L., Brandner, P., & Garaniya, V. (2016). Modelling of In-Nozzle Cavitation and Early Spray Breakup Using a Multiphase Volume of Fluid Method. *20th*

Australasian Fluid Mechanics Conference.

Yu, Y., Li, G., Wang, Y., & Ding, J. (2016). Modeling the atomization of high-pressure fuel spray by using a new breakup model. *Applied Mathematical Modelling*, *40*, 268–283. https://doi.org/10.1016/j.apm.2015.04.046

Yuan, W., Sauer, J., & Schnerr, G. H. (2001). Modeling and computation of unsteady cavitation flows in injection nozzles. *Mecanique et Industries*, *2*(5), 383–394. https://doi.org/10.1016/S1296-2139(01)01120-4

Zhu, J., Chen, Y., Zhao, D., & Zhang, X. (2015). Extension of the Schnerr–Sauer model for cryogenic cavitation. *European Journal of Mechanics / B Fluids*, *52*, 1–10. https://doi.org/10.1016/j.euromechflu.2015.01.008

Paper C

Title: Coupling method for internal nozzle flow and the subsequent spray for viscous liquids

Authors: R. Ravendran*, P. Jensen, B. Endelt, J. d. Christiansen, M. Theile, and I. Najar

Submitted to Journal: International Journal of Computational Methods and Experimental Measurements

Publisher: WIT Press [ISSN 2046-0546]

Background: This paper investigates hypothesis III in chapter 4.

Abstract: Understanding the disturbances introduced by cavitation inside spray nozzles is important, when simulating the spray formation of highly viscous liquids. In this paper a new model for cavitation-induced primary break-up is proposed, which is able to map the influence of cavitating nozzle flow on spray formation. Detailed experimental and numerical investigations of the viscous nozzle flow have been performed in order to develop an improved primary break-up model for pressure injection systems (Ravendran et al. 2017). These investigations have shown that liquid break-up is enhanced when cavitation bubbles burst at the nozzle exit. The proposed model describes the transition from the flow inside the nozzle, modelled using a homogeneous equilibrium model (HEM) method, to the first primary droplets modelled using a Eulerian-Lagrangian method. Thus, providing the boundary conditions for the calculation of the secondary break-up and spray formation. The nozzle exit is divided into a definite number of patches. Liquid momentum and density from each patch are used to initialize the primary droplets. The model has been implemented in the open-source CFD software package OpenFOAM and validation has been done using high-speed shadowgraphic imaging. The simulated spray tip penetration and spray cone angle at the near-nozzle region show a good agreement with the experiment results.

COUPLING METHOD FOR INTERNAL NOZZLE FLOW AND THE SPRAY FORMATION FOR VISCOUS LIQUIDS

RATHESAN RAVENDRAN[1,*], BENNY ENDELT[2], JESPER DE CLAVILLE CHRISTIANSEN[2], PETER JENSEN[1], MARTIN THEILE[3], IBRAHIM NAJJAR[4]

1. Hans Jensen Lubricators, 9560 Hadsund, Denmark
2. Materials and Production, Aalborg University, 9220 Aalborg, Denmark
3. FVTR GmbH, 18057 Rostock, Denmark
4. University of Rostock, 18057 Rostock, Denmark.

ABSTRACT

Understanding the disturbances introduced by cavitation inside spray nozzles is important, when simulating the spray formation of highly viscous liquids. In this paper a new model for cavitation-induced primary break-up is proposed, which is able to map the influence of cavitating nozzle flow on spray formation. Detailed experimental and numerical investigations of the viscous nozzle flow have been performed in order to develop an improved primary break-up model [1]. The proposed model describes the transition from the flow inside the nozzle, modelled using a homogeneous equilibrium model (HEM) method, to the first primary droplets modelled using a Eulerian-Lagrangian method. Thus, providing the boundary conditions for the calculation of the secondary break-up and spray formation. The nozzle exit is divided into a definite number of patches. Liquid momentum and vapor volume fraction from each patch are used to initialize the primary droplets. The model has been implemented in the open-source CFD software package OpenFOAM and validation has been done using high-speed shadowgraphic imaging. The simulated spray tip penetration and spray cone angle at the near-nozzle region show a good agreement with the experiment results.

Keywords: Spray formation, cavitation, primary break-up, numerical simulation, viscous liquids, OpenFoam

1 INTRODUCTION

Cavitation inside spray nozzles have a great importance on the break-up of liquid jets [2]–[4]. In simple pressure spray systems, liquid jet does not atomize greatly when disturbances caused by cavitation are not present [5], [6]. This is especially true for viscous liquids, which are difficult to atomize unless high fluid pressure is applied [7]. Cavitation occurs when the local pressure of the liquid drops below its vapor pressure [8], and thereby forming vapor cavities inside the liquid. The collapse of these cavities introduce disturbances to the liquid, which leads to faster break-up and greater atomization of the exiting jet [9]–[11].

Several factors influence the formation of cavitation as e.g. sharp inlet orifices, needle lift, curvature of the inlet edge, liquid properties, and system pressure [6], [12]–[14]. Ravendran et. al [1] investigated the cavitation induced atomization of viscous liquids using a transparent spray nozzle. The fluid viscosity was 0.05 Pa · s and the fluid pressure was 4 MPa. The study showed that non-axial injection conditions lead to a swirling liquid flow inside the nozzle. Thus, leading to the development of cavitation strings in the core of the liquid vortices. The degree of atomization increases significantly, when these cavitation strings extend to the exit of the nozzle. However, when the cavitation bubbles collapse in the nozzle volume, the viscous liquid is able to stabilize the disturbances introduced by cavitation.

For many decades, cavitation inside spray nozzles has been studied in order to determine the effects on droplet break-up, however the phenomenon is still poorly understood. A better understanding of cavitation demands detailed information, on the flow inside the nozzle and the subsequent spray, which is difficult to observe experimentally. This information can be obtained from a properly validated computational spray model. Several methods exist and are implemented in commercial CFD-codes for simulating the spray formation using the Lagrangian method as e.g. Taylor Analogy, Kelvin-Helmholtz and Rayleigh-Taylor break-up [3]. However, these models need sub-models to describe the transition from the nozzle flow to the primary droplet, as illustrated in Fig. 1. This coupling has been the focus of several authors, as the transition between the nozzle flow and spray formation is very complicated [15]–[17]. The majority of current coupling models employ simplified boundary conditions at the nozzle exit, as an indirect coupling to the primary droplets. Such methods often dampen or lead to the loss of the nozzle flow characteristic, which is the drawback of the Eulerian-Lagrangian approach for simulating sprays.

The simplest method for introducing the Lagrangian droplets is by the blob-method. The blob method is based on the assumption that detailed description of the atomization and drop break-up processes within the dense spray near the nozzle is not required. The Lagrangian droplets are therefore initiated by spherical droplets with a diameter equal to the nozzle hole diameter, which means the break-up occurs due to secondary aerodynamic-induced break-up.
Cavitation-induced break-up models have been developed by some researches in the recent years. The proposed break-up models are either based on one dimensional or phenomenological models of the cavitation inside the nozzle volume [18]–[20]. Arcoumanis et al. [21] included cavitation in the primary break-up by calculating an effective hole diameter (the total area of the nozzle aperture occupied by cavitation) in order to determine the initial droplet diameter of droplets. Nishimura and Assanis [22] proposed a cavitation and turbulence-induced primary break-up model for diesel sprays. This model determines the bubble dynamics inside the injector and transfers collapse energy to turbulent kinetic energy, which is then transformed to an additional break-up force included in the secondary break-up [3].

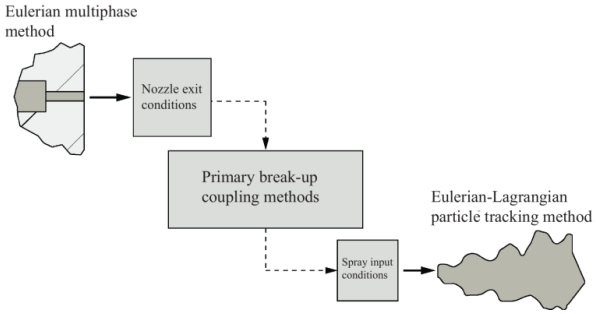

Figure 1: Illustration of the numerical simulation approach used in this study.

Baumgarten et al. [15] proposed a cavitation-induced break-up model based on experimental investigations of a quasi-stationary spray. The model defines two different zones in the nozzle volume. The first zone contains the liquid core of the jet, while the second zone consists

of a mixture of cavitation bubbles and liquid ligaments. Break-up of the different zones is treated separately. The energy from the collapse of cavitation bubbles is transferred both to the outer surface and break-up of the mixture zone, as well as to the interface between the two zones to increase turbulent energy of liquid core.

The present coupling models are related to low-viscous liquids such as diesel fuels. This means that the models are based on assumptions, which may not valid for cavitation- induced break-up of viscous liquids. This leads to the objective of this study.

In this paper, a method for coupling the internal viscous flow and the subsequent spray is proposed. The study is a continuation of the work presented in [23]. The purpose of the new primary breakup model is to describe the transition from the flow inside the nozzle to the first primary droplets. Thus, providing all starting conditions for the calculation of secondary break-up and spray formation. The input data for the new model are based on the detailed numerical investigations of the nozzle flow performed in [1]. High-speed shadowgraphic imaging has been used to validate the proposed model in spray tip penetration and spray cone angle at the near-nozzle region.

2 NUMERICAL SIMULATION APPROACH

The simulation approach is divided in two steps, as shown in Fig. 2. Firstly, the simulation of the liquid flow and cavitation inside the nozzle is performed using multiphase approach with a Schnerr-Saur cavitation model. Secondly, the simulation of the spray formation is performed using an Eulerian-Lagrangian approach using a KHRT secondary break-up model. The two simulations are connected using a coupling model, which translates the flow inside the nozzle to the first primary droplets at the nozzle exit. The focus of the following section is to describe the coupling model. Simulation of the cavitating nozzle flow is described in detail in [1] and the KHRT-model is for example documented in [16], [24].

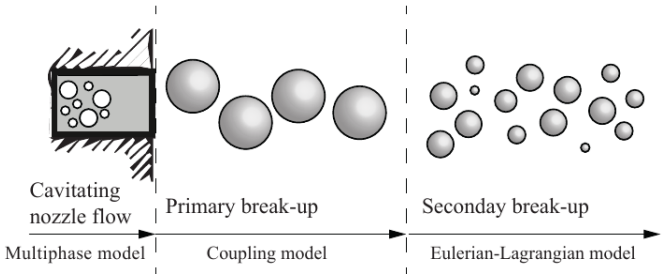

Figure 2: Overview of the numerical simulation approach.

2.1 The coupling model

The purpose of the coupling model is to initiate the primary droplets using the nozzle exit conditions. The nozzle exit is therefore separated into a defined number of boundary patches, from which liquid velocity (u) and degree of cavitation (α) are used to calculate the diameter of the primary droplet (D_i), mass flow rate ($\dot{m}_i$), and spray angle (φ_i) at each patch (i).

The location of each patch is randomly selected, in order to suppress geometrical effects when introducing a defined boundary grid. This approach makes the model flexible and applicable for different nozzle geometries. However, as patches are allowed to overlap and exceed the diameter of the nozzle, minor errors in spray angle are expected.

The first droplets at the nozzle exit are introduced using the so-called blob-method, where the assumption is that the dense spray near the nozzle can be represented by spherical droplets with uniform size. The diameter of these droplets equals the nozzle hole diameter. The number of the droplets injected per unit time is determined from the mass flow rate. The mass flow rate of the primary droplets is calculated as:

$$\dot{m}_i(t) = \rho_l \cdot A_{patch} \cdot u_i(t) \tag{1}$$

where ρ_l is the liquid density, A_{patch} is the area of the selected patch, $u_i(t)$ is the velocity of the liquid composed of the three components in x, y, and z-direction.

The direction of the droplets leaving the nozzle exit is defined using the spray angle. These parameters are highly influenced by the degree of cavitation at the nozzle exit, as bursting of cavitation bubbles leads to increased spray angle. The degree of cavitation is expressed in terms of vapor volume fraction (α_i) , which is directly extracted from the internal flow simulations. The vapor volume fraction is described by a number from 0 to 1, for $\alpha_i < 1$ the patch cavitates.

$$\varphi_i = \begin{cases} 0 & \alpha_i = 1 \\ \cos^{-1}\left(\dfrac{u_{i,plane} \cdot u_{i,y}}{\|u_{i,plane}\| \cdot \|u_{i,y}\|}\right) & \alpha_i < 1 \end{cases} \tag{2}$$

where $u_{i,y}$ is the velocity vector of the liquid perpendicular to the nozzle exit, and is defined by $u_{i,plane} = u_{i,x}^2 + u_{i,z}^2$ and describes the velocity components parallel to the nozzle exit.

2.2 Computational grid and boundary conditions

The boundary conditions were set according to the experimental conditions with a nozzle inlet pressure P_{inlet} = 4.0 MPa and outlet pressure P_{outlet} equal to the ambient pressure at 0.1 MPa. The movement of the injector needle is taken into account using an exponential ramp up of the inlet pressure corresponding to the position of the needle.

The numerical simulation of the internal flow and the spray formation is performed using OpenFOAM 3.1. The coupling routine is implemented in a MATLAB code. For all calculation a parcel injection rate of $2 \cdot 10^6$ parcels per second is used, which is considered to be sufficient for reliable results.

The computational grid is a 10×10×300 mm rectangular box with a mesh grid size of 1 mm. The mesh size is the same in all directions and kept unchanged in all of the simulations. It is well known that the mesh can play an important role when simulating sprays with the Lagrangian approach. Mesh resolution is more critical in high pressure and high density spray simulations, since liquid volume is considered small compared to the gas phase volume [18]. The simulations are performed with an adjustable time step limited by the Courant number. The Courant number is set to 0.5 and the initial time step Δt is set to 10^{-7} s.

3 EXPERIMENTAL SETUP

A schematic overview of the test setup is shown in Fig. 3. The setup consists of a HJ Lubtronic system from Hans Jensen Lubricators A/S (1), which delivers 50 mg lubrication oil per injection to a heated HJ-SIP injection valve (2). The lubrication oil is injected in to a chamber (3) with ambient atmospheric conditions. To actuate the lubricator, 7 MPa hydraulic pressure is supplied from a standard pump station (4). Fresh lubrication oil to the lubricator is delivered from a heated reservoir (5). The internal geometry of the nozzle head in the injection valve is shown in Fig. 4. The opening pressure of the injection valve is 4.0 MPa.

The high-speed camera (6) and illumination source (7) are set up at either side of the spray in order to capture the images using the shadowgraphic method, where the spray is visualised as dark in front of an illuminated background. A control system (8) is developed in order to regulate the temperature on the lubrication oil, and to initialise both the high-speed camera and the lubricator.

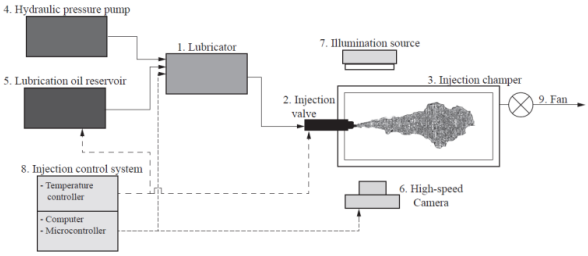

Figure 3: The layout of the experimental setup.

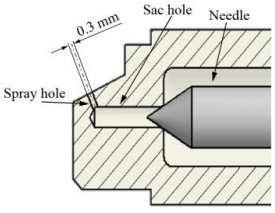

Figure 4: The internal geometry of the HJ-SIP spray injection valve.

The high-speed camera used in this study is a Photron Fastcam SA5 and a 1000W LED lamp is used as the illumination source. Images are taken with a frame rate of 15000 fps with a shutter speed of 1/171000. Both the high-speed camera and the lubricator are controlled by a computer in order to synchronize the images.

Each image is processed using a custom algorithm in MATLAB, which detects the spray boundary and computes the spray tip penetration and cone angle. The algorithm consists of several image processing steps in order to distinguish the spray from the background sufficiently. These image processing steps are shown in Fig. 5.

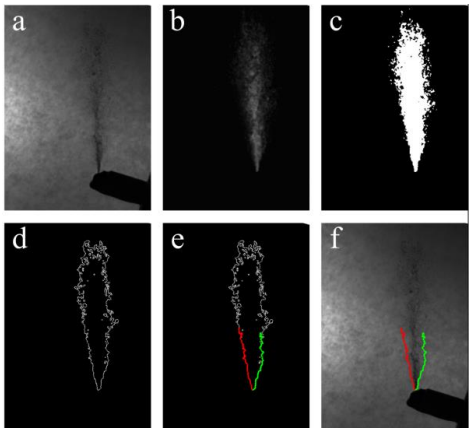

Figure 5: The image processing algorithm. (a) Unprocessed original image. (b) Background subtraction and Contrast stretching (c) Thresholding. (d) Edge detection. (e) Curve fitting. (f) Processed final image.

4 MATERIALS

The commercial lubrication oil *Mobilgard 570* is used for the spray investigations. The material properties for this oil are presented in Table 1. The properties that are highly affected by temperature change are expressed as a function.

Table 1: Lubrication oil properties used in this study. In the following equations R is the ideal gas constant, and T is the temperature of the lubrication oil expressed in Celsius.

Oil property	**Value**	**Reference**
Vapor Pressure	$P_v(T) = 10 \cdot e^{(A \cdot T - B)/((20.0 \cdot T + C)) \cdot \mathrm{R}}$ kPa The dimensionless constants are A = 1094, B = $3.458 \cdot 10^5$, and C = 5463.0.	Derived using the Clausius-Clapeyron equation
Liquid Density	$\rho_l(T) = 0.6087 \cdot T + 943.97$ kg/m^3	Measured
Liquid Viscosity	$\mu_l(T) = 0.00610 \cdot e^{1246/(\mathrm{R} \cdot T)}$ Pa · s	[25]
Vapor Density	$\rho_v = 16.05$ kg · m^{-3}	[26]
Vapor Viscosity	$\mu_v = 11.58\ \mu$Pa · s	[26]

5 VALIDATION AND RESULTS

In order to validate the proposed spray model, four injection conitions have been studied. The only difference is the temperature of the lubrication oil; Case 1: $T_{\mathrm{L}} = 100$℃, Case 2: $T_{\mathrm{L}} = 60, 80,$ and 120℃. Case 1 is used to compare the model behavior, whereas Case 2 is used evaluate the performance of different injector conditions. As shown in Figure 6, the temperature of the liquid has a significant role on the degree of cavitation and the flow inside the spray nozzle, due to the change in liquid viscosity and vapor pressure.

The nozzle exit conditions for the different injection cases, shown in Fig. 7 and Fig. 8, are used for the spray simulations. Liquid momentum and vapor volume fraction from each patch are used to initialize the primary droplets. The velocity at the nozzle exit is shown in Fig. 8, where the fringe level indicates the velocity in y-direction (U_y) and the vector field represents velocity components in the xz- plane (U_x and U_z). It is seen that the swirling flow is prominent at higher temperatures, and at low temperatures the flow is non-swirling and axisymmetric. The swirling flow leads to the cavitation strings inside the core of the liquid vortices. Fig. 8 shows, that a higher degree of cavitation is achieved when the swirling flow is more prominent. A throughout description of the internal flow and the behavior of vortex cavitation can be found in [1].

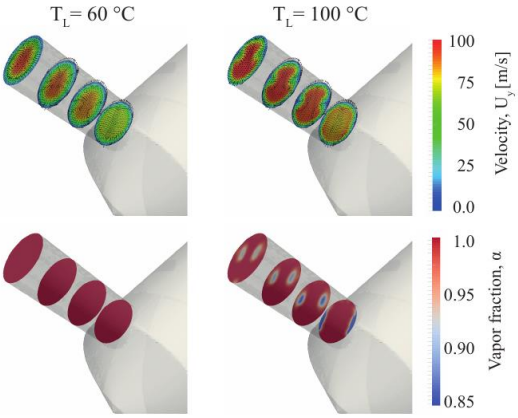

Figure 6: The numerical results of the internal nozzle flow showing liquid velocity and vapor volume fraction throughout the spray hole.

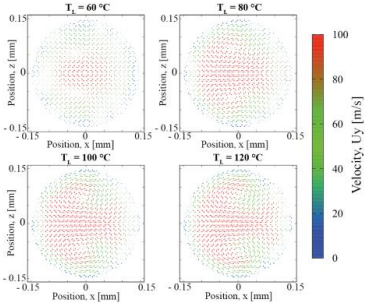

Figure 7: The numerical results for the studied injection cases showing the velocity at the nozzle exit.

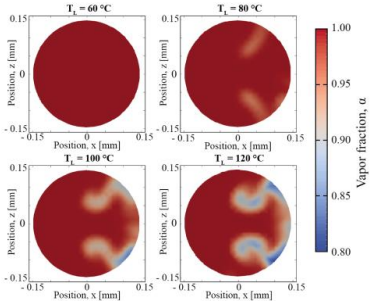

Figure 8: The numerical results for the studied injection cases showing the vapor fraction volume at the nozzle exit.

5.1 Experimental results and model validation

Fig. 9 shows the computational and experimental results of the spray formation for injection Case 1. The numerical simulations are performed using $N_P = 100$, which is the number of selected paches. The importance of this model constant is discussed in section 5.2. The simulation results show a dense liquid core in the center of the spray, and smaller dispersed ligaments away from the center. These observations agree with the experimental observations. It is also important to highlight that the proposed model is capable of predicting the spray structure and asymmetrical shape apart from the spray tip penetration.

The spray tip penetration L and cone angle θ is shown in Fig. 10. The figure shows that there is a minor difference between the simulated and measured spray penetration. The simulated spray penetrates faster through the ambient atmosphere compared to the measured spray. There is an error of 8.2% at t = 1.8 ms. It is expected, that this error relates to the interaction between the droplets and the surrounding gas. This is why this error can be minimized by adjusting the model constants for the secondary break-up e.g. by enhancing the breakup process, meaning that smaller droplets will penetrate slower than larger droplets [15].

Comparison of the computed and measured spray cone angle is shown in Fig. 10b. The measured spray cone angle is large at the beginning of the injection. As soon as the penetration increases, the resulting spray cone angle becomes smaller. The initial spray structure depends on the speed of the needle, as a slow opening result in larger spray angles, whereas a fast opening result in smaller angles. Even though the needle motion is considered in the model with a pressure boundary, the prediction of the initial spray angle is not accurate. However, a good agreement between the measured and computed steady-state spray cone angle is observed.

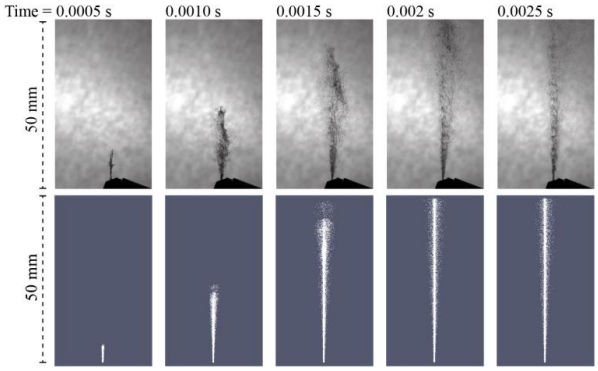

Figure 9: Spray formation due to cavitation induced breakup (Comparison between experiment and numerical simulation). The temperature of the injected liquid is $T_L = 100℃$. The numerical simulations are performed using $N_P = 100$.

The experimental images in Fig. 9 show an asymmetrical structure of the spray. This asymmetry occurs due to the asymmetrical nozzle flow and especially due to the concentration of cavitation at one side of the spray hole. Fig. 11 shows the calculated angle for each half of

the spray extracted. It is shown, that the side where cavitation is prominent leads to a higher spray angle compared to the side with less cavitation. The average of $\varphi_1 = 4.27°$ and the average of $\varphi_2 = 3.52°$, which leads to a difference of 21.3 %.

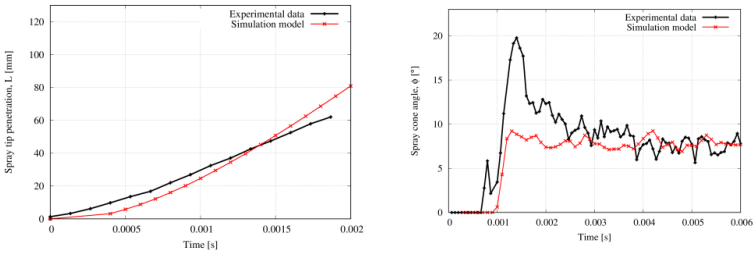

a) Spray tip penetration b) Spray cone angle

Figure 10: Comparison of the spray penetration and angle (Case 1)

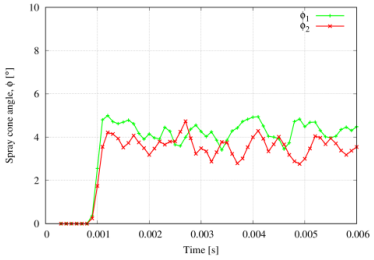

Figure 11: The asymmetrical structure of the spray represented by φ_1 and φ_2, which is the angle from the spray center to the spray contour. The angles are shown in Figure 10b. The average of $\varphi_1 = 4.27°$ and the average of $\varphi_2 = 3.52°$.

5.2 Influence of random selected patches

In the following section the influence of the number of random selected patches N_P is analyzed. Fig. 12 shows the spray penetration and spray cone angle for different values of N_P. The value of N_P depends on the area of the nozzle hole exit. The larger the area the more measurement points are needed in order to ensure a sufficient prediction of the spray formation. However, this also increases the computational time. Figure 12a shows that the penetration is not as influenced by N_P as the spray angle. Furthermore it can be concluded that N_P must be larger than 50 to ensure a sufficient prediction, when the diameter of the nozzle hole exit is 0.3 mm.

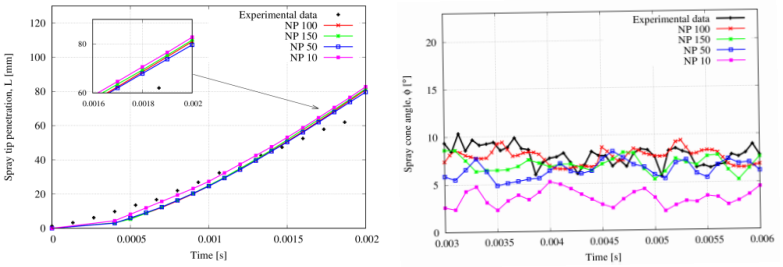

a) Spray tip penetration b) Spray cone angle

Figure 12: The influence of the number of randomly selected measurement points N_P for the proposed spray model

5.3 Influence of liquid temperature

Fig. 13 shows the computational results of the spray formation for the three injection conditions in Case 2. There is a good agreement between the computed and the measured spray cone angle. There is no break-up at $T_L = 60$ ℃, due to no cavitation at the end of the nozzle exit. This leads to a jet with a small spray cone angle, which is correctly predicted by the proposed model. As temperature increases the degree of cavitation increases, which leads to higher spray cone angles.

Regarding the spray tip penetration, there is only a good agreement between the computed and the experimental spray tip penetration at $T_L = 80$ ℃. The model overestimates the penetration length at $T_L = 60$ ℃ and 120 ℃. This overestimation is considered to be attributed to the coupling between the proposed model and the spray droplets. In this study the blob-method has been used, which assumes that the size of the droplets leaving the nozzle is the size of the nozzle hole. However, this consideration is not sufficient when having cavitation induced break-up. Droplet size and droplet behavior in the surrounding gas plays an important role, the bigger droplets result in faster penetration compared to smaller droplets. Therefore, a more accurate coupling between the droplet size and nozzle flow is needed in order to minimize the inaccuracy.

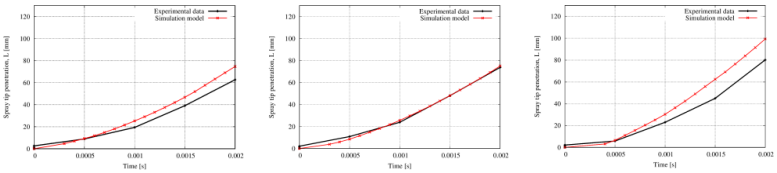

a) Spray penetration $T_L = 60$ ℃.

b) Spray penetration $T_L = 80$ ℃.

a) Spray penetration $T_L = 120$ ℃.

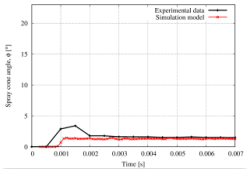

d) Spray angle $T_{\mathrm{L}} = 60$ ℃.

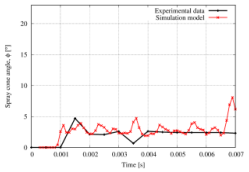

e) Spray angle $T_{\mathrm{L}} = 80$ ℃.

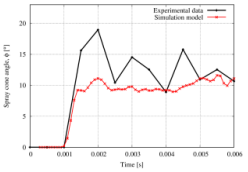

f) Spray angle $T_{\mathrm{L}} = 120$ ℃.

Figure 13: Comparison of spray penetration and spray angle of different temperatures

6 CONCLUSION

A new approach for modelling cavitation induced break-up for viscous liquids has been presented in this paper. The proposed model describes the transition from the flow inside the nozzle, modelled using a homogenous equilibrium model (HEM) method, to the first primary droplets modelled using a Eulerian-Lagrangian method. Thus, providing all starting conditions for the calculation of the secondary break-up and spray formation.

The validation of the presented approach has been done by comparison of spray structure, spray tip penetration and spray cone angle between experiments and simulations. The results showed that the simulations have the ability to reproduce the experimental trends of viscous sprays. Especially, the influence of cavitation on the spray structure is well reproduced with the presented modelling approach. Higher degrees of cavitation at the nozzle exit leads to increased droplet break-up and spray cone angle.

In order to increase the accuracy of the presented model, a more detailed coupling between nozzle flow and droplet size is needed. This has however not been the scope of this paper.

7 REFERENCES

[1] R. Ravendran, J. deClaville Christiansen, P. Jensen, and B. Endelt, “Numerical study of cavitation of high-viscous liquid spray systems,” *ILASS Am. 28th Annu. Conf.*, no. May, pp. 1–12, 2016.

[2] T. D. Fansler and S. E. Parrish, “Spray measurement technology: a review,” *Meas. Sci. Technol.*, vol. 26, no. 1, p. 012002, 2015.

[3] L. Le Moyne, “Trends in atomization theory,” *Int. J. Spray Combust. Dyn.*, vol. 2, no. 1, pp. 49–84, 2010.

[4] A. Sou, S. Hosokawa, and A. Tomiyama, “Effects of cavitation in a nozzle on liquid jet atomization,” *Int. J. Heat Mass Transf.*, vol. 50, no. 17–18, pp. 3575–3582, 2007.

[5] S. Dabiri, W. A. Sirignano, and D. D. Joseph, “Cavitation in an orifice flow,” *Phys. Fluids*, vol. 19, no. 7, 2007.

[6] C. Dumouchel, “On the experimental investigation on primary atomization of liquid streams,” *Exp. Fluids*, vol. 45, no. 3, pp. 371–422, 2008.

[7] N. Tamaki and M. Shimizu, “Enhancement of atomization of high-viscous liquid jet by pressure atomized nozzle,” *ILASS-Europe 2002*, 2002.

[8] J.-P. Franc and J.-M. Michel, *Fundamentals of Cavitation*. Springer Science +

Business Media, Inc., 2006.
[9] C. Baumgarten, J. Stegemann, and G. Merker, “A new model for cavitation induced primary break-up of diesel sprays,” *ILASS-Europe 2002*, 2002.
[10] W. Bergwerk, “Flow pattern in Diesel Nozzle Spray Hole,” *Proc. Inst. Mech. Eng.*, vol. 173, Jun. 1959.
[11] C. Dumouchel, N. Leboucher, and D. Lisiecki, “Cavitation and primary atomization in real injectors at low injection pressure condition,” *Exp. Fluids*, vol. 54, no. 6, pp. 1–17, 2013.
[12] S. Jollet, H. Hansen, K. Bitner, D. Niemeyer, and F. Dinkelacker, “Experimental and numerical investigations of 90 micrometer real-size transparent nozzles with high pressure conditions,” *ILASS-Europe 2014*, 2014.
[13] R. H. Pratama, A. Sou, Y. Wada, and H. Yokohata, “Cavitation in Mini-Sac Nozzle and Injected Liquid Jet,” *ICLASS-2015*, 2015.
[14] A. Andriotis, M. Gavaises, and C. Arcoumanis, “Vortex flow and cavitation in diesel injector nozzles,” *J. Fluid Mech.*, vol. 610, pp. 195–215, 2008.
[15] C. Baumgarten, *Mixture Formation in Internal Combustion Engine*. Springer Berlin Heidelberg, 2006.
[16] B. Mohan, W. Yang, and S. Chou, “Cavitation in Injector Nozzle Holes – A Parametric Study,” *Eng. Appl. Comput. Fluid Mech.*, vol. 8, no. 1, pp. 70–81, Jan. 2014.
[17] H. Yu, L. Goldsworthy, P. Brandner, and V. Garaniya, “Modelling of In-Nozzle Cavitation and Early Spray Breakup Using a Multiphase Volume of Fluid Method,” *20th Australas. Fluid Mech. Conf.*, 2016.
[18] B. Mohan, W. Yang, and S. K. Chou, “Development of an accurate cavitation coupled spray model for diesel engine simulation,” *Energy Convers. Manag.*, vol. 77, pp. 269–277, 2014.
[19] F. D. Santos and L. L. Moyne, “Spray atomization models in engine applications, from correlations to direct numerical simulations,” *Oil Gas Sci. Technol.*, vol. 66, no. 5, pp. 801–822, 2011.
[20] M. Herrmann, “On simulating primary atomization using the refined level set grid method,” *At. Sprays*, vol. 21, no. 4, pp. 283–301, 2011.
[21] C. Arcoumanis, M. Gavaises, and B. French, “Effect of Fuel Injection Processes on the Structure of Diesel Sprays,” *SAE Tech. Pap. 970799*, 1997.
[22] A. Nishimura and D. N. Assanis, “A Model for Primary Diesel Fuel Atomization Based on Cavitation Bubble Collapse Energy,” *ICLASS 2000*, pp. 1249–1256, 2000.
[23] R. Ravendran, B. Endelt, J. deClaville Christiansen, and P. Jensen, “Model for cavitation induced primary break-up of viscous liquid sprays,” in *Computational & Experimental Methods in Multiphase and Complex Flow*, 2017.
[24] R. D. Reitz and J. C. Beale, “Modeling spray atomization with the Kelvin-Helmholtz/Rayleigh-Taylor Hybrid model,” *At. Sprays*, vol. 9, no. 6, pp. 623–650, 1999.
[25] R. Ravendran, J. deClaville Christiansen, B. Endelt, E. A. Jensen, and P. Jensen, “Rheological behavior of lubrication oils used in two-stroke marine engines,” *Ind. Lubr. Tribol.*, vol. 69, no. 5, 2017.
[26] M. J. Assael, N. K. Dalaouti, and V. Vesovic, “Viscosity of Natural-Gas Mixtures: Measurements and Prediction,” *Int. J. Thermophys.*, vol. 22, no. 1, pp. 61–71, 2001.

8 Extended Summary

This chapter will sum up the findings and tie together the three papers presented in the previous chapters. In addition to the findings presented in the papers, this chapter will also include related work performed in this PhD thesis.

8.1 Discussion of Paper A

In Paper A, the viscosity of seven commercial lubrication oils was investigated using rotational and capillary rheometry. From a lubrication system manufacturers view point, it is important to understand the behavior of the commercial oils in order to design new applications. The study was therefore limited to the behavior of the selected groups of oils, as they were considered to be representative of oils on current market.

Commercial cylinder oils are chemically complex, as they consist of a wide variety of additives, which serves different purposes e.g. calcium carbonate detergents, viscosity modifying agents, dispersing agents, anti-wear additives and anti-oxidants. The viscosity of dispersions is first of all controlled by the continuous liquid phase which might be Newtonian or non-Newtonian, and then the added dispersed phase. Particle size, shape, amount, deformability and even the interaction between the particles can affect the viscosity (Barnes, 2001).

Figure 8.1 shows the rotational and capillary rheometry measurements for cylinder oils investigated in Paper A. As no significant change in viscosity for different shear rates is observed, the cylinder oils can be considered Newtonian fluids. Whether the oils are Newtonian or non-Newtonian can influence the fluid flow inside the injection nozzle and the subsequent spray formation. A Newtonian behavior is the natural state for any liquid like hooks law for any solid. There are two situations where the liquid can deviate from the Newtonian behavior; which is when the liquid is time and rate dependent. A time dependent fluid will change viscosity over time subjected to a constant deformation rate. This is called thixotropy if the viscosity decreases and anti-thixotropy if the viscosity increases. A rate dependent fluid will change

viscosity as function of shear rate. If the viscosity decreases the fluid is shear thinning or pseudoplastic, and if the viscosity increases it is shear thickening. Shear thinning fluids always show a Newtonian behaviour at low deformation rates, and the shear thinning effect is normally very dramatic with many decades change in viscosity.

Thixotropy, for example in the existence of a polymer network, could affect the transient behavior. This effect will be very visible in the rotational rheometry at startup of the experiment where the viscosity should change at constant shear, which was not the case for the studied lubrication oils.

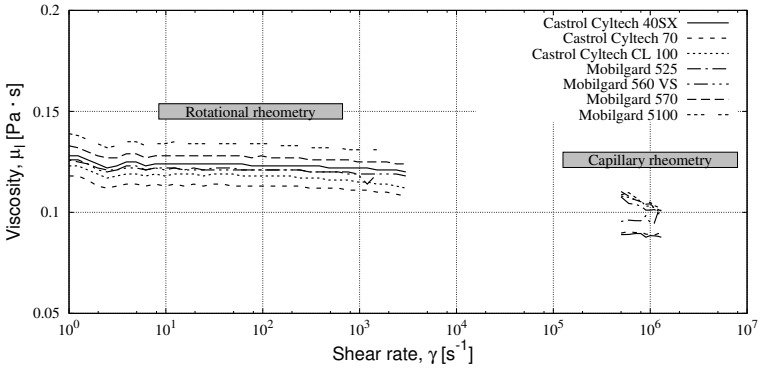

Figure 8.1: Viscosity of different lubrication oils as a function of shear rate at 50 °C.

In order to investigate the influence of high shear rates on the viscosity, capillary rheometry was made. Viscosity changes at high deformation rates can occur when the timescale of the flow is faster than the liquid can negotiate it. Hence the liquid shows deviations from the equilibrium state and the resistance to flow changes, that is the viscosity can increase or decrease, and both elastic and viscous behavior can be observed. This is formulated in the Deborah number, where $D_e = t_c/t_p$, where t_c is the characteristic time of the material (typically chosen as the Maxwell relaxation time) and t_p a characteristic time of observation, typically taken as the timescale of the process. A low Deborah number corresponds to fluid like behavior and a high Deborah number to solid like behavior. For an oil the relaxation time is in the order of 10^{-6} second (Barnes et al., 1989) and at elevated temperature much lower.

Measurements was made to investigate if the oil was shear thinning at the high deformation rates 10^6 s^{-1} close to where we might expect viscoelastic effects to occur. Therefor the flow in a capillary was measured. These measurements showed no evidence of significant non-Newtonian behavior. Small variations can be explained by shear heating. Even for highly elastic Boger fluids (highly elastic fluids that are almost Newtonian, at least in a narrow

shear rate range), a significant drop in viscosity will be observed and this was not the case.

In addition to the measurements presented in Paper A, the dynamic properties are also investigated. Rheological investigations are made in oscillatory mode where G′ and G″ are measured (Figure 8.3). There are no elasticity and G′ is so insignificant it fails to be measured. Furthermore, G″ show a pure Newtonian behavior. Using the Cox-Merz assumption, the complex viscosity is calculated (Figure 8.2). These measurements also show a pure Newtonian behavior and no elastic effects.

The conclusion from the capillary, rotational and oscillatory rheological measurements is that the lubrication oils behave Newtonian in a high shear and highly transient system, as the injection system studied in this thesis.

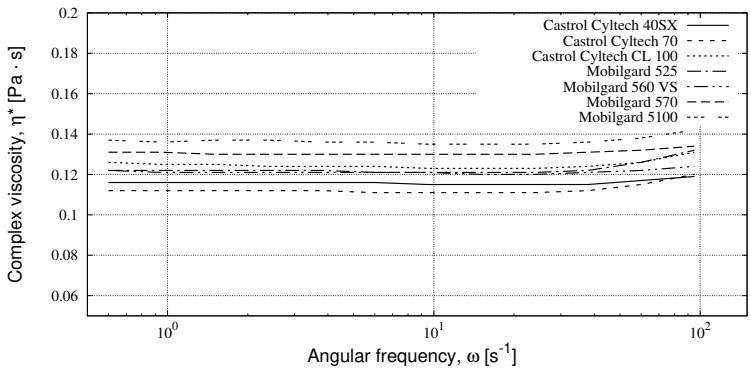

Figure 8.2: The calculated complex viscosity as a function of shear rate. Data recalculated and the straight line indicate a Newtonian behavior.

Temperature influence

The viscosity/temperature dependency of the oils was also investigated in Paper A. Figure 8.4 shows that the temperature of the liquid has a significant influence on the viscosity. More than a decade of change in viscosity is observed from 40 °C to 100 °C. This viscosity/temperature dependency was found to fit the Arrhenius model:

$$\mu_l(T) = 0.00610 \cdot \mathrm{e}^{1246/(R \cdot T)} \tag{8.1}$$

where R is the ideal gas constant and T is the temperature.

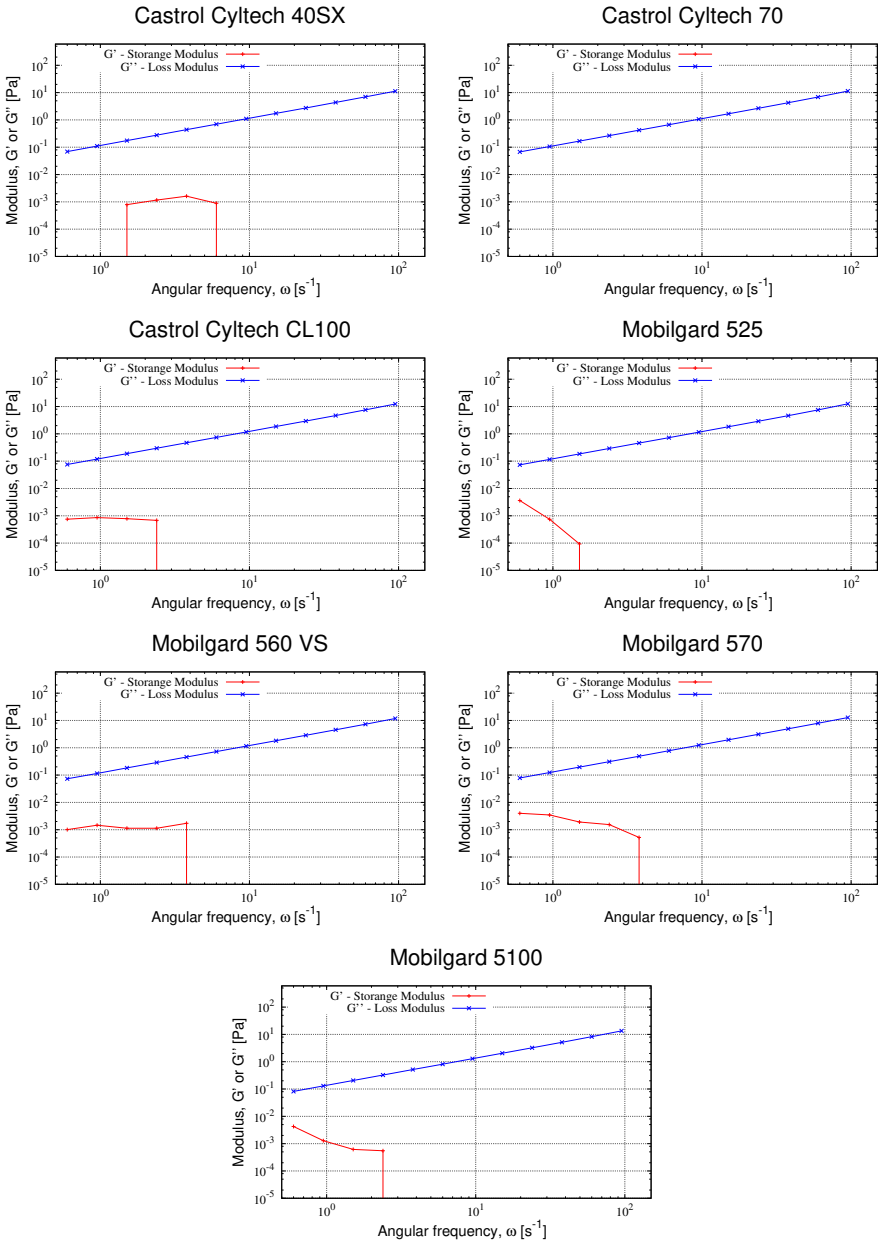

Figure 8.3: The G′ and G″ measurement of lubrication oil in oscillatory mode. There are no elasticity and G′ is so insignificant it fails to be measured. Furthermore, G″ show a pure Newtonian behavior.

In connection to the work presented in this paper, a patent has been obtained, see Patent A on page 205. This patent describes a method for controlling the temperature of the lubrication oil, and thereby ensuring right viscosity at the time of injection. The importance of the right viscosity is discussed in Paper B.

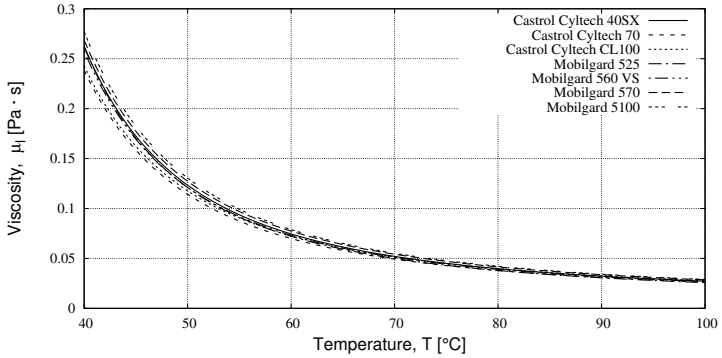

Figure 8.4: Viscosity of lubrication oils as a function of temperature.

8.2 Discussion of Paper B

In Paper B, it was shown that cavitation exists inside injectors, and that it influences the subsequent spray formation and jet break-up. Furthermore, the investigations showed that the degree of atomization is significantly enhanced when the cavitation extends to the exit of the nozzle. In contrast, when the cavitation collapses in the nozzle volume, the viscous liquid is able to stabilize the stochastic behaviour.

Experimental high-speed images of cavitation

Figure 8.5 shows the presence of cavitation inside the studied injection nozzle for different injection temperatures T_L. There is no cavitation when the liquid temperature is 60 °C. As temperature increases, cavitation emerges at the left side of the spray hole. The size of cavitation is highly dependent on the liquid temperature, as both length and width of the cavitation increase with increasing temperature and thus reduced viscosity. When the liquid temperature is above 100 °C, the cavitation extends to the nozzle exit.

The subsequent spray formation is shown in Figure 8.6. It is shown that the degree of atomization increases significantly if the cavitation extends to the end of the spray hole. This is in contrast to cases where the cavitation collapses in the nozzle volume, which results in a jet-shaped liquid stream.

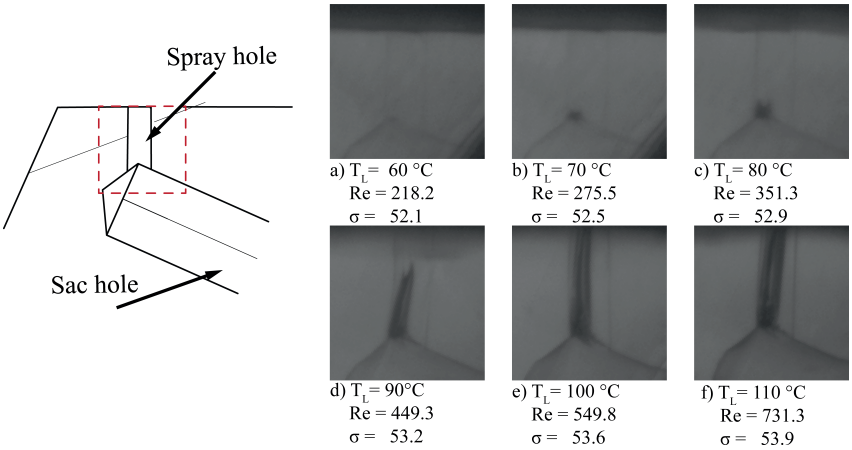

Figure 8.5: High-speed shadowgraphic images of the internal nozzle flow.

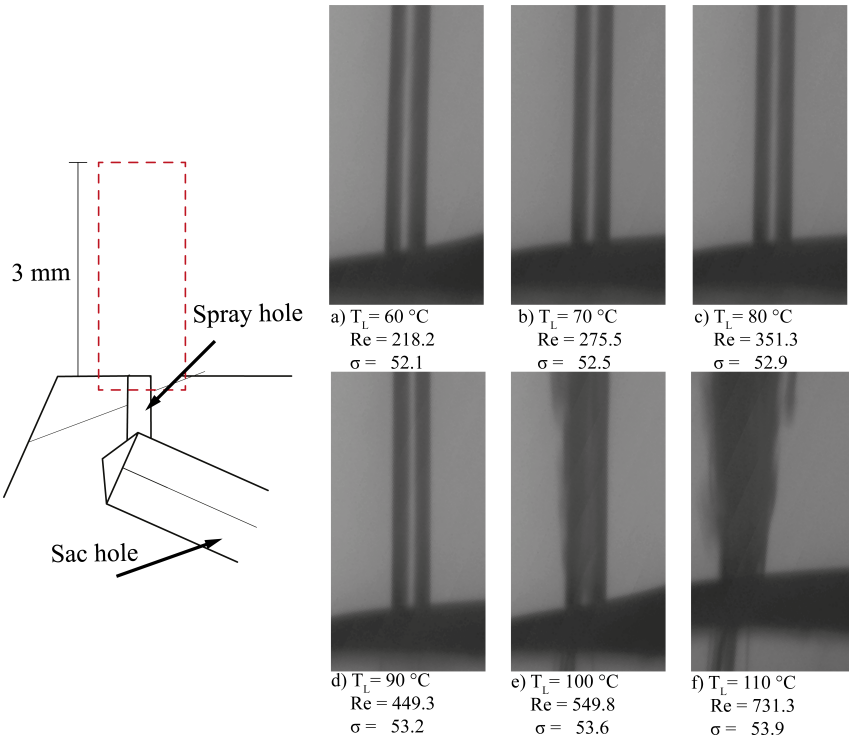

Figure 8.6: High-speed shadowgraphic images of the spray formation.

The experimental observations presented in Paper B are supported by the mass flow measurements shown in Figure 8.7, which is not included

in the publications. The measurements are made with an identical nozzle as the one analyzed in Paper B. The injection valve is substituted with a solenoid injection valve, and the lubrication oil is supplied by a pressure pump delivering constant pressure. The opening time of the solenoid valve can be controlled. Thus, it is possible to measure the mass of lubrication oil injected into a cup over fixed time (mass flow measurement). The pressure supplied to the injection valve is adjusted, thereby establishing the graph of mass flow rate as a function of pressure.

The measurements show that a stagnation point is reached at approximately 27 bar, which indicates choked flow due to the presence of cavitation inside the nozzle.

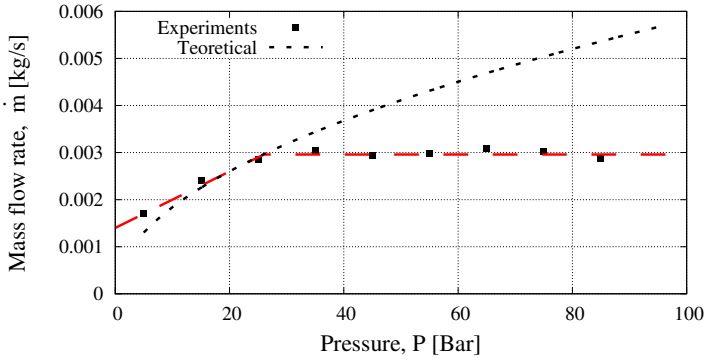

Figure 8.7: Mass flow measurement under stationary conditions using an injector with a nozzle aperture diameter of D_n =0.3 mm and the liquid temperature is $T_L = 106°C$.

Numerical modeling of cavitation

The numerical investigations presented in Paper B validate that cavitation exist inside the studied nozzle and that it is temperature dependent. Furthermore, the study reveals that it is possible to detect cavitation structures using the homogeneous mixture method with a Schnerr-Saur cavitation model.

Figure 8.8 shows the cavitation structures at different liquid temperatures, which is similar to the behavior shown experimentally (Figure 8.5). There is however a disagreement between the experimental and numerical results in terms of where the cavitation originates. In the experiments, cavitation emerges to the left side of the spray nozzle, whereas the cavitation emerges at the center of the nozzle in the simulations. This disagreement is due to the slight difference between the experimental and the simulated nozzle geometry, shown in Figure 8.9. The position of the spray hole is very important for the inflow (especially, the intersection were the sac hole and spray hole meets, see Figure 8.9). According to the simulations, the velocity gradients

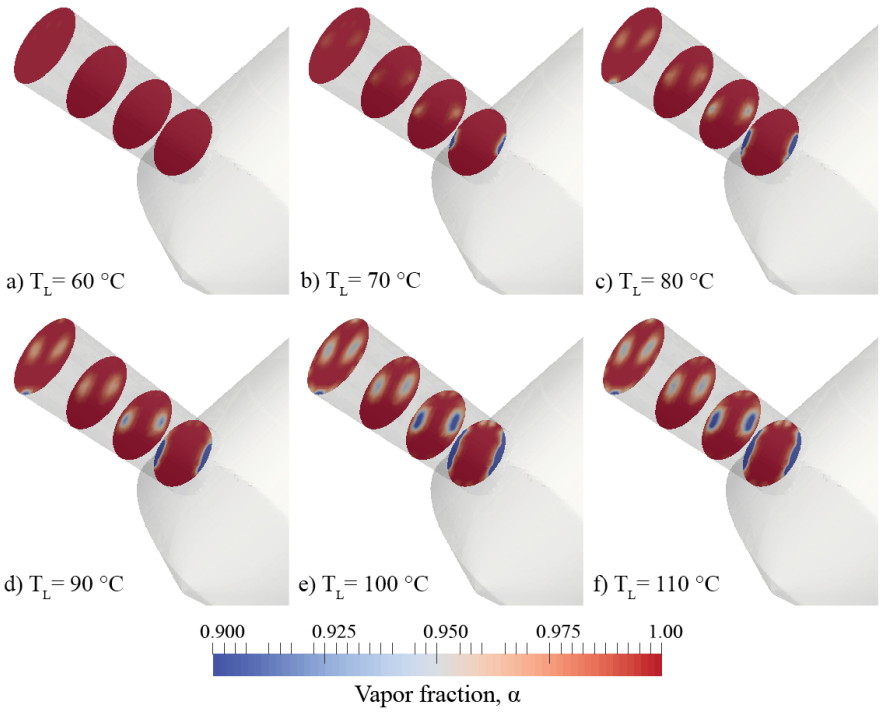

Figure 8.8: Simulation results showing cavitation structures and its dependency of temperature.

(Figure 8.10) are highest at this intersection, thus leading to origin of cavitation. It is important to highlight that the described disagreement is considered not to have an substantial impact on the conclusions made in study.

Edge-induced cavitation and string cavitation

Two types of cavitation are identified in the nozzle volume using the numerical simulations: edge-induced cavitation and string cavitation. Edge-induced cavitation is a result of sudden change in geometry such as sharp edges, while string cavitation is due to the the non-symmetrical flow paths inside the nozzle that leads to a swirling liquid flow. The swirling flow results in the development of cavitation strings in the core of the liquid vortices.

Figure 8.10 shows the velocity vector field throughout the spray hole, where the velocity is represented by the three velocity components (u_y, u_x and u_z). It is seen that the swirling flow is prominent at higher temperatures, and at low temperatures the flow is non-swirling and axisymmetric. The swirling flow leads to the cavitation strings inside the core of the liquid vortices.

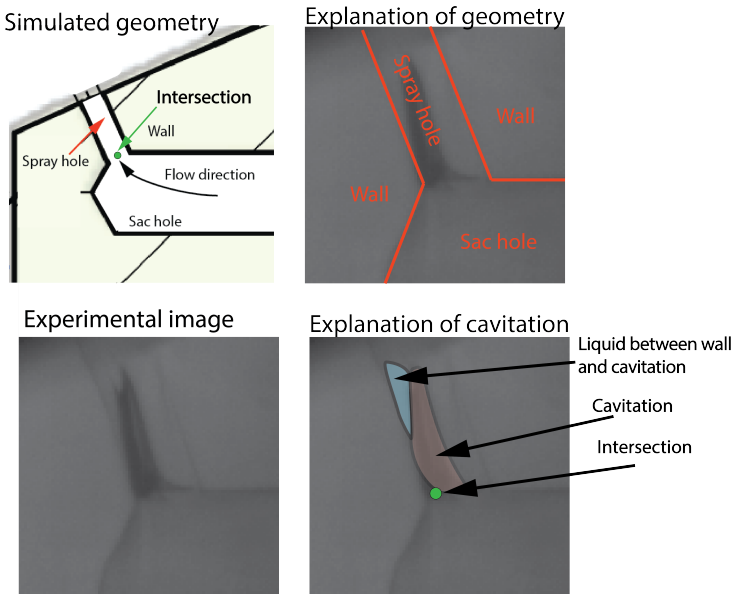

Figure 8.9: The difference between experimental and the simulated nozzle geometry. The position of the spray hole is very important for the inflow and the emerging cavitation.

Both the numerical and experimental observations made in the thesis are supported by a number recent publications revealing the presence cavitation strings in injector flows, which is similar to vortex cavitation, as observed in propeller flows. Some of the recent publications describing string cavitation inside injection nozzles:

- Miranda, R., Chaves, H., & Obermeier, F. (2002). Imaging of Cavitation, Hollow Jets and Jet Branching at Low Lift in a Real Size VCO Nozzle. ILASS-Europe 2002,
- Reid, B. A., Gavaises, M., Mitroglou, N., Hargrave, G. K., Garner, C. P., Long, E. J., & McDavid, R. M. (2014). On the formation of string cavitation inside fuel injectors. Experiments in Fluids, 55(1), 1–8.
- Andriotis, A., Gavaises, M., & Arcoumanis, C. (2008). Vortex flow and cavitation in diesel injector nozzles. Journal of Fluid Mechanics, 610, 195–215.
- Dumouchel, C., Leboucher, N., & Lisiecki, D. (2013). Cavitation and primary atomization in real injectors at low injection pressure condition. Experiments in Fluids, 54(6), 1–17.

According to the literature, it is expected that the described cavitation strings can emerge in the presence of vortex flows.

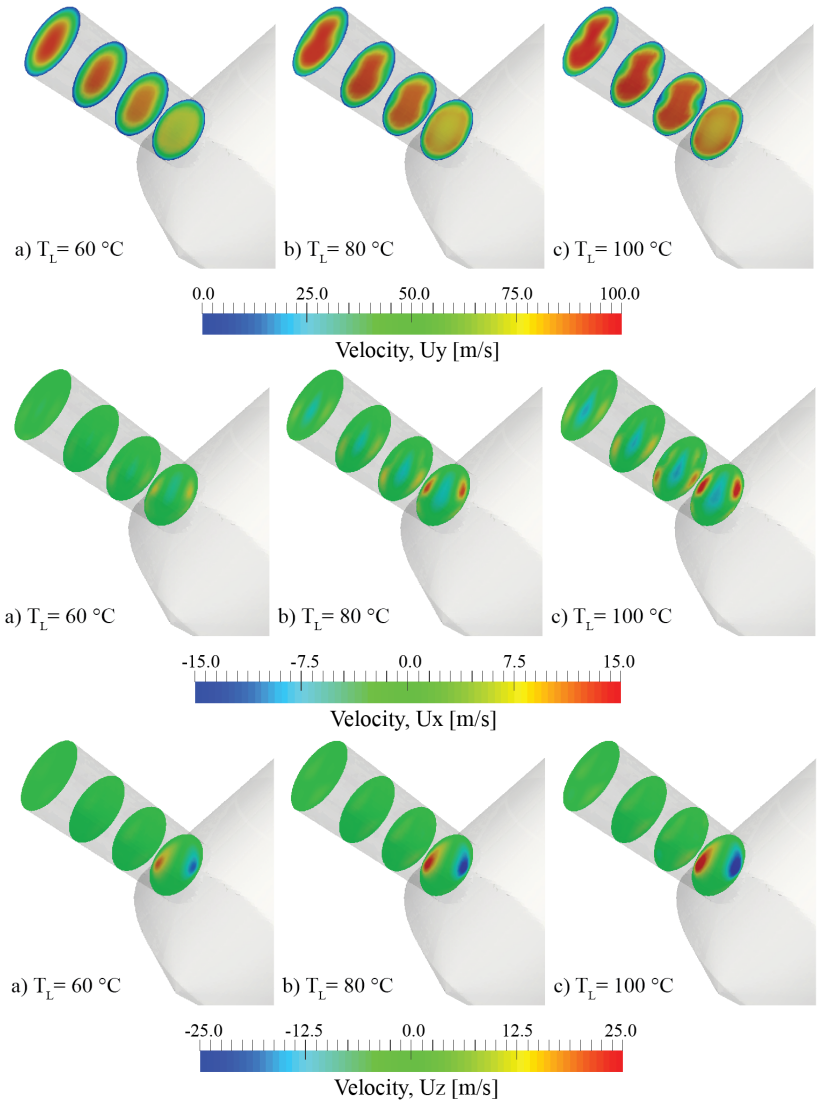

Figure 8.10: The results from the numerical simulations showing the velocity of the liquid through the nozzle exit.

Parametric study of nozzle cavitation

In addition to the work included in Paper B, a parametric study of the nozzle flow has been performed using the numerical model in order to investigate how the degree of cavitation is affected by the temperature of lubrication oil T_{L}, injection pressure P_{i}, and nozzle exit hole diameter D_{n}.

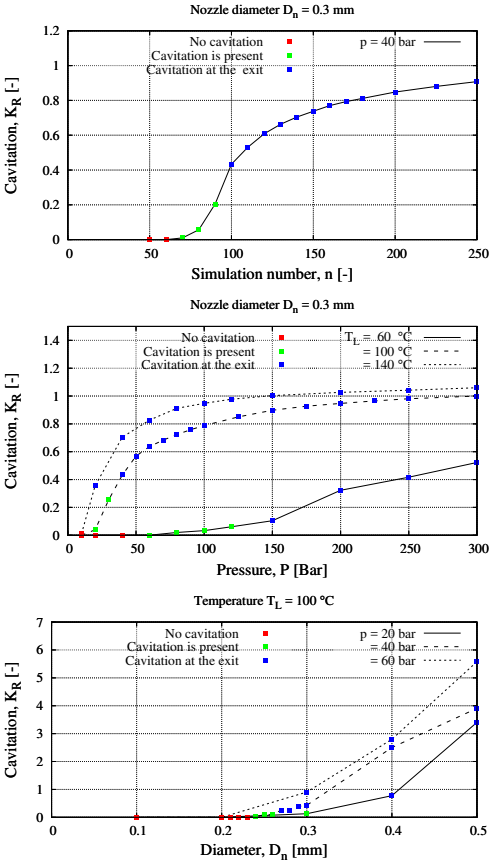

Figure 8.11: Simulation results for temperature T_L, pressure P_i and nozzle diameter D_n. It is shown when cavitation is present in the nozzle volume, and when it extends to the nozzle exit.

The results are shown in Figure 8.11, where the degree of cavitation is expressed in terms of the dimensionless cavitation factor K_R. The factor is a normalized value, which is defined as the number of computational cells that cavitate. There is no cavitation inside the nozzle volume when $K_R = 0.0$, whereas when $K_R = 1.0$ the level of cavitation equals the result at $T_L = 100$, $P_i = 40$ bar and $D_n = 0.3$ mm.

It is shown that values of $K_R > 0.0$ indicate that cavitation is present, and values of $K_R > 0.2$ indicate that the cavitation extends to the nozzle exit. As discussed previously, cavitation at the nozzle exit has a significant influence on the spray formation.

The degree of cavitation at the nozzle exit affect the spray formation, as shown in Figure 8.12 and 8.13. The measurements show the opening, steady and closing stages during an injection cycle for injection pressures $P_{\mathrm{i}} = 40$ bar and $P_{\mathrm{i}} = 60$ bar, $T_{\mathrm{L}} = 100^{\circ}$C and $D_{\mathrm{n}} = 0.3$ mm. These measurement indicates that the higher degree of cavitation at the nozzle exit leads to enhanced break-up.

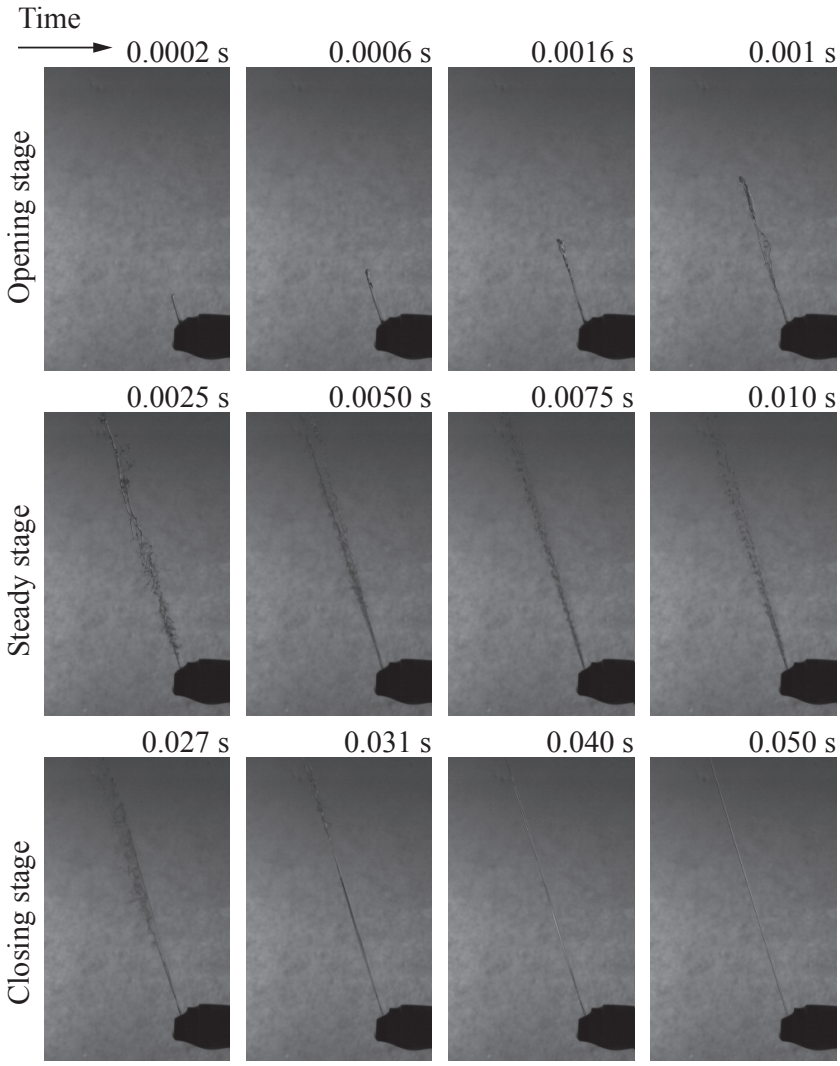

Figure 8.12: A injection cycle performed with the following conditions; $P_{\mathrm{i}} = 40$ bar, $T_{\mathrm{L}} = 100^{\circ}$C and $D_{\mathrm{n}} = 0.3$ mm.

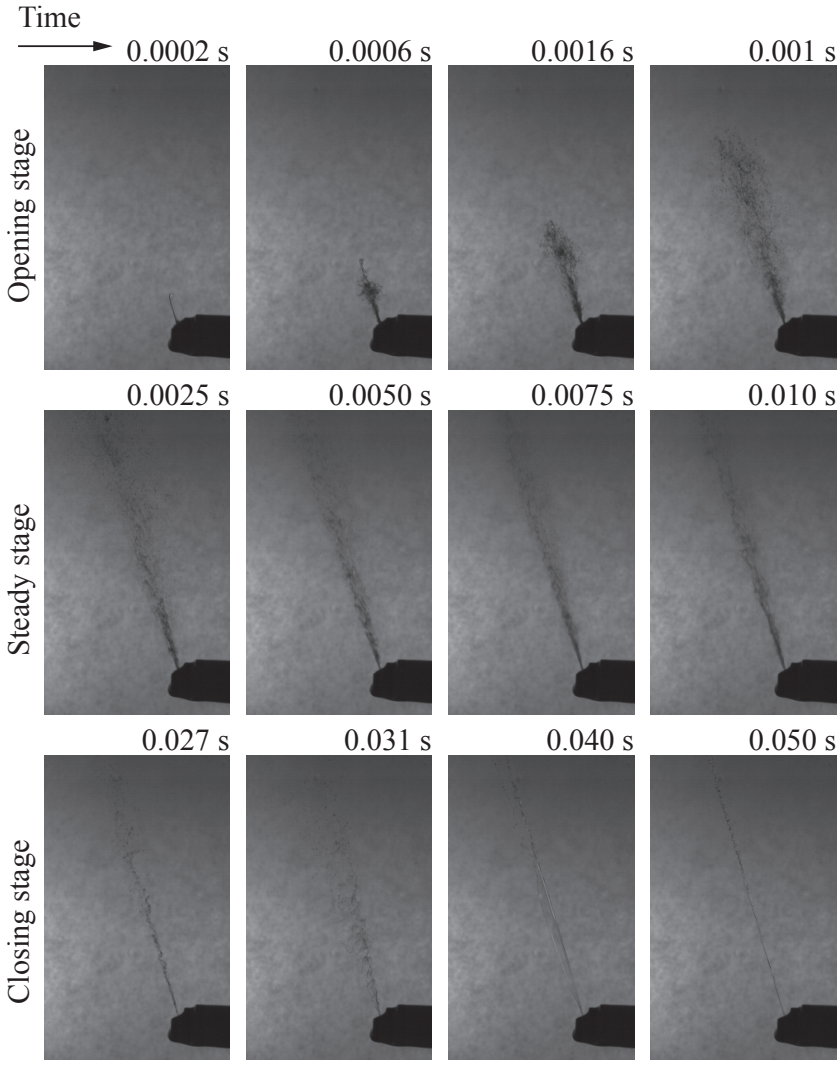

Figure 8.13: A injection cycle performed with the following conditions; $P_{\mathrm{i}} = 60$ bar, $T_{\mathrm{L}} = 100°\mathrm{C}$ and $D_{\mathrm{n}} = 0.3$ mm.

From the numerical study, equation 8.2 has been derived for the studied injection nozzle. This expression describes the relationship between viscosity μ_l, pressure P_i, nozzle diameter D_n, and the dimensionless cavitation factor K_R.

$$\begin{aligned} K_R(\mu_l, P_i, D_n) = & A_1 \cdot e^{\frac{(B_1 \cdot G_1)}{\ln(G_2 \cdot \mu_l)}} + C_1 \cdot e^{\frac{(F_1 \cdot G_1)}{ln(G_2 \cdot \mu_l)}} \\ & + A_2 \cdot e^{(B_2 \cdot P_i)} + C_2 \cdot e^{(F_2 \cdot P_i)} + A_3 \cdot D_n + B_3 \end{aligned} \tag{8.2}$$

The model constants are shown in Table 8.1. This equation can be used to determine when cavitation is present ($K_R > 0.0$), and when it extends to the nozzle exit ($K_R > 0.2$) without the time-consuming setup and calculation performed with the numerical model. The equation plotted against the numerical results for pressure, temperature and diameter, is shown in Figure D.1 in Appendix D.1.

An additional criteria for cavitation is derived by correlating the numerical results from Figure 8.11 with the Reynolds number Re, see Figure 8.14. The figure shows that cavitation is present for $Re > 450$, and that cavitation extends to the exit for $Re > 750$.

Work in this publication is implemented as design rules for injection nozzles at Hans Jensen Lubricators, and also led to a patent application, see Patent B on page 229. Further studies of geometrical nozzle parameters could be included, but they are considered to have minor influence compared to viscosity, pressure and nozzle exit hole diameter.

Table 8.1: The model constants used in equation 8.2.

Model constant	Value
A_1	0.6689
B_1	0.001233
C_1	-11.39
F_1	-0.03487
A_2	0.7888
B_2	0.000855
C_2	-1.473
F_2	-0.033
A_3	16.27
B_3	-5.28
G_1	-149.94
G_2	163.93

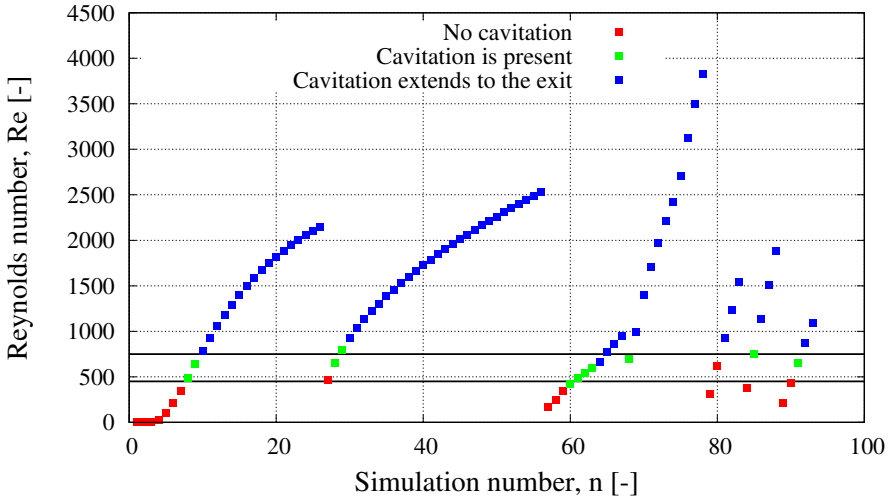

Figure 8.14: The simulation results shown in Figure 8.11 are correlated with the Reynolds number Re. The figure shows that cavitation is present for $Re > 450$, and that cavitation extends to the exit $Re > 750$.

8.3 Discussion of Paper C

In Paper C, a coupling model has been derived in order to initiate the discrete Lagrangian droplets using the nozzle exit conditions. The nozzle exit is therefore separated into a defined number of boundary patches, from which liquid velocity $\boldsymbol{u}$ and degree of cavitation α are used to calculate the diameter of the primary droplet D_i, mass flow rate $\dot{m}_i$, and spray angle ϕ_i at each patch i. The location of each patch is randomly selected in order to suppress geometrical effects when introducing a defined boundary grid.

The number of the droplets injected per unit time is determined from the mass flow rate. The mass flow rate of the primary droplets is calculated using equation 8.3.

$$\dot{m}_i(t) = \rho_\mathrm{l} \cdot A_\mathrm{patch} \cdot \boldsymbol{u_i}(t) \tag{8.3}$$

where ρ_l is the liquid density, A_patch is the area of the selected patch, $\boldsymbol{u}_i$ is the velocity of the liquid composed of the three components in x, y, and z-direction.

The direction of the droplets leaving the nozzle exit is defined using the spray angle. These parameters are highly influenced by the degree of cavitation at the nozzle exit, as busting of cavitation leads to an increased spray angle. The degree of cavitation is expressed in terms of vapor volume fraction

α, which is directly extracted from the internal flow simulations to calculate the spray in equation 8.4.

$$\phi_i = \begin{cases} 0 & \alpha_i = 0 \\ \cos^{-1}\left(\frac{u_{i,xz} \cdot u_{i,y}}{\|u_{i,xz}\| \cdot \|u_{i,y}\|}\right) & \alpha_i < 1 \end{cases} \tag{8.4}$$

The results and conclusions presented in Paper C are drawn from different nozzle flow conditions, see Figure 8.15 and Figure 8.16. The results show a good agreement between the calculated and measured spray cone angle. This is in contrast to the spray tip penetration, where there is a slight difference. The difference is attributed the insufficiency prediction of droplet break-up, which has to implemented in the coupling model or adjusted using the KHRT-model. Moreover, it is important to highlight that the proposed model is capable of predicting the spray structure and asymmetrical shape apart from the spray tip penetration and spray cone angle.

Limited attention has been placed on predicting droplet size, as sufficient droplet measuring methods have not been available in this PhD project. An approach which is not included in the publications, is to adjust the turning constants B_1 or C_3 in the KHRT break-up model according to the level of vapor in the measured patch. Another approach is to initiate droplets with difference sizes, as discussed in 3.3.

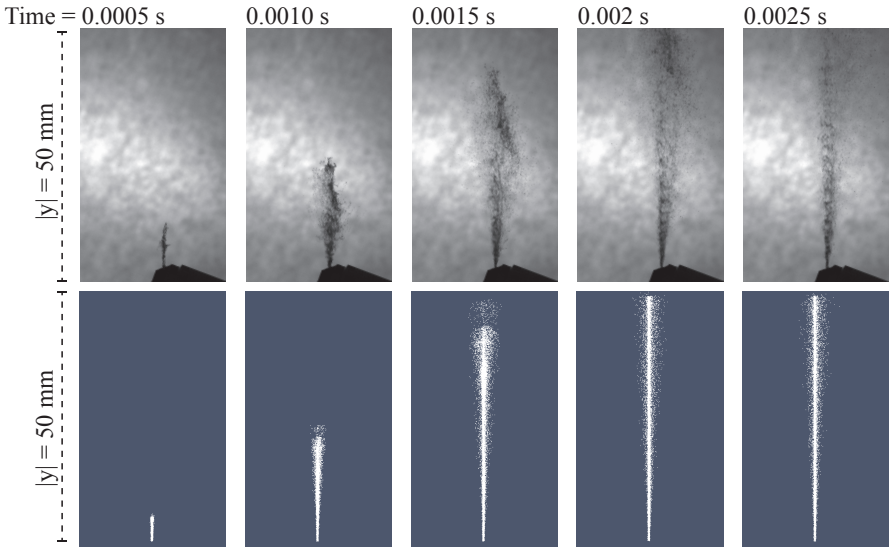

Figure 8.15: Spray formation due to cavitation-induced breakup (Comparison between experiment and numerical simulation). The temperature of the injected liquid is $T_L = 100°C$.

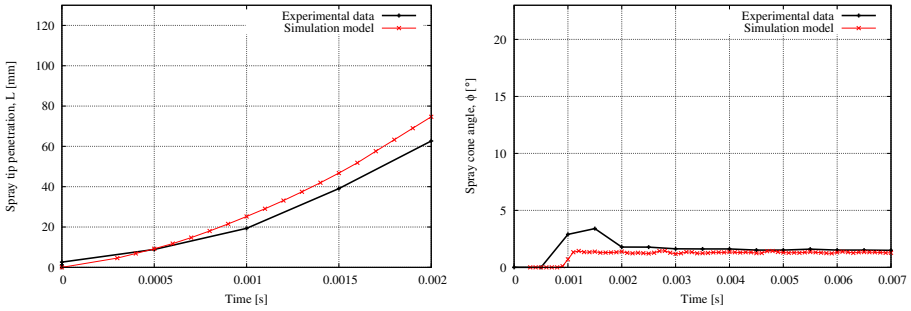

(a) Spray tip penetration and spray cone angle at $T_L = 60°C$

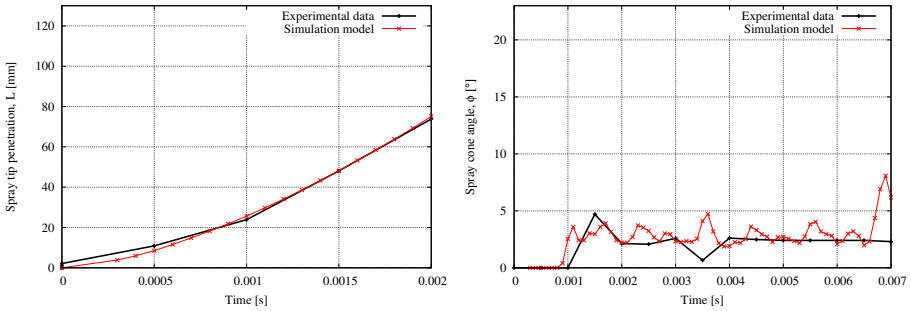

(b) Spray tip penetration and spray cone angle at $T_L = 80°C$

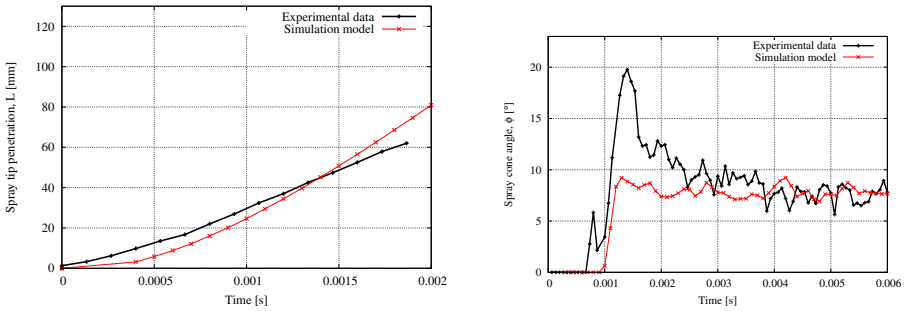

(c) Spray tip penetration and spray cone angle at $T_L = 100°C$

Figure 8.16: Comparison between experiment and numerical simulations of the spray formation.

Part V

Concluding Remarks

9 | Conclusions

The objective of the PhD project has been to create an understanding of the topics influencing the flow of cylinder lubrication oil through injection nozzles and the subsequent spray formation, thus establishing the starting point for understanding the complex process of cylinder spray lubrication systems in two-stroke marine diesel engines.

On basis of a state-of-the-art literature review, three hypotheses were formulated to constitute the basis of the three publications. The main contributions and findings from these publications are presented in the following.

1. The first publication investigated the rheological behavior of cylinder lubrication oils.

   It was shown that the viscosity of seven commercial lubrication oils are similar. Even different levels of calcium carbonate additives incorporated in the oil do not influence the viscosity.

   The lubrication oils can be considered as Newtonian fluids due to no significant change in viscosity at different shear rates. This observation simplifies the modelling of the injection process.

   Temperature has a significant influence on the viscosity. More than a decade of change in viscosity is observed from 40 to 100 °C. This viscosity/temperature dependency can be expressed by the Arrhenius model.

2. The second publication investigated break-up of liquids influenced by cavitation inside the injection nozzle.

   It was shown that cavitation inside the nozzle plays an important role on the spray formation. The growth and collapse of these vapor cavities introduces disturbances to the liquid stream that increases liquid atomization.

   Two types of cavitation are identified in the nozzle volume: edge-induced cavitation and string cavitation. Edge-induced cavitation is a result of sudden changes in geometry such as sharp corners. String

cavitation is due to the the non-symmetrical flow paths inside the nozzle that lead to a swirling liquid flow. The swirling flow results in the development of cavitation strings in the core of the liquid vortices.

When the cavitation strings extend to the exit of the nozzle, the degree of atomization is significantly enhanced. In contrast, when the cavitation collapses in the nozzle volume, the viscous liquid is able to stabilize the stochastic behaviour.

In order to take advantage of cavitation in the studied injection nozzle, design rules have been derived using the dimensionless cavitation constant K_R and Reynolds number Re. Cavitation is present for $K_R > 0.0$ and $Re > 450$, while cavitation extends to the nozzle exit for $K_R > 0.2$ and $Re > 750$.

Shadowgrapic high-speed imaging can be used to detect the cavitation inside the injection nozzle as well as the subsequent spray formation.

The homogeneous equilibrium mixture model together with Schneer-Saur cavitation model can be applied to simulate the cavitation in viscous liquids. The simulation model is able to predict similar behavior as to that observed experimentally.

3. The third publication presented a new cavitation-induced primary break-up model that translates the internal flow simulations to the discrete droplets introduced in the Eulerian-Lagrangian framework.

   It was shown that the influence of cavitation on the spray structure is well reproduced with the presented modelling approach.

   The numerical results show a good agreement with the experimental trends of viscous sprays, i.e. spray structure, spray tip penetration and spray cone angle.

   To complete the presented model, sufficient coupling between cavitation and droplet size has to be implemented.

Finally, the understanding of spray injection of cylinder lubrication oil is increased. The knowledge of cavitation-induced jet break-up in viscous pressure systems is also expanded. Factors affecting cavitation inside spray nozzles are mapped in order to enhance or oppress the degree of atomisation of viscous liquids. Ultimately, a number of tools, CFD models, and knowledge have been implemented at Hans Jensen Lubricators for further development of new products as well as for improvement of the existing ones.

10 | Future work

The current PhD project has been the initial work towards the long-term goal of an efficient cylinder lubrication for two-stroke marine diesel engine. The future challenges involve both experimental work and numerical computations, which are considered in this chapter.

1. Droplet size measurements

   Droplet size measurements are the next step in understanding the studied injection system. Such measurements cannot be performed with the imaging setup used in this PhD thesis. Two commercial imaging systems were tested during this PhD project; one based on Phase Doppler Anemometry (PDA), another based on shadow-graphic imaging. Both systems showed reliable results of droplet size and velocity. Nevertheless, an image based system is preferred due to its overall applications in terms of investigating macro-scale parameters as near-nozzle break-up, spray cone angle and spray penetration.

2. Droplet flight in the scavenging air

   The scavenging air of the engine has to taken into account, in order to determine how the lube oil is distributed on the cylinder wall. The behavior of the atomized oil droplets in the swirling flow is partially unknown. Even though optimization of the scavenge flow is important in terms of performance, efficiency and pollution levels, the details of the in-cylinder flow process are poorly understood (Sigurdsson et al., 2014). In general, experimental investigations have been limited to simplified and scaled models, due to the size of two-stroke marine diesel engines (Haider et al., 2013; Ingvorsen et al., 2013; Obeidat et al., 2014)

   It could be assumed, that large oil droplet with a high momentum might be transported directly to a collision with the surface of the cylinder, whereas smaller particles might end up in an aerosol carried along by swirl and deposited on the wall in this way or remaining in the gas until ignition. Furthermore, the droplet break-up is also affected by the cross-wind experienced by the droplet.

3. Droplet wall impingement

   Droplets of different sizes will hit the cylinder liner at different velocities. The oil is viscoelastic, which means that droplets hitting the liner will also behave elastically and might bounce back from the liner instead of staying and spreading. The same elastic phenomenon is well known from, for example, spray painting.

   When the oil droplets are attached on the cylinder liner, they will spread due to the surface tension, or meet an already covered surface to increase the thickness of the lubricating layer. Assuming the oil remain on the surface, the spreading and development of a uniform layer thickness is a time-driven process.

References

Abderrezzak, B. and Huang, Y. (2016). A contribution to the understanding of cavitation effects on droplet formation through a quantitative observation on breakup of liquid jet. *International Journal of Hydrogen Energy*, 41(35):15821–15828.

Ahmad, Z. (2006). *Principles of Corrosion Engineering and Corrosion Control*. Butterworth-Heinemann.

Aleiferis, P. G., Serras-Pereira, J., Augoye, A., Davies, T. J., Cracknell, R. F., and Richardson, D. (2010). Effect of fuel temperature on in-nozzle cavitation and spray formation of liquid hydrocarbons and alcohols from a real-size optical injector for direct-injection spark-ignition engines. *International Journal of Heat and Mass Transfer*, 53(21-22):4588–4606.

Aliseda, A., Hopfinger, E. J., Lasheras, J. C., Kremer, D. M., Berchielli, A., and Connolly, E. K. (2008). Atomization of viscous and non-newtonian liquids by a coaxial, high-speed gas jet. Experiments and droplet size modeling. *International Journal of Multiphase Flow*, 34(2):161–175.

Andriotis, A., Gavaises, M., and Arcoumanis, C. (2008). Vortex flow and cavitation in diesel injector nozzles. *Journal of Fluid Mechanics*, 610:195–215.

Arcoumanis, C., Gavaises, M., and French, B. (1997). Effect of Fuel Injection Processes on the Structure of Diesel Sprays. *SAE Technical Paper 970799*.

Baldwin, E., Grover, R., Parrish, S., Duke, D., Matusik, K., Powell, C., Kastengren, A., and Schmidt, D. (2016). String flash-boiling in gasoline direct injection simulations with transient needle motion. *International Journal of Multiphase Flow*, 87:90–101.

Barnes, H. A. (2001). *A handbook of elementary rheology*. Aberystwyth: University of Wales Institute of Non-Newtonian Fluid Mechanics, Dyfed, Wales.

Barnes, H. A., Hutton, J. F. J. F., and Walters, K. (1989). *An introduction to rheology*. Elsevier.

Baumgarten, C. (2006). *Mixture Formation in Internal Combustion Engine*. Springer Berlin Heidelberg.

Baumgarten, C., Stegemann, J., and Merker, G. (2002). A new model for cavitation induced primary break-up of diesel sprays. *ILASS-Europe 2002*.

Bergwerk, W. (1959). Flow pattern in Diesel Nozzle Spray Hole. *Proceedings of the Institution of Mechanical Engineers*, 173.

Bicer, B. (2015). *Numerical Simulation of Cavitation Phenomena inside Fuel Injector Nozzles*. PhD thesis, Kobe University, Kobe.

Bicer, B. and Sou, A. (2015). Turbulence and Bubble Dynamics Models to Simulate Transient Cavitation Flow in Fuel Injector Nozzle. *ICLASS-2015*.

Blenkey, N. (2014). Slow steaming, fuel sulfur limits present lubrication challenges: operation on distillate fuel poses different lubrication challenges. *Marine Log*, 119.

Brennen, C. E. (2005). *Fundamentals of Multiphase Flows*. Cambridge University Press, Cambridge, UK.

Bruno, B. A. (2000). *Secondary droplet breakup in periodic aerodynamic flows*. PhD thesis, Pennsylvania State University.

Castrejón-Garcia, R., Castrejón-Pita, J. R., Martin, G. D., and Hutchings, I. M. (2011). The shadowgraph imaging technique and its modern application to fluid jets and drops. *Revista mexicana de fisica*, 57(3):266–275.

Chen, G., Xiong, Q., Morris, P. J., Paterson, E. G., Sergeev, A., and Wang, Y. (2014). OpenFOAM for computational fluid dynamics. *Notices of the American Mathematical Society*, 61(4):354–363.

CIMAC Marine Lubricants Working Group (2017). The lubrication of two-stroke crosshead diesel engines. *CIMAC Recommendation 31*, 05.

Crowe, C. T., Schwarzkopf, J. D., Sommerfeld, M., and Tsuji, Y. (2012). *Multiphase Flows with Droplets and Particles*. CRC Press, 2 edition.

Crua, C. and Heikal, M. R. (2014). Time-resolved fuel injector flow characterisation based on 3D laser Doppler vibrometry. *Measurement Science and Technology*, 25(12):125301.

Dabiri, S., Sirignano, W. A., and Joseph, D. D. (2007). Cavitation in an orifice flow. *Physics of Fluids*, 19(7).

Dam, B. S. (2007). *Experimental and numerical investigations of sprays in two-stroke diesel engines*. PhD thesis, Technical University of Denmark.

Davis, J. R. (2000). *Corrosion: Understanding the basics*. ASM International.

Demoulin, F. X., Réveillon, J., Duret, B., Bouali, Z., Desjonqueres, P., and Ménard, T. (2013). Toward using direct numerical simulationto improve primary break-up modeling. *Atomization and Sprays*, 23(11):957–980.

Desantes, J. M., Garcia-Oliver, J. M., Pastor, J. M., and Pandal, A. (2016). A comparison of diesel sprays CFD modeling approaches: DDM versus Σ-Y Eulerian Atomization Model. *Atomization and Sprays*, 26(7):713–737.

Dong, P., Inaba, T., Nishida, K., and Shimo, D. (2016). Characteristics of the internal flow and the near-field spray of a single-hole injector and a multi-hole injector for diesel engines. *Proceedings of the Institution of Mechanical Engineers*, 230(5):632–649.

Dumouchel, C. (2008). On the experimental investigation on primary atomization of liquid streams. *Experiments in Fluids*, 45(3):371–422.

Dumouchel, C., Leboucher, N., and Lisiecki, D. (2013). Cavitation and primary atomization in real injectors at low injection pressure condition. *Experiments in Fluids*, 54(6):1–17.

Eriksen, L. (2003). Developments in Cylinder Liner Lubrication. In *Recent Developments in Marine Engineering Operations*. Hans Jensen Lubricators A/S.

Fansler, T. D. and Parrish, S. E. (2015). Spray measurement technology: a review. *Measurement Science and Technology*, 26(1):012002.

Franc, J.-P. and Michel, J.-M. (2006). *Fundamentals of Cavitation*. Springer Science + Business Media, Inc.

Fu, J., Lu, Y., Campbell, C. B., and Papadopoulos, K. D. (2006). Temperature and acid droplet size effects in acid neutralization of marine cylinder lubricants. *Tribology Letters*, 22(3):221–225.

Galindo-Rosales, F. J. (2017). *Complex Fluid-Flows in Microfluidics*. Springer International Publishing.

Gardhouse, T., Sercey, G. D., Crua, C., Edwards, S., and Thompson, C. (2014). Shadowgraphic characterisation of marine lubricant sprays. *ILASS-Europe 2014*.

Gavaises, M., Villa, F., Koukouvinis, P., Marengo, M., and Franc, J.-P. (2015). Visualisation and les simulation of cavitation cloud formation and collapse in an axisymmetric geometry. *International Journal of Multiphase Flow*, 68:14–26.

Ghadimi, P., Yousefifard, M., and Nowruzi, H. (2016). Applying different strategies within OpenFOAM to investigate the effects of breakup and collision model on the spray and in-cylinder gas mixture attribute. *Journal of Applied Fluid Mechanics*, 9(6):2781–2790.

Ghiji, M., Goldsworthy, L., Brandner, P. A., Garaniya, V., and Hield, P. (2017). Analysis of diesel spray dynamics using a compressible Eulerian/VOF/LES model and microscopic shadowgraphy. *Fuel*, 188:352–366.

Giannadakis, E., Gavaises, M., and Arcoumanis, C. (2008). Modelling of cavitation in diesel injector nozzles. *Journal of Fluid Mechanics*, 616:153–193.

Gjesing, R. (2008). *A new integrated numerical model of the atomization and in flight phenomena in the spray forming process*. PhD thesis, Technical University of Denmark.

Gjesing, R., Hattel, J., and Fritsching, U. (2009). Coupled atomization and spray modelling in the spray forming process using OpenFOAM. *Engineering Applications of Computational Fluid Mechanics*, 3(4):471–486.

Guo, Z., Yuan, C., Liu, P., Peng, Z., and Yan, X. (2013). Study on influence of cylinder liner surface texture on lubrication performance for cylinder liner-piston ring components. *Tribology Letters*, 51:9–23.

Haider, S., Schnipper, T., Obeidat, A., Meyer, K. E., Okulov, V. L., Mayer, S., and Walther, J. H. (2013). PIV study of the effect of piston position on the in-cylinder swirling flow during the scavenging process in large two-stroke marine diesel engines. *Journal of Marine Science and Technology*, 18(1):133–143.

He, Z., Guo, G., Tao, X., Zhong, W., Leng, X., and Wang, Q. (2016). Study of the effect of nozzle hole shape on internal flow and spray characteristics. *International Communications in Heat and Mass Transfer*, 71:1–8.

Hejranfar, K., Ezzatneshan, E., and Fattah-Hesari, K. (2015). A comparative study of two cavitation modeling strategies for simulation of inviscid cavitating flows. *Ocean Engineering*, 108:257–275.

Herrmann, M. (2011). On simulating primary atomization using the refined level set grid method. *Atomization and Sprays*, 21(4):283–301.

Hoyas, S., Gil, A., Fajardo, P., Khuong-Anh, D., and Ravet, F. (2012). Evaluation and Validation of ELSA Model in Diesel Sprays - 3D Cavitating Nozzles Case. *ICLASS-2012*.

Huang, B. and Wang, G. Y. (2011). A modified density based cavitation model for time dependent turbulent cavitating flow computations. *Chinese Science Bulletin*, 56(19):1985–1992.

Huijbregts, W. and Leferink, R. (2004). Latest advances in the understanding of acid dewpoint corrosion: corrosion and stress corrosion cracking in combustion gas condensates. *Anti-Corrosion Methods and Materials*, 51(3):173–188.

Hult, J., Simmank, P., Matlok, S., Mayer, S., Falgout, Z., and Linne, M. (2016). Interior flow and near-nozzle spray development in a marine-engine diesel fuel injector. *Experiments in Fluids*, 57(4):1–19.

Ingvorsen, K. M., Meyer, K. E., Walther, J. H., and Mayer, S. (2013). Turbulent swirling flow in a model of a uniflow-scavenged two-stroke engine. *Experiments in Fluids*, 54(3):1–17.

Jensen, P., Bach, M., Salufas, A., Tsalapatis, D., and Rolsted, H. (2016). Lubtronic SIP promise remarkably low wear rates with low CLO consumption. *CIMAC Congress 2016*.

Jensen, T. (2002). Swirl Injection Lubrication Low Cylinder Oil Consumption without Sacrificing Wear Rates. *Journal of Japan Institute of Marine Engineering*, 37(2):41–50.

Jing, D. (2005). *Experimental and Numerical Studies of Fuel Spray*. PhD thesis, University of Birmingham.

Johansson, T. B., Patwardhan, A. P., Nakićenović, N., and Gomez-Echeverri, L. (2012). *Global Energy Assessment: Toward a Sustainable Future*. Cambridge University Press.

Jollet, S., Hansen, H., Bitner, K., Niemeyer, D., and Dinkelacker, F. (2014). Experimental and numerical investigations of 90 micrometer real-size transparent nozzles with high pressure conditions. *ILASS-Europe 2014*.

Karrholm, F. P. (2008). *Numerical modelling of diesel spray injection, turbulence interaction and combustion*. PhD thesis, Chalmers University of Technology.

Kastengren, A. L., Tilocco, F. Z., Powell, C. F., Manin, J., Pickett, L. M., Payri, R., and Bazyn, T. (2012). Engine combustion network (ECN): measurements of nozzle geometry and hydraulic behavior. *Atomization and Sprays*, 22(12):1011–1052.

Kayhani, M. H., Aghaie, A. Z., and Razavi, M. R. M. (2012). Investigation of Different Numerical Models in Spray Behavior Simulation In Order To Predict The Spray Tip Penetration. *ICMAR'2012*.

Khmelev, V. N., Shalunov, A. V., and Smerdina, E. S. (2006). The cavitation spraying of the viscous liquids. *International Workshops and Tutorials on Electron Devices and Materials*, pages 269–273.

Koch, M., Lechner, C., Reuter, F., Köhler, K., Mettin, R., and Lauterborn, W. (2016). Numerical modeling of laser generated cavitation bubbles with the finite volume and volume of fluid method, using OpenFOAM. *Computers and Fluids*, 126:71–90.

Laidler, K. J., Meiser, J. H., and Sanctuary, B. C. (2003). *Physical chemistry*. Houghton Mifflin, 4. edition.

Lakshminarayanan, P. A. and Nayak, N. S. (2011). *Critical Component Wear in Heavy Duty Engines*. Wiley.

Lee, W. G. and Reitz, R. D. (2010). A Numerical Investigation of Transient Flow and Cavitation Within Minisac and Valve-Covered Orifice Diesel Injector Nozzles. *Journal of Engineering for Gas Turbines and Power*, 132(5):052802.

Lefebvre, A. (1989). *Atomization and Sprays*. Hemispheres Publishing.

Lefebvre, A. H. and Mcdonell, V. G. (2017). *Atomization and Sprays*. CRC Press, 2 edition.

Li, Z. (2014). Criteria for jet cavitation and cavitation jet drilling. *International Journal of Rock Mechanics and Mining Sciences*, 71:204–207.

Livanos, G. A. and Kyrtatos, N. P. (2007). Friction model of a marine diesel engine piston assembly. *Tribology International*, 40:1441–1453.

Marcer, R. and LeGouez, J. M. (2001). Simulation of unsteady cavitating flows in diesel injector with an improved VOF method. *ILASS-Europe 2001*.

Martinez, L., Benkenida, A., and Cuenot, B. (2010). A model for the injection boundary conditions in the context of 3D simulation of diesel Spray: methodology and validation. *Fuel*, 89:219–228.

Moeslund, T. B. (2012). *Introduction to Video and Image Processing*. Springer.

Mohamad, S. a., Lu, X., and Zheng, Q. (2015). Numerical modeling of lubrication of piston ring of two-stroke marine diesel engine considering the effect of multi-scale grooves on the cylinder liner. *Proceedings of the Institution of Mechanical Engineers*, 229(8):989–1002.

Mohan, B., Yang, W., and Chou, S. K. (2014a). Development of an accurate cavitation coupled spray model for diesel engine simulation. *Energy Conversion and Management*, 77:269–277.

Mohan, B., Yang, W., and Yu, W. (2014b). Effect of internal nozzle flow and thermo-physical properties on spray characteristics of methyl esters. *Applied Energy*, 129:123–134.

Morgut, M. and Nobile, E. (2012). Numerical Predictions of Cavitating FlowaroundModel Scale Propellers by CFD and Advanced Model Calibration. *International Journal of Rotating Machinery*, 2012:1–11.

Morgut, M., Nobile, E., and Biluš, I. (2011). Comparison of mass transfer models for the numerical prediction of sheet cavitation around a hydrofoil. *International Journal of Multiphase Flow*, 37(6):620–626.

Mostafa, A. A. and Mongia, H. C. (1987). On the modeling of turbulent evaporating sprays: Eulerian versus lagrangian approach. *International Journal of Heat and Mass Transfer*, 30(12):2583–2593.

Moyne, L. L. (2010). Trends in atomization theory. *International Journal of Spray and Combustion Dynamics*, 2(1):49–84.

Nishimura, A. and Assanis, D. N. (2000). A Model for Primary Diesel Fuel Atomization Based on Cavitation Bubble Collapse Energy. *ICLASS 2000*, pages 1249–1256.

Nordin, N. (2001). *Complex Chemistry Modelling of Diesel Spray Combustion*. PhD thesis, Chalmers University of Technology.

Nowruzi, H., Ghadimi, P., and Yousefifard, M. (2014). A numerical study of spray characteristics in medium speed engine fueled by different HFO/n-butanol blends. *International Journal of Chemical Engineering*, 2014:1–13.

Obeidat, A., Schnipper, T., Ingvorsen, K. M., Haider, S., Erik, M. K., Mayer, S., and Walther, J. H. (2014). Large eddy simulations of the influence of piston position on the swirling flow in a model two-stroke diesel engine. *International Journal of Numerical Methods for Heat & Fluid Flow*, 24(2):325–341.

Olander, P., Hollman, P., and Jacobson, S. (2013). Piston ring and cylinder liner wear aggravation caused by transition to greener ship transports-Comparison of samples from test rig and field. *Wear*, 302(1-2):1345–1350.

OpenFOAM Foundation (2014). *OpenFOAM - The Open Source CDF Toolbox*. OpenFOAM Foundation.

Payri, F., Bermudez, V., Payri, R., and Salvador, F. J. (2004a). The influence of cavitation on the internal flow and the spray characteristics in diesel injection nozzles. *Fuel*, 83(4-5):419–431.

Payri, R., Molina, S., Salvador, F., and Gimeno, J. (2004b). A study of the relation between nozzle geometry, internal flow and sprays characteristics in diesel fuel injection systems. *KSME International Journal*, 18(7):1222 – 1235.

Payri, R., Salvador, F. J., Gimeno, J., and Venegas, O. (2013). Study of cavitation phenomenon using different fuels in a transparent nozzle by hydraulic characterization and visualization. *Experimental Thermal and Fluid Science*, 44:235–244.

Pischke, P. (2014). *Modeling of Collisional Transport Processes in Spray Dynamics*. PhD thesis, RWTH Aachen University.

Powell, C., Kastengren, A., Liu, Z., and Fezzaa, K. (2011). The effects of diesel injector needle motion on spray structure. *Journal of Engineering for Gas Turbines and Power, Transactions of the ASME*, 133(1):012802.

Pratama, R. H., Sou, A., Wada, Y., and Yokohata, H. (2015). Cavitation in Mini-Sac Nozzle and Injected Liquid Jet. *ICLASS-2015*.

Reiner, M. (1964). The Deborah Number. *Physics Today*, 17:62.

Reitz, R. D. and Beale, J. C. (1999). Modeling spray atomization with the Kelvin-Helmholtz/Rayleigh-Taylor Hybrid model. *Atomization and Sprays*, 9(6):623–650.

Reitz, R. D. and Bracco, F. (1982). Mechanism of atomization of a liquid jet. *Physics of Fluids*, 25(10):1730.

Ronnedal, P. and Yamamoto, H. (2013). Challenges for Cylinder Liner Development. *CIMAC Congress 2013*.

Roohi, E., Zahiri, A. P., and Passandideh-Fard, M. (2013). Numerical simulation of cavitation around a two-dimensional hydrofoil using VOF method and LES turbulence model. *Applied Mathematical Modelling*, 37(9):6469–6488.

Salvador, F., Romero, J.-V., Roselló, M.-D., and Martínez-López, J. (2010). Validation of code model cavitation phenomena in diesel injector nozzles. *Mathematical and Computer Modelling*, 52(7):1123–1132.

Salvador, F. J., Romero, J. V., Rosello, M. D., and Jaramillo, D. (2016). Numerical simulation of primary atomization in diesel spray at low injection pressure. *Journal of Computational and Applied Mathematics*, 291(1):94–102.

Santos, F. D. and Moyne, L. L. (2011). Spray atomization models in engine applications, from correlations to direct numerical simulations. *Oil and Gas Science and Technology*, 66(5):801–822.

Sauer, J. and Schnerr, G. H. (2000). Unsteady cavitating flow: a new cavitation model based on a modified front capturing method and bubble dynamics. *FEDSM'00, ASME Fluids Engineering Summer Conference*, pages 11–15.

Sautermeister, F. A. and Priest, M. (2012). Physical and Chemical Impact of Sulphuric Acid on Cylinder Lubrication for Large 2-Stroke Marine Diesel Engines. *Tribology Letters*, 47(2):261–271.

Schmidt, D. P. and Corradini, M. L. (2001). The internal flow of diesel fuel injector nozzles: a review. *International Journal of Engine Research.*, 2(1):1–22.

Schmidt, D. P. and Rutland, C. J. (2004). Reducing grid dependency in droplet collision modeling. *Journal of Engineering for Gas Turbines and Power*, 126(2):227.

Schramm, J., Henningsen, S., and Sorenson, S. (1994). Modelling of Corrosion of Cylinder Liner in Diesel Engines Caused by Sulphur in the Diesel Fuel. *SAE Technical Paper 940818*.

Sherrington, I. (2011). Oil film thickness measurement: a contribution to the understanding and control of lubrication in the piston-ring packs of IC engines. *Proceedings of the Institution of Mechanical Engineers, Part J: Journal of Engineering Tribology*, 225(7):595–601.

Shi, Y., Ge, H.-W., and Reitz, R. D. (2011). *Computational Optimization of Internal Combustion Engines*. Springer-Verlag London Limited.

Sigurdsson, E., Ingvorsen, K. M., Jensen, M. V., Mayer, S., Matlok, S., and Walther, J. H. (2014). Numerical analysis of the scavenge flow and convective heat transfer in large two-stroke marine diesel engines. *Applied Energy*, 123:37–46.

Soriano, O. J. and Rotondi, R. (2008). Linking nozzle flow and primary breakup of high pressure diesel jets using CFD. *ILASS-Europe 2008*.

Soriano-Palao, O. J., Sommerfeld, M., and Burkhardt, A. (2014). Modelling the influence of the nozzle geometry on the primary breakup of diesel jets. *International Journal of Spray and Combustion Dynamics*, 6(2):113–146.

Sou, A., Bicer, B., and Tomiyama, A. (2014). Numerical simulation of incipient cavitation flow in a nozzle of fuel injector. *Computers and Fluids*, 103:42–48.

Sou, A., Hosokawa, S., and Tomiyama, A. (2007). Effects of cavitation in a nozzle on liquid jet atomization. *International Journal of Heat and Mass Transfer*, 50(17-18):3575–3582.

Stachowiak, G. and Batchelor, A. W. (2013). *Engineering Tribology*. Elsevier Science, 4 edition.

Subramaniam, S. (2013). Lagrangian-Eulerian methods for multiphase flows. *Progress in Energy and Combustion Science*, 39(2-3):215–245.

Tamaki, N. and Shimizu, M. (2002). Enhancement of atomization of high-viscous liquid jet by pressure atomized nozzle. *ILASS-Europe 2002*.

Taylor, G. (1950). The instability of liquid surfaces when accelerated in a direction perpendicular to their planes. I. *Proceedings of the Royal Society of London. Series A, Mathematical and Physical Sciences*, 201(1065):192–196.

Toft, O. and Thomsen, J. (2007). Some common field experience with large bore 2-stroke engines. In *CIMAC Congress 2007*.

Tropea, C., Yarin, A. L., and Foss, J. F. (2007). *Springer handbook of experimental fluid mechanics*. Springer Science+Business Media.

Valenti, G., Colombo, L., Murgia, S., Lucchini, A., Sampietro, A., Capoferri, A., and Araneo, L. (2013). Thermal effect of lubricating oil in positive-displacement air compressors. *Applied Thermal Engineering*, 51(1-2):1055–1066.

Vallier, A. A. (2013). *Simulations of cavitation – from the large vapour structures to the small bubble dynamics*. PhD thesis, Lund University.

Versteeg, H. and Malalasekera, W. (2007). *An Introduction to Computational Fluid Dynamics - The Finite Volume Method*. Pearson Education Limited, 2 edition.

Vølund, A. (2003). *Measurement and Calculation of Frictional Loss in Large Two-Stroke Engines*. PhD thesis, Technical University of Denmark.

von Berg, E., Edelbauer, W., Alajbegovic, A., Tatschl, R., Volmajer, M., Kegl, B., and Ganippa, L. C. (2005). Coupled Simulations of Nozzle Flow, Primary Fuel Jet Breakup, and Spray Formation. *Journal of Engineering for Gas Turbines and Power*, 127(4):897.

Wan, Z. (2016). Three steps to a green shipping industry: it is time to crack down on the emissions and destructive development caused by vast container vessels that pollute the air and seas. *Nature*, 530(7590):275–277.

Wang, G., Senocak, I., Shyy, W., Ikohagi, T., and Cao, S. (2001). Dynamics of attached turbulent cavitating flows. *Progress in Aerospace Sciences*, 37(6):551–581.

Wang, X. and Su, W. (2009). A numerical study of cavitating flows in high-pressure diesel injection nozzle holes using a two-fluid model. *Chinese Science Bulletin*, 54(10):1655–1662.

Weisser, G., Schulz, R., Wright, Y. M., and Boulouchos, K. (2004). Progress in Computational Fluid Dynamics (CFD) Application for Large Diesel Engine Development. In *CIMAC Congress 2004*.

Wierzba, A. (1990). Deformation and breakup of liquid drops in a gas stream at nearly critical Weber numbers. *Experiments in Fluids*, 9(1-2):59–64.

Winkler, M. (2010). The use of tribology and wear metal analysis in two-stroke engines to optimize oil feed rates and reduce liner wear. *CIMAC Congress 2010*.

Wolff, A. (2014). Simulation based study of the system piston–ring–cylinder of a marine two-stroke engine. *Tribology Transactions*, 57(4):653–667.

Woodyard, D. (2009). *Pounder's marine diesel engines and gas turbines*. Elsevier/Butterworth-Heinemann.

Wu, R. C., Campbell, C. B., and Papadopoulos, K. D. (2000). Acid-Neutralizing of Marine Cylinder Lubricants: Effects of Nonionic Surfactants. *Industrial & Engineering Chemistry Research*, 39(10):3926–3931.

Xue, F., Luo, F., Cui, H., Moro, A., and Zhou, L. (2017). Numerical analyses of transient flow characteristics within each nozzle hole of an asymmetric diesel injector. *International Journal of Heat and Mass Transfer*, 104:18–27.

Yarin, A. L., Roisman, I. V., and Tropea, C. (2017). *Collision Phenomena in Liquids and Solids*. Cambridge University Press.

Yu, H., Goldsworthy, L., Brandner, P., and Garaniya, V. (2016a). Modelling of In-Nozzle Cavitation and Early Spray Breakup Using a Multiphase Volume of Fluid Method. *20th Australasian Fluid Mechanics Conference*.

Yu, Y., Li, G., Wang, Y., and Ding, J. (2016b). Modeling the atomization of high-pressure fuel spray by using a new breakup model. *Applied Mathematical Modelling*, 40:268–283.

Yuan, W., Sauer, J., and Schnerr, G. H. (2001). Modeling and computation of unsteady cavitation flows in injection nozzles. *Mécanique & Industrie*, 2(5):383–394.

Zhang, X., Moon, S., Gao, J., Dufresne, E. M., Fezzaa, K., and Wang, J. (2016). Experimental study on the effect of nozzle hole-to-hole angle on the near-field spray of diesel injector using fast X-ray phase-contrast imaging. *Fuel*, 185:142–150.

Zhu, J., Chen, Y., Zhao, D., and Zhang, X. (2015). Extension of the Schnerr–Sauer model for cryogenic cavitation. *European Journal of Mechanics / B Fluids*, 52:1–10.

Part VI

Appendix

A | Corrosive Wear in Diesel Engines

In general, corrosive wear occurs there is a combination of abrasive or adhesive wear and a corrosive environment. The rate of material loss can be very high, and many times higher than the individual wear process or corrosion alone. This is because loose corrosion products are easily removed by wear and continually replaced new metal from the beneath, which in turn can corrode quickly (CIMAC Marine Lubricants Working Group, 2017). Corrosive wear on the cylinder walls is divided into two types (Woodyard, 2009):

- **Low-temperature corrosion** is introduced when the temperature at the cylinder liner is below the dew point of sulphuric acid, which leads to the condensation of sulphuric acid vapour formed during combustion (Lakshminarayanan and Nayak, 2011).
- **High-temperature corrosion** is introduced by the vanadium in the heavy fuel, which combines with sodium and sulphur during the combustion process to form eutectic compounds. At temperatures higher than the compounds melting point at $530^{\circ}C$, the compounds weld at the cylinder wall. These molten compounds are very corrosive and attack the protective oxide layers on steel and exposing it to corrosion. Besides high-corrosion, the compounds deposit out during combustion, leading to abrasive wear on the cylinder liner and piston ring (Woodyard, 2009).

A shift in the marine industry to slow steaming has introduced new stresses on existing marine diesel engines, which were originally built to operate at higher service speeds (Blenkey, 2014). Slow steaming induces the diesel engines to operate at higher pressure and lower temperature, which challenges both the fuel oil and cylinder lubrication oil. Fuel oils are of a fairly low quality and generally have a high sulphur content (2-5%) which leads to the formation of sulphuric acids (Wu et al., 2000). To prevent corrosive wear, lubrication oils have been formulated with neutralising agents to

avoid most of the corrosive wear (Olander et al., 2013). This low-temperature corrosive wear is described in this chapter.

A.1 What is corrosion?

Most commonly used metals are unstable in the atmosphere. These unstable metals are produced by reducing ores artificially, and therefore they tend to return to their original state or to similar metallic compounds when exposed to the atmosphere (Davis, 2000). The formation and decomposition of steel products are shown in Figure A.1. For most materials, this means formation of the oxides or sulphides from which they originally started when they were taken from the earth (Ahmad, 2006).

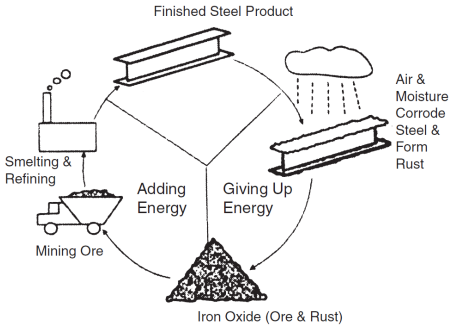

Figure A.1: The formation and decomposition of steel products (Davis, 2000).

The changes in metals are electrochemical reactions that follow the laws of thermodynamics. This is why both the dimensions of chemistry and electricity must be understood in order to explain the corrosion process of a cylinder liner.

A.2 Low-temperature corrosion

As presented in Section A.1, the main force driving the corrosion mechanism is the tendency of iron returning to its thermodynamic state. The iron (Fe^0) is unstable and therefore tends to oxidize to form rust ($Fe(OH)_2$ or $Fe(OH)_3$) (Ahmad, 2006).

The corrosion reactions can be considered as an anordic-cathodic reaction. This is when electrons leave the iron at anodic areas (equation A.1), and at

the cathodic areas, reduction of oxygen takes place (A.2).

$$Fe \rightarrow Fe^{2+} + 2e \tag{A.1}$$

$$O_2 + 2H_2O + 4e \rightarrow 4OH^- \tag{A.2}$$

The OH ions react with the Fe^{2+}ions produced and thereby forming:

$$\mathrm{Fe}^{2+} + 2\mathrm{OH}^- \rightarrow \mathrm{Fe(OH)}_2 \tag{A.3}$$

$\mathrm{Fe(OH)}_2$ oxidizes to form $\mathrm{Fe(OH)}_3$, with access to more air and water:

$$4\mathrm{Fe(OH)}_2 + \mathrm{O}_2 + 2\mathrm{H}_2\mathrm{O} \rightarrow 4\mathrm{Fe(OH)}_3 \tag{A.4}$$

And later $4Fe(OH)_3$ loses its water and to form hydrated ferric oxide or rust:

$$4\mathrm{FE(OH)}_2 + \mathrm{O}_2 \rightarrow 2\mathrm{Fe}_2\mathrm{O}_3 \cdot \mathrm{H}_2\mathrm{O} + 2\mathrm{H}_2\mathrm{O} \tag{A.5}$$

An illustration of the aqueous corrosion cycle is shown in Figure A.2. The rust formed at the anodic areas creates a protective surface film in which further corrosion is either eliminated or retarded. The protective film may be as thin as 2-10 nm (Ahmad, 2006).

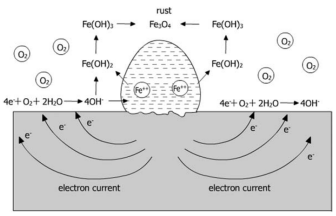

Figure A.2: Aqueous corrosion cycle (Ahmad, 2006).

A.3 Development of corrosive sulfuric acids

The sulphur in diesel fuel reacts completely in the combustion chamber to form sulphur dioxide (SO_2). Further oxidation yields to 0.3-7% sulphur trioxide(SO_3), which rapidly reacts with water to form sulphuric acid (H_2SO_4) at various concentration (Sautermeister and Priest, 2012). These reactions are shown in equation A.6 and A.7.

$$2\mathrm{SO}_2(\mathrm{g}) + \mathrm{O}_2(\mathrm{g}) \rightarrow 2\mathrm{SO}_3(\mathrm{g}) + \mathrm{heat} \tag{A.6}$$

$$\mathrm{SO}_3(\mathrm{g}) + \mathrm{H}_2\mathrm{O}(\mathrm{l}) \rightarrow \mathrm{H}_2\mathrm{SO}_4(\mathrm{aq}) + \mathrm{heat} \tag{A.7}$$

The resulting sulphuric acid condenses on the cylinder wall. The higher the dew point, the more rapidly the condensation occurs. As shown in Figure A.3, the dew point of sulphuric acid depends on three factors: sulphur content, temperature and pressure. The dew point temperature of SO_3 with H_2O can be expressed in terms of a dew point equation shown in, for example, (Huijbregts and Leferink, 2004).

Studies of exhaust gas composition and phase diagrams for vapor of sulphuric acid and water have shown that concentrations of sulphuric acid between 5 and 80 wt.% can be expected to condensate on the cylinder wall (Sautermeister and Priest, 2012).

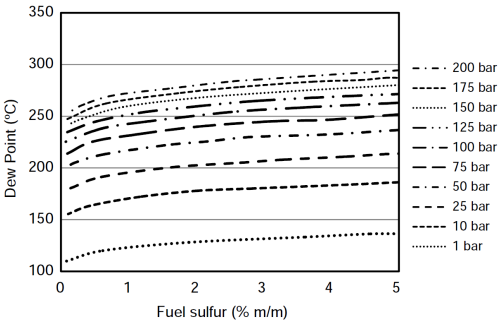

Figure A.3: Dewpoint of sulphuric acids dependent on sulphur content and pressure.

Dilute sulphuric acid reacts with iron via a single displacement reaction due to the polarity of the acid. The reaction produces hydrogen gas and iron sulphate:

$$\mathrm{Fe(s) + H_2SO_4(aq) \rightarrow H_2(g) + FeSO_4(aq)} \tag{A.8}$$

However, concentrated sulphuric acid is a strong oxidizing agent and does not react with iron in the same way. Here, the sulphuric acid is able to accept electrons in order to produce sulphur dioxide, water and sulphate:

$$\mathrm{2H_2SO_4 + 2e^- \rightarrow SO_2 + 2H_2O + SO_4^{2-}} \tag{A.9}$$

Electrons used for the reaction in equation A.9, can be delivered from the reactive iron from the cylinder wall. This leads to the development of anodic areas, that promote corrosion through the corrosion mechanism described through equation A.1 to A.5.

A.4 Neutralisation of sulphuric acids

As described in Chapter 5, the neutralization of sulphuric acids is conducted by an alkaline reserve in the marine cylinder lubricants. The alkaline reserve is usually added into the lubricant by dispersing calcium carbonate particles as reversed micelles (Sautermeister and Priest, 2012).

In general, the calcium carbonate exists as sulphonates, salicylates, or phenates. When these complex molecules contain a large excess of base, they are referred to over-based detergents. As shown in Figure A.4, the over-based sulfonates and salicylates form of a reserve micelles with mixed alkyl-aryl shell which makes the detergent soluble. The over-based phenates likewise form a reverse micelle, though with a shell having a polymeric structure (Wu et al., 2000). The calcium carbonate core of a typical over-based sulphonate reverse micelle has a diameter of 4 and 14 nm and together with the stabilizing surfactant layer, an overall diameter of between 8 and 18 nm (Wu et al., 2000).

When the sulphuric acid migrates to the calcium carbonate core and acid-base reaction takes place, as shown in equation A.10. This chemical reaction between sulphuric acids and calcium carbonate is possible, as the sulfuric acid is a strong acid and the calcium carbonate is a weak base. (Fu et al., 2006; Wu et al., 2000).

$$H_2SO_4(l) + CaCO_3(s) \rightarrow CaSO_4 + H_2O(l) + CO_2(g) \tag{A.10}$$

The reaction will result in crystal calcium sulfate hydrates and carbon dioxide.

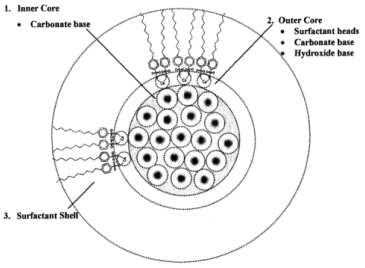

Figure A.4: Schematic structure of calcium carbonate (Fu et al., 2006).

B Determination of Vapour Pressure

Vapour pressure of the cylinder lubrication oil is estimated in this appendix using the Clausius-Clapeyron equation. It is necessary to known the vapour pressure of a liquid in order to determine at which pressures the liquid begins to cavitate.

The Clausius-Clapeyron equation is shown in equation B.1, which describes, for a pure substance, the relation between the pressure and temperature for conditions of equilibrium between two phases (Laidler et al., 2003).

$$\ln\left(\frac{P2}{P1}\right) = \frac{\Delta H_{\mathrm{v}}}{R}\left(\frac{1}{T_1} - \frac{1}{T_2}\right) \tag{B.1}$$

where ΔH_{v} molar enthalpy of vaporization and R is the ideal gas constant. It is possible to calculate ΔH_{v} using sublimation, when using the boiling point $T_{\mathrm{b}} = 589.15$ K and the vapour pressure $P_{\mathrm{v}} = 13$ Pa at $T_{\mathrm{v}} = 293.15$ K from the *material safety data sheet* for Mobilgaard 570. This lead to the following expression:

$$\Delta H = \mathrm{R} \cdot \ln\left(\frac{P_{\mathrm{v}}}{P_{\mathrm{atm}}}\right)\left(\frac{1}{T_{\mathrm{b}}} - \frac{1}{T_{\mathrm{v}}}\right)^{-1} = 32\,\mathrm{kJ/mol} \tag{B.2}$$

Having the molar enthalpy of vaporization ΔH_{v} and boiling point T_{b} for the lubrication oil, the vapor pressure as a function of temperature can be determined using equation B.1. This leads to this following simplified expression in equation B.3.

$$P_{\mathrm{v}}(T) = 10000.0\,\mathrm{e}^{(54.72 \cdot T - 32.24 \cdot 10^3)/\mathrm{R} \cdot T} \tag{B.3}$$

In equation B.3, the temperature is expressed in terms of Kelvin. An equivalent function expressed in terms of Celsius is therefore derived:

$$P_{\mathrm{v}}(T) = 10000 \cdot \mathrm{e}^{(A \cdot T - B)/((20.0 \cdot \mathbf{T} + C) \cdot \mathrm{R})} \tag{B.4}$$

Where the dimensionless constants are $A = 1094$, $B = 3.458 \cdot 10^5$, and $C = 5463.0$. Figure B.1 shows a graph of the vapor pressure as a function of temperature.

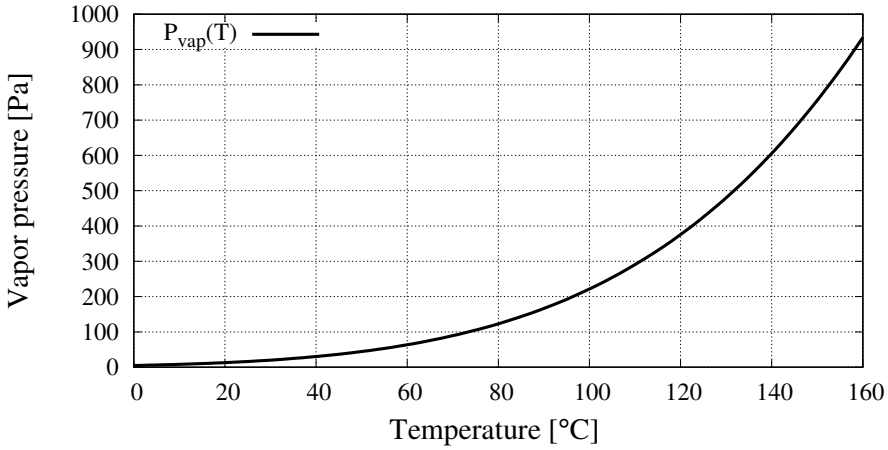

Figure B.1: The vapour pressure of the studied cylinder lubrication oil as a function of temperature. The curve is derived by the the Clausius-Clapeyron equation.

C | HJ Lubricators

The commercial Lubtronic system from Hans Jensen Lubricators (HJ Lubtronic) is used as a lubricator. The system is hydraulically driven and electronically controlled. There are a variety of customized HJ Lubtronic systems available. The important features of the system used in this thesis are:

- Piston diameter, D_{pd}= 6.5 mm
- Number of lube points, N_{lp}= 10
- Maximum stroke length, S_{l} = 9 mm
- Hydraulic supply pressure, P_{supply} = 7 MPa

A CAD drawing of the HJ Lubtronic and a cross-sectional view of the lubricator is shown in Figure C.1.

There are two electrically controlled solenoid valves in a lubricator, a primary (1) and a backup (2). When one of these solenoid valves is activated, system oil pushes the hydraulic pistons (3) in order to move the hydraulic actuator (4) and the distributor plate (5). This plate activates a number of pistons (6) that force lubrication oil out of the cavity (7), and into the pipes (8) connecting the lubricator and the injection valves.

When the solenoid valves are deactivated, a spring (9) pushes the distributor plate to its starting position. Thus, fresh lubrication oil is filled in the cavity and the next lubrication stroke can be initiated.

The quantity of oil delivered to each injector can be varied by adjusting the stroke length of the lubrication pistons (6). This is done by the adjustment screw (10) and controllable DC motor (11). A potentiometer (12) ensures that the right stroke setting is achieved. The delivered quantity (m_{injected}) is determined using the following equation:

$$m_{\mathrm{injected}} = \rho_{\mathrm{l}} \cdot V_{\mathrm{lube}} = \rho_{\mathrm{l}} \cdot \left(\frac{D_{\mathrm{ph}}}{2}\right)^2 \cdot \pi \cdot S_{\mathrm{L}} \tag{C.1}$$

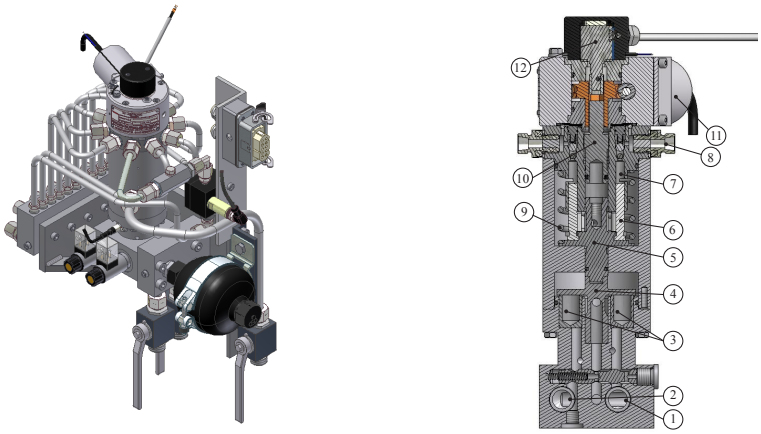

(a) A CAD drawing of the HJ Lubtronic system used in this thesis.

(b) Cross sectional view of the HJ Lubtronic

Figure C.1: The HJ Lubtronic system delivers lubrication oil to the injection valve. The systems consist of: (1) primary solenoid, (2) backup solenoid, (3) hydraulic pistons, (4) hydraulic actuator, (5) distributor plate, (6) lubrication pistons, (7) lube oil cavity, (8) connecting pipes, (9) spring, (10) adjustment screw, (11) DC-motor, and (12) potentiometer.

where ρ_{l} is the liquid density, V_{lube} is the volume of the lubrication oil cavity (102). This volume can be expressed in terms of the piston diameter D_{ph} and stroke length S_{L}.

D | Cavitation constant K_R

From the numerical study, equation 8.2 has been derived for the studied injection nozzle. This expression describes the relationship between viscosity μ_l, pressure P_i, nozzle diameter D_n, and the dimensionless cavitation factor K_R.

$$\begin{aligned} K_\mathrm{R}(\mu_\mathrm{l}, P_\mathrm{i}, D_\mathrm{n}) = & A_1 \cdot \mathrm{e}^{\frac{(B_1 \cdot G_1)}{\ln(G_2 \cdot \mu_\mathrm{l})}} + C_1 \cdot \mathrm{e}^{\frac{(F_1 \cdot G_1)}{ln(G_2 \cdot \mu_\mathrm{l})}} \\ & + A_2 \cdot \mathrm{e}^{(B_2 \cdot P_\mathrm{i})} + C_2 \cdot \mathrm{e}^{(F_2 \cdot P_\mathrm{i})} + A_3 \cdot D_\mathrm{n} + B_3 \end{aligned} \tag{D.1}$$

The model constants are shown in Table D.1. This equation can be used to determine when cavitation is present ($K_\mathrm{R} > 0.0$), and when it extends to the nozzle exit ($K_\mathrm{R} > 0.2$) without the time consuming setup and calculation performed with the numerical model. Figure D.1 shows the equation plotted against the numerical results for pressure, temperature and diameter.

Table D.1: The model constants used in equation 8.2.

Model constant	Value
A_1	0.6689
B_1	0.001233
C_1	-11.39
F_1	-0.03487
A_2	0.7888
B_2	0.000855
C_2	-1.473
F_2	-0.033
A_3	16.27
B_3	-5.28
G_1	-149.94
G_2	163.93

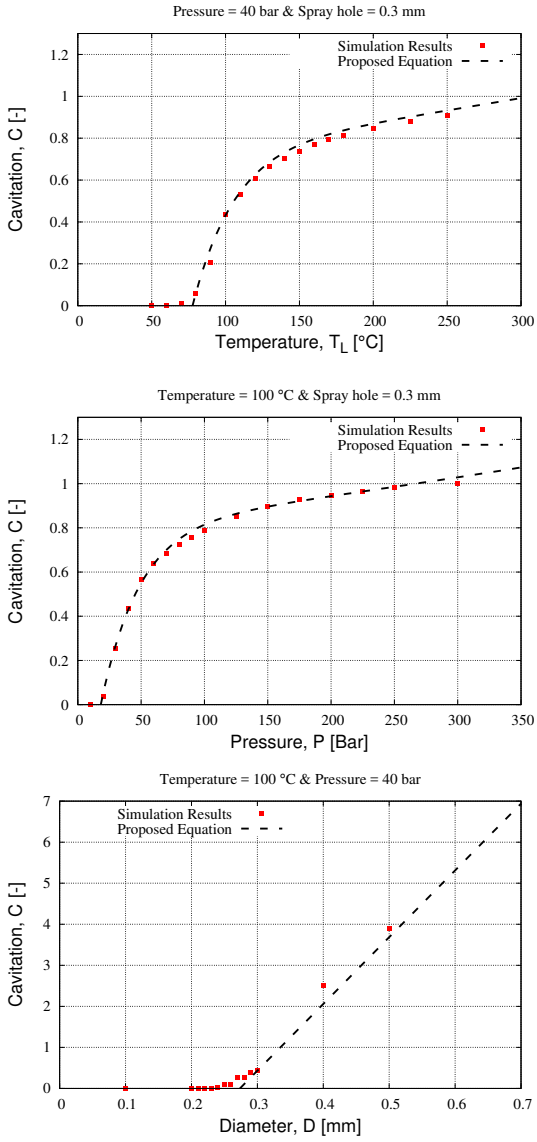

Figure D.1: Simulation results for temperature, pressure and nozzle diameter plotted against the dimensionless cavitation number K_R. The value K_R is a normalised value, which is defined as the number of computational cells that cavitates.

Part VII

Additional Publications

Paper D

Title: Numerical study of cavitation of high-viscous liquid spray systems

Authors: R. Ravendran*, J. d. Christiansen, P. Jensen, and B. Endelt

Publisher: Proceedings of ILASS Americas 28th Annual Conference on Liquid Atomization and Spray Systems

Conference: ILASS-AMERICA 2016

Background: This paper investigates hypothesis II in chapter 4.

Abstract: Understanding the disturbances introduced by cavitation inside spray nozzles is important, when simulating the spray formation of highly viscous liquids. In this paper a new model for cavitation-induced primary break-up is proposed, which is able to map the influence of cavitating nozzle flow on spray formation. Detailed experimental and numerical investigations of the viscous nozzle flow have been performed in order to develop an improved primary break-up model for pressure injection systems (Ravendran et al. 2017). These investigations have shown that liquid break-up is enhanced when cavitation bubbles burst at the nozzle exit. The proposed model describes the transition from the flow inside the nozzle, modelled using a homogeneous equilibrium model (HEM) method, to the first primary droplets modelled using a Eulerian-Lagrangian method. Thus, providing the boundary conditions for the calculation of the secondary break-up and spray formation. The nozzle exit is divided into a definite number of patches. Liquid momentum and density from each patch are used to initialize the primary droplets. The model has been implemented in the open-source CFD software package OpenFOAM and validation has been done using high-speed shadowgraphic imaging. The simulated spray tip penetration and spray cone angle at the near-nozzle region show a good agreement with the experiment results.

ILASS Americas 28th Annual Conference on Liquid Atomization and Spray Systems, Dearborn, MI, May 2016

Numerical study of cavitation of high-viscous liquid spray systems

R. Ravendran*, J. d. Christiansen, P. Jensen and B. Endelt.
Hans Jensen Lubricators A/S
Aalborg University
9560 Hadsund, Denmark

Abstract

It is difficult to atomize high-viscous liquids using pressure spray systems unless high fluid pressure is applied. To enhance the degree of liquid atomization of high-viscous sprays, the internal nozzle geometry can be designed so that cavitation is promoted. Cavitation in the nozzle affects the subsequent atomization behavior, because it introduces a stochastic behavior of the liquid stream and destabilizes the jet. In the present work, a numerical simulation model of an injection nozzle is developed to predict cavitation of high-viscous liquids. The modelling is carried out in the open-source CFD software package OpenFOAM using a standard incompressible multiphase flow solver. The in-nozzle cavitation phenomenon is captured using the Schneer-Saur cavitation model. The numerical simulation model is validated using high-speed shadow graphic images of a transparent acrylic nozzle with an orifice diameter of 0.3 mm.

*Corresponding Author: rra@hjlubri.dk

Introduction

New pressure spray systems provide lubrication in to the cylinder of two-stroke marine diesel engines to lubricate the piston and cylinder liner. Traditionally, lubrication has been provided by non-return injection valves introducing oil into a groove around the liner circumference (Figure 1). Vertical distribution across the cylinder is provided by the moving piston. The need of lubrication is greatest at the top of the cylinder [1, 2], this means that in order to properly lubricate the top there is a tendency to over-lubricate lower regions.

Pressure spray systems provide a more efficient coverage of the cylinder wall. In this study, the focus will be on the *HJ-SIP* spray lubrication system developed by Hans Jensen Lubricators A/S. Spray injection valves, placed at the liner circumference, directs the lubricating oil spray upwards. The oil is delivered into the engines scavenging air aiding the vertical delivery and thus the oil is distributed at the top of the cylinder [3].

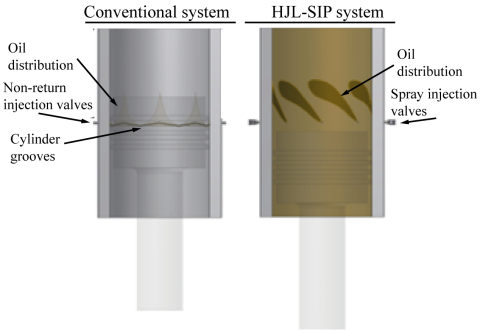

Figure 1: Illustration of conventional and HJ-SIP lubrication systems.

The viscosity grade of commercial cylinder oils is typically SAE50, and is therefore considered as being high-viscous compared to e.g. diesel fuel oil. It is difficult to atomize high-viscous liquids using pressure spray systems unless high fluid pressure is applied [4]. The internal geometry of the HJ-SIP spray nozzle investigated in this study is shown in figure 2. The spray nozzle hole is 0.3 mm and the fluid pressure is 3.7 MPa, which means that the Reynolds number is << 2000. The flow inside the spray nozzle is therefore considered to be laminar.

Gardhouse *et al.* [5] showed that cavitation in the HJ-SIP spray nozzle affects the liquid atomization. Cavitation is the formation of vapor bubbles and cavities due to liquid evaporation. This evaporation occurs when change in geometry, through which the liquid flows, leads to the decrease of static pressure below the vapor pressure [6]. Cavitation emerges at the intersection between the sac hole and spray hole in the HJ-SIP valve.

Cavitation in the nozzle affects the subsequent atomization behavior, because it introduces a stochastic behavior of the liquid stream and destabilizes the subsequent jet. To enhance the degree of liquid atomization of high-viscous sprays, the internal nozzle geometry can be designed so that cavitation is promoted [4, 7, 8].

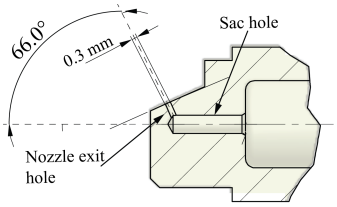

Figure 2: The internal dimensions of the HJ-SIP injection valve studied in this work.

Development of accurate Computational Fluid Dynamics (CFD) simulation models has been studied intensively in the recent years, and different approaches have been proposed for modelling the in-nozzle cavitating flow [9–13]. However, the authors are focusing on modelling low viscous liquids such as water and diesel fuel, and not much work has been performed on modelling high-viscous cavitating flow inside spray nozzles.

One of the popular approaches to model cavitation inside the nozzle is the homogenous mixture two-phase method (HEM) [14], which assume that the liquid and gas phases are perfectly mixed in a cell. This means that there is only one set of equations, hence reducing computational time. The most difficult part of this method is to determine the conditions that closes the system of equations. A bartropic law is often used to calculate the growth and collapse of cavitation [14, 15].

The scope of this paper is to investigate whether the in-nozzle cavitating flow of high-viscous can be modelled using CFD simulations. As mentioned, there are different methods by which the cavitation can be modelled. However, in this study a homogeneous mixture method will be used together with

the cavitation model proposed by Schneer-Saur [16].

Numerical Setup

The Governing Equations

The internal flow is modelled using a homogeneous equilibrium two-phase mixture method (HEM), which assumes that vapor and liquid are perfectly mixed in each cell [14]. There is therefore only one set of equations. The continuity equation and the momentum equations for the mixture is described as follows:

$$\frac{\delta \rho_m}{\delta t} + \nabla \cdot (\rho_m \mathbf{U}) = 0 \tag{1}$$

$$\frac{\delta \rho_m}{\delta t} + \nabla \cdot (\rho_m \mathbf{U}\mathbf{U}) = -\nabla P + \nabla \cdot \{\mu_m [\nabla \mathbf{U} + (\nabla \mathbf{U})^T]\} \tag{2}$$

where t is time, $\mathbf{U}$ and P is the velocity and the pressure of the mixture. ρ_m and μ_m is the mixture density and mixture viscosity, which is determined by the volume fraction of the liquid phase α_l: using the following equations:

$$\rho_m = (1 - \alpha_l)\rho_v + \alpha_l \rho_l \tag{3}$$

$$\mu_m = (1 - \alpha_l)\mu_v + \alpha_l \mu_l \tag{4}$$

The subscripts l and v indicates the liquid and vapor phase respectively.

Cavitation Modelling

The mass transfer rate between liquid and vapor phase is described using equation 5.

$$\frac{\delta \alpha_L \rho_L}{\delta t} + \nabla \cdot (\alpha_L \rho_L \mathbf{U}) = R_c + R_e \tag{5}$$

where R_c and R_e are the mass transfer source terms for condensation and evaporation, respectively. These source terms are calculated using the Schnerr-Saur cavitation model describing growth and collapse of cavitation. This model is a simplified form of the Rayleigh-Plesset equation, where viscous terms, surface tension, incondensable gas, and high-order terms are ignored [14]. The mass transfer rate for the evaporation R_e and the condensation R_c is given in equation 6 and 7. The equations takes vapor saturation pressure P_v, as a threshold for evaporation and condensation.

$$R_e = -C_v \frac{3\rho_l \rho_v}{\rho_m} \frac{\alpha_l (1 - \alpha_l)}{R_b} sgn(P_v - P_l) \cdot \sqrt{\frac{2|P_v - P_l|}{3\rho_l}}, \quad P_l < P_v \tag{6}$$

$$R_c = -C_c \frac{3\rho_l \rho_v}{\rho_m} \frac{\alpha_l (1 - \alpha_l)}{R_b} sgn(P_l - P_v) \cdot \sqrt{\frac{2|P_v - P_l|}{3\rho_l}}, \quad P_v < P_l \tag{7}$$

where R_b is the initial bubble radius, C_c and C_v are the rate constants for condensation and evaporation. The rate constants are both set to 100, and R_b is set to 1 10^{-5}m in all the present simulations. Furthermore, the nuclei number density per unit volume n_c is set to be $10^{14} m^3$.

The Schneer-Saur model allows turbulence viscosity to be included [16]. However, turbulence is not taken into account in the present simulations, because a Reynolds number below 2000 indicates a laminar flow. If turbulence viscosity is taken into account, it will lead to a higher total viscosity which results in decreased dynamic pressure and therefore less cavitation.

Computational grid and boundary conditions

The computational grid is shown in figure 3, which is made of a structured grid with 339,688 hexahedral cells and 31.9 μm in minimum cell size. The interPhaseChangeFoam solver in OpenFOAM 3.0 is used to perform the numerical simulations. Gauss Upwind scheme is used for numerical discretization. The simulations are performed with adjustable time step limited by the Courant number. The Courant number is set to 0.5 and the initial timestep Δt is set to 10^{-7}s. The results in this study shows the steady state solution at 0.2 ms.

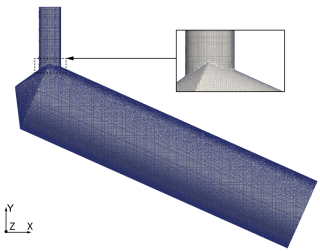

Figure 3: The employed mesh of the internal spray nozzle.

The operating conditions were set according to the experimental conditions with a inlet pressure P_{inlet} = 3.7 MPa and outlet pressure P_{out} equal to

environment pressure at 0.1 MPa. The oil properties used for the simulations are shown in Table 1. Oil temperature of 60 °C, 90 °C, and 120 °C are investigated to evaluate the validity of the simulations. The oil properties are temperature dependent, however only the influence of viscosity change is analyzed. Thus viscosity is expected to be the dominant factor, as it decreases exponentially.

Oil property	Value	Reference
Vapor Pressure	$P_v = 13$ [MPa]	[17]
Liquid Density	$\rho_l = 937$ $[kg/m^3]$	[17]
Liquid Viscosity		
at 60 °C	$\mu_{60} = 0.074$ [Pa·s]	Measured
at 90 °C	$\mu_{90} = 0.032$ [Pa·s]	Measured
at 120 °C	$\mu_{120} = 0.021$ [Pa·s]	Measured
Vapor Density	$\rho_v = 0.2$ $[kg/m^3]$	Estimated
Vapor Viscosity	$\mu_v = 0.00018$ [Pa·s]	Estimated

Table 1: Material properties used in this study.

Experimental setup

High-speed images of the internal flow are used to validate the numerical simulations. Figure 4 shows the experimental setup. The setup consists of a *HJ Lubtronic* system from Hans Jensen Lubricators A/S, which delivers 85 mg lubrication oil per injection to a heated HJ-SIP injection valve. The opening pressure of the injection valve is 3.7 MPa. The lubricator is supplied with 6 MPa in hydraulic pressure from a pump station and fresh lubrication oil from a heated tank. The oil used in this study is *Mobilgaard 560VS*, which is a commercial lubrication oil from ExxonMobil.

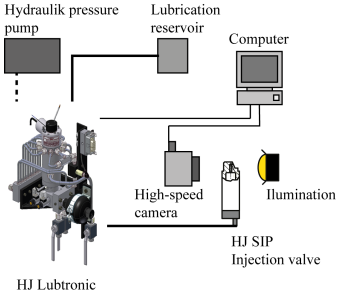

Figure 4: The experimental setup used to detect the internal nozzle cavitation.

The spray nozzle is manufactured in a transparent PMMA material in order to capture cavitation using a shadowgraphic imaging technique. The refractive index of lubrication oil and PMMA material was found out to match, and therefore refraction appears only at the phase interface between the liquid and vapor. This means that phase interfaces will appear as a dark shadow on the image.

The high-speed camera used in this study is a Photron Fastcam SA5. Images are taken with a frame rate of 7200 fps with a shutter speed of 7200. A 1000W halogen lamp was used as illumination source.

Results and Discussion

High-speed images of the transparent nozzle is shown in Figure 5. The images show the internal nozzle flow, when steady state is reached at approximately 2 ms after needle lift.

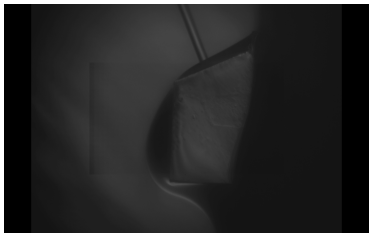

(a) Liquid temperature of 60 °C .

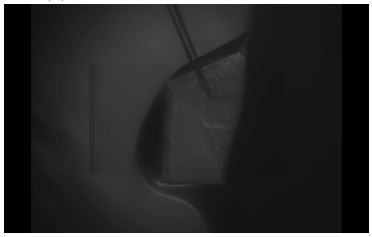

(b) Liquid temperature of 90 °C .

(c) Liquid temperature of 120 °C .

Figure 5: High-speed images of the transparent spray nozzle at different liquid temperatures. The images show the nozzle flow at approximately 2 ms.

Figure 5a shows that cavitation does not exist, when the temperature of the lubrication oil is 60 °C. However, cavitation emerges and develops in the spray hole, when the temperature increases to 90 °C and 120 °C. When comparing figure 5b and 5c, it seen that the degree of cavitation increases with increasing temperature. Furthermore, the images show that the cavitation emerges at one side of the spray hole and extents to the nozzle exit, and indicating hydraulic flip [7].

The numerical simulations

Figure 6 shows the liquid pressure P_l, velocity in y-direction U_y, and volume fraction α_l at liquid temperature of 90 °C. It is seen that the liquid velocity accelerates and exceeds 80 m/s, when the liquid enters from sac hole to spray hole. This is due to the Bernoulli principle.

Furthermore, it is seen that the liquid pressure is below the vapor pressure at transition between the sac hole and the spray hole, which correctly leads to cavitation. However, the size of the cavitation does not correlate with the experimental result shown in Figure 5b. The numerical results underestimates the size of the cavitation.

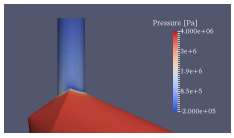

(a) Liquid pressure P_l.

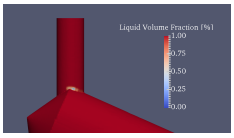

(b) Liquid volume $\alpha_l l$.

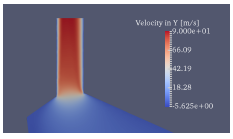

(c) Liquid velocity U_y.

Figure 6: Numerical simulations of the internal nozzle at a liquid temperature of 90 °C.

The influence of liquid temperature

Figure 7 shows the degree of cavitation at liquid temperature of 60 °C, 90 °C and 120 °C. Cavitation does not exist at 60 °C, but increases with increasing temperature. The Reynolds number is below 2000 in all three simulations, which indicates laminar flow.

When comparing Figure 5 and Figure 7, it is seen that the numerical simulations underestimate the size of cavitation. However, correctly predicts the scenario where cavitation does not exist in the nozzle.

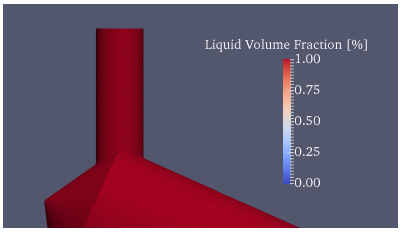

(a) The liquid volume fraction at 60 °C. Reynolds number $Re \approx 187$.

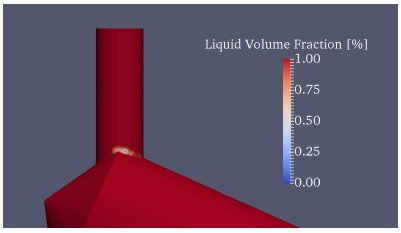

(b) The liquid volume fraction at 90 °C. Reynolds number $Re \approx 510$.

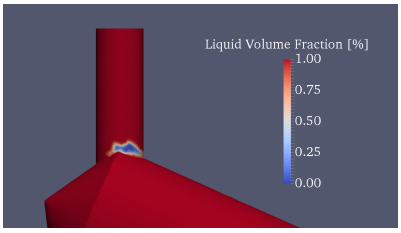

(c) The liquid volume fraction at 120 °C. Reynolds number $Re \approx 822$.

Figure 7: Cavitation at the internal nozzle

.

To achieve better numerical results that correlate with the experimental results, there are a few elements that can be revised in the simulation model:

- The constants describing the bubble dynamics in the Schneer-Saur cavitation model can be adjusted.
- The prediction of cavitation can be based on another criteria than saturation pressure e.g. total stress criteria or critical pressure. [14, 18]

Velocity at the nozzle exit

Figure 8 shows the velocity vector field at the nozzle exit. The fringe level indicates the velocity in y-direction (U_y), whereas the vector field represents velocity components in the xy- plane (U_x and U_z).

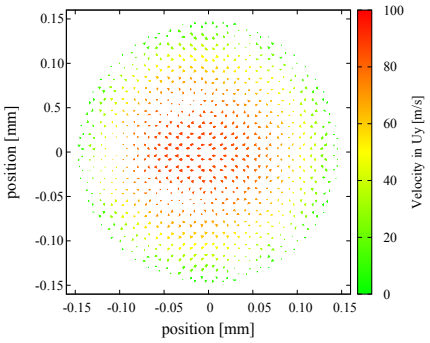

(a) Liquid temperature of 60 °C.

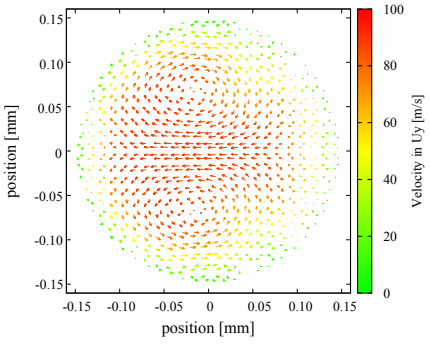

(b) Liquid temperature of 90 °C.

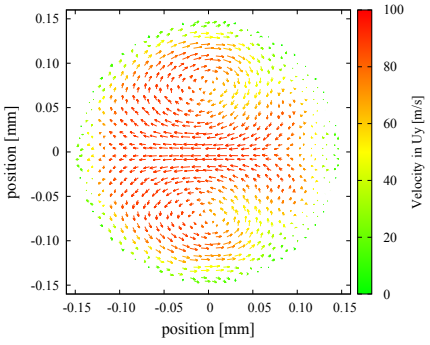

(c) Liquid temperature of 120 °C.

Figure 8: Velocity vector field at the nozzle exit.

When the liquid temperature is 60°C, the velocity component U_y is uniform and can be described using a elliptic paraboloid with maximum at center of the nozzle exit. Furthermore, the velocity components U_x and U_z is small compared U_y.

As temperature increases in Figure 8b and 8c, U_y becomes non-uniform and the magnitude of U_x and U_z increases. This leads to vortices in the nozzle, which becomes more prominent as the temperature increases. Furthermore, it is seen that symmetry across x-axis is still present.

The ratio between the velocity components is important for the break-up of liquid jets. A smaller ratio between U_y and the velocity components in x- and z-direction means that more disturbance is introduced to the liquid flow, which leads to an increased degree of droplet breakup.

Conclusion

In this present study, the internal nozzle flow of HJ-SIP spray injection valves has been studied using numerical simulations. These spray injection valves are used to deliver high-viscous lubrication oil into the cylinder of two-stroke marine diesel engines. Shadow graphic high-speed images showed that cavitation exits inside the spray hole, which may enhance the degree of atomisation. A numerical simulation model was set up using a homogeneous mixture model together with Schneer-Saur cavitation model. The numerical results showed that cavitation exists, and the degree of cavitation increases with increasing temperature. However, the numerical simulations underestimate the size of cavitation compared to the experimental results. The experimental results indicate that hydraulic flip is present in the nozzle.

Nomenclature

α	volume fraction
μ	viscosity [Pa·s]
ρ	density [kg/m^3]
l	liquid phase
m	mixture phase
n_c	nuclei number density per unit volume [m^3]
P	Pressure [Pa]
P_v	vapor pressure [v]
R_c	rate constants for condensation
R_v	rate constants for evaporation
R_b	initial bubble radius [m]
t	time [s]
$\mathbf{U}$	velocity [m/s]
v	vapor phase

References

[1] Martin F. Jensen, Jørgen Bøttiger, Henrik H. Reitz, and Michael E. Benzon. *Wear*, 253:1044–1056, 2002.

[2] C L Felter, a Vølund, T Imran, and P Klit. *Proceedings of the Institution of Mechanical Engineers, Part J: Journal of Engineering Tribology*, 224(9):877–883, 2010.

[3] Leif Eriksen. *Recent Developments in Marine Engineering Operations*, pp. 1–8. Hans Jensen Lubricators A/S, 2003.

[4] N Tamaki and M Shimizu. (September), 2002.

[5] Tim Gardhouse, Guillaume De Sercey, Cyril Crua, Simon Edwards, and Céline Thompson. *ILASS Europe, 26th Annual Conference on Liquid Atomization and Spray Systems*, 2014.

[6] Mitja Morgut, Enrico Nobile, and Ignacijo Biluš. *International Journal of Multiphase Flow*, 37(6):620–626, 2011.

[7] Akira Sou, Shigeo Hosokawa, and Akio Tomiyama. *International Journal of Heat and Mass Transfer*, 50(17-18):3575–3582, aug 2007.

[8] Cyril Crua and Morgan R Heikal. *Measurement Science and Technology*, 25(12):125301, 2014.

[9] Yusong Yu, Guoxiu Li, Yong Wang, and Jiawei Ding. *Applied Mathematical Modelling*, 40:268–283, 2013.

[10] Florin Mariasiu. *Tribology Transactions*, 56(2):161–168, 2013.

[11] Oscar J. Soriano-Palao, Martin Sommerfeld, and Axel Burkhardt. *International Journal of Spray and Combustion Dynamics*, 6(2):113–146, jun 2014.

[12] Akira Sou, Bari Biçer, and Akio Tomiyama. *Computers and Fluids*, 103(January 2016):42–48, 2014.

[13] Sven Jollet, Hauke Hansen, Konstantin Bitner, Dirk Niemeyer, and Friedrich Dinkelacker. pp. 8–10, 2014.

[14] Spray Systems. *ICLASS 2015, 13th International Conference on Liquid Atomization and Spray Systems*, pp. 1–8, Tainan, Taiwan, 2015.

[15] Ehsan Roohi, Amir Pouyan Zahiri, and Mahmood Passandideh-Fard. *Applied Mathematical Modelling*, 37(9):6469–6488, 2013.

[16] Weixing Yuan, Jürgen Sauer, and Günter H. Schnerr. *Mecanique et Industries*, 2(5):383–394, 2001.

[17] ExxonMobil. Material Safety Data Sheet - Mobilgard 570. Technical report, 2012.

[18] S. Dabiri, W. A. Sirignano, and D. D. Joseph. *Physics of Fluids*, 19(7):072112, 2007.

Paper E

Title: Model for cavitation induced primary break-up of viscous liquid sprays

Authors: Rathesan Ravendran*, B. Endelt, J. d. Christiansen, and P. Jensen

Publisher: WIT Transactions on Engineering Sciences [ISSN 1743-3533]

Journal: Multiphase Flow 2017, 115

Background: This paper investigates hypothesis III in chapter 4.

Abstract: In this paper a new model for cavitation induced primary break-up is proposed, which is able to map the influence of cavitating nozzle flow on spray formation. The model is applicable for viscous liquid sprays, where the Reynolds number is below 800. For such viscous spray systems, liquid break-up is enhanced when cavitation bubbles burst at the nozzle exit. The proposed model describes the transition from the flow inside the nozzle, modelled using a homogeneous equilibrium model (HEM) method, to the first primary droplets modelled using a Eulerian-Lagrangian method. Thus, providing the boundary conditions for the calculation of the secondary break-up and spray formation. The nozzle exit is divided into a definite number of patches, and liquid momentum and density from each patch are used to initialize the primary droplets. Using this method, the influence of bursting cavitation bubbles and asymmetrical properties of viscous sprays can be identified. The model has been implemented in the open-source CFD software package OpenFOAM and a first validation has been done using high-speed shadowgraphic imaging.

MODEL FOR CAVITATION INDUCED PRIMARY BREAK-UP OF VISCOUS LIQUID SPRAYS

R. RAVENDRAN, B. ENDELT, J.D. CHRISTIANSEN & P. JENSEN
Department of Materials and Production, Aalborg University, Denmark
Hans Jensen Lubricators A/S, Denmark

ABSTRACT

In this paper a new model for cavitation induced primary break-up is proposed, which is able to map the influence of cavitating nozzle flow on spray formation. The model is applicable for viscous liquid sprays, where the Reynolds number is below 800. For such viscous spray systems, liquid break-up is enhanced when cavitation bubbles burst at the nozzle exit. The proposed model describes the transition from the flow inside the nozzle, modelled using a homogeneous equilibrium model (HEM) method, to the first primary droplets modelled using a Eulerian-Lagrangian method. Thus, providing the boundary conditions for the calculation of the secondary break-up and spray formation. The nozzle exit is divided into a definite number of patches, and liquid momentum and density from each patch are used to initialize the primary droplets. Using this method, the influence of bursting cavitation bubbles and asymmetrical properties of viscous sprays can be identified. The model has been implemented in the open-source CFD software package OpenFOAM and a first validation has been done using high-speed shadowgraphic imaging.

Keywords: spray formation, cavitation, primary break-up, numerical simulation, viscous liquids, OpenFoam.

1 INTRODUCTION

It is generally accepted that cavitation inside spray nozzles have a great importance on the break-up of liquid jets [1]–[5]. Cavitation is the formation of vapor cavities inside the liquid due to evaporation, which takes places, when the local pressure of the liquid drops below the vapor pressure. The subsequent collapse of these cavities introduces disturbances to the liquid stream that lead to a faster breakup of the exiting jet [6]–[8].

Even in high pressure spray systems, the liquid jet does not atomize greatly when disturbances caused by cavitation are not present [9]. This is especially true for viscous liquids, which are difficult to atomize using pressure spray systems unless high fluid pressure is applied [10], [11].

The internal nozzle cavitation has been studied intensively, and research has shown that cavitation is promoted by a variety of factors as e.g. sharp inlet orifices, needle lift, curvature of the inlet edge, liquid properties, and system pressure [12]–[15].

Ravendran [15], investigated the atomization of viscous liquids, and showed that the non-axial injection conditions lead to a swirling liquid flow inside the nozzle. Thus, leading to the development of cavitation strings in the core of the liquid vortices. Fig. 1 shows, shadowgraphic images of the two cavitation strings inside the studied transparent spray nozzle.

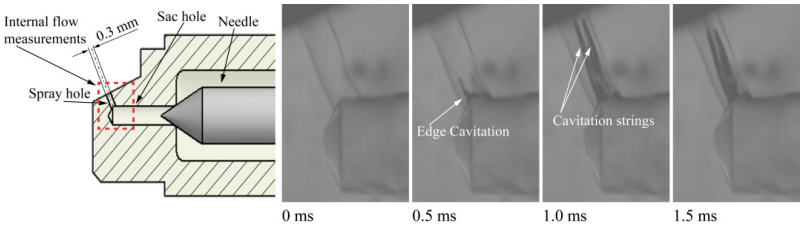

Figure 1: Shadowgraphic images of the developing cavitation strings inside the studied transparent spray nozzle.

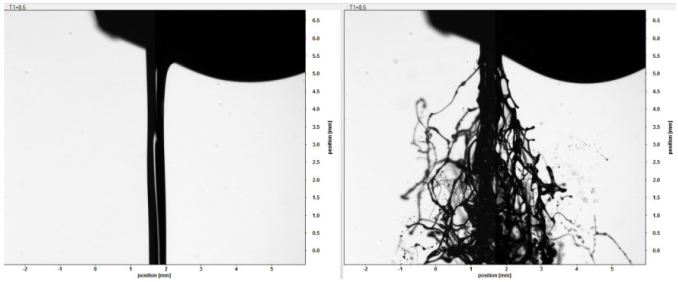

Figure 2: Near-nozzle images of the spray formation. Images are taken with a shadow imaging system from LaVision. (a) Cavitation collapses in the nozzle volume; (b) Cavitation bursts outside the nozzle exit.

It was shown that the cavitation strings increase the degree of atomization greatly, this is only the case when the cavitation strings extends to the exit of the nozzle. However, when the cavitation collapses in the nozzle volume, the viscous liquid is able to stabilize the stochastic disturbances introduced by the cavitation. Fig. 2(a) shows an image of the exiting spray, when the cavitation collapses in the nozzle volume, whereas Fig. 2(b) shows a case where the liquid break-up is enhanced due to bursting cavitation bubbles at the nozzle exit.

Several methods exist and are implemented in commercial CFD-codes for simulating the spray formation using the Lagrangian method as e.g. Taylor Analogy, et al., Break-up [16]. However, these models need sub-models to describe the transition from the nozzle flow to the primary droplet, as illustrated in Fig. 3. This coupling has been the focus of several authors, as accurate numerical simulation of spray formation is of great interest [6], [17], [18]. Especially, there is a high interest of modeling low viscous liquids such as water and diesel fuel, and not much work has been performed on cavitation induced primary break-up of viscous liquids. This leads to the objective of this study.

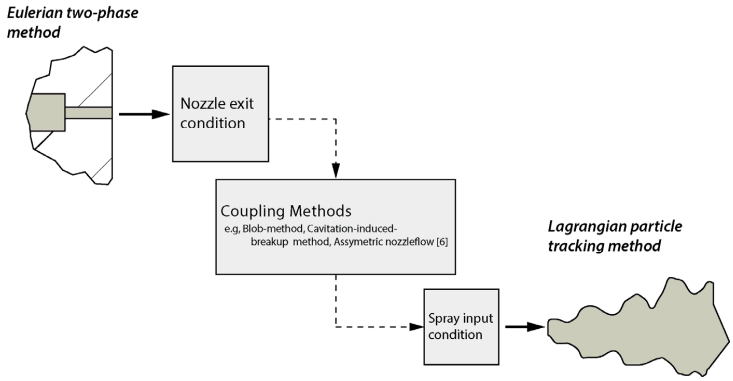

Figure 3: Illustration of the numerical simulation approach used in this paper.

In this paper, a method for coupling the internal flow and the subsequent spray is proposed. The purpose of the new primary breakup model is to describe the transition from the flow inside the nozzle to the first primary droplets, and thereby providing all starting conditions for the calculation of secondary break-up and spray formation. The input data for the new model are based on the detailed numerical investigations of the nozzle flow performed in [15]. The first validation of the model has been done using high-speed shadowgraphic imaging, however this has not been the scope of this paper.

2 NUMERICAL APPROACH

The simulation approach is divided in two steps, as illustrated in Fig. 4. Firstly, simulation of the liquid flow and cavitation inside the nozzle is done using the two-phase fluid mixture Schneer and Saur model [15], [19], [20]. Secondly, simulation of the spray formation is done using a standard Lagrangian KHRT secondary break-up model. The two simulation steps are connected using a coupling model, which translates the flow inside the nozzle to the first primary droplets at the nozzle exit and provide the starting conditions for the spray formation.

The focus of the following section is therefore to describe the proposed coupling model, as the simulation of the internal flow is described in detail in [15], and the standard KHRT-model is for example documented in [6], [18], [21].

2.1 Primary break-up model

The purpose of the coupling model is to initiate the primary droplets using the nozzle exit conditions. The nozzle exit is therefore separated into a defined number of boundary patches, from which liquid velocity (U) and degree of cavitation (α) are used to calculate the diameter of the primary droplet (D_i), mass flow rate ($\dot{m}_i$), and spray angle (φ_i) at each patch (i).

The location of each patch is randomly selected, in order to suppress geometrical effects when introducing a defined boundary grid. This approach makes the model flexible and applicable for different nozzle geometries. However, as patches are allowed to overlap and exceed the diameter of the nozzle, minor errors in spray angle are expected.

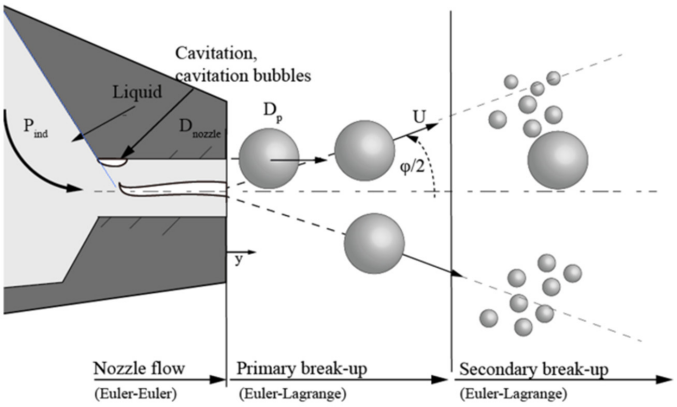

Figure 4: Illustration of the purpose of the different coupling methods.

The first droplets at the nozzle exit is introduced using the so-called blob-method, where the assumption is that the dense spray near the nozzle can be represented by spherical droplets with uniform size. The diameter of these droplets equals the nozzle hole diameter. The number of the droplets injected per unit time is determined from the mass flow rate. The mass flow rate of the primary droplets is calculated using eqn (1).

$$m_i(t) = \rho_l \cdot A_{patch} \cdot U_i(t), \tag{1}$$

where ρ_l is the liquid density, A_{patch} is the area of the selected patch, $U_i(t)$ is the velocity of the liquid composed of the three components in x, y, and z-direction.

The direction of the droplets leaving the nozzle exit is defined using the spray angle. These parameters are highly influenced by the degree of cavitation at the nozzle exit, as busting of cavitation bubbles leads to increased spray angle (φ_i). The degree of cavitation is expressed in terms of vapor volume fraction (α_i) , which is directly extracted from the internal flow simulations. The vapor volume fraction is described by a number from 0 to 1, for $\alpha_i < 1$ the patch cavitates. The spray angle (φ_i) is determined using eqn (2).

$$\varphi_i = \begin{cases} 0 & \alpha_i = 1 \\ \cos^{-1}\left(\frac{U_{i,plane} \cdot U_{i,y}}{\|U_{i,plane}\| \cdot \|U_{i,y}\|}\right) & \alpha_i < 1 \end{cases}, \tag{2}$$

where $U_{i,y}$ is the velocity vector of the liquid perpendicular to the nozzle exit, and is defined by $U_{i,plane} = U_{i,x}^2 + U_{i,z}^2$ and describes the velocity components parallel to the nozzle exit.

2.2 Boundary conditions

The internal flow and droplet breakup simulations are performed using the open source finite-volume CFD software OpenFoam 3.0. The proposed coupling model is a subroutine written in Matlab.

The boundary conditions for the simulations are based on experimental data, which are thoroughly described in [15]. However, the experimental conditions are summarised in Table 1.

3 RESULTS AND DISCUSSION

The results of the nozzle flow simulations are shown in Fig. 5. The velocity at the nozzle exit is shown in Fig. 5(a), where the fringe level indicates the velocity in y-direction (U_y) and the vector field represents velocity components in the xz- plane (U_x and U_z). It is seen that the swirling flow is prominent at higher temperatures, whereas at low temperatures the flow is non-swirling and axisymmetric.

Fig. 6 shows the computational and experimental results of the spray formation for injection case 1. The numerical simulations are performed using $N_P = 100$. The simulation results show a dense liquid core in the center of the spray, and smaller dispersed ligaments away from the center. These observations agree with the experimental observations. It is also important to highlight that the proposed model is capable of predicting the spray structure and asymmetrical shape apart from the spray tip penetration.

Table 1: Experimental test conditions.

1. Pressure system	Pressure pump	HJ – Lubtronic
	Pressure supply	70 bar
	Piston diameter	6 mm
	Oil temperature	60, 80, 100℃
	Oil type	Mobilgaard 570
2. Injector nozzle	Injector type	HJ - SIP
	Opening pressure	40 bar
	Ambient pressure	1 bar
	Ambient temperature	25
3. Camera Settings	Camera type	Photron Fastcam SA5
	Illumination	1000 W LED-lamp
	Frame rate	1/15000 fps
	Shutter speed	1/15000 s

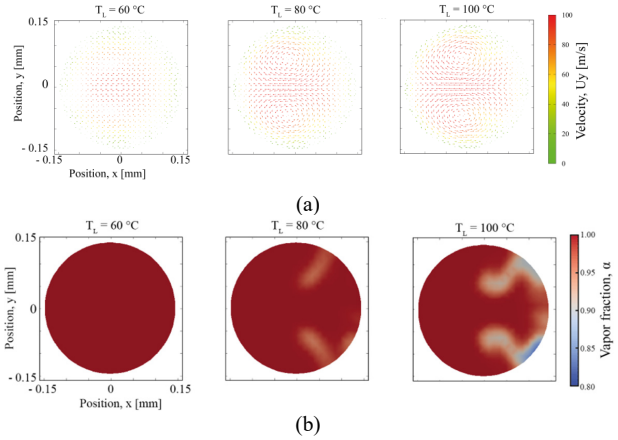

Figure 5: The results of the internal nozzle simulations. (a) Velocity vector field at nozzle exit; (b) The results of the internal nozzle simulations.

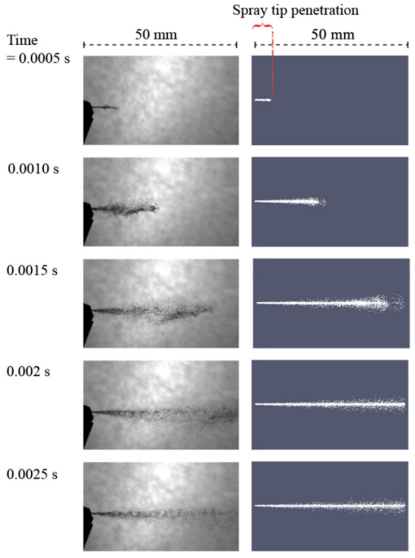

Figure 6: Spray formation due to cavitation induced breakup (Comparison between experiment and numerical simulation). The temperature of the injected liquid is $T_L = 100°C$. The numerical simulations are performed using 100 patches.

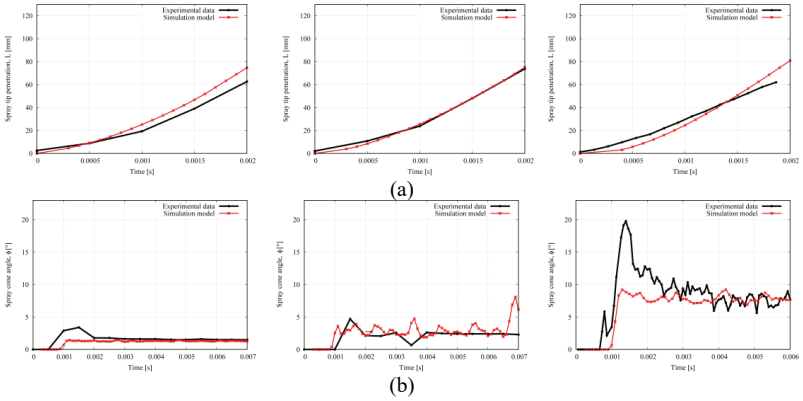

Figure 7: The results of the internal nozzle simulations. (a) Velocity vector field at nozzle exit; (b) The results of the internal nozzle simulations.

The spray tip penetration L and cone angle φ is shown in Fig. 7. There is a good agreement between the calculated and measured spray tip penetration, which is due to the good prediction of the liquid flow from the internal nozzle flow simulations.

Fig. 7(b) shows, that the computed spray angle for different nozzle flow cases can be predicted adequately. When the liquid temperature is 60℃, there is no cavitation at nozzle exit, thus the exiting liquid is a jet. As the degree of cavitation increases in $T_L = 80℃$ and $T_L = 100℃$, the spray angle increases as well. There is a very good agreement between the calculated and measured spray cone angle.

4 CONCLUSION

In this study a new method for simulating cavitation induced breakup for viscous liquids is proposed. The proposed model describes the transition from the flow inside the nozzle, modelled using a homogeneous equilibrium model (HEM) method, to the first primary droplets modelled using a Eulerian-Lagrangian method. Thus, providing all starting conditions for the calculation of the secondary break-up and spray formation.

The model is able to predict the spray angle and spray tip penetration sufficiently for different nozzle flow cases, where the degree of cavitation differs.

Further investigations have to be performed in order to determine whether the droplet size can be predicted using the proposed method. Furthermore, the importance of the model constants used for the simulation is not discussed in this study.

REFERENCES

[1] Fansler, T.D. & Parrish, S.E., Spray measurement technology: a review. *Meas. Sci. Technol.*, **26**(1), p. 12002, 2015.

[2] Le Moyne, L., Trends in atomization theory. *Int. J. Spray Combust. Dyn.*, **2**, pp. 49–84, 2010.

[3] Dong, P., Inaba, T., Nishida, K. & Shimo, D., Characteristics of the internal flow and the near-field spray of a single-hole injector and a multi-hole injector for diesel engines. *Proc. Inst. Mech. Eng. Part D J. Automob. Eng.*, **230**(5), pp. 632–649, 2016.

[4] Jollet, S., Heilig, A., Bitner, K., Niemeyer, D. & Dinkelacker, F., Comparison of experiments and numerical simulations of high pressure transparent injection nozzles Experimental test-rig. pp. 1–4, 2013.
[5] Sou, A., Hosokawa, S. & Tomiyama, A., Effects of cavitation in a nozzle on liquid jet atomization. *Int. J. Heat Mass Transf.*, **50**(17–18), pp. 3575–3582, 2007.
[6] Baumgarten, C., *Mixture Formation in Internal Combustion Engine*. Springer:Verlag Berlin Heidelberg, 2006.
[7] Bergwerk, W., Flow pattern in diesel nozzle spray holes. *Arch. Proc. Inst. Mech. Eng.*, **173**(1959), pp. 655–660, 1959.
[8] Dumouchel, C., Leboucher, N. & Lisiecki, D., Cavitation and primary atomization in real injectors at low injection pressure condition. *Exp. Fluids*, **54** (6), 2013.
[9] Dabiri, S., Sirignano, W.A. & Joseph D.D., Cavitation in an orifice flow. *Phys. Fluids*, **19**(7), p. 72112, 2007.
[10] Tamaki, N. & Shimizu, M., Enhancement of atomization of high-viscous liquid jet by pressure atomized nozzle. *ILASS Eur. 12th Trienn. Int. Conf. Liq. At. Spray Syst.*, 2002.
[11] Khmelev, V.N., Shalunov, A.V. & Smerdina, E.S., The cavitation spraying of the viscous liquids. *Int. Work. Tutorials Electron Devices Mater. EDM - Proc.*, pp. 269–273, 2006.
[12] Jolletm, S., Hansenm, H., Bitner, K., Niemeyer, D. & Dinkelacker, F., Transparent nozzles with high pressure conditions. *ILASS Eur. 26th Annu. Conf. Liq. At. Spray Syst.*, pp. 8–10, 2014.
[13] Pratama, R.H., Sou, A., Wada, Y. & Yokohata, H., Cavitation in mini-sac nozzle and injected liquid jet. *ICLASS 2015, 13th Int. Conf. Liq. At. Spray Syst.*, **1**, pp. 3–9, 2015.
[14] Andriotis, A., Gavaises, M. & Arcoumanis, C., Vortex flow and cavitation in diesel injector nozzles. *J. Fluid Mech.*, **610**, pp. 195–215, 2008.
[15] Ravendran, R., deClaville Christiansen, J., Jensen, P. & Endelt, B., Numerical study of cavitation of high-viscous liquid spray systems. *ILASS Am. 28th Annu. Conf.*, pp. 1–12, 2016.
[16] Baumgarten, C., Stegemann, J. & Merker, G., A new model for cavitation induced primary break-up of diesel sprays. *Zaragoza*, **9**(11), 2002.
[17] Soriano-Palao, O.J., Sommerfeld, M. & Burkhardt, A., Modelling the influence of the nozzle geometry on the primary breakup of diesel jets. *Int. J. Spray Combust. Dyn.*, **6**(2), pp. 113–146, 2014.
[18] Mohan, B., Yang, W. & Chou, S.K., Development of an accurate cavitation coupled spray model for diesel engine simulation. *Energy Convers. Manag.*, **77**, pp. 269–277, 2014.
[19] Yuan, W., Sauer, J. & Schnerr, G.H., Modeling and computation of unsteady cavitation flows in injection nozzles. *Mec. Ind.*, **2**(5), pp. 383–394, 2001.
[20] Mohan, B., Yang, W. & Chou, S., Cavitation in Injector Nozzle Holes – A Parametric Study. *Eng. Appl. Comput. Fluid Mech.*, **8**(1), pp. 70–81, 2014.
[21] Reitz, R.D. & Beale, J.C., Modeling Spray Atomization With the Kelvin-Helmholtz/Rayleigh-Taylor Hybrid Model. *At. Sprays*, **9**(6), pp. 623–650, 1999.

Paper F

Title: Consequences of oil film degradation

Authors: R. Ravendran* and P. Jensen

Publisher: The Motorship

Journal: The Motorship Magazine - June 2017

Website: `http://www.motorship.com/news101/fuels-and-oils/consequences-of-oil-film-degradation`
[Accessed: 11/07/2017]

Abstract: In a review of recent studies into two-stroke lubrication, Rathesan Ravendran and Peter Jensen of Hans Jensen Lubricators highlight the importance of cylinder oil distribution.

Preparing cylinder for SIP lubrication in Singapore

Consequences of oil film degradation

In a review of recent studies into two-stroke lubrication, **Rathesan Ravendran** and **Peter Jensen** of Hans Jensen Lubricators highlight the importance of cylinder oil distribution.

IT IS IMPORTANT to address degradation of cylinder lubrication oil in two-stroke marine diesel engines in order to ensure optimal engine-running conditions. Oil degradation (also known as oil starvation) means the change in physical and chemical properties of the lubricants that results in deterioration of its performance (CIMAC Working Group 8, 2004, Oil Degradation. *Guidelines for Diesel Engines Lubrication*, 22).

The oil film on the cylinder wall can be considered as an oil reservoir, consisting of several elements needed to ensure sufficient lubrication. When the lubrication oil is in service, the oil film will be exposed to stresses degrading the lubricating properties of the oil. The ability of the oil to treat oil stresses is therefore a key factor to ensure longer life of cylinder liners and piston rings.

Oil stresses are in general classified in four categories, which are all related to engine/operating conditions and the properties of the lubrication oil and the fuel oil (Hammett, J, 2014, Utilising the Latest Findings Engine Oil Stress from Field & Laboratory Engine Testing, 49(3), 6-13). The four categories are:

- **Humidity stress:** Water absorbed in the lubricant compromises its ability to deal with insoluble particles and promotes depletion of the alkalinity reserve.
- **Acid stress:** Sulphuric acid formed by the combustion corrodes the cylinder liner. This must be prohibited (in a certain degree) by the neutralizing agents in the lubricant.
- **Insoluble stress:** The lubrication oil has to clean insoluble particles in order to avoid deposit formation and wear. These particles include; non-combusted fuel components or contaminants (asphalthenes, cat fines), neutralization products (CaSO4, FeSO4) and metal debris from the abrasive wear.
- **Thermal stress:** Temperature and exposure time determine the extent of thermal degradation of lubricant components. It is influenced by engine load, combustion characteristics and cylinder piston cooling.

Large two-stroke engines place greater physical and chemical stresses on the lubricant because of high power output, low oil consumption and long intervals between injections of fresh lubricants.

The rate of oil degradation varies in relation to the oil film thickness. The thinner the oil film the faster degradation. However, distribution of fresh lubricant with non-return valves is inhomogeneous and lubricant was found to stay in the engine for up to 30 minutes (Doyen et al, 2007, Advanced applied research unravelling the fundamentals of 2-stroke engine cylinder lubrication—an innovative on-line measurement method based on the use of radioactive tracers). Studies have shown that the residence time increases at lower engine loads and also feed rates (Hammett, 2014). This means that the risk of oil degradation is higher when the engine is slow-steaming and when the engine consumes low lubrication oil.

Several studies have shown that the wear of cast iron, caused by reciprocating piston ring under lubrication, is more severe at top dead centre and bottom dead centre than between these reversal points (Felter, C. L. et al, 2010, Development of a model capable of predicting the performance of piston ring-cylinder liner-like tribological interfaces). Furthermore, sulphuric acid and carbon soot in the lubrication increased the wear drastically (Yahagi, 1987, Corrosive wear of diesel engine cylinder bore. *Tribology International,* 20(6), 365-373). The level of sulphuric acid in the lubricating oil influences the corrosive wear. The carbon soot on the other hand increases abrasive wear, due to the hard carbon particles rubbed against the surface.

Oil stress measurements are as important as oil thickness measurements in order to prevent significant liner wear or damage of sliding surfaces. However, oil stress may be difficult to measure as several locations must be measured to understand the physical and chemical properties of the lubrication oil film.

Lubrication oil injection at each piston stroke will refresh the oil film at each piston stroke and thereby minimise the stress level of the oil film on the cylinder liner. Degradation of the oil film will therefore be prevented and low wear rates can be obtained. Furthermore, by injecting only the required amount of lubrication reduces furthermore the accumulation of oil additives, such as calcium carbonate particles which will lead to scuffing.

Flexibility in the delivery of the required amount of fresh lubrication oil at each engine stroke has been highly prioritized by Hans Jensen Lubricators. For this purpose, the HJ Lubtronic system operates with automated stepless stroke adjustment and timed lubrication. Combining HJ Lubtronic system and HJ SIP valves is said to ensure good engine condition. The HJ SIP spray injection valves, placed at the liner circumference, direct the lubricating oil spray upwards and into the engines scavenging air. Thus fresh oil is distributed at the top of the cylinder, where the oil film is highly exposed to degrading oil stresses. MS

Patent A

Title:	Method and system for dosing lubricating oil into cylinders, preferably in two-stroke diesel engines, and use of such method and system
Inventor:	Rathesan Ravendran
Applicant:	Hans Jensen Lubricators A/S
Application number:	DKPA201670169 20160323
IPC :	F 01 M 1/08 (2006.01)
Original Language	Danish
Status:	Published
Priority date:	12/12/2016
Background:	This patent is formulated during the work made during investigation of hypotheses I in chapter 4.
Abstract:	There is disclosed a method and a system for dosing lubricating oil in two-stroke diesel engines. A use thereof is also disclosed. The method comprises steps for delivering lubricating oil under pressure from a lubricating oil reservoir via a forced lubrication system to injectors provided in the cylinder walls. A number of injectors are used, each adapted for injecting a dosed amount of lubricating oil into each cylinder.

(19) DANMARK

(10) DK 178732 B1

(12) PATENTSKRIFT

Patent- og Varemærkestyrelsen

(51) Int.Cl.: *F 01 M 1/08 (2006.01)*

(21) Ansøgningsnummer: **PA 2016 70169**

(22) Indleveringsdato: **2016-03-23**

(24) Løbedag: **2016-03-23**

(41) Alm. tilgængelig: **2016-12-12**

(45) Patentets meddelelse bkg. den: **2016-12-12**

(73) Patenthaver: **Hans Jensen Lubricators A/S, Smedevænget 3, 9560 Hadsund, Danmark**

(72) Opfinder: **Rathesan Ravendran, Jyllandsgade 5, 2 th., 9000 Aalborg, Danmark**

(74) Fuldmægtig: **PATRADE A/S, Fredens Torv 3 A, 8000 Århus C, Danmark**

(54) Benævnelse: **Fremgangsmåde og anlæg til dosering af smøreolie i cylindre, fortrinsvis i 2-takts dieselmotorer samt anvendelse af sådan fremgangsmåde og anlæg**

(56) Fremdragne publikationer:
EP 2484875 A1
US 2006112925 A1
JP S59145312 A
CN 104110288 A

(57) Sammendrag:
**Der beskrives en fremgangsmåde og et anlæg til dosering af smøreolie i 2-takts dieselmotorer.
Der beskrives også en anvendelse heraf. Fremgangsmåden omfatter trin for levering af smøreolie under tryk fra et smøreoliereservoir via et tryksmøringsanlæg til injektorer, der er anbragt i cylindrenes vægge. Der anvendes et antal injektorer, der hver er indrettet for indsprøjtning af en doseret mængde smøreolie i hver cylinder.
Fremgangsmåden omfatter endvidere trin for- etablering af data der angiver temperatur i cylinderforinger, - etablering af data der angiver smøreoliens temperatur i smøreoliereservoiret, - lagring af nævnte temperaturdata for cylinderforinger og smøreolien i en computer, -etablering af mindst en temperaturreguleringsenhed, der styres af computeren og som er i forbindelse med den leverede smøreolie for etablering af en temperaturregulering af smøreolien før indsprøjtning i cylinderen, - styring af temperaturreguleringen af smøreolien i afhængighed af cylinderforingernes temperatur samt smøreoliens temperatur i smøreoliereservoiret idet computeren styrer opvarmning/afkøling i temperaturreguleringsenheden for påvirkning af smøreoliens viskositet således at der etableres en ensartet indsprøjtning uafhængig af cylinderforingernes temperatur.**

Fortsættes ...

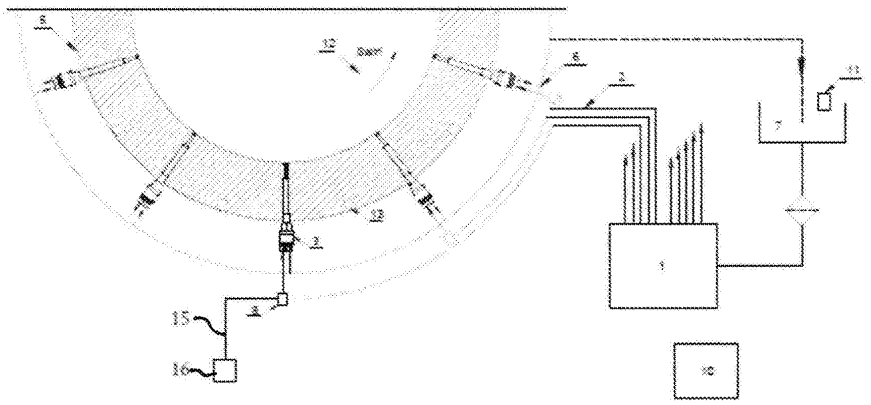

FIG. 2

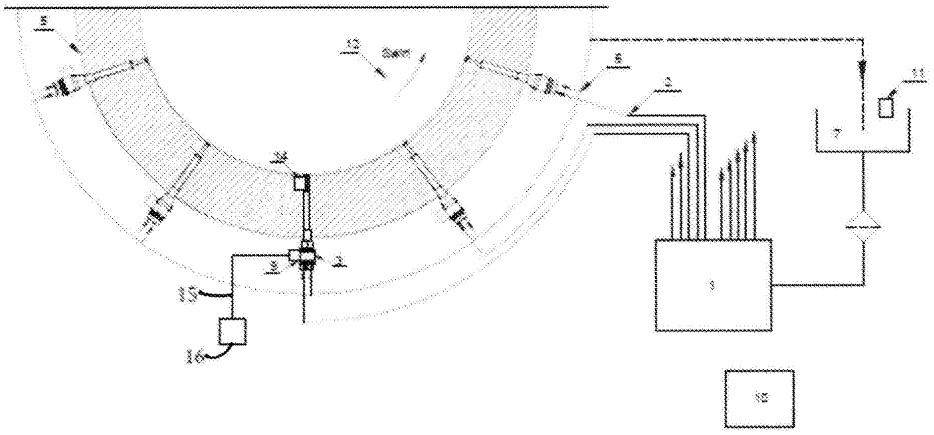

FIG. 3

Fremgangsmåde og anlæg til dosering af smøreolie i cylindre, fortrinsvis i 2-takts dieselmotorer samt anvendelse af sådan fremgangsmåde og anlæg

Opfindelsens område

Den foreliggende opfindelse angår en fremgangsmåde til dosering af smøreolie i cylindre, fortrinsvis i 2-takts dieselmotorer, for eksempel skibsmotorer, hvilken fremgangsmåde omfatter trin for;

- levering af smøreolie under tryk fra et smøreoliereservoir via et tryksmøringsanlæg til injektorer, der er anbragt i cylindrenes vægge, idet der anvendes et antal injektorer, der hver er indrettet for indsprøjtning af en doseret mængde smøreolie i hver cylinder
- etablering af data, der angiver temperatur i smøreolien i injektoren, i cylinderforingen eller i injektoren eller en kombination af disse,
- lagring af nævnte temperaturdata i en computer,
- etablering af mindst en temperaturreguleringsenhed, der styres af computeren, og som er i forbindelse med den leverede smøreolie for etablering af en temperaturregulering af smøreolien før indsprøjtning i cylinderen.

Opfindelsen angår endvidere et anlæg til dosering af smøreolie i cylindre, fortrinsvis i 2-takts dieselmotorer, for eksempel skibsmotorer, hvilket anlæg

- et smøreoliereservoir,
- et tryksmøringsanlæg der er forbundet med smøreoliereservoiret
- injektorer, der er forbundet med tryksmøringsanlægget og som er anbragt i cylindrenes vægge, idet der anvendes et antal injektorer, der hver er indrettet for indsprøjtning af en doseret mængde smøreolie i hver cylinder idet smøreolien under tryk leveres fra tryksmøringsanlægget til injektorer,
- måleenheder for etablering af data, der angiver temperatur i smøreolien i injektoren, i cylinderforingen eller i injektoren eller en kombination af disse,
- computer for lagring af nævnte temperaturdata,
- mindst en temperaturreguleringsenhed, der styres af computeren, og som er i forbindelse med den leverede smøreolie for etablering af en temperaturregulering af smøreolien før indsprøjtning i cylinderen for påvirkning af smøreoliens viskositet, således at der etableres en ensartet indsprøjtning.

Opfindelsen angår endvidere en anvendelse af fremgangsmåden eller anlægget i et tryksmøreanlæg hvor injektorer tilsluttes en fælles olieforsyningsledning, der har konstant forsyningstryk.

Opfindelsens baggrund

I traditionelle cylindersmøringssystemer, hovedsageligt til store 2-taktsdieselmotorer, anvendes der centrale tryksmøringsanlæg der kan omfatte et eller flere smøreapparater, der hver sørger for smøring af steder på en enkelt eller flere cylindere, dvs. ved tilførsel af mængder af olie under tryk gennem respektive forbindelsesledninger til de forskellige steder, der skal smøres, med relevante tidsintervaller. Se for eksempel DK/EP 0678152. Disse relevante intervaller kan typisk være, når stempelringene er anbragt overfor det relevante smøringssted i løbet af kompressionsslaget, når stemplet bevæger sig opad.

Smøreapparaterne er traditionelt udformet som pumpeenheder, der er monteret i nær tilslutning til deres respektive cylindre, og som er forbundet med et føderesservoir for smøreolie og med smøresteder i form af olieinjektorer på forskellige steder af cylindervæggen. Hver pumpeenhed omfatter flere stempelpumper, der forsyner forskellige smøresteder med olie, og som drives af en fælles, roterende styreaksel med påsatte knaster. Ved akslens rotation samvirker knasterne med trykhoveder på respektive aksialt forskydelige stempler, der er fjederbelastede i retning mod styreakslen, således at stemplerne ved akslens rotation vil udføre frem- og tilbagegående bevægelser for aktivering af stempelpumpernes stempler.

Smøreapparater har i en lang årrække arbejdet under den driftsbetingelse, at afgangstrykket fra stempelpumperne ikke har skullet være særligt stort, idet det er en fast standard, at olien skal injiceres i cylinderen under det opadgående returslag af motorstemplet, dvs. under kompressionsforløbet, men dog inden det efterfølgende arbejdsslag ved den antændte forbrænding. Det har herved været aktuelt at arbejde med injektions- eller pumpetryk af størrelsesordenen op til 10 bar.

Et tryksmøreanlæg kan også være tilvejebragt som et smøresystem til et antal cylindre. Hver cylinder er udstyret med et antal injektorer, der er tilsluttet en fælles smøre-

olieforsyningsledning, der har et konstant forsyningstryk, f.eks. i størrelsesordenen 30 – 100 bar. Forsyningstrykket leveres af en hydraulisk pumpe enhed, som forsynes fra et smøreoliereservoir. Pumpestationen kan omfatte pumper, filtre, kontraventiler, som forhindrer, at smøreolien løber tilbage gennem en stillestående pumpe.

Indenfor de senere år er det bragt i forslag at effektivisere smøringen ved at indsprøjte olien gennem trykforstøvningsdyser for opnåelse af en spraysmøring under stemplets opadgående bevægelse. Herved tilføres olien dog ved et langt højere tryk til sikring af en ønsket forstøvning gennem trykforstøvningsdyser, f.eks. et tryk på op til 100 bar eller mere.

Således kendes to-takts marine diesel motorer hvor der anvendes SIP injektorer fremstillet af Hans Jensen Lubricators til cylindersmøring.

Smøreolien sprayes ud i motorens skylleluft, hvorved olien fordeles i et tyndt og jævnt lag på cylindervæggen. I modsætning til andre smøreolieinjektorer på markedet, har SIP-injektorerne den fordel at der opnås en mere optimal dækning af toppen af cylindervæggen, hvor behovet for cylindersmøring er størst.

Indsprøjtningsmønsteret er, for traditionelle indsprøjtningssystemer, i høj grad styret af indsprøjtningsdysens design, væskens inerti og væskens egenskaber.

Ohnesorge-diagrammet, som er vist i Fig. 4, viser den eksperimentelle sammenhæng mellem disse faktorer udtrykt ved hjælp af Reynoldstal (Re) og Ohnesorgetallet (Z).

$$Re = \frac{u \cdot D \cdot \rho}{\mu} \quad (1)$$

$$Z = \frac{\mu}{\sqrt{\sigma \cdot \rho \cdot D}} \quad (2)$$

Hvor u er væskens hastighed, D er dysehullets størrelse, ρ er væskens densitet, μ er væskens viskositet og σ er væskens overfladespænding.

Der er to mekaniske måder hvorpå SIP-ventilens indsprøjtningsmønster kan ændres, enten kan dysens design ændres eller cylinderoliens leveringstryk kan ændres.

Leveringstrykket justeres ved at ændre karakteristikken for fjederen i SIP-ventilen. Når disse parametre er fastlagt, er det ikke muligt at ændre indsprøjtningsmønsteret uden manuelt indgreb.

Overfladespænding, densitet og viskositet er stort set ens for kommercielle cylinderolier. Viskositeten er dog, i modsætning til overfladespænding og densitet, særlig afhængig af oliens temperatur.

Der er empirisk målt viskositeten af en lang række kommercielle cylinderolier, og deraf bestemt at viskositeten kan beskrives ved hjælp af Arrhenius ligning, det vil sige som en funktion af temperaturen (T) ved hjælp af ligning 3.

$$\mu(T) = 0.0061 \cdot e^{1246/8.314 \cdot T} \qquad (3)$$

Denne ligning viser at cylinderoliens viskositet falder eksponentielt ved stigende temperatur. Derfor vil temperaturen på cylinderolien, jævnfør Ohnesorge-diagrammet, have en signifikant effekt på indsprøjtningsmønsteret.

Fig. 5 viser hvilken effekt temperaturen har på viskositeten for flere forskellige smøreolier. Der er et drastisk fald i viskositeten i intervallet mellem 40 og 300 °C. Ved temperaturer over 100 °C, ses det at kurven flader ud og at temperaturændring kun medfører meget begrænset ændring af viskositeten.

Sammenlignet med de to førnævnte metoder hvorpå indsprøjtningsmønsteret kan ændres, vil temperaturstyring være en mere fleksibel løsning.

I Sigurdsson, E. et al., 2014. "Numerical analysis of the scavenge flow and convective heat transfer in large two-stroke marine diesel engines". Applied Energy, 123, pp.37–46 omtales det at cylinderforingens temperatur ved cylinder hoved er ca. 250 °C og at der ved skylleporte i bunden af cylinderforingen er ca. 50 °C. Fra cylinder hoved til skylleporte aftager temperaturen med et andengradspolynomium.

Injektorerne i cylindervæggen vil have den samme temperatur som stedet på foringerne, hvor injektoren er placeret.

Der optræder således en stor variation i injektorernes temperatur og dermed også temperatuen i den smøreolie der indsprøjtes af injektorerne. Disse temperaturafvigelser påvirker smøreoliens viskositet og dermed det indsprøjtningsmønster der etableres.

Fra EP 2.484.875 A1 kendes et anlæg og en fremgangsmåde af den indledningsvis nævnte type. Der er ikke i dette skrift en beskrivelse af en registrering af temperaturdata for olien i smøreoliereservoiret.

Der er et ønske om at kunne styre indsprøjtningsmønsteret for at sikre en ensartet og korrekt smøring under anvendelse af mindst mulig smøreoliemængde.

Opfindelsens formål

Det er formålet med nærværende opfindelse at anvise en fremgangsmåde og et anlæg, som gør det muligt at kunne undgå ulemper ved uensartet og varierende temperatur i den indsprøjtede smøreolie og derved etablere en ensartet indsprøjtning.

Beskrivelse af opfindelsen

Dette opnås ifølge den foreliggende opfindelse med en fremgangsmåde af den indledningsvis nævnte type, der er særpræget ved, at fremgangsmåden endvidere omfatter trin for

- etablering af data der angiver smøreoliens temperatur i smøreoliereservoiret,
- lagring af nævnte temperaturdata i en computer,
- styring af temperaturreguleringen af smøreolien i afhængighed af nævnte temperatur i smøreolien i injektoren, i cylinderforingen eller i injektoren eller en kombination af disse samt smøreoliens temperatur i smøreoliereservoiret idet computeren styrer opvarmning/afkøling i temperaturreguleringsenheden for påvirkning af smøreoliens viskositet således at der etableres en ensartet indsprøjtning.

Anlægget ifølge opfindelsen er særpræget ved, at anlægget endvidere omfatter

- måleenheder for etablering af data der angiver smøreoliens temperatur i smøreoliereservoiret.

De data der angiver temperatur i cylinderforingen eller i injektoren eller en kombination af disse benyttes som udtryk for temperaturen i den indsprøjtede smøreolie. Dette benyttes i de situationer hvor det ikke er muligt at måle smøreolietemperaturen direkte ved indsprøjtningen gennem injektoren. Alternativt kan smøreolietemperaturen måles direkte i smøreolien der strømmer gennem injektoren. Alternativt kan der anvendes en kombination af disse temperaturmålinger.

Ved at regulere temperatuen på smøreolien i injektorerne bliver det på enkel måde muligt at regulere oliens viskositet. Ved at kunne styre temperaturen kan der således skabe en ensartet indsprøjtning.

Det er vigtigt at pointere, at der ikke kun er tale om en komplet forstøvning. Med opfindelsen vil det med temperaturstyringen være muligt for at styre graden af forstøvning. Lav viskositet vil føre til lav forstøvningsgrad, og høj viskositet vil føre til en høj forstøvningsgrad.

Ved at kunne styre temperaturen vil der kunne kompenseres for uensartet og varierende temperatur i smøreolien ved at foretage en temperaturregulering og derved påvirke smøreoliens viskositet og derved skabe en ensartet indsprøjtning for hver smøreolietilførsel.

I nærværende patentansøgning anvendes udtrykket indsprøjtning som udtryk for den måde hvorpå smøreolien indføres i cylinderen. Dette kan ske med større eller mindre tryk således at smøreolien optræder som en atomiseret spray eller som en helt eller delvis kompakt jet. Ligeledes kan indføringen ske på en måde så olien i nærmest kan siges at flyde ind i cylinderen frem for at sige at den sprøjtes ind i cylinderen.

En anvendelse af en fremgangsmåde ifølge opfindelsen eller et anlæg ifølge opfindelsen i et tryksmøreanlæg hvor injektorer tilsluttes en fælles olieforsyningsledning, der har konstant forsyningstryk giver særlige fordele.

Der opnås ydermere en fordel i tryksmøreanlæg hvor forsyningstrykket leveres af en hydraulisk pumpeenhed, som forsynes med smøreolie fra et smøreoliereservoir. Da viskositeten er en betegnelse for væskens indre friktion vil temperaturændring medfø-

re at det på enkel måde bliver muligt at foretage en regulering af den smøreoliemængde som indenfor et givet tidsinterval leveres af tryksmøreanlægget hvor injektorer tilsluttes en fælles olieforsyningsledning, der har konstant forsyningstryk.

Således vil en øget temperatur i den indsprøjtede smøreolie medføre en sænket viskositet. Dette betyder at der optræder mindre friktion i smøreolien og således kan der indenfor et givet tidsinterval indsprøjtes en større smøreoliemængde.

I tryksmøresystemer hvor indsprøjtningstiden styres er det således muligt at anvende opfindelsen for at regulere mængden af smøreolie som indsprøjtes inden for det givne tidsinterval.

Ifølge en yderligere udførelsesform er fremgangsmåden ifølge opfindelsen særpræget ved, at fremgangsmåden endvidere omfatter trin for

- etablering af en algoritme eller en tabel i computeren for sammenhængen mellem smøreoliens temperatur og viskositet.

Ved at etablere en algoritme kan der i computeren ske en styring ud fra en formel og aktuelt målte værdier.

Alternativt kan reguleringen også ske ved, at der forud er bestemt empiriske sammenhængstal, som er indlagt i en tabel. I begge situationer vil der ud fra algoritme eller tabel kunne foretages en justering af temperaturen, således at der opnås en ønsket viskositet i smøreolien og sikrer, at der opnås et ensartet indsprøjtningsmønster uafhængigt af temperaturvariationer i cylinderforingen og i injektorer.

Ifølge en yderligere udførelsesform er fremgangsmåden ifølge opfindelsen særpræget ved,

- måling af temperaturen i smøreolien i injektoren, i cylinderforingen eller i injektoren foretages med temperaturmålere i det område, hvor injektorerne er anbragt i cylindrenes vægge eller med temperaturmålere der er inkorporeret i injektorerne.

Ved at foretage en direkte måling af temperaturen i cylinderforingen ved injektorerne eller i selve injektorerne opnås en indirekte måling af den temperatur som optræder i

den indsprøjtede smøreolie. Såfremt temperaturmåleren der er inkorporeret i injektorerne måler direkte på smøreolietemperaturen opnås en måling af den temperatur som optræder i den indsprøjtede smøreolie. Der kan således kompenseres med opvarmning/afkøling af smøreolien.

Ifølge en yderligere udførelsesform er fremgangsmåden ifølge opfindelsen særpræget ved,

- registrering af motorens driftsforhold, for eksempel belastning af motoren, og anvendelse af sådanne data som angivelse af temperaturen i smøreolien.

I visse tilfælde kan det være hensigtsmæssigt, at benytte driftsparametre, som for eksempel motorbelastning i styringen. Motorens driftsforhold vil påvirke temperaturforhold i cylindervæggen. Alternativt vil driftsforhold som belastning kunne benyttes i en styring for at justere andre parametre end smøreolietemperaturen. Således kan parameter for belastning af motoren også benyttes for at justere en fordeling af smøreolien over cylindervæggens højde. Ligeledes er det muligt at anvende temperaturforhold sammen med andre driftsparametre, som for eksempel cylindertemperaturen eller udstødningsgastemperaturen.

Ifølge en yderligere udførelsesform er fremgangsmåden ifølge opfindelsen særpræget ved, at

- temperaturreguleringen foretages før smøreoliens passage gennem injektoren, idet temperaturreguleringsenheden er anbragt i serie med injektoren, eller
- temperaturreguleringen foretages under smøreoliens passage gennem injektoren, idet temperaturreguleringsenheden er indbygget i injektoren.

I visse tilfælde foretrækkes det at placere temperaturreguleringsenheden i serie med injektoren. Dette kan for eksempel være nødvendigt af pladshensyn. I andre situationer foretrækkes det, at temperaturreguleringsenheden er indbygget i injektoren. Herved opnås den mest præcise temperaturregulering i smøreolien umiddelbart før den indsprøjtes af injektoren.

Ifølge en yderligere udførelsesform er fremgangsmåden ifølge opfindelsen særpræget ved, at fremgangsmåden endvidere omfatter trin for

- registrering af den aktuelle temperatur i smøreolien ved hjælp af temperaturmålere i smøreoliereservoiret.

Ved at registrere smøreoliens temperatur i smøreoliereservoiret kan der foretages en regulering af smøreolien ikke alene i injektorerne, men også i smøreoliereservoiret. Således kan olien i smøreoliereservoiret bibringes en temperatur, som er så nær den ønskede smøreolietemperatur i injektoren. Herved reduceres behovet for opvarmning/afkøling i temperaturreguleringsenheden, som er tilvejebragt i tilknytning til injektoren. Dette sker ved, at en temperaturreguleringsenhed er placeret i tilknytning til smøreoliereservoiret. En sådan temperaturreguleringsenhed ved smøreoliereservoiret kan således benyttes i kombination med temperaturreguleringsenhederne ved injektorerne.

Ifølge en yderligere udførelsesform er fremgangsmåden ifølge opfindelsen særpræget ved,

- opvarmning/afkøling i temperaturreguleringsenheden foretages ved at cirkulere væske, fortrinsvis vand, der er i varmeudvekslingsforbindelse med smøreolien, og at
- væskecirkulationens hastighed reguleres for derved at påvirke temperaturreguleringen.

I de fleste større motorer findes der et kølevæskesystem. Derfor vil det være særligt hensigtsmæssigt at opvarmning/afkøling foretages med en varmeudveksling mellem cirkulerende kølevæske og smøreolien. Det er på enkelt måde muligt at foretage reguleringen ved at regulere vandcirkulationens hastighed.

Som alternativ til opvarmning/afkøling med vand kan der anvendes andre væsker ligesom der også kan anvendes gas eller el i temperaturreguleringsenheden.

Ifølge en yderligere udførelsesform er fremgangsmåden ifølge opfindelsen særpræget ved,

- temperaturreguleringen af smøreolien foretages indenfor et temperaturinterval mellem 0 og 250 °C, fortrinsvis mellem 0 og 100 °C.

Som omtalt tidligere kan cylinderforingens temperatur variere mellem ca. 50 og 250 °C. Derfor vil et temperaturinterval fra 0 – 250 °C være et hensigtsmæssigt område for temperaturregulering. Da det endvidere viser sig, at der i temperaturintervallet fra 100 – 250 °C ikke er stor forskel på viskositeten, kan det i særlige tilfælde være en fordel at foretage en regulering alene i temperaturintervallet 0 – 100 °C. I en sådan situation vil det antages, at viskositeten i temperatur over 100 °C er sammenlignelig med viskositeten ved 100 °C.

Temperaturen på smøreolien enten kan reguleres af en enhed, der opvarmer olien, inden den passerer igennem injektoren eller en enhed, der er indbygget i injektoren.

Ifølge en yderligere udførelsesform er anlægget ifølge opfindelsen særpræget ved, at
- temperaturreguleringsenheden er anbragt i serie med injektoren, således at temperaturreguleringen foretages før smøreoliens passage gennem injektoren, eller
- temperaturreguleringsenheden er indbygget i injektoren, således at temperaturreguleringen foretages under smøreoliens passage gennem injektoren.

Som omtalt ovenfor i forbindelse med fremgangsmåden kan pladshensyn gøre det hensigtsmæssigt at placere temperaturreguleringen i serie med injektoren eller indbygget i injektoren.

Ifølge en yderligere udførelsesform er anlægget ifølge opfindelsen særpræget ved, at det omfatter temperaturmålere i det område, hvor injektorerne er anbragt i cylindrenes vægge for måling af temperaturen i cylinderforingen i dette område eller temperaturmålere der er inkorporeret i injektorerne.

En temperaturmåler kan på enkel vis placeres i cylinderens væg eller være inkorporeret i injektoren. Således opnås der ved måling af temperaturen i cylinderforingen ved injektoren eller temperaturen i injektoren eller ved måling af temperaturen i smøreolien i injektoren en meget præcis indikation af temperaturen i smøreolien der indsprøjtes således at der kan foretages temperaturregulering og dermed etablere ensartet indsprøjtning.

Ifølge en yderligere udførelsesform er anlægget ifølge opfindelsen særpræget ved, at

det omfatter en varmevekslingsenhed, hvor væske, fortrinsvis vand cirkuleres i varmeudvekslingsforbindelse med smøreolien for derved at etablere opvarmning/afkøling i temperaturreguleringsenheden.

Som omtalt ovenfor er en varmeudvekslingsenhed, hvori der benyttes cirkulerende vand, hensigtsmæssig i forbindelse med større to-taksmotorer, idet disse ofte er forsynet med et kølevandsanlæg.

De omtalte og viste systemer er kun eksempler på et system ifølge opfindelsen. Således kan systemet være opbygget på andre måder som for eksempel med injektorer i form af injektionsdyser omfattende en dysestav med et deri forskydeligt ventillegeme, således at ventil er placeret i umiddelbar nærhed af dyseåbningen.

For funktionsduelighed vil flere elementer være nødvendige. Kun de elementer der er væsentlige for at forklare opfindelsen er omtalt.

Injektoren kan enten være forsynet med en forstøverventil eller en ventil med en eller flere stråler/kompakte jets.

Injektoren kan laves i en udførelsesform, hvor man kun forsyner den med tryksat smøreolie og uden returledninger. Typiske forsyningstryk på mellem 30 og 100 bar.

Tegningsbeskrivelse

Opfindelsen vil herefter blive forklaret nærmere under henvisning til den medfølgende tegning, hvor

Fig. 1 illustrerer en udførelsesform for et kendt system,

Fig. 2 illustrerer en første udførelsesform for et system ifølge opfindelsen,

Fig. 3 illustrerer en anden udførelsesform for et system ifølge opfindelsen,

Fig. 4 viser et Ohnesorge-diagram, som viser den eksperimentelle sammenhæng mellem Reynoldstal (Re) og Ohnesorgetallet (Z), og

Fig. 5 viser sammenhængen mellem temperatur og viskositet for forskellige smøreolier.

Detaljeret beskrivelse af opfindelsen

I Fig. 1 2 og 3 vises et antal injektorer 3, der er anbragt med passende intervaller i en cylinderforing 5. Disse injektorer er sat til at åbne ved et bestemt tryk i en olieledning 2, der går fra et smøreapparat 1 til de enkelte injektorer 3.

For enden af injektoren 3 umiddelbart indenfor den indre cylinderflade er der monteret en dyse 4 med dyseåbninger, hvorigennem olien forstøves, når trykket i olieledningen 2 når en bestemt forudindstillet værdi. Alternativt kan olien indsprøjtes uden forstøvning.

Olien tilføres hver olieledning 2 fra smøreapparatet 1, der består af et antal små pumper, en til hver olieledning 2, der modtager olie fra et oliereservoir 7.

Oliepumperne er i stand til at afgive en afmålt portion olie ved givne tidsintervaller og kan eksempelvis være et traditionelt tidsindstillet cylindersmøreapparat som beskrevet i internationalt patentansøgning WO 96/09492. Disse injektorer 3 er konstrueret således, at hvis der sker olieudslip, er der tilvejebragt et tilbageløb 6 til udsivet olie, som fører tilbage til oliereservoiret 7. Injektorerne kan være indrettet for mekanisk eller elektronisk bestemmelse af indsprøjtningstidspunktet.

J indikerer en strøm af olieindsprøjtning fra en injektor 3, og A indikerer den perifere udstrækning af cylindervæggens område, hvorimod denne stråle er rettet.

Fig. 2 viser en første udførelsesform for et system svarende til det i Fig. 1 viste og hvor en temperaturreguleringsenhed 8 er koblet på olieforsyningen til injektorerne 3.

Fig. 3 viser en anden udførelsesform for et system svarende til det i Fig. 1 viste og hvor en temperaturreguleringsenhed 9 er inkorporeret i injektorerne 3.

Smøreolien sprayes ud i motorens skylleluft, der beskriver en swirl 12 hvorved olien fordeles i et tyndt og jævnt lag på indersiden af cylindervæggen 5.

Det er ligeledes muligt at sprøjte smøreolie ind på stemplet eller under stemplet hvor der ikke er skylleluft. Dette kan ske som alternativ eller i kombination med indsprøjtning over stemplet.

I cylindervæggen 5 er der monteret en eller flere temperaturmålere 13 (kun en er vist) i området for injektorerne 3. Temperaturmålere 14 (kun vist i Fig. 3) er inkorporeret i injektorerne. Temperaturmåleren 14 kan måle temperaturen i injektoren eller temperaturen i smøreolien, der indsprøjtes gennem injektoren eller en kombination af disse temperaturer.

Disse temperaturmålere 13,14 er forbundet med en computer 10 enten via ledninger (ledninger ikke vist) eller via trådløs kommunikation.

I oliereservoiret 7 er der anbragt en temperaturmåler 11, der er forbundet med computeren 10 enten via ledninger (ledninger ikke vist) eller via trådløs kommunikation.

Computeren 10 er forbundet med temperaturreguleringsenheden 8/9 enten via ledninger (ikke vist) eller via trådløs kommunikation.

Temperaturreguleringsenheden 8/9 er via en ledning 15 forbundet med et varmelegeme/kølelegeme 16, således at der enten ved elektrisk/medie varmeudvekslingsforbindelse etableres opvarmning/afkøling i temperaturreguleringsenheden 8/9.

PATENTKRAV

1. Fremgangsmåde til dosering af smøreolie i cylindre, fortrinsvis i 2-takts dieselmotorer, for eksempel skibsmotorer, hvilken fremgangsmåde omfatter trin for;

- levering af smøreolie under tryk fra et smøreoliereservoir via et tryksmøringsanlæg til injektorer, der er anbragt i cylindrenes vægge, idet der anvendes et antal injektorer, der hver er indrettet for indsprøjtning af en doseret mængde smøreolie i hver cylinder,
- etablering af data, der angiver temperatur i smøreolien i injektoren, i cylinderforingen eller i injektoren eller en kombination af disse,
- lagring af nævnte temperaturdata i en computer,
- etablering af mindst en temperaturreguleringsenhed, der styres af computeren, og som er i forbindelse med den leverede smøreolie for etablering af en temperaturregulering af smøreolien før indsprøjtning i cylinderen,

kendetegnet ved, at fremgangsmåden endvidere omfatter trin for

- etablering af data der angiver smøreoliens temperatur i smøreoliereservoiret,
- lagring af nævnte temperaturdata i en computer,
- styring af temperaturreguleringen af smøreolien i afhængighed af nævnte temperatur i smøreolien i injektoren, i cylinderforingen eller i injektoren eller en kombination af disse samt smøreoliens temperatur i smøreoliereservoiret idet computeren styrer opvarmning/afkøling i temperaturreguleringsenheden for påvirkning af smøreoliens viskositet således at der etableres en ensartet indsprøjtning.

2. Fremgangsmåde ifølge krav 1, **kendetegnet ved, at** fremgangsmåden endvidere omfatter trin for

- etablering af en algoritme eller en tabel i computeren for sammenhængen mellem smøreoliens temperatur og viskositet.

3. Fremgangsmåde ifølge krav 1 eller 2, **kendetegnet ved,**

- måling af temperaturen i smøreolien i injektoren, i cylinderforingen eller i injektoren foretages med temperaturmålere i det område hvor injektorerne er anbragt i cylindrenes vægge eller med temperaturmålere der er inkorporeret i injektorerne.

4. Fremgangsmåde ifølge krav 1 eller 2, **kendetegnet ved,**

- registrering af motorens driftsforhold, for eksempel belastning af motoren, og anvendelse af sådanne data som angivelse af temperaturen i smøreolien.

5. Fremgangsmåde ifølge et hvilket som helst af de foregående krav, **kendetegnet ved, at**

- temperaturreguleringen foretages før smøreoliens passage gennem injektoren idet temperaturreguleringsenheden er anbragt i serie med injektoren, eller
- temperaturreguleringen foretages under smøreoliens passage gennem injektoren idet temperaturreguleringsenheden er indbygget i injektoren.

6. Fremgangsmåde ifølge et hvilket som helst af de foregående krav, **kendetegnet ved, at** fremgangsmåden endvidere omfatter trin for

- registrering af den aktuelle temperatur i smøreolien ved hjælp af temperaturmålere i smøreoliereservoiret.

7. Fremgangsmåde ifølge et hvilket som helst af de foregående krav, **kendetegnet ved, at**

- opvarmning/afkøling i temperaturreguleringsenheden foretages ved at cirkulere væske, fortrinsvis vand, der er i varmeudvekslingsforbindelse med smøreolien og at
- væskecirkulationens hastighed reguleres for derved at påvirke temperaturreguleringen.

8. Fremgangsmåde ifølge et hvilket som helst af de foregående krav, **kendetegnet ved, at**

- temperaturreguleringen af smøreolien foretages indenfor et temperaturinterval mellem 0 og 250 °C, fortrinsvis mellem 0 og 100 °C.

9. Anlæg til dosering af smøreolie i cylindre, fortrinsvis i 2-takts dieselmotorer, for eksempel skibsmotorer, hvilket anlæg

- et smøreoliereservoir,
- et tryksmøringsanlæg der er forbundet med smøreoliereservoiret
- injektorer, der er forbundet med tryksmøringsanlægget og som er anbragt i cylindrenes vægge, idet der anvendes et antal injektorer, der hver er indrettet for indsprøjtning af en doseret mængde smøreolie i hver cylinder idet smøreolien under tryk leveres fra tryksmøringsanlægget til injektorer, - måleenheder for etablering af data der angiver

temperatur i smøreolien i injektoren, i cylinderforingen eller i injektoren eller en kombination af disse,

- computer for lagring af nævnte temperaturdata,
- mindst en temperaturreguleringsenhed, der styres af computeren og som er i forbindelse med den leverede smøreolie for etablering af en temperaturregulering af smøreolien før indsprøjtning i cylinderen for påvirkning af smøreoliens viskositet således at der etableres en ensartet indsprøjtning, **kendetegnet ved, at** anlægget endvidere omfatter
- måleenheder for etablering af data, der angiver smøreoliens temperatur i smøreolie-reservoiret.

10. Anlæg ifølge krav 9, **kendetegnet ved, at**

- temperaturreguleringsenheden er anbragt i serie med injektoren således at temperaturreguleringen foretages før smøreoliens passage gennem injektoren, eller
- temperaturreguleringsenheden er indbygget i injektoren således at temperaturreguleringen foretages under smøreoliens passage gennem injektoren.

11. Anlæg ifølge krav 9 eller 10, **kendetegnet ved, at** det omfatter temperaturmålere i det område hvor injektorerne er anbragt i cylindrenes vægge for måling af temperaturen i cylinderforingen i dette område eller temperaturmålere der er inkorporeret i injektorerne.

12. Anlæg ifølge krav 9, 10 eller 11, **kendetegnet ved, at** det omfatter en varmevekslingsenhed hvor væske, fortrinsvis vand cirkuleres i varmeudvekslingsforbindelse med smøreolien for derved at etablere opvarmning/afkøling i temperaturreguleringsenheden.

13. Anvendelse af en fremgangsmåde ifølge et hvilket som helst af kravene 1- 8 eller et anlæg ifølge et hvilket som helst af kravene 9 – 12 i et tryksmøreanlæg hvor injektorer tilsluttes en fælles olieforsyningsledning, der har konstant forsyningstryk.

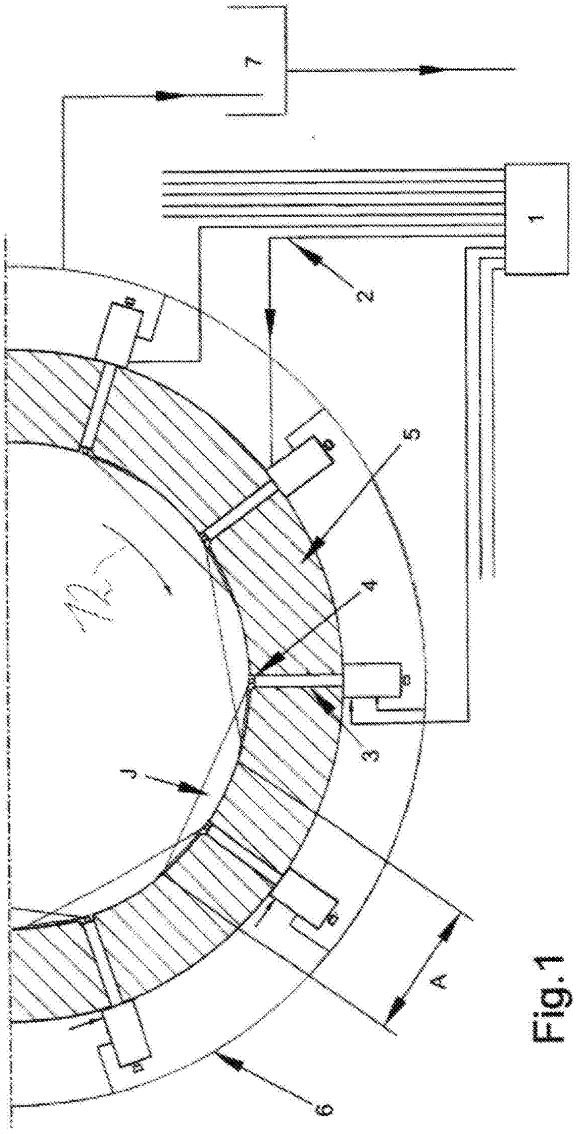

Fig.1

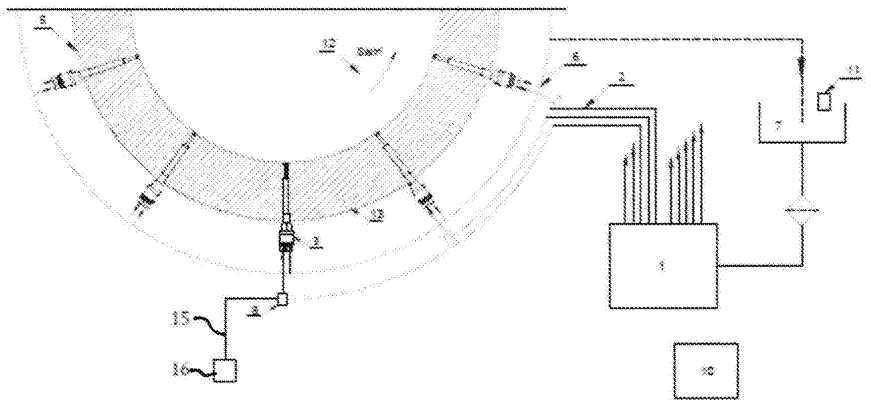

FIG. 2

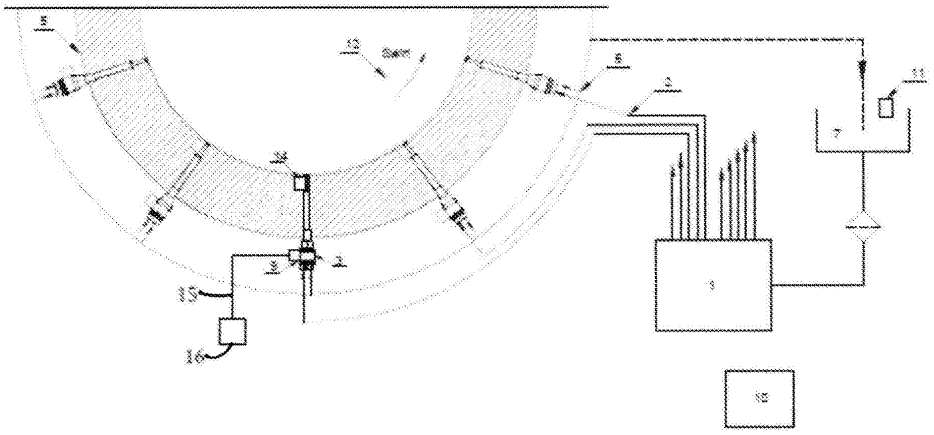

FIG. 3

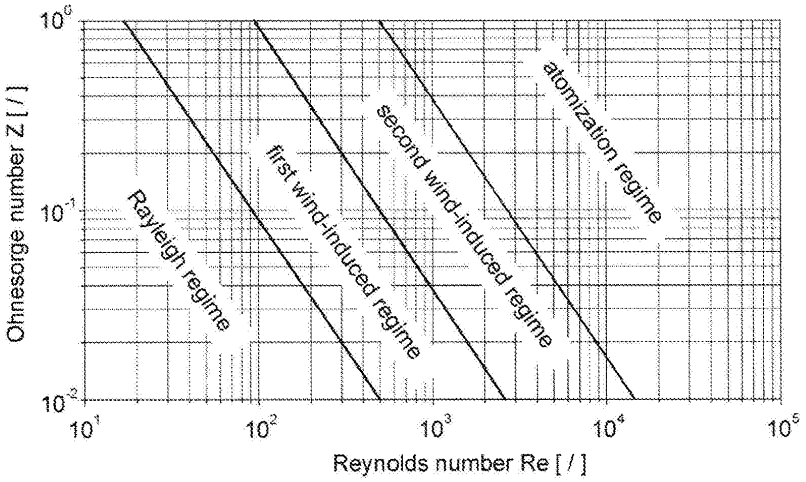
Ohnesorge number Z [/]
Reynolds number Re [/]
Rayleigh regime
first wind-induced regime
second wind-induced regime
atomization regime

FIG. 4

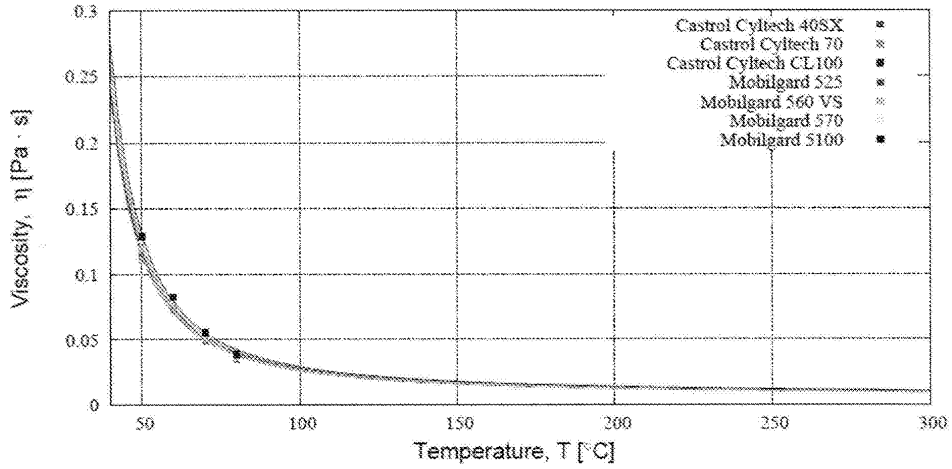
Viscosity, η [Pa · s]
Temperature, T [°C]
Castrol Cyltech 40SX
Castrol Cyltech 70
Castrol Cyltech CL100
Mobilgard 525
Mobilgard 560 VS
Mobilgard 570
Mobilgard 5100

FIG. 5

Patent B

Title:	Method for lubricating large two-stroke engines using controlled cavitation in the injector nozzle.
Inventor:	Rathesan Ravendran
Applicant:	Hans Jensen Lubricators A/S
Application number:	PA 2017 70382
Application country :	Denmark
Original Language	English
Status:	Granted
Application date:	26/05/2017
Background:	This patent is formulated during the work made during investigation of hypotheses II in chapter 4.
Abstract:	A method for lubricating a large slow-running two-stroke engine. The lubricant viscosity and pressure is selected such that cavitation is provided in the nozzle and potentially is extending to the nozzle exit.

SUMMARY

Cylinder lubrication oil is an important component for the operation of large two-stoke marine diesel engines. It controls the mechanical friction loss and wear on cylinder liner and piston rings by providing a thin oil film between the sliding interfaces. The lubrication oil is injected as a spray into the scavenging air swirl inside the cylinder, thereby providing an even coverage of the oil at the top of the cylinder, where the need of lubrication is highest.

Over the last decades, there has been an increasing focus on optimising the lubrication oil consumption in order to reduce the operational costs of marine diesel engines. As of today, the analysis has been documented by an experimental trial and error approach. Numerical investigations of the spray injection process have not been performed in order to establish an understanding of the complex process. This PhD thesis will serve as a starting point for the investigations by covering the topics influencing the flow of cylinder lubrication oil through the injection nozzle and the subsequent spray formation.

ISSN (online): 2446-1636
ISBN (online): 978-87-7210-055-5

AALBORG **UNIVERSITY PRESS**